UNIVERSIDAD NACIONAL DE INGENIERÍA

FACULTAD DE CIENCIAS

UNIDAD DE POSGRADO

# “ PARTICLE IDENTIFICATION ALGORITHMS FOR THE MEDIUM ENERGY ($\sim$ 1.5-8 GeV) MINER$\nu$A TEST BEAM EXPERIMENT ”

TESIS

PARA OPTAR EL GRADO ACADÉMICO DE MAESTRO EN CIENCIAS CON MENCIÓN EN FÍSICA

PRESENTADA POR:

**ANTONIO FEDERICO ZEGARRA BORRERO**

ASESOR:

DR. CARLOS JAVIER SOLANO SALINAS

UNIVERSIDAD NACIONAL DE INGENIERÍA

LIMA-PERÚ

2016

*Dedicado a todos aquellos que hicieron posible*
*la realización de este trabajo.*

## Acknowledgements

Agradezco en primer lugar a mi asesor el Dr. Javier Solano por el apoyo brindado durante el tiempo en que realizaba mis estudios de maestría en la Facultad de Ciencias de la UNI y por su confianza en mi persona para realizar un trabajo de investigación en el Fermi National Accelerator Laboratory (Fermilab). Un agradecimiento especial al Dr. Orlando Pereyra (actual decano de la Facultad de Ciencias) por las mismas razones.

Un agradecimiento enorme y muy especial para el CONCYTEC, por el apoyo financiero brindado que me permitió dedicarme por completo a mis estudios de maestría y de esa forma haber terminado con éxito este trabajo de investigación. Este proyecto de invertir en el talento me parece muy importante y permitirá a nuestro país avanzar en Ciencia y Tecnología, único camino en mi opinión de salir del subdesarrollo.

A toda la colaboración MINER$\nu$A, en especial a los científicos Dr. Jorge Morfin, Dr. Leo Bellantoni y Dra. Deborah Harris por su asesoría y apoyo brindado durante mi pasantía en Fermilab. A todos los Test-Beam-Experts por su enorme apoyo, en especial a Aaron Bercellie, Robert Fine, Anne Norrick y demás estudiantes y Post-Docs cuyas sugerencias han sido cruciales para el desarrollo de este trabajo: Edgar Valencia, David Martínez, Dipak Rimal, Trung Le, Chris Marshall, Nuruzzaman entre muchos otros.

A la Unidad de Posgrado de la Facultad de Ciencias, en especial a la secretaria Karen Soto por su cordial apoyo brindado en todo lo referido a trámites necesarios para poder presentar este trabajo.

Quiero agradecer también a mi familia y a los profesores de la Facultad de Ciencias de la UNI que han contribuido a mi formación científica durante mis estudios de maestría.

## Abstract

This thesis is focused on the construction of algorithms to isolate specific kinds of particle species present in the secondary beam of the current Test Beam (taking data at medium energies $\sim$ 1.5-8 GeV) of the MINER$\nu$A experiment at Fermilab. For that purpose it was necessary to analyze many variables related to specific devices along the beamline (Time of Flight, Cerenkov, Veto) and the main detector (a miniature version of the MINER$\nu$A detector). Results on the particle composition of the secondary beam ($\%\ p^{\pm}, \pi^{\pm}, \mu^{\pm}, e^{\pm}$) are presented for different energies and polarities of the beam together with a methodology to get those results. The usage of ROOT via C++/python was mandatory as well as the generation of Monte Carlo simulations of single particles passing through the Test Beam detector to test the cuts (logic conditions) used for the isolation of specific particle species (for all energies) and to perform an Efficiency-Purity analysis in order to find the optimum cuts (for the 2GeV sample).



**Keywords: MINER$\nu$A experiment, Fermilab, medium energies, Test Beam, Monte Carlo, ROOT, secondary beam, beamline, cuts, Efficiency-Purity analysis.**



## Resumen

Esta tesis está enfocada en la construcción de algoritmos para aislar tipos específicos (especies) de partículas presentes en el haz secundario del actual Test Beam (tomando datos a energías medias $\sim$ 1.5-8 GeV) del experimento MINER$\nu$A en Fermilab. Para dicho fin ha sido necesario el análisis de muchas variables relacionadas a dispositivos específicos a lo largo de la línea del haz (Time of Flight, Cerenkov, Veto) y al detector principal (una versión en miniatura del detector MINER$\nu$A). Resultados de la composición del haz secundario ($\%\ p^{\pm}, \pi^{\pm}, \mu^{\pm}, e^{\pm}$) son presentados para diferentes energías y polaridades del haz junto con la metodología seguida para dicho fin. El uso de ROOT vía C++/python ha sido necesario así como la generación de simulaciones Monte Carlo del paso de partículas específicas a través del detector del Test Beam para verificar los cortes (condiciones lógicas) usados para el aislamiento de especies específicas de partículas (para cualquier energía) así como para realizar un análisis de Pureza-Eficiencia con el fin de encontrar los cortes óptimos (para la muestra de 2GeV).



**Palabras clave: experimento MINER$\nu$A, Fermilab, energías medias, Test Beam, Monte Carlo, ROOT, haz secundario, línea del haz, cortes, análisis de Pureza-Eficiencia.**

# Introduction

The MINER$\nu$A collaboration [1] is currently interested in studying neutrino (neutrinos coming from a high-intensity beam called NuMI [2]) interactions at medium energies ($\sim$ 1.5-8 GeV [3]) taking place inside its main detector (located underground). In order to test the Monte Carlo simulation of the final-state particles (arising from those interactions) passing through this detector it has been necessary to initiate a second Test Beam effort (it was a previous one set for low energies $\sim$ 0.35-2.0 GeV [4]) at the Fermilab Test Beam Facility [5]. It is very important for the MINER$\nu$A experiment as well as for the Accelerator Division (in charge of delivering the beam for both the Test Beam and for NuMI) to understand the particle-composition (% of protons, pions, muons, electrons, kaons) of the (secondary) beam of particles entering the Test Beam detector (a miniature version of the MINER$\nu$A main detector). This work presents different particle ID algorithms that have been developed and applied to Test-Beam-Data in order to estimate the composition of this (secondary) beam at different energies and polarities with the aid of many variables related to the Test Beam devices. The structure of this thesis is the following:

**Chapter 1** provides a general overview of the main goals of the current Medium-Energy Test-Beam experiment, explaining the way in which a beam of a specific composition, energy and polarity can be set to enter the Test Beam detector with the aid of different experimental devices (Triggering, Tracking and particle-ID devices) located along its beamline. It is also pointed out the importance of this Medium-Energy Test Beam for the MINER$\nu$A experiment as well as an overview of the way in which the MINER$\nu$A main detector works.

**Chapter 2** presents an introduction to neutrino physics and the main neutrino interactions taking place inside the MINER$\nu$A main detector. This is relevant because the particles present in the final state have a specific way of depositing energy inside the detector (an issue which permits the reconstruction of events) and are the ones we analyze as single-events in the Test Beam.

**Chapter 3** explains the software tools needed to perform Data Analysis (ROOT via C++/python) and the different ways in which particles passing through matter manage to deposit energy (via Ionization, Electromagnetic-Showers and Hadronic-Showers). It also provides some features about Arachne, a software developed by the MINER$\nu$A collaboration in order to "visualize" particle tracks inside its detector.

**Chapter 4** establishes the most important conditions (logic statements in a script) we need to impose on Data in order to retain physically meaningful events to fulfill the main goal of the Test Beam (to put a single particle "per unit time" of known energy and polarity in a miniature version of the MINER$\nu$A detector) and presents the initial approach that was taken to find the beam composition as well as some early results.

**Chapter 5** presents RESULTS on the composition of the secondary beam (% $p^{\pm}, \pi^{\pm}, \mu^{\pm}, e^{\pm}$) for different energies and polarities from the usage of a systematic approach useful for 4, 6 & 8 GeV data samples. For the 2GeV sample a more sophiticated tool was constructed in order to separate $\mu$ and $\pi$ present in the ToF (Time of Flight) $\pi$-peak. In order to test the validity of the results, Monte Carlo simulations of single particles passing through the detector were developed in order to compare patterns (2D histograms of key-variables) of isolated-particles (from Data) and pure-particles (Monte Carlo).

**Chapter 6** shows an Efficiency-Purity analysis developed to find the optimum-cut to separate $\mu^+$ from $\pi^+$ for the 2GeV sample (and in this way reduce systematic uncertainties), for this purpose a change in the logic was needed as well as Monte Carlo simulations of different kinds of species passing through the detector in order to find the best way of discriminating between them via the construction of histograms of many Detector-Variables ($Var\_i\_\beta$). The same method was applied to construct the optimum-cut to separate $e^+$ from $\mu^+$ and $e^+$ from $\pi^+$, respectively. The general way to proceed in order to peform a Particle-ID analysis for Test Beam data was established after this analysis.

Regarding the Appendex, there are presented only some of the most important scripts (there were too many scripts containing thousands of lines of code each one) in pyroot to show their main structure (Appendix A, B, C, D), some plots of important histograms relevant for the analysis presented in Chapter 6 (Appendix E, F, G) & a final Apprendix (H) in which some of the main contributions of this work to the MINER$\nu$A experiment and other relevant physical issues are summarized.

# Contents

# Chapter 1

# Overview of the Medium Energy Test Beam of the MINER$\nu$A experiment

This chapter starts presenting a short review of the MINER$\nu$A experiment [1] in Section 1.1, discussing its main goals and the way in which they can be achieved. Emphasis is put in the necessity of using a Test-Beam to measure how well the Monte Carlo simulation (MC) of the detector response of particles produced from neutrino interactions describes the data. Right now the MINER$\nu$A collaboration is taking data at Medium Energies, they already took Low Energy data during the period of time from March 2010 to April 2012 and studied interactions of neutrinos and anti-neutrinos at an energy of few GeV. For that analysis the MINER$\nu$A collaboration already worked in a previous Test-Beam (1) for the energy range 0.35 to 2.0 GeV [4] and is currently working on a new Test-Beam (2) effort for the energy of current interest (1.5 to 8 GeV, although at the beginning even greater energies were expected [3]). Section 1.2 outlines the main goals of the current Test-Beam 2 project and how a work on the particle composition of the secondary beam is valuable for its purposes. In Section 1.3 all the necessary devices along the beamline for taking good data are presented, they can be divided as Triggering, Tracking and Particle-ID devices. In Section 1.4 some features about the Test-Beam detector and the difference it has with respect to the MINER$\nu$A main detector (underground) are described, emphasis is put on the 2 configurations used for taking the data currently used for the particle-ID analysis. Due to the importance of the Time of Flight system for particle ID purposes, there is an entire Section (1.5) dedicated to explain how it works, from the experimental part through the electronics and the variables to look at data acquired from the usage of that equipment. At the end there is Section (1.6) in which the importance that a Detector Expert plays in the experiment to ensure that the data is properly taken is presented. There are presented some issues about the training needed to become a Detector Expert and things to look at when there is a problem with the data acquisition (DAQ).

## 1.1 Overview of the MINER$\nu$A experiment at Fermilab

MINER$\nu$A (Main INjector ExpeRiment $\nu$-A) is a few GeV neutrino-nucleus scattering experiment designed to study low energy neutrino (in a first stage) interactions both in support of neutrino oscillation experiments and as a pure weak probe of the nuclear medium. The experiment uses a fine-grained, high resolution detector. The active region is composed of plastic scintillator with additional targets of helium, carbon, iron, lead and water placed upstream of the active region.

The **NuMI** [2] (Neutrinos at the Main Injector) is an intense $\nu_\mu$, $\overline{\nu}_\mu$ **beam** located at Fermilab[6], with the purpose of serving different neutrino experiments, short and long-baseline, such as MINER$\nu$A (see Figure 1.1), MINOS, ArgoNeut and NO$\nu$A [7]. The MINER$\nu$A experiment is located in the NuMI hall (next to the MINOS Near Detector [8]), about 1 km downstream of the NuMI-target and 100 meters underground in order to get the flux for the neutrino cross section measurements. NuMI is a tertiary beam which results from the decay of secondary kaons and pions produced in the NuMI target. A 120 GeV/c proton beam that is extracted from the Main Injector storage ring bombards a graphite NuMI target producing mostly kaons and pions. These charged mesons are focused by a system composed of two toroidal magnets called horns into a 675 meters decay pipe and then decay primarily into $\mu$ and $\nu_\mu$. Then they travel through a region of 240 m of unexcavated rock that stop the remnant hadrons and leptons, leaving only the neutrinos (see Figure 1.2).

**Figure 1.1:** MINER$\nu$A installation at the NuMI Hall

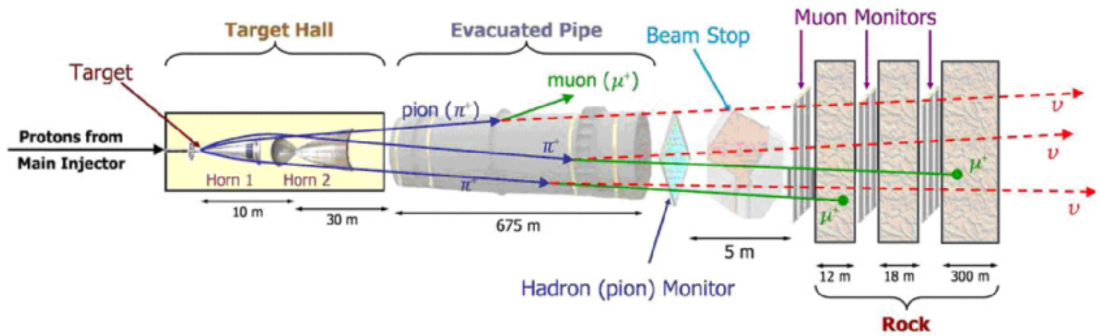


**Figure 1.2:** The NuMI main components.

**The MINER$\nu$A Detector:** consits of an inner tracker volume made of active plastic scintillator surrounded by electromagnetic and hadronic calorimeters and a set of different passive nuclear targets: helium, carbon, iron, lead and water (see Figure 1.3). The detector has 120 modules of hexagonal shape with an inner portion surrounded by an outer steel support frame. This frame is 56 cm wide and partially instrumented with scintillator and serves as a hadronic calorimeter. The content of the inner portion depends on the part of the detector the module is located: the tracker, calorimeters or nuclear targets.

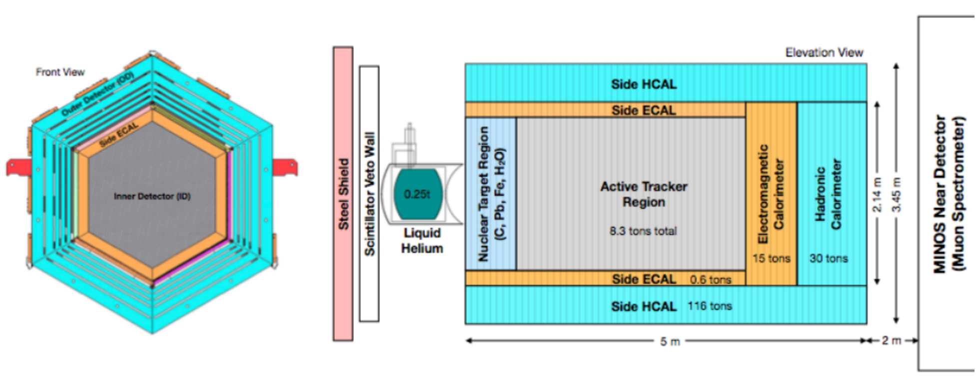


**Figure 1.3:** Minerva Detector Schematic.

Details about the inner detector which is composed of the Nuclear Targets, Tracker Region, Electromagnetic and Hadronic calorimeters (ECAL and HCAL respectively), and the outer detector can be found in [9]. In Section 1.4 there is more information about the Tracker, ECAL and

HCAL regions but for the Test Beam detector (which is a miniature version of the MINER$\nu$A main detector). This because the present thesis is more focused on the Test-Beam 2 rather than in the MINER$\nu$A neutrino experiment. In that Section it is explained how the data is acquired from light (produced by charge particles passing through the scintillators) to electric charge (which is stored in an FEB) and then digitized to be stored as information in a DST (which is a ROOT file). Specific and detailed information about the Data Acquisition (DAQ) System for the MINER$\nu$A experiment (for the Test Beam the DAQ system is almost the same) can be found in [10].

## 1.2 Goals of the Test-Beam 2 and of a particle-ID analysis

All particle physics experiments rely on computer simulations of their detectors to make measurements, but neutrino experiments struggle to test these simulations using particles that are created from the neutrino beam itself. Neutrino interactions often produce charged particles such as muons or electrons (that knock one or more protons or neutrons out of the nucleus) and also quark-antiquark pairs called pions. Each of these different particles gives us a view inside the nucleus, but to make these precise measurements, MINER$\nu$A needs to understand what these particles do once they exit the nucleus and enter the rest of the detector.

We could simply trust a computer package (called **Geant4**) that simulates particle interactions, but to be rigorous, we need to verify that package. To do this we use a well-calibrated low-energy beam of pions, protons, muons and electrons from the Fermilab Test Beam Facility (**FTBF**) [5] and a scaled-down version of the full MINER$\nu$A detector that is made of planes of **scintillator, lead and steel**. This smaller detector, which can be configured to replicate the downstream third of the neutrino detector (in the ECAL configuration), uses the same materials, electronics and calibration strategy as the MINER$\nu$A (underground) main detector.

The MINER$\nu$A collaboration already operated a scaled-down replica of the solid scintillator tracking and sampling calorimeter regions of the MINER$\nu$A detector in a hadron test beam at the FTBF. They reported measurements with samples of protons, pions, and electrons from 0.35 to 2.0 GeV/c momentum [4] and the calorimetric response to protons, pions, and electrons was obtained from these Data. These measurements are used to tune the MINER$\nu$A detector simulation and evaluate systematic uncertainties in support of the MINER$\nu$A neutrino cross section measurement program.

In the next Figure there is shown a diagram of the beamline used in Test Beam 1, it is relevant to notice that they used a tertiary beam, which is generated from the collision of pions (of $\sim 16GeV$) from the secondary beam, which was generated previously from the collision of $120GeV$ protons (primary beam), as will be explained below. This Figure is relevant to be shown for comparison with the beamline elements along the secondary beam in Test Beam 2, the purpose and working mechanism of those elements is explained in Section 1.3 only for Test-Beam-2 elements.

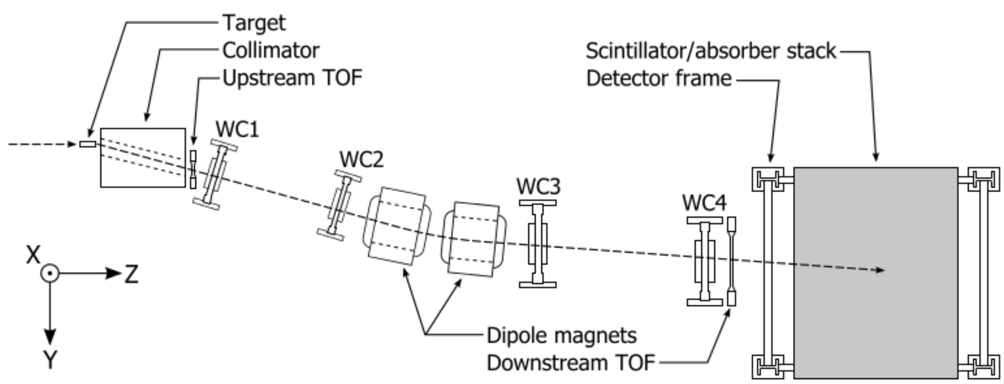


**Figure 1.4:** Diagram of the beamline built for the Test Beam 1 experiment, viewed from above with the beam going from left to right.

For the Test Beam it is possible to select a beam of a given polarity (ie. to select a beam of positive or negative particles) by changing the direction of the fields in the magnets, located upstream the detector, as will be shown next. It is very important to be able to know what specific particles are passing through the detector; in fact, **the goal of the Test Beam experiment** (for both TB 1 and 2) is to **validate the Monte Carlo simulation** used for simulating particles passing through the detector **by putting single particles of known type and energy into a smaller version of the main detector** [11]. For this reason it is necessary to perform a particle Identification (particle ID) of the species composing the beam entering the detector. For TB-1 this was performed with the aid of a Time of Flight (ToF) device, which permits to separate particles considering that particle species having different masses spend a different time travelling from one point to another (as is explained in Section 1.5) and Wire Chambers to calculate the momentum of the particles (and follow their trajectory). Thus by constructing a 2D histogram of ToF time and momentum, as shown in the next Figure they were able to study the composition of the beam. For TB-2 it is not possible to rely on the Wire Chambers because there is no tertiary beam (which helped them to calculate the momentum with the aid of magnets placed between them, as shown in the previous Figure). In next Figure there is also shown the detector response to pions for TB-1, the idea for TB-2 is to get also the response to electrons and protons at the extrapolated energy interval.

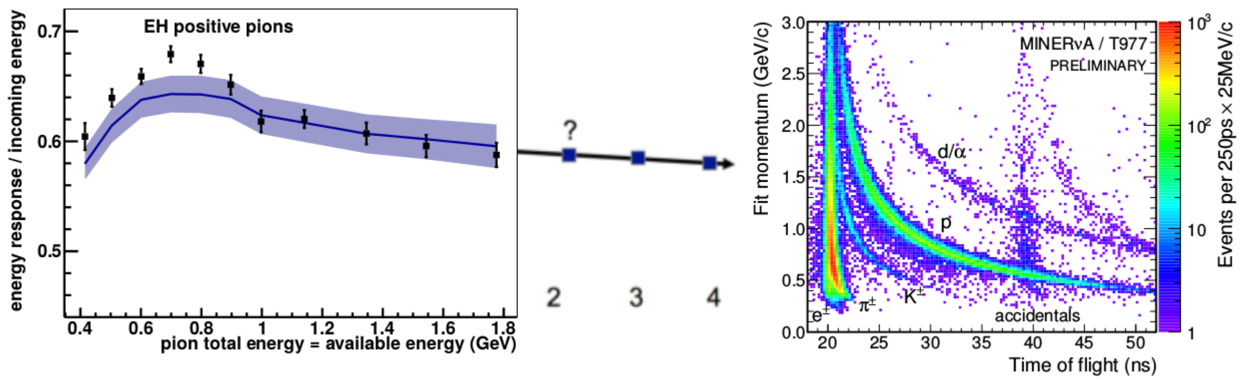


**Figure 1.5:** Test Beam 1 Results. Left: Energy Response of the Detector, the idea is to get results for greater values of energy. Right: The measured momentum (from Wire-Chambers) and time-of-flight used to separate different particle species and backgrounds (2D histogram presented).

For TB-2, as already explained, it is more difficult to perform a particle ID analysis due to the following reasons: At higher energies (greater than 8GeV) the ToF system is not able to separate pions from protons, there is no tertiary beam that can permit us to discriminate particles based on their momentum, a dE/dx analysis is also more difficult and useless to separate pions from protons. Fortunately for the MINERνA experiment at higher energies there is a complete different process (DIS: Deep Inelastic Scattering) that dominates neutrino Interactions and for which is not mandatory to study the passage of hadron particles like pions and protons inside the detector at energies higher than 8GeV. Notwithstanding that, it is still very important to find the composition of the beam at hand because for TB-2 the collaboration knows more about the devices and the detector but less about the beam, and also as a way to find out how well the MC simulation of the secondary beam (still in progress) is being performed.

To be able to do a proper particle-ID analysis of the secondary beam it is necessary to understand how the beam is produced and how all the elements along the beamline affect it, each of these devices gets specific information using scintillators and PMTs (Photomultiplier Tubes, used to convert light into an electric signal) when a charged particle passes through them. The DAQ works in such a way that this information is digitized and stored in a root file called a DST, so it is also mandatory to understand how to analyze those files using ROOT [12](a software for Data Analysis). To sum up, to perform a proper particle-ID analysis it is necessary to have a clear understanding of the devices affecting the beam and to write down scripts in ROOT to isolate particles looking at specific variables (Branches) that are related to a specific physical property of the particle we are trying to isolate. For example, a proton and a pion have a completely different time of flight (for energies $<$ 8GeV) because of their difference in mass and a muon will deposit energy in the detector (via ionization) in a different way than a pion (via hadronic showers).

## 1.3 Devices along the secondary beam of the Test-Beam (TB)

To study the **secondary beam** (composed mainly of pions, though there are also protons, electrons, muons and very few kaons) which enters the Test Beam detector, we need to understand the way it is generated upstream. It is generated from the collision of 120 GeV protons (which composed the **primary beam**) on a target of Aluminium, where a bunch of particles of different energies are produced from the interaction. After that, this initial part of the secondary beam passes through a magnet called MT4W (MT stands for Meson Test) which will make particles of different momentum to travel along a curve with a different radius as shown in Figure 1.6 (the higher the momentum the less the radius) and will also give the beam a given polarity (positive and negative particle will travel along opposite directions).

Just downstream that magnet there is a movable momentum-selector which have an aperture (the remaining is a calorimeter to avoid other particles to pass through) to select particles travelling at a specific trajectory (which means they have a specific momentum, because the magnet already created a correlation between position and momentum). Downstream that momentum selector and along the beamline there is located the ToF-1 (start or UPstream) station, which have a scintillator with PMTs attached to it to record the passage of any charged particle through it. Since the creation of the secondary beam upstream a lot of radiation was produced from the interaction of particles, for that reason there is a second magnet called MT5E which is used to reject neutral particles and radiation (that is why this magnet is called as the sweeper) and ensure in that way that the downstream beam is composed of charge particles of a given momentum and polarity (+ or - sign of their charge).

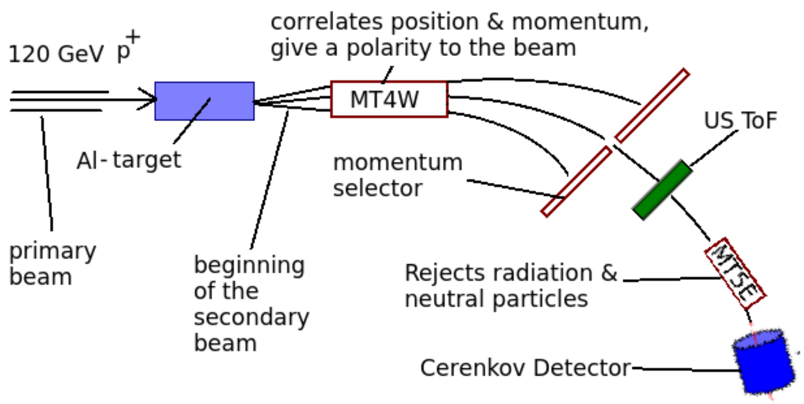


**Figure 1.6:** Elements upstream the secondary beam, produced from the collision of a bunch of 120GeV protons (primary beam) with a target of Al.

After that we encounter some important elements in the downstream part of the secondary beam, these devices are divided as Triggering (Cerenkov, MT6SC$1 \rightarrow 4$), Tracking (MWPC$1 \rightarrow 4$) and Particle-ID devices (Cerenkov, ToF Upstream & Downstream). These elements are extremely important to study the beam, they permit to select specific kinds of particles we want to get at the Detector (located downstream), follow their trajectory, find their momentum, avoid the entrance of more than 1 particle at at time to the detector (this is the role of the Veto) and send a signal (the Trigger) to the DAQ system to inform that it should start taking data. All the way in which data is acquired in each element and the way in which a specific bunch of protons (which are not being sent continuously but with a certain periodicity of $\sim 19ns$ == 1 bucket) is sent by the Acceleration Division (AD) is a very complex process that will not be explained in this thesis. The remaining part of this section just shows a glimpse about what these important elements are and do, special emphasis will be put on the ToF device (Section 1.5) because of its importance in the particle-ID analysis.

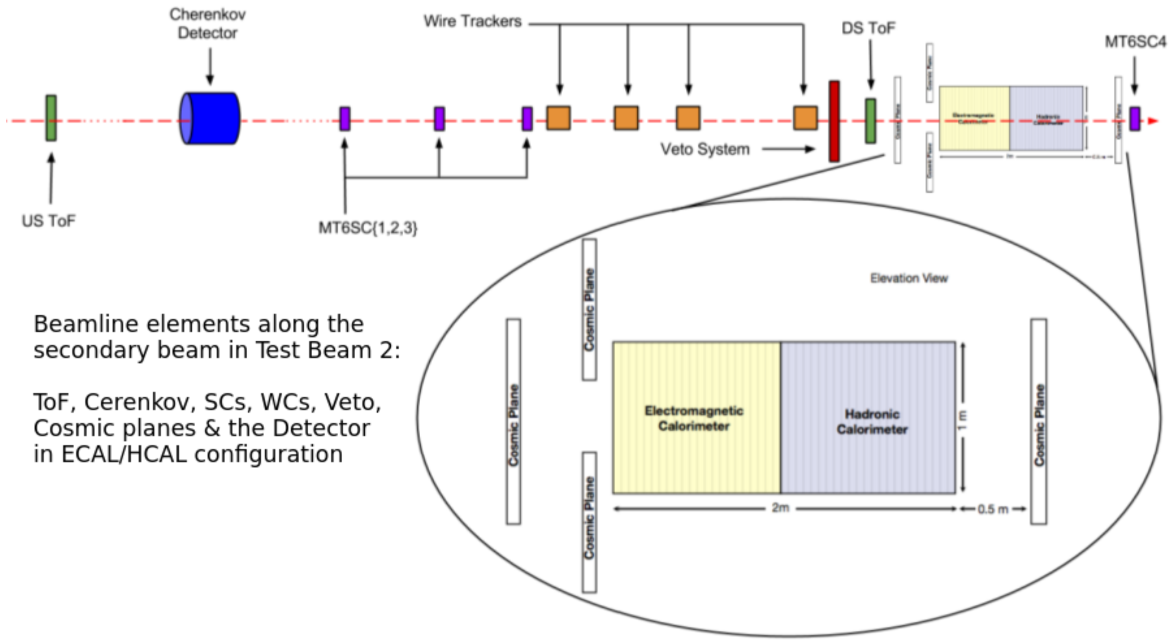


**Figure 1.7:** Important elements downstream the secondary beam. They can be divided as Triggering, Tracking & Particle-ID devices. At the end of the beamline we have the Test Beam Detector (in this case in an ECAL/HCAL configuration). This figure does not show the MT5E magnet.

The Fermilab Test Beam Facility (FTBF) [5] has a number of instrumentation systems to help users with Triggering (send a signal to tell the DAQ to start taking data), Tracking (follow the trajectory of charged particles), and Particle ID (Identify the specific species of particles composing the beam). The cosmic planes are used when the beam is off (out of spill) for calibrations (taking data from cosmic muons that usually pass through the detector). Only some of these elements are being used by the MINERνA collaboration for their Test Beam effort, as shown in the previous 2 figures.

### 1.3.1 Triggering Devices

Among the Triggering devices we have the Cerenkov (MT5&6CC) and 4 scintillator counters (MT6SC1→4), the first is used to select or anti-select electrons (there is also a Lead shield, not in the figures, that is used to reduce as much as possible the amount of electrons when we do not want them in our sample). All 4 scintillator counters are attached to PMTs (Photomultiplier Tubes, which convert light into an electric signal) whose voltages are controlled from RR7 in

MS4 (a location inside the FTBF) and can be read out through ACNET (Accelerator Control NETwork, which is a system of computers that monitors and controls the accelerator complex). All these PMTs only have 1 single channel (as those attached to the Veto and the ToF stations), only PMTs at the detector have 64 channels. These scintillator counters are important in the formation of the TRIGGER (SC1→3 + SPILL, a signal sent by AD) which tells the DAQ to start taking data.

### 1.3.2 Tracking Devices

Among the Tracking devices at the FTBF there are the SWICs (3 in total), The Si-Pixel Telescope and the Multi Wire Proportional Chambers (MWPC1 $\rightarrow$ 4), where only the 4 MWPCs are used in MINER$\nu$A Test Beam 2. They basically detect if a charged particle passes and get the trajectory of that particle. The MWPC tracking system is made up of 4 stations, and an associated DAQ system. Each Station consists of 2-plane(X,Y) wire chamber and the necessary hardware to support it. Each plane has 128 wires, perpendicular spacing between wires is 1 mm. Accurate relative positioning of the planes within a chamber is automatic. The four chambers are read out with LeCroy 3377 CAMAC TDC modules in CAMAC crates. By the way, the CAMAC is composed also by the Veto, the ToF system and the Cerenkov (they used the same Readout Electronics). A didatic explanation about the working mechanism of the MWPCs and the way to study them (using ROOT) can be found in [13].

### 1.3.3 Particle-ID Devices

For particle ID purposes, the FTBF provides the Cerenkov and the Time of Flight (ToF) systems, the first one is based on the Cerenkov effect which takes place whenever a charged particle travels at a speed faster than the speed of light in a medium ($v_{light} = c/n$, $n$ being the index of refraction and $c$ the speed of light in vaccuo). It has been used to select or antiselect electrons, so it is important for taking data without electrons (a Lead shield is also necessary for this purpose, because of the inefficiency of the device) and to do electron/pion separation. The ToF system, on the other hand, takes advantage of the fact that different species with the same momentum have different velocities (because of their difference in mass) so they spend a different time in travelling from one point (Upstream or Start ToF station) to another (Downstream or Stop ToF station), and it is very efficient in separating pions and protons. Details about the ToF system are presented in Section 1.5.

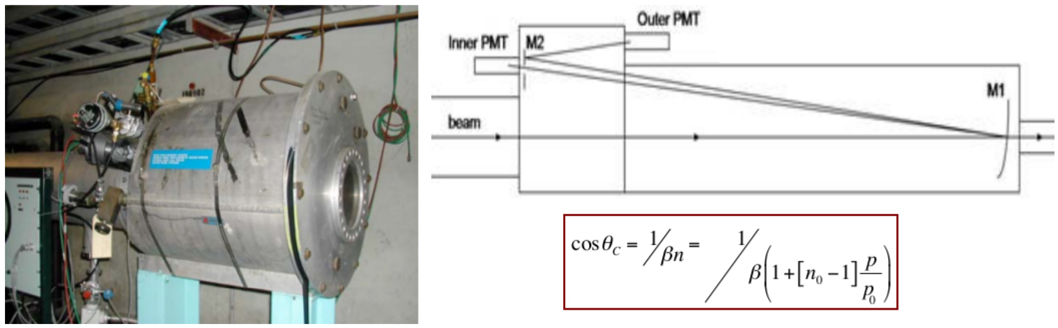


**Figure 1.8:** Left: Cherenkov system, located in MT6.1, is $\geq 98\%$ efficient for electron detection. Right: Differential Cerenkov Counter Optics and the equation that tells the angle (in general momentum dependent) at which the shockwave is emitted with respect to the direction of the particle travelling faster than light in that media.

### 1.3.4 Veto system

The veto system is a set of scintillator paddles that surrounds the central region and looks for particles entering the detector outside of the direct beamline. We want to only have one particle in the detector within a 300 ns window (centered at the time the Trigger signal is sent), because anything smaller than that, we might have trouble resolving. There are 12 Veto paddles, each of them attached to a PMT, that fire (send a signal) whenever a charged particle passes through it. Understanding this variables and knowing the spatial location of the paddles is relevant for an analysis of the spatial distribution of the beam (Section 4.5).

## 1.4 Details of the TB-Detector and the 2 configurations used for the DAQ

In order to understand how the Test Beam detector works we need to review how the MINER$\nu$A (underground) Main Detector works, the way in which the data is acquired and the componentes

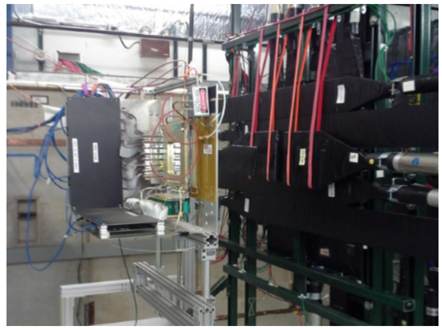

**Figure 1.9:** Veto system (the black paddles are shown) located just downstream (at the right hand side) of one of the MWPCs

inside the detector that make this possible. This because the Test Beam detector is just a miniature version composed of almost the same material elements (scintillators, steel and lead) and acquires information in the same way (from light to charge to digital information). For that reason let us review what materials compose the Tracker, ECAL and HCAL regions of the MINER$\nu$A main detector, understand why they are needed and what other elements are necessary to take data (WLS, PMTs, FEBs). After that it is really easy to understand what are the 42 planes (modules) in the Test Beam detector (relevant for a particle-ID analysis inside the detector, like a dE/dx calculation over modules as an approach to separate muons from pions) and how the 2 different configurations (ECAL/HCAL and Tracker/superHCAL), used for taking the data under analysis, lead to a different pattern in which particles deposit energy inside the detector and consequently to different plots in Arachne (as is explained in Section 3.3).

### 1.4.1 Composition of the Tracker, ECAL & HCAL regions of the MINER$\nu$A main detector

The MINER$\nu$A detector (Figure 1.3) consists of an inner tracker volume made of active plastic scintillator surrounded by electromagnetic and hadronic calorimeters and a set of different passive nuclear targets: helium, carbon, iron, lead and water. The Inner Detector (ID) has a hexagonal shape of apothem 1.07 m and is composed of 120 **modules** divided in four regions: the nuclear target region, **the tracker, the downstream electromagnetic calorimeter (ECAL) and the downstream hadronic calorimeter (HCAL)**. It also includes the side electromagnetic calorimeter.

***Tracker Region:**

Modules in the **Tracker Region** contain three layers of finely segmented scintillator planes as shown in Figure 1.10 to allow three dimensional track reconstruction. Each plane is composed of 127 strips of extruded polystyrene scintillator that are triangular in cross section (17.0 mm height x 33.4 mm base). The triangular shape ensures energy deposition in two strips per plane for most particle paths, improving the position resolution of the reconstruction. A 1.2 mm diameter green wavelength shifting fiber (**WLS**) down the middle of each strip guides the generated light to a **single pixel of a 64 anode PMT**. The way in which light is generated inside the scintillators is the following: When a charged particle passes through a material, it can ionize the atoms it passes, pulling electrons free. When those electrons recombine with an atom, photons are released. They come in many varieties and types: There are gaseous, liquid and solid scintillators. The time to recombine and release light is also different from material to material.

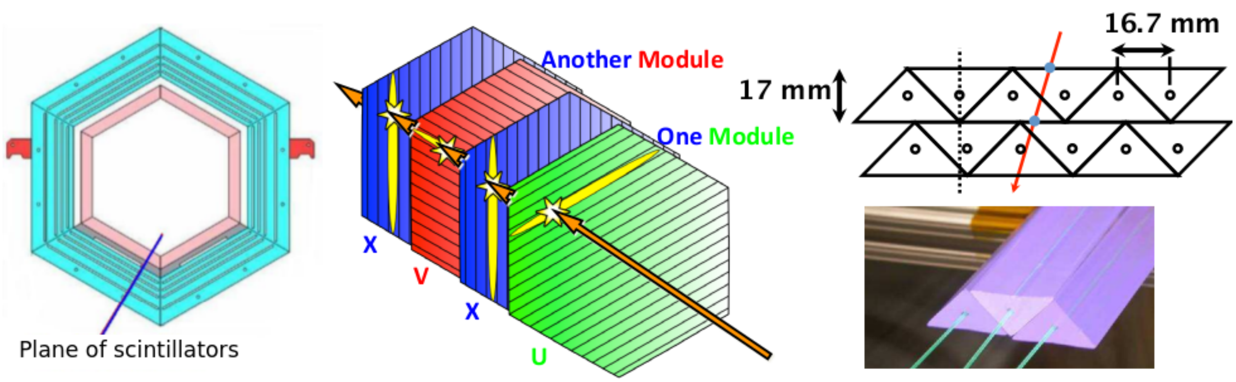


**Figure 1.10:** Left: One active (tracker) module and its three planes: X,U and V. V and U are rotated ±60 degrees with respect to the X. Right: Triangular scintillator strips arranged so charged particles hit more than one strip, giving better position resolution (∼3 mm).

***Downstream Electromagnetic Calorimeter (ECAL):**

High energy photons are detected through the pair-production/bremsstrahlung process that lead to a shower of $e^{\pm}$ and $\gamma$. The photons energy regime in the detector is of the order of a few GeV, so 99% of the energy is expected to be contained within 4 cm of Pb, which is about 7 radiation lengths (the **Radiaton Length** $X_0$ is an important physical concept to be discussed in Section 3.2). The downstream electromagnetic calorimeter consists of 20 layers of Pb, each 2 mm thick, interleaved with one layer of scintillator, consisting of the standard 1.7 cm thick layer of triangular strips, which gives an energy resolution of approximately $6\%/\sqrt{E}$ , with $E$ in GeV. The idea is to contain almost completely the EM energy deposited. The side ECAL is not covered in this work.

***Downstream Hadronic Calorimeter (HCAL):**

The downstream hadron calorimetry consists of 20 layers of iron, each 2.54 cm thick, interleaved with one layer of scintillator between plates, downstream of the electromagnetic calorimeter. The combined thickness of the 4 cm of Pb and 50 cm of Fe stop muons up to about 600 MeV and protons up to about 800 MeV. One **nuclear interaction length** (The nuclear interaction length $\lambda_I$ is an important physical concept discussed in Section 3.2) is 16 cm for Fe, so higher energy protons (or pions) will also generally be stopped. With this HCAL all hadron showers are contained so information about their presence inside the detector is not lost.

### 1.4.2 Elements necessary to take Data (Electronics Structure)

The light acquired from abouth 30.000 scintillators in the MINER$\nu$A detector has to be converted to electric pulses with an amplitude proportional to the deposited energy and the time. In order to accomplish this objetive, the MINER$\nu$A experiment uses multi-anode photomultiplier tubes (PMTs) R7600U-00-M64, each with 64 pixels or channels, provided by Hamamatsu Photonics [14]. Each XU/XV module employs 19 PMT that are the MINER$\nu$A fundamental detection instrument. There are 500 PMTs totalling about 32.000 channels. Each PMT is covered by a cilindrical box of steel called “PMT Box”, in order to isolate the PMTs from backgrounds of light or electromagnetic fields.

The input signal for each PMT is acquired from the scintillator strips through wavelength shifting fibers (WLS) that are installed at the center of each triangular scintillator strip (see Figure 1.10). The WLS fibers collect the blue scintillation light from the scintillating fibers and shift it to green, that is reflected internally in the fiber reducing the loss of signal significantly. This signal input is amplified and read out using MINER$\nu$A’s front end boards or FEBs to be later translated to physical quantities.

The MINER$\nu$A electronic requirements are motivated by the following objetives: 1)Fine-grained spatial resolution, exploiting light-sharing between neighboring scintillator strips. 2)Identification of $\pi^{\pm}$ , $K^{\pm}$ and $p$, using $dE/dx$ information. 3)Efficient pattern-recognition, using timing to identify track direction and separate interactions occurring during a single spill. 4)Ability to identify strange particles, and muon decay, using delayed coincidence. 5)Negligible deadtime within a spill.

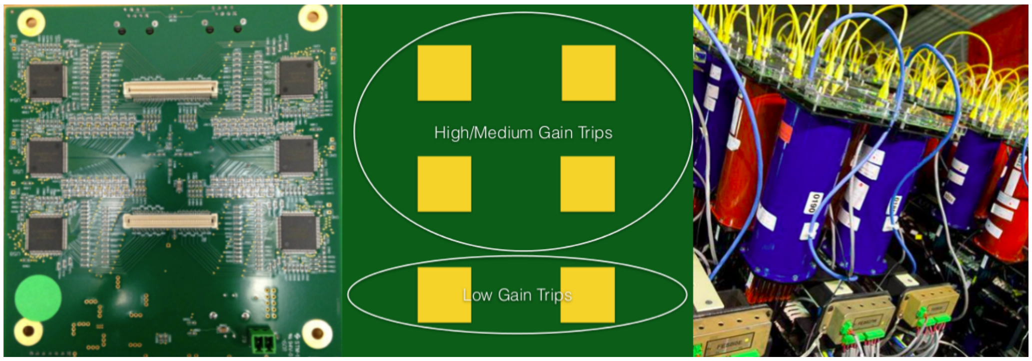


**Figure 1.11:** Each Front End Board (FEB) has four subsections that look at one type of charge, and two that carry another type of charge called Trip Chips (each chip has 16 channels). Right: PMT boxes attached to the Detector, on each PMT there is an FEB attached which provides the voltage and stores charge to be digitized.

The Front End Boards (FEBs) are in charge of: providing high voltage to the photomultiplier tubes (PMTs) via the Cockroft-Walton generator [15] and reading out the PMT anode charge. The standard operating mode of the readout system is to open a collection readout window (gate) on the FEBs synchronously with the delivery of neutrino beam spills of 16 $\mu s$ each. This gate is opened $0.5 \mu s$ before and ends $5.5 \mu s$ after the beam spill (see Figure 1.12, Left).

Each readout system channel has a discriminator threshold, so when the charge crosses this threshold, the TriP-Ts integrates the charge and stores it along with the hit time information (this happens 150 ns after the discriminator is fired). After this, there is a 20 ns time lapse in which the channels cannot be readout (**Dead Time**). This allows up to 5 readouts per gate.

All FEBs are daisy-chained together in groups of nine or ten and connected to a custom VME module called Chain Readout Controller (CROC) that serves up to four of these chains. CROCs receive timing information from another VME custom module called CROC Interface Module (CRIM), that collects timing information from the NuMI and from MINOS. The second information is used for matching events between MINER$\nu$A and MINOS detectors, since MINER$\nu$A

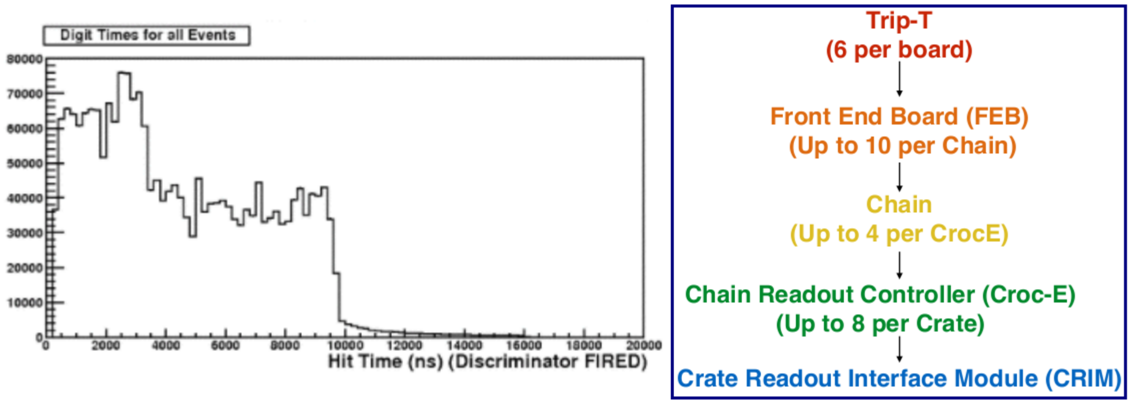


**Figure 1.12:** Left: Accelerator Division sends us a signal, telling us that they are going to send protons to the target, then we wait a specified amount of time ($0.5\mu s$) and then we "open our eyes" $16 + 5.5\mu s$ to watch for the neutrinos. Right: Structure of the Electronics, controlled through the trigger in the Master Timing Module, there is 1 CRIM for the Test Beam and 2 for the MINER$\nu$A detector underground.

uses the MINOS Near Detector as a muon spectrometer. MINER$\nu$A has two VME crates each housing a CAEN V2718 Crate Controller, two CRIMs and eight CROCs. These crates are accessed through a CAEN A2818 PCI Card that interact with the V2718 Crate Controller.

### 1.4.3 Test Beam detector configurations

As it was said previously, Test Beams are used in neutrino experiments to make sure we understand our detector's response to the charged particles that are produced in neutrino interactions. Most neutrino experiments do some sort of "Test Beam" measurement at some point in the course of their lifetimes [16]. TB-1 looked at Pions, protons, electrons from ∼400 MeV to ∼2 GeV (Positive and negative polarity) and TB-2 has been looking at Pions, protons, electrons from ∼2 Gev to 8 GeV (Positive and negative polarity). The TB detector only has 42 planes of scintillators and is reconfigurable, which means that we can slide Lead or Steel in front of scintillator planes as we wish. We put particles of known Type and Energy into this smaller detector and measure its response. The planes for this detector are squared and have 63 nested, triangle-shaped scintillator strips each with length 107 cm and thickness 1.7 cm. It shares the same 3-view UXVX sequence of planes as the main detector but unlike that one, this has removable absorber planes that allow to take exposures in 2 configurations [4].

One configuration (**ECAL/HCAL**) has 20+1/2 planes with 1.99 mm thick lead absorber (ECAL) followed by 21 planes with 26.0 mm thick iron absorber (HCAL). The absorber is interleaved by placing one absorber upstream of each scintillator plane, note that this configuration is equivalent to the last dowsntream part of the main detector (ECAL/HCAL downstream calorimeters). The other configuration known as (**Tracker/superHCAL**) has 20 planes of Scintillator, 4 planes of Steel/Scintillator, 11 planes of Double Steel/Scintillator and 6 planes of Steel/Scintillator. **Data Run 1** refers to the data taken between 6-21 April in ECAL/HCAL configuration and **Data Run 2** refers to the data we taken between 23-30 April in Tracker/superHCAL configuration [17], the main goal of Data Run 2 was to study both electrons and high-energy ($\geq 4GeV$) pion shower shape, Test Beam experts wanted to look at initial shower development (which is the part of current electron ID that seemed suspicious) and look at the back leakage for very high energy pions ($\geq 10GeV$), as there seemed to be large Data/MC disagreements.

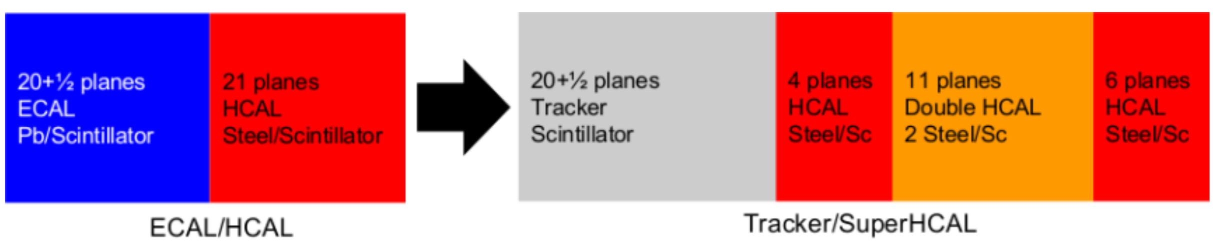


**Figure 1.13:** Left: ECAL/HCAL configuration used for taking Data Run 1. Right: Tracker/superHCAL configuration used for taking Data Run 2.

These Data Sets are extremely important for the particle ID analysis presented in Chapters 4, 5 & 6. It is also worthy to mention that this Data was initially separated in 3 different Files: MWPC data was stored in a txt File, CAMAC data (containing ToF, Veto and Cerenkov information) was in another txt File and TB-Detector data in a DST (ROOT File) so they needed to be merged into what we called the **merged-DSTs** [18] located in Folders labeled with the Energy of particles, the Type of particles (a beam mainly composed of electrons or pions, the Cerenkov and Lead shield used for this separation) and the Polarity of the beam (positive or negative particles, the upstream magnets used for this separation).

The readout chain from scintillator to wavelength-shifting (WLS) fiber to photomultiplier tube (PMT) to digitization is almost identical between the Test Beam and the MINERvA detectors, some of the slight differences for Test Beam 1 (that remain valid for TB 2) are outlined in [4].

The fact is that the MINER$\nu$A collaboration currently knows more about the Detector and the DAQ for TB 2 (than for TB 1) but less about the beam, and that is why a study of its structure becomes valuable. Referring to the concept of a **module**, it is important to say that for the main detector each module consits of 2 planes of scintillators but for the Test Beam of only 1 plane, where different modules in the TB detector are located in regions where different materials are placed between scintillators (see Figure 1.13) so in order to calculate the energy deposited (using a function called **ModuleMultipler**, as explained in Chapter 4) in a given plane, one has to multiply the number of photoelectrons (PE) by a number which depends on the specific plane inside the Detector (& take into account passive material present there).

## 1.5 Details of the Time-of-Flight (ToF) device

This section is dedicated to a review of the ToF system, what elements compose it at the FTBF, how this device takes Data, how one can expect to get different peaks related to energy deposited (hits) by different species in the histogram of the **Measured Time** variable containg peaks at different times (hits at specific times) and also some initial results from its usage are presented. These initial results, that can be found in the ToF Technical note [19], were obtained from Data taken in February 2015 and are important because we can compare them with results using modern Data, which corresponds to Data Run 1 and 2 (taken during the month of April of 2015, as explained in Section 1.4.3). It is also relevant to say that the energy of the beam and its corresponding uncertainty can be calculated with the aid of this device, although there is a fixed relative error in the energy of the beam of $\sim 3\%$ set by the Accelerator Division (AD).

As part of its 2014-2015 TestBeam effort, the MINER$\nu$A collaboration needed to determine the response of its detector to different hadrons of different energies to the level of a few percent. The beam, particularly at lower energies like 1GeV, will have some non-negligible $p/\pi$ ratio. There is not a good way to distinguish the species of hadron from shower shape or other detector variables in MINER$\nu$A, but different hadrons will, as a result of having different cross-sections for different processes, produce different detector responses.

Consequently, a time of flight system, consisting of a START (or UPstream) station in MT3-4 (locations at the FTBF) located at the old MT5SC location, a STOP station in MT6.2 and readout via NIM/CAMAC electronics was installed in MTest. This information will also be used in validation of a MARS / TURTLE simulation of the beamline (which is a still in progress Monte Carlo simulation of the secondary beam) that will be of great value in predicting the properties of the beam under a variety of usage scenarios.

The **START station** (Figure 1.14, Left) was constructed for an earlier edition of a Time-of-Flight facility for the MTest beamline, and was rebuilt for this rendition. This station contains 4 fast PMT tubes all looking at a single 5mm thick piece of polyvinyltolune based scintillator (Bicron 400). The scintillator is approximately an octagon of 10cm side-to-opposing-side. It is located just upstream of the vertical bend magnet MT5VT1, and is supported with Unistrut that is bolted to the floor, to ease removal and replacement. The PMTs are 2 inch diameter "fast"(1.3ns with a jitter of about 0.3ns) Ampex model PM2106 PMTs. A fast PMT is one which has a small value of rise-time.

The **STOP station** (Figure 1.14, Right) was constructed for the MINERvA testbeam. It is located just in front of the MINERvA testbeam structure, but will be relocated when the system is re-purposed for other users. This station contains 2 not-so-fast PMT tubes (a higher value of rise-time), both looking at a single 25.4mm thick piece of polyvinyltolune based scintillator (Bicron 404). The scintillator is a 130 x 130mm square, in order to completely cover the span of the "Fenker" MWPC trackers that are commonly used. The PMTs are Thorn- EMI (Now ET Enterprises) model 9954 units; also 2 inch diameters. Their rise time is 3.0ns, with a jitter of about 0.4ns.

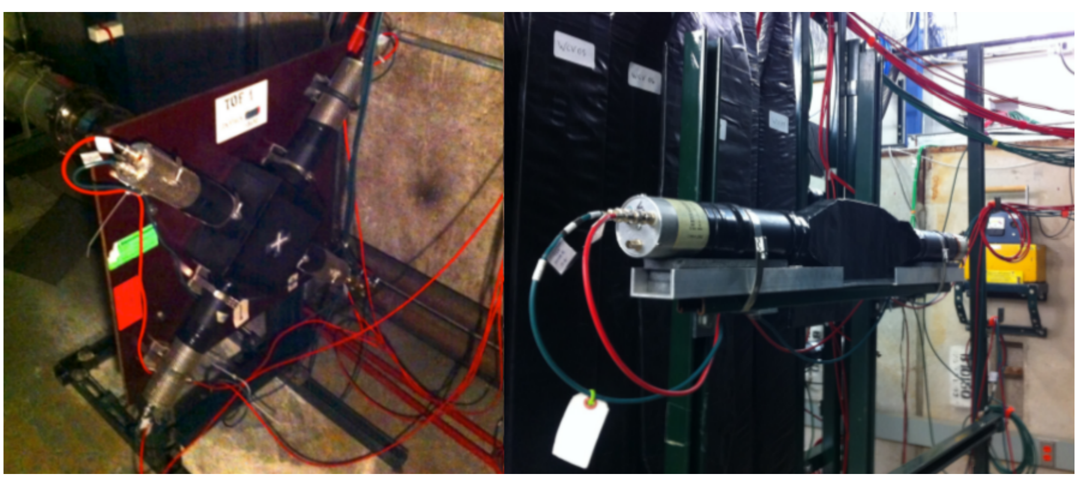

**Figure 1.14:** Left: The installed START station in MT3-4 (4 PMTs looking at a single scintillator). Right: The STOP station, installed in MT6.2 (2 PMTs looking at a single scintillator).

The rise time of the PMTs is useful for setting the delay of the Constant Fraction Discriminators (CFDs); the measurement desired for that use is the time from when the pulse reaches 20% of its maximum amplitude to the time when it reaches 100% of its maximum amplitude. The 100% point is difficult to find easily with a scope, but the 20% - 80% rise time can be found almost automatically. The average reading on 50 samples was 1.57ns on the START station PMTs (with a scatter of 0.26ns) and 2.81ns (with scatter 0.33ns) on the STOP station PMTs. The specification rise time of the scope is 0.7ns. Scaling the numbers by (100-20%)/(80-20%) and subtracting 0.7ns from the rise time (but not the scatter) gives the values listed above.

In the START station, PMTs are numbered 1-4 in a counter clockwise direction starting from the 2nd quadrant as one faces the device in the beamwise (i.e. from upstream to downstream) direction. In the STOP station the PMTs are labeled L and R (left and right) based again on their position as seen in the beamwise direction.

In this thesis there is no information about the HV settings, discriminator thresholds, cabling, Constant Fraction Discriminators (CFDs), delays and TDC (Time to Digital Converter) which are important for the electronics and DAQ of the ToF system but irrelevant for an analysis on particle-ID, for more information about those topics look at [19]. However, it is important to present some of the initial results obtained with old data in order to get the physics behind this system and to compare them with results using modern data (Data Run 1 & 2).

Considering that ALL particles in the beam have the same momentum (selected upstream using the momentum selector) and that the distance between the 2 ToF stations is known, we can calculate the time spent by each kind of particle in travelling from ToF-Start to ToF-Stop stations and the time difference between particles of different mass, like protons, pions, kaons and so on. Each time a particle passes through both stations a point in recorded (due to signals sent from the 6 PMTs) in a histogram of the measured time, as is presented below, where we expect a time different between hits coming from particles of different masses. For the analysis of Chapters 4 & 5 a point is attached to such a histogram each time the 6 PMTs sent a signal (within a time window specified by the Electronics of the system that also takes into the account the Trigger signal).

Figure 1.15 presents the relativistic equations for calculating the time spent by a particle in travelling between the 2 ToF stations, what is important is the time difference between particles (we can fix a zero of time arbitrarily) although the exact time spent by protons can be calculated sending a single bunch of protons (primary beam) and measure the total time spent. For particle ID purposes it is only imporant to measure a difference in time to make a cut and in that way separate the protons present in the sample from the other particles (pions and muons have almost the same mass and are found inside a single peak, electrons can be rejected using the Lead Shield and the Cerenkov). Regarding the masses of particles in the secondary beam we expect to see first hits from electrons, then from muons, pions, kaons and protons (the greater the mass the greater the time difference).

$$\boxed{p = \gamma m v} \qquad \boxed{v = c\sqrt{\frac{p^2}{p^2 + (mc)^2}}}$$

$$\boxed{\gamma = \frac{1}{\sqrt{1 - (v/c)^2}}} \quad \Longrightarrow \quad \boxed{t = \frac{distance}{v}}$$

$$\boxed{\Delta t = t_p - t_\pi = \frac{distance}{pc}\left[\,\sqrt{p^2 + (m_p c)^2} - \sqrt{p^2 + (m_\pi c)^2}\,\right]}$$

**Figure 1.15:** Relativistic equations to calculate the time spent by a particle travelling between both ToF Stations and time difference between 2 different kinds of particle species.

Figure 1.16 shows the distribution of $(PMT1 + PMT2 + PMT3 + PMT4)/4 - (PMTL + PMTR)/2$ (which account for the measured time) in 2GeV "pion" beam (electrons rejected using a Lead shield and the Cerenkov), taken in early February 2015. Corrections for channel-to-channel offsets due to cable length and TDC offsets were determined from 120GeV beam and applied to each of the 6 channels before constructing the plot; events where any of the 6 readings are absent are not included (so we considered ToF events of quality one, as explained in Chapters 4 & 5).

Because of scattering in MT6, and because the ToF device is fairly far downstream, loss of particles before reaching the STOP counters is considerable. Only 48% of the triggered events have hits in STOP under these conditions; that fraction can be raised to 67% by introducing the FTBF provided He filled tubes to reduce scattering.

In Figure 1.16, vertical bars are drawn to show where we would expect to see $\pi, \mu, K$ and $p$ to appear, assuming a distance between the stations of 88.122 m and exactly 2 GeV/c of beam momentum. Evidently, either the energy was lower or the beamline was longer! As was expected from earlier experiments, the beam is mostly electrons, pions and a few protons. The proton fraction is about $9.00 \times 10^{-3}$ , but much work needs to be done to really understand the beam composition (that is why a particle-ID analysis is important).

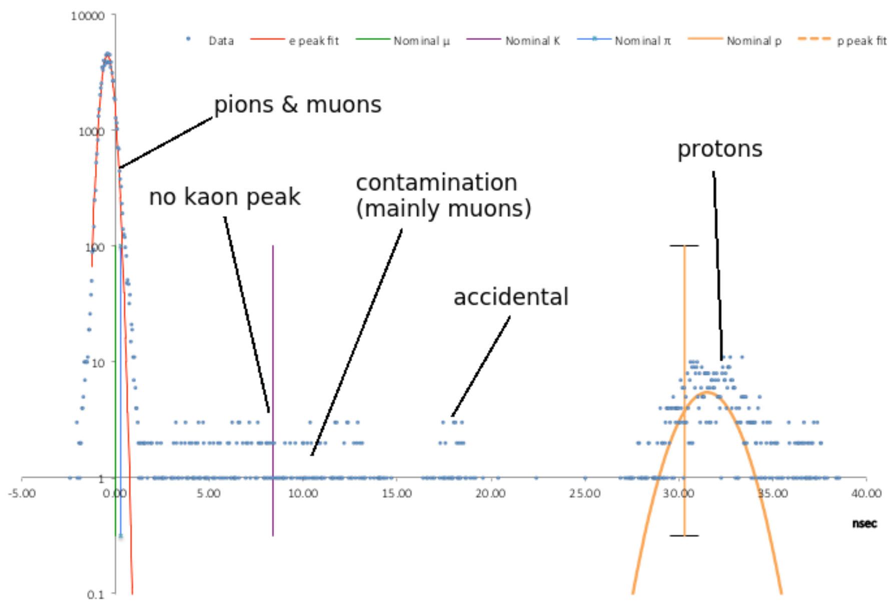


**Figure 1.16:** Initial results with 2 GeV "pion" beam.

The horizontal error bar for the expected proton position shows the spread that would be created as a result of a 2.7% full span variation in beam energy; that is the nominal energy spread for this beamline. There is also evidently some level of either intermediate speed particles (contamination), or very off-momentum halo particles, possibly a result of decays in flight. We can see that there is no kaon peak, which would imply that almost all kaons produced upstream already decayed; however there is certainly certain amount of contamination at the right of the pion peak (composed maily by muons as will be seen in Chapter 4) that ends at 15 ns. There is also an accidental peak maybe due to particles from the second bucket, although we did not know a priori their identity (scanning how those events look at the detector may say something about their identity).

Figure 1.17 is the same distribution in 4GeV "pion" beam, we notice that the proton and pion peaks are closer, they actually merge at energies higher than 8GeV and in the ultrarelativistic limit the difference between the peaks is as small as the resolution of the device ($\sim$ 200 ps), we also see a larger proton fraction, of about $26 \times 10^{-3}$, as expected (these protons may come from the Al target or from energetic protons from the primary beam that did not have enough time to interact).

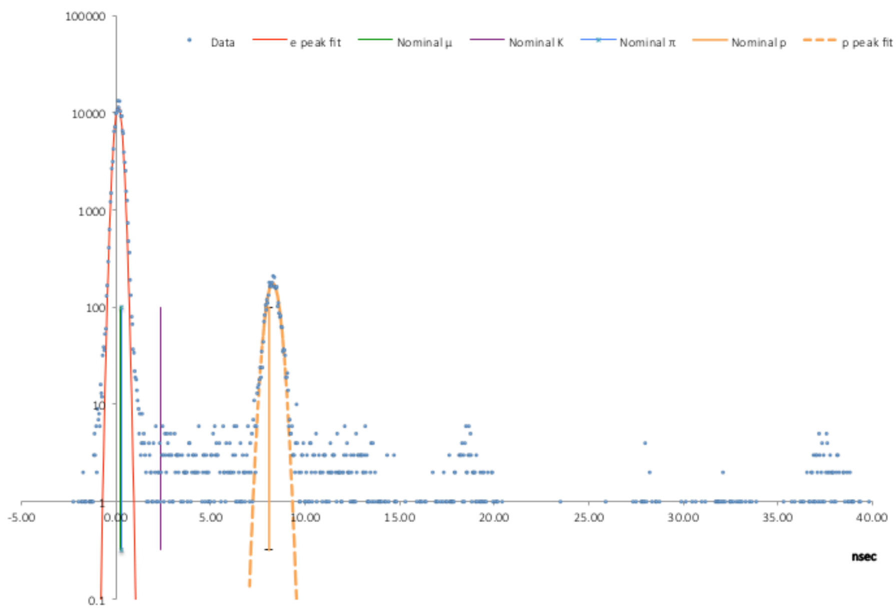


**Figure 1.17:** Initial results with 4 GeV "pion"beam.

The width of the electron peaks in these plots is $\sigma = 288ps$ in the 2 GeV data and $190ps$ in the 4GeV data. The widths of the proton peaks are $1398ps$ and $325ps$, respectively. However, the fits shown here are really only based on events in the centers of the peaks; there are substantial tails not yet included in the fit. If we assume a $500ps$ width in the electron peak (to allow that there will be a tail from relatively indistinguishable pions) and a $300ps$ width in the proton peak, then there should be $3\sigma$ of electron-proton separation up to 8.5GeV.

It is also possible to calculate the beam momentum and its uncertainty using this ToF device, considering that there is a relation between the time difference and the momentum of the beam (see the equations in Figure 1.15), if we find the uncertainty in the time difference between pions and protons then we can find the uncertainty of the beam momentum (energy). It can be shown that the uncertainty increases as the beam energy increases, the way in which this calculation is performed can be found in [19], there are some results validating this assuming an accuracy in ToF of $\sim 100ps$ (taken as the resolution of the ToF system).

## 1.6 Working as a Detector Expert

For the MINER$\nu$A experiment it is extremely important to assure that good quality data is being taken 24 hours a day, for this reason there is always a shifter at the ROC (Remote Operations Center) West located at the Fermilab Wilson Hall who is in charge of checking that data is properly taken looking at monitors which indicate different issues related to the data acquisition (DAQ): the status of the beam, the current Run and subrun being processed, the status of different hardware components of the detector and also the status of the MINOS near detector (which is used by MINER$\nu$A as a muon spectrometer).

Every 12 hours 2 types of calibration data are taken: Light Injections and Pedestals. The idea behind light injections is to put a known amount of light into the PMT and measure the charge output of the PMT, this allows us to calculate the "gain" of the PMT and to see if there is any dead channel (more than one in a given region will indicate a problem) which permits to detect a problem in an FEB or PMT. The idea behind pedestals is that when there are no particles passing through the detector, we take a gate's worth of data just to see what the background levels are, we subtract off the average value for each channel from the data in order to "suppress the pedestal ".

In order to solve any specific problem related to the DAQ, which may be a software or hardware issue, there is a Detector Expert available for a week which is responsible to solve any problem the shifter cannot solve. To become a Detector Expert there is a training provided by the MINER$\nu$A Run Coordinator (Dr. Howard Budd) in which we have to test PMTs at Lab-G (a specific location inside Fermilab), there we take some Pedestals and Light Injections using PMTs that present specific (already known) problems, familiarize ourselves with the way in which hardware components in the main detector and in the Test Beam are located and how a DST (root file) is made up and read (to check any problem like a light leak by looking at specific histograms). All the procedure to test PMTs at Lab-G can be found in [20], the procedure for replacing FEBs in [21] and the way in which the MINER$\nu$A detector is turn ON and OFF in

[22]. All this implies working with both the Run Control and Slow Control Interfaces and to follow a specific procedure for each case as is indicated in the cited references. When the problem cannot be fixed remotely it may be necessary to go underground to make a replacement of an FEB. The philosophy behind being a Detector Expert is to be able to have the DAQ working properly, the most important part related to this can be found in [22].

# Chapter 2

# Neutrino Physics & Interactions

This Chapter summarizes the basic concepts we must know in the field of neutrino physics, these include their history and the way different flavors were discovered through many different experiments, how it was found that this "ghostly" particle can change its flavor (oscillate) & in that way have a non-zero mass. The study of neutrinos is important because it may provide also information about the imbalance in the ratio of matter/antimatter in our Universe. It is very important to study its interaction channels in detail because they provide information about their identity and this is important in the study of Neutrino Oscillations. These interactions take place in the MINER$\nu$A detector located underground (at Fermilab) & the way each interaction is studied is via the reconstruction of specific events based on the specific pattern of energy deposited inside the detector by particles present in the final state.

Even though I have worked analyzing Data coming from the Medium Energy ($\sim 1.5 - 8GeV$) MINER$\nu$A Test Beam detector & beamline elements and not from the MINER$\nu$A main detector (located underground), it is extremely important to understand the neutrino interactions taking place inside the MINER$\nu$A main detector because particles present in the final state are the Events we analyze in the Test Beam, where each Event corresponds to each of these final state particles, which are mainly electrons, pions, protons and muons. The Identification of these particles is extremely important for the reconstruction of the specific neutrino interaction and the calculation of its cross-section (probability of taking place). It is also vital to point out that by studying neutrino interactions we can undestand better why at different interaction energies different processes dominate over others, a feature which permits us to justify the need for this second Test Beam (taking data at medium energies) experiment notwithstanding the fact that a previous Low-Energy Test Beam experiment was already studied (The Energy Range of the interaction has a great effect in the expected cross sections for each process). The same information provided here can be found in [9], where more details on the Muon Charged Current Quasi-Elastic channel are presented.

## 2.1 History & General overview of Neutrinos

Experiments in 1911 by Otto Hahn and Lise Meitner [23], and by James Chadwick in 1914 [24] suggested that the beta decay spectrum was continuous rather than discrete. In 1927, Ellis and Wooster confirmed this result [25]. That is, electrons were ejected from the atom with a range of energies, rather than the discrete amounts of energies that were observed in gamma and alpha decays. This was a problem for nuclear physics at the time, because it indicated that energy was not conserved in the beta decays.

On 4th December 1930, the Austrian physicist Wolfgan Ernst Pauli proposed the neutrinos existence, in his famous letter to the "Dear Radioactive Ladies and Gentlemen" who had gathered in a Physics conference in T$\ddot{u}$bingen (Germany), in order to explain the apparent contradiction to the law of conservation of energy produced in beta decays. This particle should have a neutral electric charge and be extremely light, reason for which in 1933, Enrico Fermi proposed the name of *neutrino* to this particle, which is the italian equivalent of "little neutral one". Fermi developed a beta decay theory (the first theoretical model ever known for weak interactions), in which the neutrino played an important role.

Frederick Reines and Clyde Cowan reported the first neutrino evidence in 1956, using a fission reactor as (anti)neutrinos source. The anti-neutrinos interacted with the protons inside a target made of water mixed with cadmium chloride, originating a positron ($e^+$) and a neutron. This reaction is actually the inverse beta decay[1]:

$$\overline{\nu}_e + p \longrightarrow n + e^+ \tag{2.1}$$

In 1957, the Italian physicist Bruno Pontecorvo formulates a theory of neutrino oscillations,

[1]The positron interacts via $e^- - e^+$ annihilation producing two photons. The neutron decelerates before being eventually captured by a cadmium nucleus, originating a photon emission about 15 $\mu s$ after the $e^+$. These photons are detected and the 15 $\mu s$ of difference identify the neutrino interaction

showing that neutrino-antineutrino transitions may occur, if different flavors of neutrinos exist [26]. Although such matter-antimatter oscillation has not been observed, this idea formed the foundation for the quantitative theory of neutrino flavor oscillation, which was first developed by Maki, Nakagawa, and Sakata in 1962 [27] and further elaborated by Pontecorvo in 1967 [28].

The muon-neutrino ($\nu_\mu$) was discovered in 1962 by a group of scientist of Brookhaven Laboratory and Columbia University, using a proton beam at the Brookhaven's Alternating Gradient Synchrotron [29] in order to produce a shower of pions that traveled about 21 meters through a 5 tons wall of steel. In the process, they decayed into muons and neutrinos, but only the neutrinos went through the whole wall, reaching a spark chamber detector. There, the neutrino interaction with the aluminium plates produced a trace of muons that were detected and photographed, demonstrating the muon neutrino existence ($\nu_\mu$). Leon Lederman, Melvin Schwartz and Jack Steinberger won the Nobel prize for this discovery (see Figure 2.1).

**Figure 2.1:** Leon Lederman, Melvin Schwartz and Jack Steinberger, Nobel prize winners for the discovery of the muon neutrino.

In 1973, a group at CERN [30], used a buble chamber (Gargamelle) with a muon neutrino beam produced by the CERN Proton Synchrotron in the search of weak neutral currents. This led to the experimental observation of the weak neutral currents that was announced in July 1973, shortly after their theoretical prediction by Sheldon Glashow, Abdus Salam and Steven Weinberg.

Two years later, the $\tau$ lepton is discovered by a group led by the physicist Martin Perl at SLAC (Stanford Linear Accelerator Center), which later led to the evidence of a third neutrino flavor, the tau neutrino $\nu_\tau$ [31] which was discovered in 2000 in the DONUT [32] experiment at FERMILAB.

### 2.1.1 Neutrino Flavors

The number of neutrinos participating in the electroweak interaction can be determined by the $Z^0$ decay width. It was confirmed at LEP (CERN) [33] [34] [35] [36] long before the observation of the $\nu_\tau$ , that there are only three light neutrinos.

LSND (Liquid Scintillator Neutrino Detector[2]) claimed in 1995 that three neutrinos were not enough to explain their results and introduced a sterile neutrino [37]. This sterile neutrino does not undergo weak interactions nor interacts in any other way but gravity. However, MiniBooNE results from late March 2007 showed no evidence of muon neutrino to electron neutrino oscillations in the LSND region, refuting a simple 2-neutrino oscillation interpretation of the LSND results. More advanced analyses of their data are currently being undertaken by the MiniBooNE collaboration [38].

### 2.1.2 Helicity

An experiment carried out by C.S Wu [39] in 1957 determined that the weak interaction maximally violates parity conservation. Applying this result to massless neutrinos leads to the condition that neutrinos must be fully polarised with a helicity of $+1$ or $-1$. In 1958, an experiment by Goldhaber [40] measured the helicity of the neutrino and determined that only left-handed neutrinos (spin anti-parallel to neutrino direction) and right-handed antineutrinos (spin parallel to anti-neutrino direction) participate in the weak interaction.

### 2.1.3 Solar Neutrinos

The Sun is a powerful source of electron neutrinos with energies of about 1 MeV, produced in thermonuclear fusion reactions in the core of the Sun [41]. Since neutrino interactions with

[2]Scintillation counter at Los Alamos National Laboratory that measured the number of neutrinos being produced by an accelerator neutrino source.

matter are extremely weak, most of the neutrinos pass through the Sun and go to space.

The flux of solar neutrinos that get to the Earth is enormous but its detection is quite difficult and require big detectors due to the low cross section rates neutrinos have. These detectors are installed underground in order to protect them from cosmic rays.

The pioneering experiment in this field was performed deep in the Homestake Gold Mine in South Dakota starting in the early 1970s [42]. A large tank was filled with 100 000 gallons of $C_2Cl_4$ , an ordinary cleaning fluid. Electron neutrinos reacted with the chlorine in the solution to produce Argon-37. The tank was periodically purged with Helium gas and any Argon atoms were captured in a charcoal trap, that then decayed producing electrons and detected. The number of electrons were proportional to the electron neutrino flux at the mine. But the average neutrino flux measured was only 28% of the flux predicted by the standard solar model[43].

In the 1990s, different experiments, SAGE [44], GALLEX [45], Kamiokande, Super-KamioKande [46], also measured solar neutrino rates with the similar results. SAGE measurements were only 51% of the flux predicted by the standard solar model, GALLEX 53%, KamioKande 42% and Super-K 37%.

The discrepancies related to the solar neutrinos remained until the SNO experiment (Sudbury Neutrino Observatory [47]) contributed significantly into the topic. The detector consisted of 1 000 tonnes of heavy water ($D_2O$) enclosed in a transparent plastic vessel measuring 12 meters across. The vessel was itself enclosed in 7 000 tonnes of pure normal water, lodged in an immense 22 meters wide and 34 meters high cavity. The acrylic vessel was surrounded by a geodesic dome equipped with 9 600 detectors that sensed the presence of neutrinos. The frequency of neutrino detection was one per hour. Unlike previous experiments, SNO was able to detect the three flavors of neutrinos. Electron neutrinos $\nu_e$ are produced at the core of the Sun, but during their travel to Earth, they could oscillate into $\nu_\mu$ and $\nu_\tau$ , explaining these discrepancies.

### 2.1.4 Atmospheric Neutrinos

Another source of neutrinos is the upper atmosphere. Primary cosmic rays consisting mainly of high energy protons and electrons bombard the earth's atmosphere continuously from all directions. The protons interact with nuclei in the superior atmosphere producing mainly pions that decay as [48]:

$$\pi^+ \to \mu^+ + \nu_\mu \,, \quad \pi^- \to \mu^- + \overline{\nu}_\mu \tag{2.2}$$

Muons decay into electrons and electron neutrinos through the following process:

$$\mu^+ \to e^+ + \nu_e + \overline{\nu}_\mu \,, \quad \mu^- \to e^- + \overline{\nu}_e + \nu_\mu \tag{2.3}$$

Many experiments measured the ratio of muon to electron events. A double ratio $R$ was also conventionally calculated, which is the ratio of the $\mu/e$ ratio measured by experiment to the $\mu/e$ ratio predicted by Monte Carlo simulations, and is expected to be 1 if the data is correctly described by the Monte Carlo. Figure 2.2 shows the double ratio $R$ for different experiments: Kamiokande Sub-GeV, Super-Kamiokande Sub-GeV (where Sub-GeV means the visible energy measured is less than 1 330 MeV), Kamiokande Multi-GeV, Super-Kamiokande Multi-GeV (where Multi-GeV means the visible energy $E_{vis} > 1\,330 MeV$) [49], IMB (Sub-GeV and Multi-GeV) [50], Soudan 2 [51], Fréjus [52], NUSEX [53], where only NUSEX and Fréjus did not see a significant deviation from the unity.

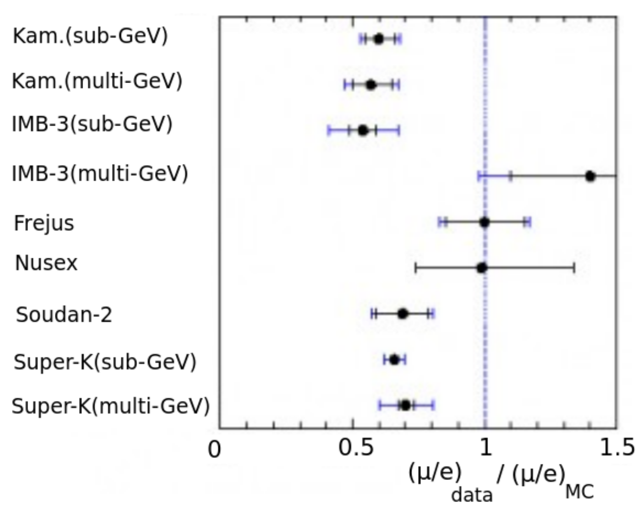


**Figure 2.2:** The atmospheric neutrino anomaly [54].

The Super-Kamiokande [55] experiment delivered the most precise results on the Atmospheric Neutrinos Anomaly. Super-Kamiokande is a 50 Kiloton water Cherenkov detector constructed under Mt. Ikenoyama located at the central part of Japan, giving it a rock over-burden of 2 700 m water-equivalent. The fiducial mass of the detector for atmospheric neutrino analysis is 22.5 kiloton. The experiment found substantial difference between the flux of neutrinos produced above the detector and the ones produced in the antipode region in South Atlantic. This observation could be explained with the oscillation of $\nu_\mu$ neutrinos into $\nu_\tau$ when traveling more than 12 km through the earth.

## 2.2 Neutrinos in the Standard Model, Neutrino-Mass & Neutrino-Oscillations

### Neutrinos in the Standard Model

In the seventies, S. Glashow, S. Weinberg and A. Salam, proposed the electro-weak model, which unify electromagnetic and weak interactions postulating four massless gauge bosons, ordered in an isovector triplet under the $SU(2)$ group and an isoscalar singlet under the $U(1)$ group. The model is referred to the group $SU(2)_L \otimes U(1)_Y$.

The spontaneous symmetry breaking $SU(2)_L \otimes U(1)_Y$ allow bosons to acquire mass while interacting with a scalar field (Higgs boson) that permeates the whole space. The massive bosons are denoted $W^\pm_\mu$ and $Z^0_\mu$ while one, the photon $A_\mu$ remains massless [56].

In relativistic quantum mechanics, fermions with spin $\frac{1}{2}$ and mass $m$ are described by the Dirac equation (using Einstein notation and considering $\hbar = c = 1$) [57]:

$$(i\gamma^\mu \frac{\partial}{\partial x^\mu} - m)\psi = 0 \tag{2.4}$$

where $\psi$ denotes a spinor of four components and $\gamma^\mu$ are the matrices $4 \times 4$ denoted by[3] :

$$\gamma^0 = \begin{pmatrix} 0 & \sigma^0 \\ \sigma^0 & 0 \end{pmatrix} \quad , \quad \gamma^i = \begin{pmatrix} 0 & \sigma^i \\ -\sigma^i & 0 \end{pmatrix} \tag{2.5}$$

where $\sigma^i$, are the Pauli matrices $2 \times 2$ [48]:

[3] This is the quiral representation (Weyl) for $\gamma^\mu$.

$$\sigma^0 = I = \begin{pmatrix} 1 & 0 \\ 0 & 1 \end{pmatrix}, \ \sigma^1 = \begin{pmatrix} 0 & 1 \\ 1 & 0 \end{pmatrix}, \ \sigma^2 = \begin{pmatrix} 0 & -i \\ i & 0 \end{pmatrix}, \ \sigma^3 = \begin{pmatrix} 1 & 0 \\ 0 & -1 \end{pmatrix} \tag{2.6}$$

The four components of $\psi$, correspond to particles and anti-particles with two possible projections $J_Z = \pm\frac{1}{2}$ equivalent to the two helicities $\mathcal{H} = \frac{\vec{s}\bullet\vec{p}}{|\vec{p}|} = \pm 1$, where $\vec{s}$ and $\vec{p}$ are the particle spin and momentum. Neutrinos are leptons of spin $\frac{1}{2}$ as other fermions, however, it is an experimental fact that only left-handed neutrinos ($\mathcal{H} = -1$) and right-handed anti-neutrinos are observed ($\mathcal{H} = +1$)[57].

Hence, a spinor of two components (Weyl spinors) should be enough to describe them. In a four-components theory, this is obtained with the help of the operators $P_{L,R} = \frac{1}{2}(1 \mp \gamma^5)$ [48]

$$\psi = (P_L + P_R)\psi = \frac{1}{2}(1 - \gamma^5)\psi + \frac{1}{2}(1 + \gamma^5)\psi = \psi_L + \psi_R \tag{2.7}$$

where $\gamma^5 = i\gamma^0\gamma^1\gamma^2\gamma^3 = \begin{pmatrix} -\sigma^0 & 0 \\ 0 & \sigma^0 \end{pmatrix}$

The elementary particles are arranged in a weak isospin $SU(2)_I$ that consists of doublets for chiral left-handed fields and singlets for right-handed fields in the form:

$$\begin{pmatrix} e \\ \nu'_e \end{pmatrix}_L \begin{pmatrix} \mu \\ \nu_\mu \end{pmatrix}_L \begin{pmatrix} \tau \\ \nu'_\tau \end{pmatrix}_L \begin{pmatrix} u \\ d' \end{pmatrix}_L \begin{pmatrix} c \\ s' \end{pmatrix}_L \begin{pmatrix} t \\ b' \end{pmatrix}_L$$
$$e_R \quad \mu_R \quad \tau_R \quad u_R \quad d_R \quad s_R \quad c_R \quad b_R \quad t_R$$

The Glashow-Weinberg-Salam lagrangian using electromagnetic charged and neutral currents is:

$$\mathcal{L} = -e\mathcal{J}^\mu_{EM}A_\mu - \frac{g}{\cos(\theta_W)}\mathcal{J}^\mu_{NC}\mathcal{Z}_\mu - \frac{g}{\sqrt{2}}((J^\mu_{CC})^+W^+_\mu + J^\mu_{CC}W^-_\mu) \tag{2.8}$$

where, $\mathcal{J}^\mu_{EM}$ is the electromagnetic current, $\mathcal{J}^\mu_{NC}$ the weak neutral current, and $(J^\mu)^+$ , $J^\mu$ the weak charged current and the coupling associated with the photon field $A_\mu$, the field of the boson $W^\pm_\mu$ and the boson $Z_\mu$.

The lepton currents (quiral representation) are given by [57], [58]:

$$\begin{cases} \mathcal{J}^{\mu}_{EM} = \bar{l}_L\gamma^{\mu}l_L + \bar{l}_R\gamma^{\mu}l_R = \bar{l}\gamma^{\mu}l \\ \mathcal{J}^{\mu}_{NC} = \frac{1}{2}\overline{\nu}_{l_L}\gamma^{\mu}\nu_{l_L} - \frac{1}{2}\bar{l}_L\gamma^{\mu}l_L - (\sin\theta_W)^2\mathcal{J}^{\mu}_{EM} \\ (J^{\mu}_{CC})^{+} = \overline{\nu}_{l_L}\gamma^{\mu}l_L \\ J^{\mu}_{CC} = \bar{l}_L\gamma^{\mu}\nu_{l_L} \end{cases} \tag{2.9}$$

Or in Dirac representation [59]:

$$\begin{cases} \mathcal{J}^{\mu}_{EM} = \bar{l}_L\gamma^{\mu}l_L + \bar{l}_R\gamma^{\mu}l_R = \bar{l}\gamma^{\mu}l \\ \mathcal{J}^{\mu}_{NC} = \frac{1}{2}\overline{\nu}_l\gamma^{\mu}(\frac{1-\gamma^5}{2})\nu_l - \frac{1}{2}(1-2(\sin\theta_W)^2)\bar{l}\gamma^{\mu}(\frac{1-\gamma^5}{2})l + (\sin\theta_W)^2\gamma^{\mu}(\frac{1-\gamma^5}{2})l \\ (J^{\mu}_{CC})^{+} = \overline{\nu}_l\gamma^{\mu}(\frac{1-\gamma^5}{2})l \\ J^{\mu}_{CC} = \bar{l}\gamma^{\mu}(\frac{1-\gamma^5}{2})\nu_l \end{cases} \tag{2.10}$$

Where $\theta_W$ is the Weinberg angle, such that: $\sin\theta_W = e/g$

**Neutrino Mass:**

Massless particles in the Standard Model formulation [60] guarantee gauge invariance under $SU(2)$ or $U(1)$ transformations; however, it is an experimental fact that particles and gauge bosons $W^{\pm}, Z^0$ do have mass (which makes the weak force to be short range)[4].

In the standard model, mass addition is accomplished through the spontaneous symmetry breaking via Higgs Mechanism. In order to break $SU(2)$ symmetry, a fundamental complex weak doublet of scalar (spin-0) fields for the charged and neutral states is introduced:

$$\phi = \begin{pmatrix} \phi^{+} \\ \phi^{0} \end{pmatrix} \tag{2.11}$$

which leads us to add the so called Yukawa coupling to the Standard Model lagrangian for each lepton family:

[4]The weak force range is about $10^{-18}m$, in comparison to the infinite range of electromagnetic forces with the photon as its gauge boson, which is massless

$$\mathcal{L}_{Yuk} = -c_l[\overline{\nu}_L \phi^+ l_R + \bar{l}_L \phi^0 l_R] + h.c. \tag{2.12}$$

where $c_l$ is an arbitrary constant coupling and $h.c.$ the hermitian conjugate.

After the spontaneous symmetry breaking, the values for the $\phi$ field come from a particular configuration selected called *vacuum* space, motivated by the fact that such space has an electrically neutral state, where the vacuum expectation values of the Higgs field are: $<\phi^+>=0$ and $<\phi^0>=v/\sqrt{2}$, where $v \simeq 246\ GeV$, making neutrinos massless and charged leptons $e, \mu, \tau$ with a mass term coming from:

$$\mathcal{L}_D = -(m_D^l)\bar{l}_L l_R + h.c. \tag{2.13}$$

where $m_D^l = c_l v/\sqrt{2}$, and the coupling constant $c_l$ is experimentally obtained.

However, it is also an experimental fact that neutrinos have mass, reason why the right-handed chiral neutrino component is introduced, obtaining a lagrangian similar to the ones for the charged leptons:

$$\mathcal{L}_D^{\nu_l}(x) = -\nu_{\alpha_L}(x) m_{\alpha\beta} \nu_{\beta_R} + h.c. \tag{2.14}$$

where $m_{\alpha\beta}$ is a complex matrix, than can be represented in diagonal form with the help of two unitary matrices:

$$m_{\alpha\beta} = (U_{\alpha i}^L)^* m_i U_{\beta i}^R \tag{2.15}$$

here, $m_i$ are three real and positive masses. $U^L$ , $U^R$ are the unitary matrices.

Considering the Standard Dirac lagrangian density [48]:

$$\mathcal{L} = i\psi_L^+ \widetilde{\sigma}^\mu \partial_\mu \psi_L + i\psi_R^+ \sigma^\mu \partial_\mu \psi_R - m(\psi_L^+ \psi_R + \psi_R^+ \psi_L) \tag{2.16}$$

Where $\sigma^\mu, \widetilde{\sigma}^\mu$ are in function of the Pauli matrices defined in (2.6):

$$\sigma^\mu = (\sigma^0, \sigma^1, \sigma^2, \sigma^3), \ \ \widetilde{\sigma}^\mu = (\sigma^0, -\sigma^1, -\sigma^2, -\sigma^3) \tag{2.17}$$

and $\psi_L$ , $\psi_R$ come from the four-component Dirac field

$$\psi = \begin{pmatrix} \psi_L \\ \psi_R \end{pmatrix} = \begin{pmatrix} \psi_L \\ 0 \end{pmatrix} + \begin{pmatrix} 0 \\ \psi_R \end{pmatrix} \tag{2.18}$$

Then, we can define:

$$\nu_{i_L}(x) = (U^L_{i\alpha})^* \nu_{\alpha_L}(x) \tag{2.19}$$

$$\nu_{i_R}(x) = (U^R_{i\alpha})^* \nu_{\alpha_R}(x) \tag{2.20}$$

and replace in 2.14, getting:

$$\mathcal{L}^{\nu_l}_D(x) = -m_i(\nu^+_{i_L}\nu_{i_R} + \nu^+_{i_R}\nu_{i_L}) \tag{2.21}$$

Which resembles the mass term in the standard lagrangian density in terms of $\psi_L$ and $\psi_R$ in (2.16).

However, due to the fact that neutrinos are neutral particles, it would be possible to define them in a different way, considering the neutrino is its own anti-particle. In a Majorana field we have [61]:

$$\nu = \nu_L + \nu^C_L \tag{2.22}$$

which satisfies the Majorana condition:

$$\nu^C = \nu \tag{2.23}$$

The mass term in the Majorana Lagrangian density is given by [48]:

$$\mathcal{L}_{\mathcal{M}}(x) = -\frac{1}{2}\nu^T_\alpha(-i\sigma^2)\nu_\beta m_{\alpha\beta} + h.c. \tag{2.24}$$

where $\alpha, \beta$ take values of the three neutrino flavors $e, \mu, \tau$ , and $\nu_\alpha, \nu_\beta$ are chiral left-handed neutrinos ($L$ subscript are omitted for better clarity) and $m_{\alpha\beta}$ is an arbitrary complex matrix.

If we consider $m_{\alpha\beta} = m_{\beta\alpha}$ , we can then write:

$$m_{\alpha\beta} = U_{\alpha i} m_i U_{\beta i} \tag{2.25}$$

where $m_i$ are three positive masses, and we can define:

$$\nu_i(x) = U_{\alpha i}\nu_\alpha(x) \tag{2.26}$$

where the equation 2.24 becomes:

$$\mathcal{L}_{\mathcal{M}}(x) = -\frac{1}{2}m_i\nu_i^T(-i\sigma^2)\nu_i + h.c. \tag{2.27}$$

where:

$$\nu_\alpha(x) = U_{\alpha i}^*\nu_i(x) \tag{2.28}$$

**Neutrino Oscillations**

Neutrino oscillations are related to the fact that the mass of neutrinos is not zero, which is why it requires extending the Standard Model.

In the neutrino oscillation model, the neutrinos that are produced by weak interactions (weak eigenstates) are not states of a definite mass but a linear superposition of mass eigenstates instead. This can be expressed in the form of a mixing matrix, if we assume only two neutrino species, then such matrix would be:

$$\begin{pmatrix} \nu_\alpha \\ \nu_\beta \end{pmatrix} = \begin{pmatrix} \cos\theta & \sin\theta \\ -\sin\theta & \cos\theta \end{pmatrix} \begin{pmatrix} \nu_1 \\ \nu_2 \end{pmatrix} \tag{2.29}$$

where $(\nu_\alpha, \nu_\beta)$ are the weak eigenstates and $(\nu_1, \nu_2)$ the mass eigenstates and $\theta$ is the neutrino mixing angle. Also, $\alpha, \beta$ are the neutrino flavors and you could associate two masses $m_1, m_2$ to the mass eigenstates.

Hence, using equation 2.29, a neutrino weak eigenstate at a time $t = 0$ would then be:

$$|\nu_\alpha(t = 0) >= \sin\theta|\nu_1 > + \cos\theta|\nu_2 > \tag{2.30}$$

However, for a time $t \neq 0$, the mass eigenstate propagates with a different phase factor, as following:

$$|\nu_\alpha(t)>= \sin\theta e^{-iE_1t-px}|\nu_1> + \cos\theta e^{-iE_2t-px}|\nu_2> \tag{2.31}$$

where $E_1$ , $E_2$ are the mass eigenstates energies with a momentum $p$. If we consider the extreme relativistic approximation for very small neutrino masses $m \ll p$, then:

$$E_{1,2} \approx p + \frac{m_{1,2}^2}{2p} \tag{2.32}$$

So, using 2.32 in 2.31:

$$|\nu_\alpha(t)>= |\nu_1> \cos\theta e^{-\frac{-im_1^2L}{2E}} + |\nu_2> \sin\theta e^{-\frac{im_2^2L}{2E}} \tag{2.33}$$

where $E = p$ and $L$ is defined as the distance from the neutrino production to the neutrino detection. So, after that distance propagation $L$, the probability to find a different neutrino flavor is defined as:

$$P(\nu_\alpha \longrightarrow \nu_\beta, t) = |<\nu_\beta|\nu_\alpha(t)>|^2 = (\sin 2\theta)^2(\sin\{\Delta m^2 L/4E\})^2 \tag{2.34}$$

where $\Delta m^2 = m_2^2 - m_1^2$ is the mass square difference.

### 2.2.1 Neutrino main Interaction Channels

The interest in neutrino interactions has recently increased in the physics community due to the need of it for neutrino oscillation data interpretation. Neutrino scattering results on both charged current (CC) and neutral current (NC) interaction channels.

Neutrinos cross sections can be expressed as:

$$\sigma = \sigma^{CC} + \sigma^{NC} \tag{2.35}$$

and each one of these inclusive cross sections can be broken up in three basic processes which are described in Sections presented below: Quasi-Elastic $\sigma^{QE}$ , Resonance $\sigma^{RES}$ and Deep Inelastic $\sigma^{DIS}$ each of which has its own model and associated uncertainties.

$$\sigma^{CC,NC} = \sigma^{QE} + \sigma^{RES} + \sigma^{DIS} \tag{2.36}$$

For the sake of simplicity, small contributions to the total cross section in the few GeV energy range, such as coherent and elastic $\nu e^-$ scattering, were omitted from the expression above.

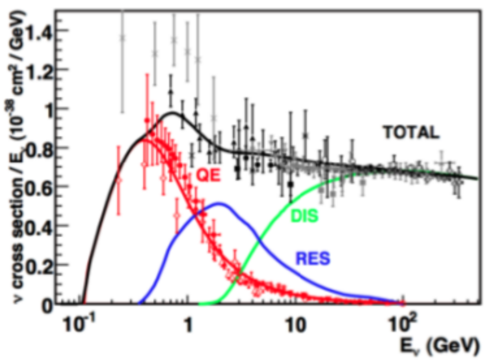


**Figure 2.3:** Existing muon neutrino charged-current cross section measurements and predictions as a function of neutrino energy. The contributing processes in this energy region include QuasiElastic (QE) scattering, Resonance Production (RES), and Deep Inelastic Scattering (DIS)[62].

### 2.2.2 Deep Inelastic Scattering

This is the dominant channel at high neutrino energies (see Figure 2.3). The term "deep" is due to the fact that the interaction is produced at the quark level. It is characterized by a high momentum transfer $q$. The associated wavelength of the propagator $1/|q|$ is at the size scale of the nucleon constituents.

Neutrinos have the unique ability to taste particular flavors of quarks, hence playing an important role in the extraction of *Parton Distribution Functions* (PDFs)[5], which represent probability densities to find a parton carrying a momentum fraction $x$ at a squared energy scale $Q^2$ [63]. In charged current DIS, the $\nu$ interact with $d, s, \overline{u}$ and $\overline{c}$ while the $\overline{\nu}$ interact with $u, c, \overline{d}$ and $\overline{s}$. This is due to charge conservation i.e: $\nu(0) + d(-1/3) \longrightarrow \mu^-(-1) + u(2/3)$.

The main interactions for charged and neutral current can be expressed in the equations presented in the next Figure:

[5] The Parton name was proposed by Richard Feynman in 1969 as a generic description for any particle constituent within the proton, neutron and other hadrons. These particles are referred today as quarks and gluons.

Charged Current :

$\nu_l + N \to l^- + X$

$\bar{\nu}_l + N \to l^+ + X$

Neutral Current :

$\nu_l + N \to \nu_l + X$

$\bar{\nu}_l + N \to \bar{\nu}_l + X$

$N = p, n$

$X$ denotes any final hadron state

**Figure 2.4:** Main interactions for charged and neutral currents.

### 2.2.3 Resonance Production

In this interaction process, a resonant state is produced due to the excitation of the nucleon during the interaction process. These excited states decay to their fundamental states producing a combinations of nucleons and mesons.

Resonant reactions can be expressed as:

$$\nu + N \longrightarrow \nu + R \tag{2.37}$$

$$\nu + N \longrightarrow l^- + R \tag{2.38}$$

The resonant production in neutrino interactions represents a significant fraction of the total cross section for the few GeV range as seen in Figure 2.3.

This channel is also the main background source for experimental quasi-elastic analyses, which is a channel with very high statistics, and the main channel studied in [9]. There, in particular, resonant processes where single pions are produced were analyzed.

#### Resonance Single Pion Production

As mentioned previously, resonance reactions involve a nucleon that is excited into a resonance state. At **low neutrino energies**, these resonance states are composed of isospin $1/2(N^*)$ and $3/2\Delta$ states, which generally decay into a nucleon and a single pion final state (See next Figure):

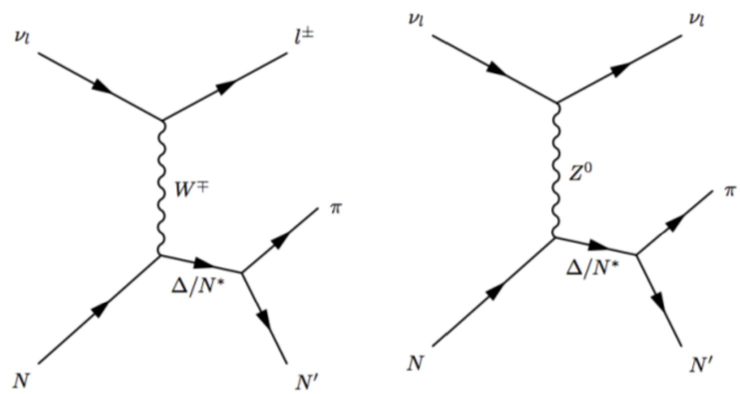


**Figure 2.5:** (left) Charged and (right) Neutral Current resonance pion production.

Resonance reactions in which intermediate resonance states like $\Delta(1232)$ are produced are given in the equations shown in the next Figure (**charged current & neutral current reactions**):

Charged Current:

$$\nu_\mu + p \rightarrow \mu^- + p + \pi^+ \quad , \quad \bar{\nu}_\mu + p \rightarrow \mu^+ + p + \pi^-$$
$$\nu_\mu + n \rightarrow \mu^- + n + \pi^+ \quad , \quad \bar{\nu}_\mu + n \rightarrow \mu^+ + n + \pi^-$$
$$\nu_\mu + n \rightarrow \mu^- + p + \pi^0 \quad , \quad \bar{\nu}_\mu + p \rightarrow \mu^+ + n + \pi^0$$

Neutral Current:

$$\nu_\mu + p \rightarrow \nu_\mu + p + \pi^0 \quad , \quad \bar{\nu}_\mu + p \rightarrow \bar{\nu}_\mu + p + \pi^0$$
$$\nu_\mu + n \rightarrow \nu_\mu + n + \pi^0 \quad , \quad \bar{\nu}_\mu + n \rightarrow \bar{\nu}_\mu + n + \pi^0$$
$$\nu_\mu + p \rightarrow \nu_\mu + n + \pi^+ \quad , \quad \bar{\nu}_\mu + p \rightarrow \bar{\nu}_\mu + n + \pi^+$$
$$\nu_\mu + n \rightarrow \nu_\mu + p + \pi^- \quad , \quad \bar{\nu}_\mu + n \rightarrow \bar{\nu}_\mu + p + \pi^-$$

**Figure 2.6:** Charged & Neutral current reactions for the **Resonant**-Single-Pion-Production process.

The single pion production from baryonic resonances is predicted using the **Rein & Sehgal model** [64] , which works well for high energy neutrino interactions, but are poorly constrained by neutrino data at lower energies (below 2 GeV) [65].

### 2.2.4 Coherent Pion Production

In coherent pion production, very little energy is exchanged between the neutrino and the target. The nucleus remains intact in its fundamental state but a single pion exists in the final state from the coherent sum of scattering from all the nucleons, with the same charge as the boson involved in the interaction [66]. Coherent charged and neutral current processes are expressed in the equations presented in the next Figure:

Neutral Current

$$\nu_\mu + A \to \nu_\mu + A + \pi^0 \quad , \quad \bar{\nu}_\mu + A \to \bar{\nu}_\mu + A + \pi^0$$

Charged Current

$$\nu_\mu + A \to \mu^- + A + \pi^+ \quad , \quad \bar{\nu}_\mu + A \to \mu^+ + A + \pi^-$$

**Figure 2.7:** Charged & Neutral current reactions for the **Coherent**-Single-Pion-Production process.

Just as in the resonance pion production case, the **Rein and Sehgal model** [64] is also used for predicting these reactions but more data is necessary to constrain the model. There has been many pion analyses currently on-going on the Miner$\nu$a experiment [101] from both neutrino and anti-neutrino resonant and coherent channels. The work developed in particle-ID for the Test Beam actually contributed to analyze these processes in which there is a charged pion present in the final state.

### 2.2.5 Quasi-Elastic Scattering

This is the dominant channel below $2GeV$ as Figure 2.3 shows. The neutrino scatters off a nucleon inside the nucleus of an atom by the exchange of the $W$ boson (for charged current interactions) or the $Z$ boson (for neutral current interactions) and one nucleon (or multiple nucleons) come out from the target. The term “quasi” for charged current interactions is due to the fact the the neutrino can change its identity to a charged lepton and the neutron can suffer a quark flip becoming a proton. For neutral current interactions, this process is referred simply as *elastic scattering*.

**Charged Current Quasi-Elastic Scattering**

The charged current quasi-elastic reactions for neutrinos and anti-neutrinos are[6] :

$$\nu_l + n \longrightarrow p + l^- \tag{2.39}$$

$$\overline{\nu}_l + p \longrightarrow n + l^+ \tag{2.40}$$

where $l = e, \mu, \tau$.

The differential cross section can be expressed in the **Llewellyn-Smith formalism** [67]. This formalism allows to describe the cross section in terms of functions that only depend on the four-momentum transfer $Q^2$. The neutrino cross section is then written as the next Figure shows:

$$\boxed{\frac{d\sigma_{CC}^{\nu_l n, \bar{\nu}_l p}}{dQ^2} = \frac{G_F^2 |V_{ud}|^2 m_N^4}{8\pi \left(p_\nu \cdot p_{N_i}\right)^2} \left[A\left(Q^2\right) \pm B\left(Q^2\right) \frac{s-u}{m_N^2} + C\left(Q^2\right) \frac{(s-u)^2}{m_N^4}\right]}$$

$$\boxed{s - u = 4ME_\nu - Q^2 - m_l^2}$$

$*$ A, B, C are in function of $Q^2$:

$$\boxed{\begin{aligned} A = \frac{m_l^2 + Q^2}{m_N^2} \Big\{ &(1+\tau) F_A^2 - (1-\tau)(F_1^V)^2 + \tau(1-\tau)(F_2^V)^2 + 4\tau F_1^V F_2^V \\ &- \frac{m_l^2}{4m_N^2} \left[ \left(F_1^V + F_2^V\right)^2 + (F_A + 2F_P)^2 - \left(\frac{Q^2}{m_N^2} + 4\right) F_P^2 \right] \Big\} \end{aligned}}$$

$$\boxed{B = \frac{Q^2}{m_N^2} F_A \left(F_1^V + F_2^V\right)} \qquad \boxed{C = \frac{1}{4}\left(F_A^2 + (F_1^V)^2 + \tau (F_2^V)^2\right)}$$

**Figure 2.8:** Expression for the differential cross section for the CCQE process in the **Llewellyn-Smith** formalism.

In the expression presented in the previous Figure $\tau = Q^2/4m_N^2$. Notice that neutrinos and anti-neutrinos just differ in the cross section formula by the sign in the $B$ term.

[6]The equation 2.40 with $l = e$ is also called inverse beta decay and has been used in historical experiments such as in the Cowan and Reines experiment, where neutrinos where observed for the first time.

In other words, the cross section can be expressed in terms of **four form factors**: $F_1^V$, $F_2^V$, $F_A$ and $F_P$.

The vector form factors $F_{1,2}^V$ can be expressed considering the conserved vector current hypothesis (CVC) [68] in terms of the Dirac and Pauli electromagnetic form factors $F_1^{p,n}$, $F_2^{p,n}$:

$$F_{1,2}^V = F_{1,2}^p - F_1^n \tag{2.41}$$

These electromagnetic form factors have been measured in electron scattering experiments, and can be written in the Galster et all formalism [69]:

$$F_1^{p,n} = \frac{G_E^{p,n} + \tau G_M^{p,n}}{1+\tau} \tag{2.42}$$

$$F_2^{p,n} = \frac{G_M^{p,n} + \tau G_E^{p,n}}{1+\tau} \tag{2.43}$$

where $\tau = -q^2/m_N^2$. The $G_E$ and $G_M$ are called the Sachs form factors and are parameterized in terms of the **dipole form factor** $(G_D)$ as shown in next Figure:

$$\boxed{\begin{aligned} G_E^p(Q^2) &= G_D(Q^2) \\ G_E^n(Q^2) &= 0 \\ G_M^p(Q^2) &= \mu_p G_D(Q^2) \\ G_M^n(Q^2) &= \mu_n G_D(Q^2) \end{aligned}} \qquad \boxed{G_D(Q^2) = \frac{1}{1+Q^2/M_V^2}}$$

$$\boxed{\begin{array}{l} \text{vector mass} \\ M_V = 0.843 \text{ GeV} \end{array}}$$

**Figure 2.9:** Sachs form factors parameterized in terms of the **dipole form factor** $G_D$.

The pseudo-scalar form factor $F_P$ and the axial form factor $F_A$ can be related by requiring partially conserved vector current (PCAC) [70]:

$$F_P(Q^2) = \frac{2m_N^2}{Q^2 + m_\pi^2} F_A(Q^2) \tag{2.44}$$

The axial form factor commonly adopts the following dipolar form:

$$F_A(Q^2) = g_A/[1 + \frac{Q^2}{M_A^2}] \tag{2.45}$$

where the average axial mass constant $M_A = 1.026\ GeV$ and the best axial vector constant coming from beta decay experiments [71] $g_A = -1.267$. For a detailed discussion of the axial structure of the nucleon, see [72].

It is important to notice that the neutrino energy $E_\nu$ and the four-momentum transfer $Q^2$ can be expressed in terms of the muon kinematics as following:

$$\boxed{E_\nu^{QE} = \frac{(2M_n - E_B)E_\mu - \left[(M_n - E_B)^2 + m_\mu^2 - m_p^2\right]}{2\left[(M_n - E_B) - E_\mu + \sqrt{E_\mu^2 - m_\mu^2}\cos\theta_\mu\right]}}$$

$$\boxed{Q_{QE}^2 = -m_\mu^2 + 2E_\nu^{QE}(E_\mu - \sqrt{E_\mu^2 - m_\mu^2}\cos\theta_\mu)}$$

**Figure 2.10:** Neutrino energy $E_\nu$ and the four-momentum transfer $Q^2$ in terms of the $\mu$ kinematics. $E_B$ is called the *binding energy* and is equivalent to $34MeV$ in this model.

### 2.2.6 Short Range Correlations

Quasi-elastic scattering is traditionally viewed as scattering off single nucleons, as described previously. However, when nucleons are too close from each other ($< 15fm$), strong short-range forces increase their relative momentum and push the nucleons far off-shell. This is known as short range correlations (SRCs) [73] and are predicted to involve the nucleon 20% of the time and most of them are neutron-proton correlations [74] [75]. These effects are not included in the simulation but have a significant impact in the mea- surement. Details on this can be found in [76].

### 2.2.7 Meson Exchange Currents

This is another mechanism that is not included in the standard quasi-elastic formalism. Meson exchange currents are two-body currents carried by a virtual meson which is exchanged between two nucleons in the nucleus. This leads to the emission of two nucleons in the hadronic final state. See [77] for more details.

## 2.3 A particular Analysis Motivation

Quasi-elastic interactions were extensively studied in between the 1970s and 1990s using deuterium-filled bubble chambers. This could be called the first generation of neutrino quasi-elastic experiments, where the main interest was to measure the **axial-vector form factor** of the nucleon [78]. The **Llewellyn-Smith** formalism was used to describe the quasi-elastic scattering.

The modern neutrino quasi-elastic experiments no longer use deuterium as a target, but **heavier nuclei** with $A > 2$ instead. By doing so, nuclear effects become important and produce considerable modifications to the standard quasi-elastic differential cross section described in Equation presented in Figure 2.8.

Figure 2.11 shows the comparison of the $\nu_\mu$ CCQE cross-section as a function of neutrino energy for different experiments and models. Here, MiniBooNE [79] and NOMAD [80] are both modern neutrino experiments with high-statistics and carbon-based targets, but some disparity can be appreciated between both measurements.

NOMAD experimental data is consistent with a neutrino quasi-elastic scattering on a free nucleon target, as described in Llewellyn-Smith formalism with the standard axial mass constant $M_A \approx 1.03$. MiniBooNE data on the other hand, prefers an axial mass of $M_A = 1.35$.

Notice that the neutrino energy range is different in both experiments. MiniBooNE has neutrino energies less than $2GeV$ while NOMAD cross sections have neutrino energies greater than $3GeV$.

It is currently believed that nuclear effects are responsible for these discrepancies. In particular, nucleon-nucleon correlations and two-body exchange currents can improve the accuracy of describing neutrino quasi-elastic scattering. These effects yield significantly enhanced cross sections (larger than the free scattering case) which, in some cases, appear to better match the experimental data [81].

These nuclear effects also produce final states that include multiple nucleons, implying a “quasi-elastic” definition should not be restricted to a single nucleon. Nowadays, the fact that nuclear effects may play an important role in neutrino quasi-elastic scattering has made both theorists and experimentalists to put a lot of effort in these studies

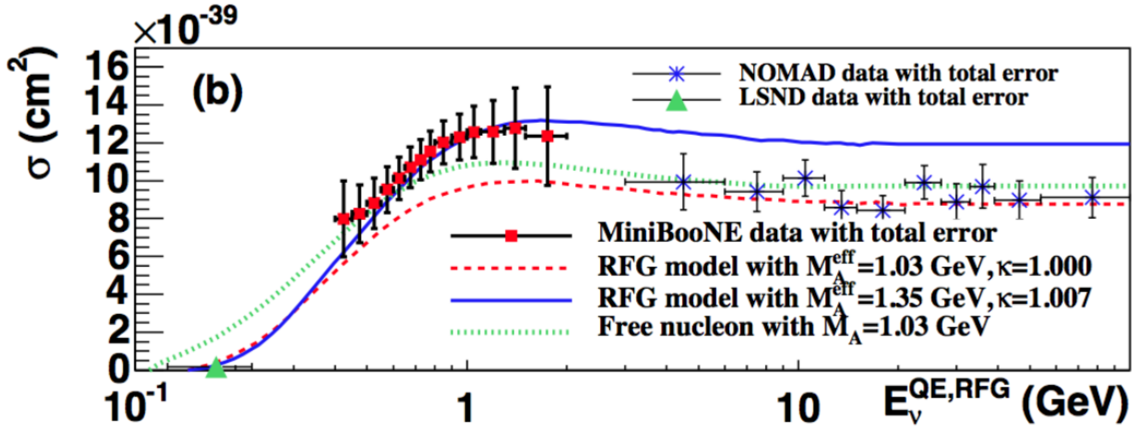


**Figure 2.11:** Flux unfolded $\sigma(E_\nu)$ Data for MiniBoone and NOMAD.

Since the total cross sections $\sigma(E_\nu)$ and the axial mass are model dependent quantities, especially when scattering off nucleon targets, there is a strong preference to report differential cross section results in term of observables instead. MiniBooNE measured single differential cross section as a functions of $Q^2$ and a double differential cross section in terms of the muon kinetic energy and the scattering angle [82] for $E_\nu < 2GeV$.

Figure 2.12 shows a single differential quasi-elastic cross section as a function of $Q^2$ compared to different models in the MINER$\nu$A experiment. The purity of the sample is about 49% and the background is removed with a MC-driven background subtraction technique that constrains the background models with MINER$\nu$A own data [83] in order to lessen the model dependency. The analysis developed in [9] aimed to improve the purity of the MINER$\nu$A quasi-elastic sample by extending the reconstruction to identify the protons and rejecting pion backgrounds that decay into michel electrons. The analysis perfomed there measured Quasi-Elastic Like events, which are events that a detector can see (because of the specific particles present in the final state), with a neutrino energy $1.5\,GeV < E_\nu < 10.0\,GeV$.

In order to lessen the model dependency, it also aimed to measure a double differential cross section as a function of two observables: the longitudinal ($P_Z$ ) and transverse ($P_T$) momentum of the muon. This phase space was chosen instead of the $T_\mu \cos\theta_\mu$ phase space used by MiniBoonE because the muon scattering angles are more forward in MINER$\nu$A due to the higher

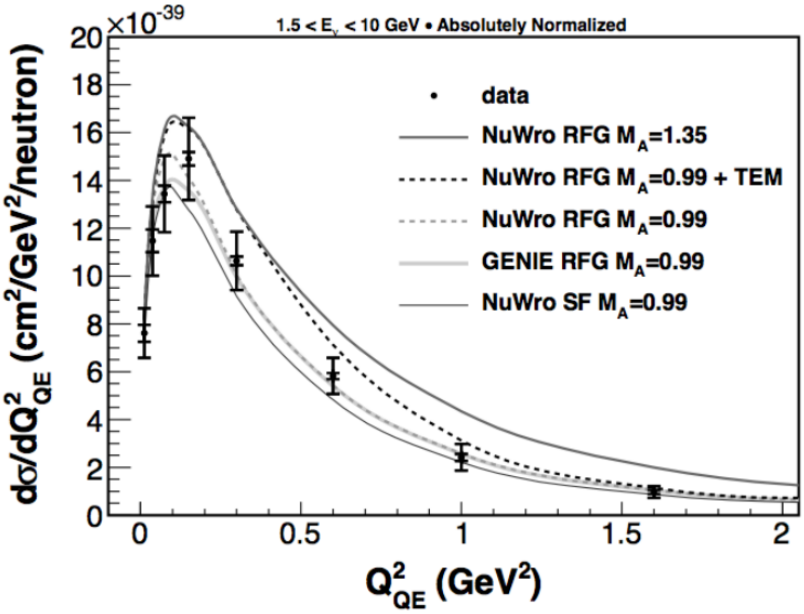


**Figure 2.12:** Minerva single differential cross section $d\sigma/dQ^2$.

neutrino energies from the NuMI beam, and because this acceptance is limited more by the requirement of these muons to match into the MINOS Near Detector[7] (more about this in the next Chapter). Figure 2.13 shows how different constant values of the neutrino energy and the four-momentum transfer $E_\nu^{QE}$, $Q^2_{QE}$ calculated under the quasi-elastic assumption from the muon kinematics (see Figure 2.10) look like in this phase space.

[7]This Detector is used as a $\mu$ spectrometer, it has a magnetic field which tells us the $\mu$ charge & momentum

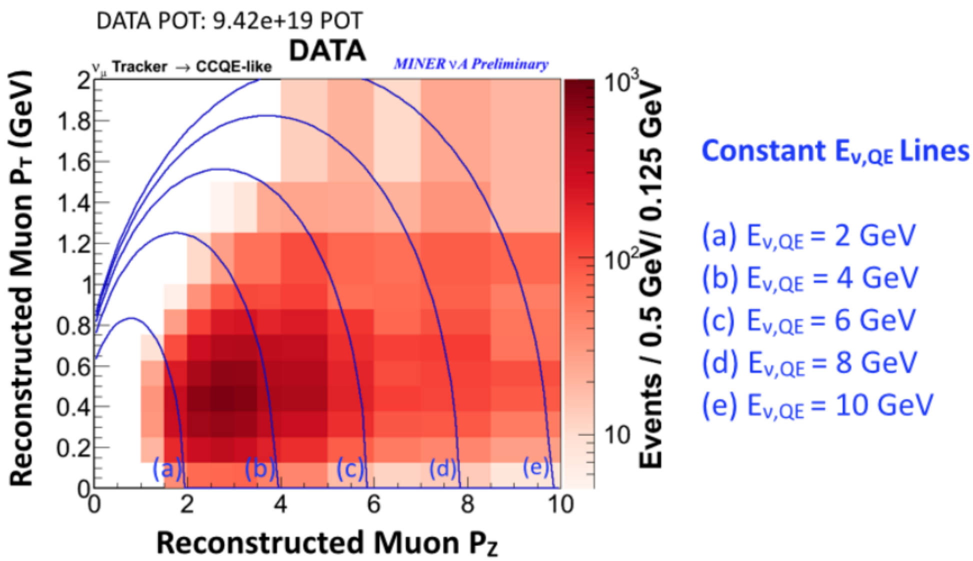


(a) Constant lines of different $E_\nu^{QE}$ values in the muon $P_Z - P_T$ phase space.

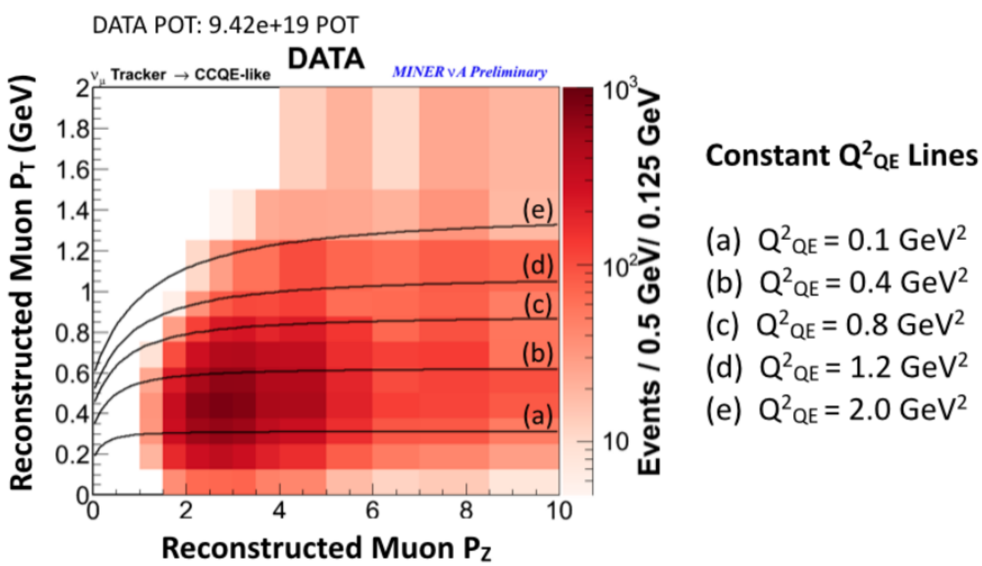


(b) Constant lines of different $Q^2{}_{QE}$ values in the muon $P_Z - P_T$ phase space.

**Figure 2.13:** Constant lines of $E_\nu^{QE}$, $Q^2_{QE}$ values in the muon $P_Z - P_T$ phase space. Events shown here are data events taken from March to July 2010 after passing a "selection criteria" described in [9].

# Chapter 3

# Tools for Data Analysis

To be able to perform Data Analysis it is mandatory to understand how to use the software needed for that purpose, in the area of High Energy Physics, ROOT [12] is the software most widely used to analyze data. It is also relevant to have some experience in programming, specially in C++, because most of the ROOT syntax is actually C++ syntax. Python is another language that can be use, we just need to import the ROOT libraries (which turns python into pyroot) and in that way be able to define and use ROOT objects in a python script (the scripts for the analysis performed in this thesis have been written in python). The concepts of objects and classes, which are part of the paradigm of Object Oriented Programming (OOP), are extremely important because in ROOT we deal with Data-objects like Chains, Branches, Trees and Result-objects like histograms and functions. A nice and didatic introduction to OOP in C++ can be found in [84]. In Section 3.1 all basic feactures about ROOT and OOP in C++ are covered.

The idea is to be able to create histograms (and later fit them) of events of interest, to get these events we require to isolate them from all the sample taken and for this we require to loop over all events in a Chain (which is make by adding many Trees) and put conditions on them (cuts) in order to retain the events we seek to analyze. To perform a proper cut we require to understand the physics behind the Branch on which we are imposing conditions, this can be made with a Monte Carlo simulation (to create simulated-data which can tell us what specific events to look at), with a scatterplot of different variables to see if cutting on one of them can improve our DataSet (for example, to reject events of high $\chi^2$) or using some physical criteria to tell which Branch intervals are physically meaningful.

For the last way to perform a proper cut, if we want to identify different kinds of particles inside the detector, we need to understand the different mechanisms in which they deposit energy as they pass through matter. This permits to separate protons from pions or muons from pions in a given sample by looking at specific variables related to the energy deposited in a specific region of the detector.

All the issues related to the ways in which particles deposit energy, which can be via ionization (dE/dx), via Electromagnetic Showers or Hadronic Showers, are outlined in Section 3.2. For the MINER$\nu$A and Test Beam detectors, which have a specific way to read the energy deposited by charged particles (as explained in Section 1.4), there is a software called Arachne [85] (developed by the MINER$\nu$A collaboration) which permits visualizations of the hits deposited inside the modules and in that way permits to perform an eye scanning of events of interest to test if the cuts performed were useful, a review of what it means is covered in Section 3.3.

## 3.1 Basic Concepts in ROOT

The software ROOT is already installed in the Fermi machines, so we just need to access one of these machines via SSH (Secure Shell) using the Kerberos Network Authentication Protocol. With the aid of this software we can create scripts (Macros) to open DSTs (root files) containing Trees (we can also open many Trees into what is called a Chain), which are datasets with different Branches (physical variables), and be able to create histograms, fit functions, perform cuts, among many other things. A good and didatic ROOT tutorial which tell us what is needed to start a basic analysis (the template of the script) can be found in [86].

Let us do a basic review of ROOT, all features about the important topic of Object Oriented Programming in C++ are not covered in this report but a good summary about it can be found in [87] and [84]. With the aid of ROOT we can plot a function (and manipulate it, change its domains and axis-labels), create a histogram (specify the number of bins and the axes limits), fill a histogram with random outcomes from a given probability distribution function (gaussian, poisson, Landau, etc), fit a histogram with a function, save and open a Canvas (a space where we can plot functions or histograms), use the TBrowser (a GUI interface) to open Trees and look at histograms of specific branches in an easy way and the most important thing is that there is a command (actually a C++ function) called MakeClass() that creates a (polymorphic) class for our analysis, which has a (virtual) function in which we specify all we need for our analysis (definition of objects of interest, loops to do cuts and presentation of results).

In the remaining of this section an interactive usage of ROOT is presented with some figures showing the results of the commands typed in the ROOT command line, then it is explained how to make a Class for our analysis and what is the structure of the python scripts used for the analysis presented in Chapters 4, 5 & 6. Keeping in mind that functions and histograms in ROOT are actually C++ objects, we define them in the same way we do in a C++ program. In Figure 3.1 we can see the way to define a given function (C++ object) and the result of using the function Draw (a method of the class TF1 whose objects are 1D functions), which plots the function inside a Canvas.

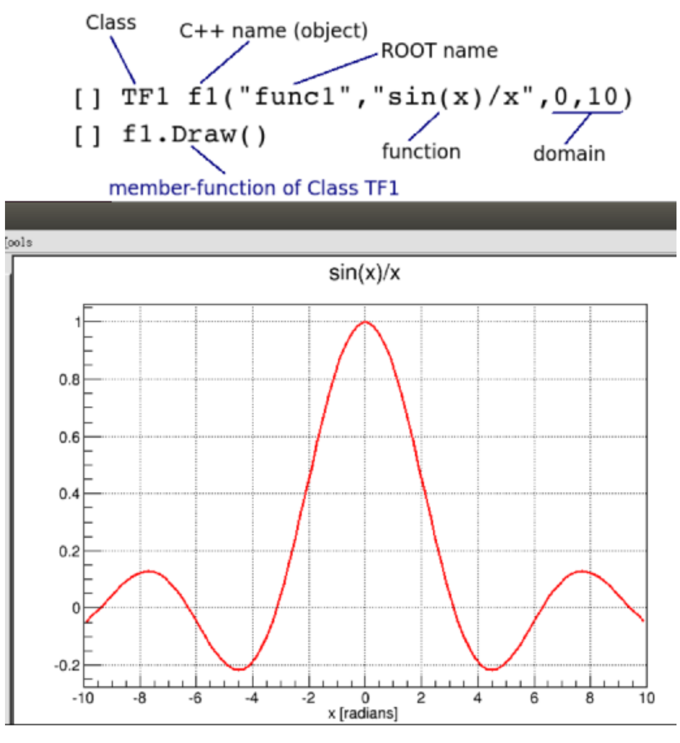


**Figure 3.1:** Definition and plot of a function in ROOT.

Figure 3.2 presents the way in which a (non-standard) gaussian function can be defined in order to generate random outcomes from it that are used later to fill a histogram, and the way to draw that histogram with error bars, that indicate the statistical uncertainty. When putting error bars, the width of those statistical errors is reduced as we increase the number of Entries due the Law of Large Numbers (this is relevant for the analysis in this thesis because only raw data was used so all the errors are of statistical nature):

$$Relative\ Error(X) \equiv \frac{\sqrt{Var(X)}}{< X >} = \frac{\sigma}{\mu} \sim \frac{1}{\sqrt{N}} \longrightarrow 0 \quad as \quad N \longrightarrow \infty \tag{3.1}$$

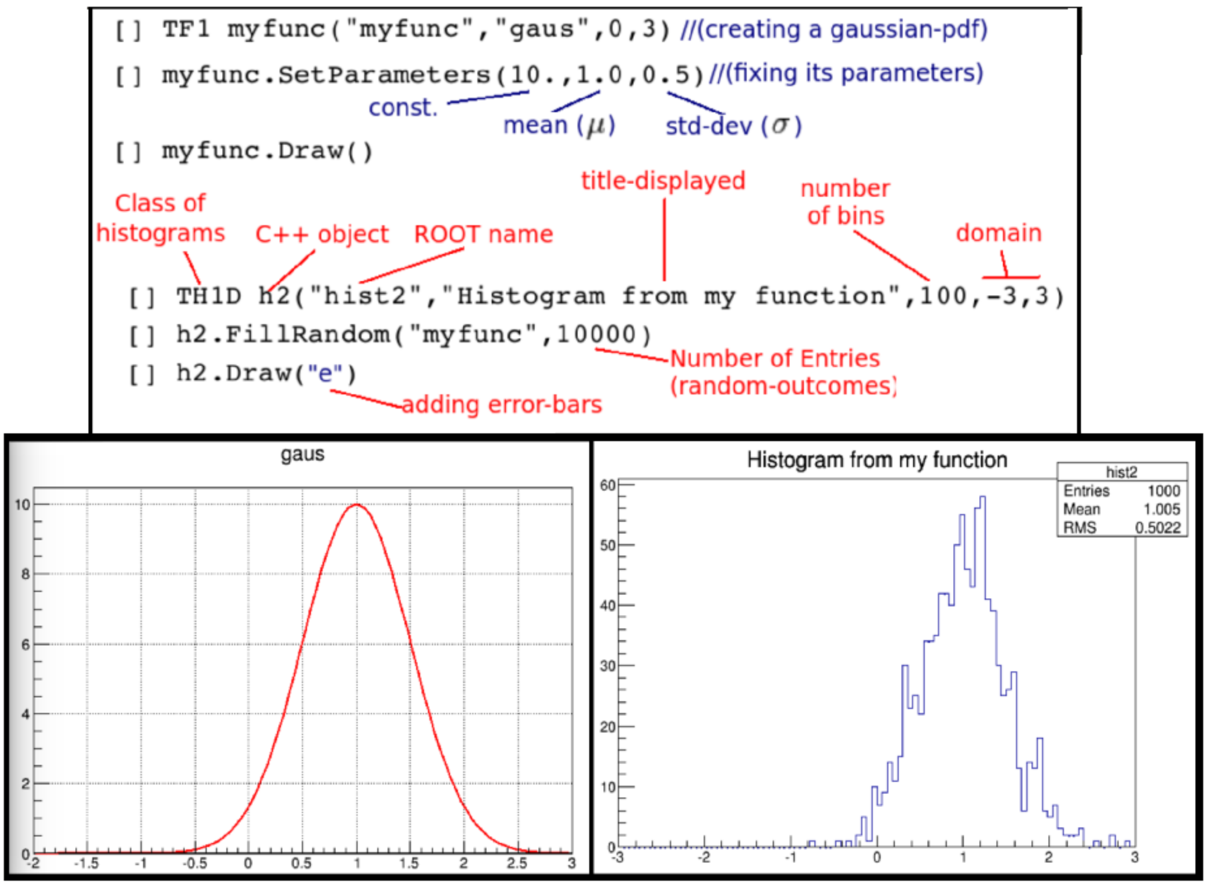


**Figure 3.2:** Definition of a non-standard gaussian function (Left) used to fill a histogram (Right).

We can use the TBrowser to explore the contents of any root file, for example in [86] there is a file called histogram.root which contains a complex histogram which is fitted by the sum of two non-standard gaussian functions. Figure 3.3 shows this histogram (with error bars) and the fitted function (in red) inside the TBrowser GUI, the value of $\chi^2/ndf$ is also presented, which indicates how good the fit was performed ($\sim 1$ for a good fit, the parameters of the fit are displayed at the top right of the Canvas).

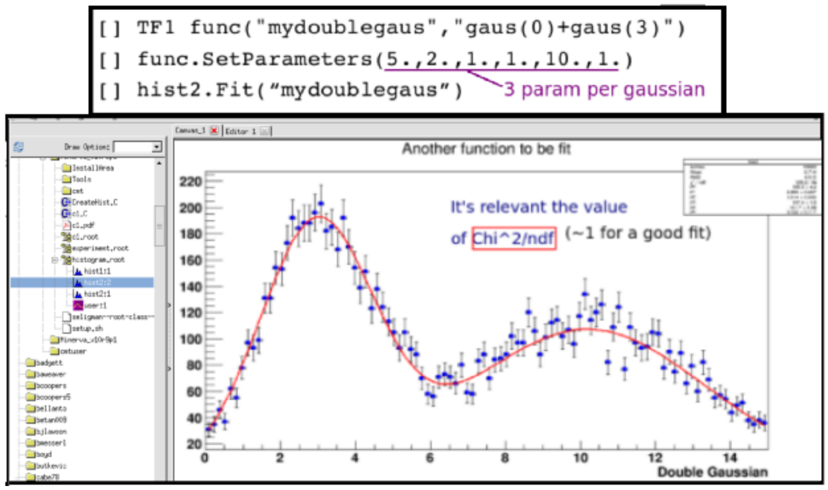


**Figure 3.3:** Definition of the double gaussian function to be fitted in the histogram shown in the TBrowser.

It is possible to open a File with ROOT commands, do any modification we want and then save the File with these modifications. It is sometimes useful to open a ROOT File contaning a Tree and analyze the Tree (containing many Branches) interactively before creating a Macro for a more specific analysis. Figure 3.4 shows the way to open a File and save the modifications and also some basic commands to analyze a Tree (it is possible to add many Trees, each comming from a specific root file, into what is called a Chain, as is explained below).

```
[] TFile file1("histogram.root","UPDATE")   Opening the File "histogram.root"
[] hist2.Draw()                             which contains the C++ object
[] TF1 func("user","gaus(0)+gaus(3)")       hist2 (a certain histogram)
[] func.SetParameters(5.,2.,1.,1.,10.,1.)
[] hist2.Fit("user")   The Write() command
[] hist2.Write()       permits us to Save the
[] func.Write()        fitted function.
[] file1.Close()
[] tree1->Scan() (To display the TTree-data)
[] tree1->Print() (display only the name of vars & size of TTree)
[] tree1->Draw("ebeam")(to create a histogram of 1 var.)
[] tree1->Draw("ebeam:px") (scatterplot, to measure correlations)
[] tree1->Draw("zv","zv<20")    (To perform specific cuts )
[] tree1->Draw("ebeam","zv<20")
[] tree1->Draw("ebeam","px>10 && zv<20")
```

**Figure 3.4:** A way to open a root file and save modifications (above), and some commands that can be applied to a root file containing a Tree (below).

So until now we have seen how some basic commands can be written down in the ROOT command prompt to plot functions, construct, fill and fit histograms, and make some cuts in a Tree. However, to perform an analysis we usually require to work with many histograms, apply multiple cuts (usually we open many Trees into a Chain and loop over all Events there), plot many histograms or functions of interest and save our results into a (PDF) file.

For that reason ROOT provides a method (actually a C++ function) called **MakeClass()**, which creates 2 files in the working directory: a **.h** file which contains the body of a polymorphic class with the name we wish and a **.C** file which contains the body of the virtual function (member of the previous mentioned class) called **Loop()**, is inside this file that we can make histograms of 1 or more quantities we seek to analyze, draw scatterplots to find correlations (and in that way perform cuts), calculate our own (derived) variables (eg. Transverse momentum, angle made by the beam), apply specific cuts to calculate the frequency of a given conditional event and reject events with high $\chi^2$, write histogram to a File (instead of showing them directly), among many other things relevant for our analysis. Figure 3.5 shows the way in which an analysis class is created and the way to run the code inside the .C file which consists of 3 main parts: 1)Set-Up: Open files, define variables, create histograms, etc; 2)Loop: for each event in the Tree or Chain perform some taks, calculate values, apply cuts, fill histograms, etc; 3)Wrap-Up: display results, save histograms.

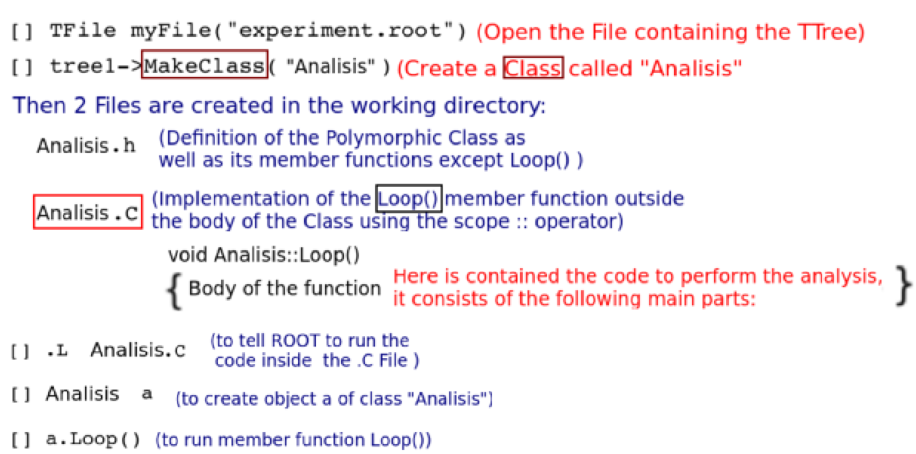


**Figure 3.5:** A way to open a root file containing a Tree, create an analysis class to perform analysis on that Tree and run the .C file.

The way to perform an analysis using the C++ approach (which uses a lot of pointers to objects) is very important, specially when doing a more complex analysis which involves the usage of Gaudi (when one needs to create a new branch not in the avaible DSTs); However, for a basic analysis it is often easier to use pyroot (python with the ROOT libraries imported), in this way it is not necessary to use pointers but just the objects themselves. When using pyroot it is not necessary to rely in the MakeClass() command, we just import ROOT libraries and start looking at the DST's (root files containing Trees) Branches. For all the analysis presented in this thesis pyroot codes (except for some plots of data with errors) were used with the following characteristics:

*A python Class (HTML) and a function (DrGranCoolTool) were created to be able to construct HTML-Files (Arachne-Links) of the events of interest to see how those selected events look at the detector.

*The usage of dictionaries was important for several reasons like keeping histograms and Arachne-Links for different folders (keys of the dictionaries) and for constructing histograms of new (user-defined) variables, like the total Energy deposited in the Detector and the value of dE/dx for a given module of the detector.

*Many cuts were used that ensure physical things like: the beam was on, there was activity in the detector, the event occurred in the trigger slice (more about the slices in Section 3.3), the time interval in the ToF was fixed (to separate pions and protons for example), the total value of energy deposited was in a given range (to separate muons from pions for example)

So the pyroot scripts used for the particle-ID analysis permit us not only to construct histograms (for different energies, which means root files in different folders) of the events of interest (and save those histograms in a PDF file) but also to construct Arachne Links for those events to be able to perform an eye-scanning and test in that way how efficient were the cuts in separating the particles of our interest.

## 3.2 Interaction of particles passing through matter

From neutrino interactions different kinds of particles are present in the final state, these particles have a specific way in which they deposit energy in the scintillators, lead and steel present in the MINER$\nu$A and Test Beam detectors. The 3 main ways in which particles loss energy as they pass through matter (Figure 3.6) are [88]: **Ionization** (primary mechanism for muons), **Electromagnetic showers** (for photons and electrons) and **Hadronic showers** (for hadrons like pions or protons). The concepts of Radiation and Nuclear Interaction lenghts ($X_0$ & $\lambda_I$) become important because due to its composition, the detector posseses specific values of that parameters in different modules, which imply we will have a particle depositing energy in a certain region with a given probability. This permits to be able to identify a particle based on the way its energy was deposited inside the detector as it passed through it. For example, in the ECAL/HCAL configuration of the TB detector, we expect most electrons to shower in the ECAL region and many pions to shower inside the detector (if they not shower in the ECAL, there is a big chance they will do it in the HCAL).

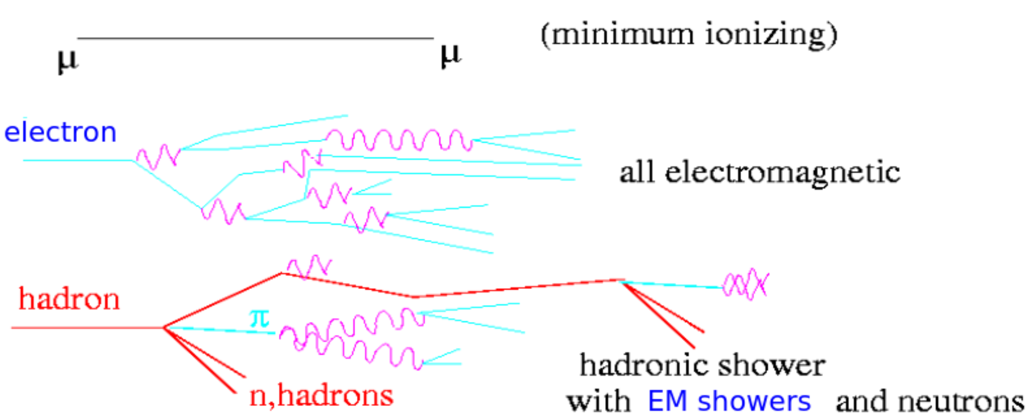


**Figure 3.6:** Three kinds of particle signatures, related to different kinds of interaction.

### 3.2.1 Energy loss by ionization

Primary mechanism for muons in energies of modern neutrino experiments, if a particle is too slow to start producing showers, it will loose energy through ionization. This occurs for hadrons within a distance less than the nuclear interaction lenght ($\lambda_I$) and for electrons within a distance less than the radiation lenght ($X_0$). This kind of energy loss can be used to ID particles in range of momentum, because from the Bethe-Bloch equation $dE/dx = f(\beta = v/c)$, and the value of $dE/dx$ in common detector materials determines how long an event will be in the detector. Figure 3.7 shows the Bethe-Bloch equation and the function $dE/dx$ vs momentum for different kinds of particles (useful for discriminating between hadrons like pions and protons before they shower), it also presents a table of the $dE/dx$ values in common materials used in detectors. For example, in the T2K experiment, to contain a 700MeV muon, it is required 350 cm of water (or scintillator) or 65 cm of steel.

$$\frac{dE}{dx} \propto z^2 \frac{Z}{A} \frac{1}{\beta^2} \left[ \frac{1}{2} \ln \frac{2 m_e c^2 \beta^2 \gamma^2 T_{max}}{I^2} - \beta^2 - \frac{\delta}{2} \right]$$

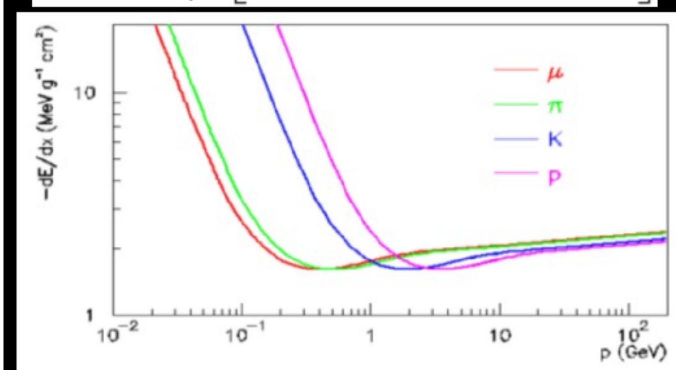


| Detector Material | Minimum Ionizing dE/dx (MeV/cm) |
|---|---|
| Liquid Argon | 2.1 |
| Water | 2.0 |
| Steel | 11.4 |
| Scintillator (CH) | 1.9 |
| Lead | 12.7 |

**Figure 3.7:** From the Bethe-Bloch equation $dE/dx = f(\beta = v/c)$, which permits a particle ID in range of momentum.

### 3.2.2 Electromagnetic Showers

For electrons above the critical energy, they will create photons through Bremsstrahlung which then go on to produce $e^-e^+$ pairs. As those produced $e^+$ and $e^-$ travel, they also will create photons until the energy of particles in the shower goes below the critical energy, then particles lose energy by bremsstrahlung and these last photons do not have enough energy to produce pairs again. The **Radiation lenght** $X_0$ is defined as the distance over which electrons lose $1/e$ of their energy by radiation, this is equivalent to say that roughly, every $X_0$ an electron will emit a photon through bremsstrahlung. The distance over which photons will pair produce is related ($\lambda = 9/7X_0$) and the Transverse EM shower development is determined by the Moliere radius. Figure 3.8 shows some of these relations and a table with the values of $X_0$ for different materials.

$$E_C = \frac{800 \text{ MeV}}{Z + 1.2}$$

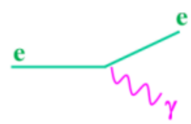


$$X_0 = \frac{716.4A}{Z(Z+1)\ln(287/\sqrt{Z})} \left[\frac{\text{g}}{\text{cm}^2}\right]$$

Moliere radius $R_M = X_0 \frac{21.2 \text{ MeV}}{E_C}$

| Material | $X_0$ (cm) |
|---|---|
| Liquid Argon | 14 |
| Water | 37 |
| Steel | 1.76 |
| Scintillator (CH) | 42 |
| Lead | 0.56 |

**Figure 3.8:** Critical energy for an electron above which starts to shower, value of $X_0$ as a function of the atomic number $Z$, Moliere radius and table of $X_0$ for different materials.

### 3.2.3 Hadronic Showers

Similar to electromagnetic showers, but different underlying interaction means vital statistics are different (here there is strong interaction beside the EM one). Instead of a radiation length, now there is a **Nuclear Interaction Length** $\lambda_I$ defined by the average distance a hadron travels before it undergoes a strong (nuclear) interaction. It is relevant to keep in mind that sometimes neutral pions are produced which decay to photons which then proceed electromagnetically and that sometimes neutrons are made in the shower, which then may show no visible energy in the detector.

Radiation lenghts are always shorter than Nuclear interaction lenghts and EM showers are shorter and narrower than hadronics, for incoming particles of the same energy. If we look at the dependence of these parameters on the materials the nuclear interaction probability is a function of the atomic number $A$, whereas the electromagnetic interaction probability follows a dependence of the form $A/Z^2$. Figure 3.9 presents some features of this interaction and a table with the energy dependence of the different interactions for different particles (showing their primary energy loss mechanism).

| Particle | Characteristic Length | Dependence |
|---|---|---|
| Electrons | Radiation length ($X_o$) | Log(E) |
| Hadrons | Interaction length ($\lambda_{INT}$) | Log(E) |
| Muons | dE/dx | E |
| Taus | Decays first | $\gamma ct = \gamma 87 \mu m$ |

| Material | $X_o$ (cm) | $\lambda_{INT}$(cm) | $\frac{dE}{dx}$ (MeV/cm) | Density (g/cm$^3$) |
|---|---|---|---|---|
| Liquid Argon | 14 | 83.5 | 2.1 | 1.4 |
| Water | 37 | 83.6 | 2.0 | 1 |
| Steel | 1.76 | 17 | 11.4 | 7.87 |
| Scintillator (CH) | 42 | ~80 | 1.9 | 1 |
| Lead | 0.56 | 17 | 12.7 | 11.4 |

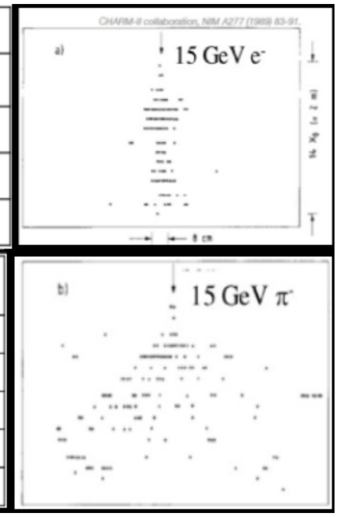


**Figure 3.9:** Table showing the characteristic lenghts for different particles, values of these lenghts for different materials and a comparison of an EM (electrons) and a hadronic shower (pions) for particles of the same energy (15GeV).

## 3.3 Importance of the eye-scanning (Arachne)

As it was previously stated, once we are able to retain events of interest (performing cuts) it is usually important to see how those events look at the detector. Considering the way in which different particles species deposit energy, we expect to see a difference between them. As a particle passes through the detector it deposits energy in different modules, so there is a specific number of hits in different strips for a given module (a module is a plane in the TB), it means that is possible to have a visualization of the tracks of particles by assigning a color intensity to a given strip proportional to the number of hits (and photoelectrons, PE) on it.

It is relevant to point out what we mean by a specific event: when data is taken we consider many Runs, for each Run there are many other Subruns, for each subrun there are many gates (see Section 1.4.2) and for each gate (which lasts for $\sim 16\mu s$) there can be many events taking place. We consider an event to take place inside the detector if there is enough energy deposited, so for a given gate we have many slices (intervals over which the previous condition holds) and we are usually interested in the Triggered Slices (the slice that represents the events that fired the Trigger). Figure 3.10 shows some slices for a given gate, one of those slices represent the event that made the Trigger to fire (for the TB).

The activity taking place inside the detector is visually represented with a web-based tool called

Arachne. Data are retrieved from a central server via AJAX, and client-side JavaScript draws images into the user's browser window using the draft HTML 5 standard. These technologies allow neutrino interactions in the MINER$\nu$A main detector and passage of particles in the TB detector to be viewed by anyone with a web browser, allowing for easy eye-scanning of particle interactions [85].

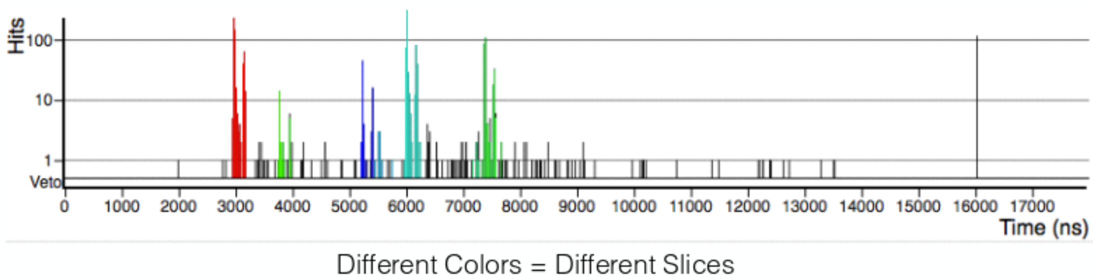


**Figure 3.10:** We look for concentrations of hits in time and divide those into things called "slices", which represent physical events. One of them corresponds to the triggered slice.

In the python scripts used for the particle-ID analysis there is a class called HTML and a function called DrGranCoolTool, that permits us to create Arachne-Links of events of interest. The **most important condition for these events to be physically meaningful is that they occurred in the triggered slice**, this piece of code is mandatory and goes beside any other cut one is interested in performing (more details about this in Chapter 4). The Arachne-Link for each event also indicates the Run/Subrun/Gate and Tiggered Slice for the event of interest. In that link one can see the number of hits, total PE in each strip for each module and also the track of the particle in 3 different views: XZ, UZ and VZ (related to the planes U, V and X discussed in Section 1.4.1).

Considering the way in which different particle species deposit energy in the detector (Section 3.2) and the lengths $X_0$ and $\lambda_I$ for the TB detector components in the ECAL/HCAL configuration (see Section 1.4.3) we can calcuate the survival probabilities of electrons and pions (survival means they passed along the whole detector whithout showering). For example, in the ECAL (8.17 radiation lengths and 0.77 interaction lengths) the Probability(An electron not shower in the ECAL)= exp(-8.17)$\sim$ $0.03\%$ and the Probability(A pion not shower in the

ECAL)= exp(-0.77)$\sim$ 46%. This means that almost all electrons will shower in the ECAL and that 54% pions shower in the ECAL, the remaining 46% will shower in the HCAL or pass through the whole detector without showering and so looking like a muon. Figure 3.11 presents a table with the accumulated radiation and interaction lengths for the TB detector in ECAL/HCAL configuration and probabilities of survival for electrons and muons in each part of the detector.

| | ECAL | HCAL |
|---|---|---|
| Accumulated radiation lengths through volume | 8.17 | 38.64 |
| Electron survival probability through volume | $e^{-8.17} \approx 0.028\%$ | $e^{-38.64} \approx$ Insignificant |
| Accumulated interaction lengths through volume | 0.77 | 4.36 |
| Pion survival probability through volume | $e^{-0.77} \approx 46\%$ | $e^{-4.36} \approx 1.3\%$ |

**Figure 3.11:** Total radiation and nuclear interaction lenghts for the ECAL & HCAL parts of the TB detector and probabilities of survival for electrons and protons in each region.

Now we can look at how we expect to look in the detector the tracks for different particles (Figure 3.12): A beam muon does not shower so will look like a straight line that passes along the whole detector. A pion may shower in the ECAL or HCAL so we expect a certain initial regime in which it deposites energy like a muon (via $dE/dx$) but a point in which it showers. An electron will certainly shower in the ECAL region and we do not expect to see any region in which it looks like a muon considering that the energy (8GeV) is certainly above the critical needed for the electron to start showering. A proton may be more difficult to locate since it will look like pion; however, before showering it has a greater value of dE/dx so we would expect to see a darker color. There maybe events which do not have any specific pattern but for that reason one always makes a spreadsheet to count events and see if we have enough events of interest for our cuts to be reliable. Chapter 4 presents some of these spreadsheets for an eye-scanning of events (contamination) between the proton and pion peaks.

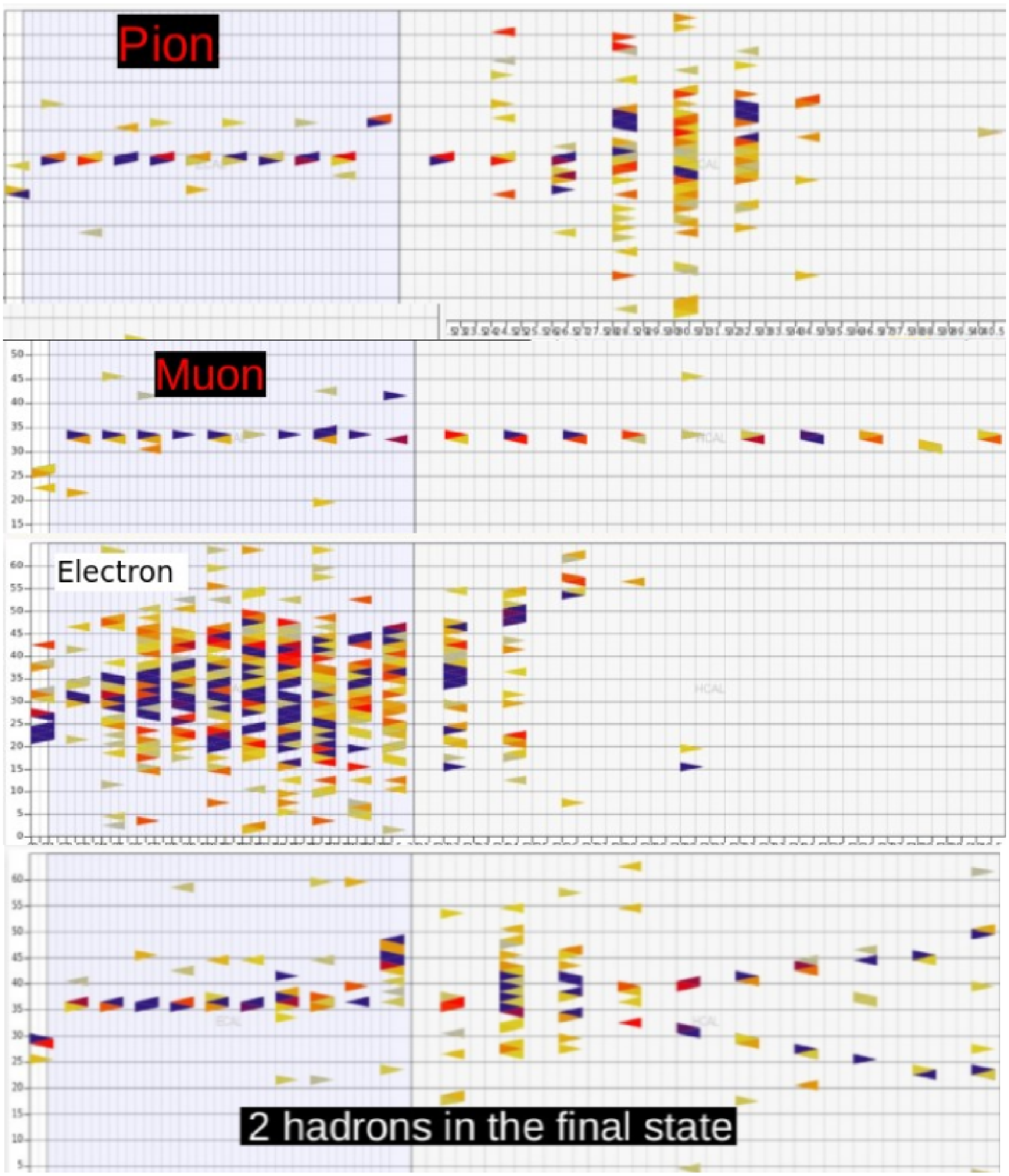


**Figure 3.12:** Different tracks in the TB Detector (in ECAL/HCAL configuration) for different particles passing through it, as is seen in Arachne for a given view (XZ).

# Chapter 4

# Initial Results (& Technical issues) in the ID of particles composing the secondary beam

The goal of a particle ID analysis is to develop tools (scripts) for the identification of particle species, in this particular case for particles composing the secondary beam used by the MINER$\nu$A collaboration for their Test-Beam-2 effort. The way this secondary beam is generated and the elements along its beamline were already explained in Section 1.3. It is important to present results on the percentage of different particles species ($\%\ p^{\pm}, \pi^{\pm}, \mu^{\pm}, e^{\pm}$) in the secondary beam, that information is useful both for MINER$\nu$A and for the Acceleration Division. Right now there is not yet a Monte Carlo simulation of this beam (it is still in progress) so it would be interesting to make comparisons between these results using current Data and the predictions of that simulation (when it is ready) regarding the composition of the beam.

It is relevant to say that for this analysis one looks at DSTs (root files) in specific folders that indicate: the configuration of the TB Detector (Data-Run-1 or Data-Run-2), the specific energy, the "type" of beam (composed mainly by pions or electrons) and its polarity (beam composed of positive or negative particles). For this early results only Pion-Folders were analyzed, to get this data we put a Lead Shield and use the Cerenkov to reject electrons and get only pions, with some protons (always present, that are separate using the ToF system) and muons (which come mainly from the decay of pions).

The scripts for doing this analysis are written in pyroot (python with the import of ROOT libraries) and use specific functions related to the Detector configuration (like the ModuleMultipler function, line 47 of Appendix-A), a function to generate Arachne links of selected events (DrGranCoolTool function, line 32 of Appendix-A) and loops to perform important tasks like for example to add many Trees (each one belonging to a specific DST in a specific Folder) into a Chain to loop over all events in the Folder (line 133 of Appendix-A). The branches of interest are related to the Time of Flight ($ToF\_quality$ & $ToF\_measured\_time$), the Veto (the 12 counters and the $Veto\_Count$ branch) and the Detector (number of hits, PE and module of a specific hit, etc) devices.

In this Chapter we review the initial procedure followed, starting from the construction of the ToF histograms (where we can isolate the protons), the scanning of the events between the pion and proton peaks (contamination interval), some ways in which we can separate the muons from the pions in the pion peak, a way to visualize the spatial distribution of the beam by looking at the Veto Counters, the importance of the Veto in the events of interest and the efficiency of the mandatory cuts (which isolate the events physically meaningful). All results presented are discussed and the pieces of code relevant to get them (the specific lines) are referred so they can be found in the respective Appendix.

## 4.1 Main Cuts used in the scripts

To retain events of interest there are some mandatory cuts beside those related to ToF, this is because we require the beam to be ON ($event.In\_spill > 0.5$), that there is activity in the detector ($event.n\_slices > 0$) and the event to take place in the triggered slice (conditions if triggered and if sliced to be true, as shown in lines 184 and 194 of Appendix-A). After that we require that All 6 PMTs in the ToF stations to send a signal (which represent the greates amount of information from the ToF device), this requirement is fullfilled if we only take events for which $event.ToF\_quality == 1$. The meaning of this branch is the following:

$ToF\_quality == 1$: All 6 PMTs with hits

$ToF\_quality == 2$: 3 upstream, 2 downstream

$ToF\_quality == 3$: 4 upstream, 1 downstream

$ToF\_quality == 4$: 3 upstream, 1 downstream

$ToF\_quality == 5$: 4 upstream, 0 downstream

$ToF\_quality == 6$: 3 upstream, 0 downstream

and anything that doesn't fall into those categories has quality score 7 (the worst condition in which there were no hits in any PMT). After retaining these good ToF events we can fill a histogram containing them. These histograms are shown in the next Section for both Data-Run-1 and Data-Run-2. They clearly show the proton and pion peaks separated (for energies below 8GeV) which means that we can perform a time cut to isolate protons and pions (with muons also there), and that there is also some contamination between them. At this stage stage the Veto was not taken into account (the piece of code related to it is commented, as shown in line 41 of Appendix-A) because as the ToF stations and the Veto paddles almost don't overlap in space, so we though the effect of the Veto (to reject events in which the Veto fire, which means we only consider single-particle events) was going to be negligible, but it is not the case as discussed in Section 4.6.

It is relevant to indicate that the script in Appendix-A is written to construct histograms for Data-Run-1 folders, if we want to do the same for Data-Run-2 we need to modify the ModuleMultipler function to consider passive material in the other configuration of the detector, choose other list of directories (line 94), choose other address where the files are located (line 119), change the name of the pdf file to be created (line 204) and of course to replace by “Run2” everywhere we see “Run1 ” written down.

## 4.2 Application of the scripts to Data Run 1 & 2. Interpretation of Results

Below are the ToF histograms (in logarithmic scale) of the Pion-folders for both Data-Run-1 and Data-Run-2, the contamination interval (containing unknown events), which is located between the pion and proton peaks, is also indicated for each of the folders. For each of the histograms the contamination interval was already located, there we can perform a time-cut (to restrict the branch $ToF\_measured\_time$ to be in a certain interval) and save Arachne links of those events to perform an eye-scanning.

**Data-Run-1 ToF histograms**

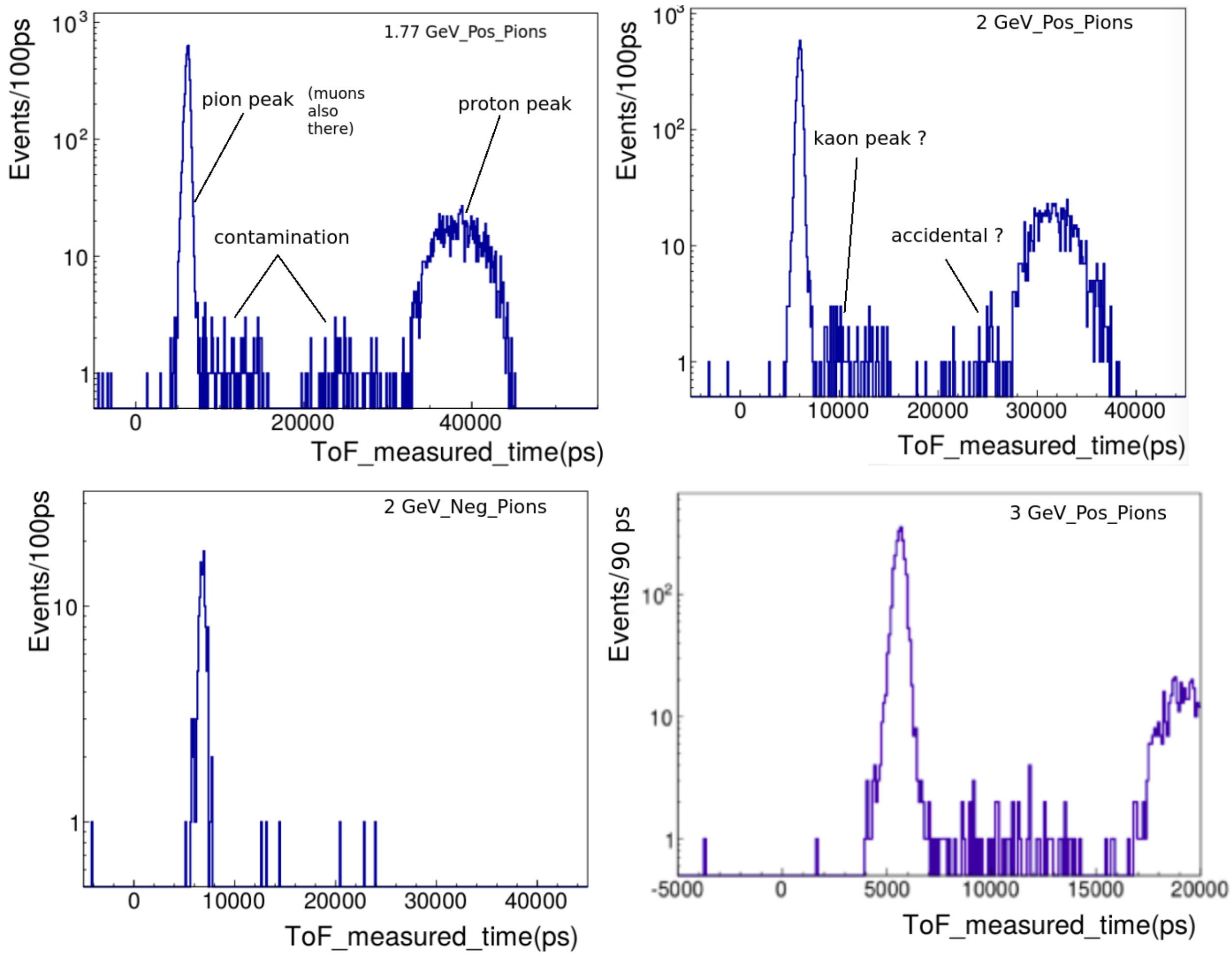


**Figure 4.1:** ToF histograms for events in the $1.77GeV\_Pos\_Pions$ (contamination interval $\sim$ $[9\ 000, 30\ 000](ps)$), $2GeV\_Pos\_Pions$ (contamination interval $\sim$ $[7\ 500, 20\ 600](ps)$), $2GeV\_Neg\_Pions$ (contamination interval $\sim$?) and $3GeV\_Pos\_Pions$ (contamination interval $\sim$ $[7\ 500, 15\ 000](ps)$) folders (Data-Run-1). There was no data for negative runs neither for the 1.77GeV nor for the 3 GeV samples.

Figure 4.1 shows the ToF histograms for low energy samples, we notice that for positive runs it is possible to distinguish clearly the pion (left) and proton (right) peaks and also the contamination present in between. For negative runs it is more difficult to locate the proton peak (and also the contamination interval) because the production rate for antiprotons is smaller than the one corresponding to protons & they are less stable. It is also generally more difficult to get negative data, so the statistics is worse (as can be seen in the $2GeV\_Neg\_Pions$ sample) and in other cases it was not possible (for 1.77 and 3 GeV samples) to take this data.

It is noticeable that for low energy samples there is a signal at the right of the pion peak that ends at 15 ns, a region where we would expect to find a peak for kaons (although there is no such a peak) so we still need to study more about the composition of the contamination to tell what is actually in between those peaks.

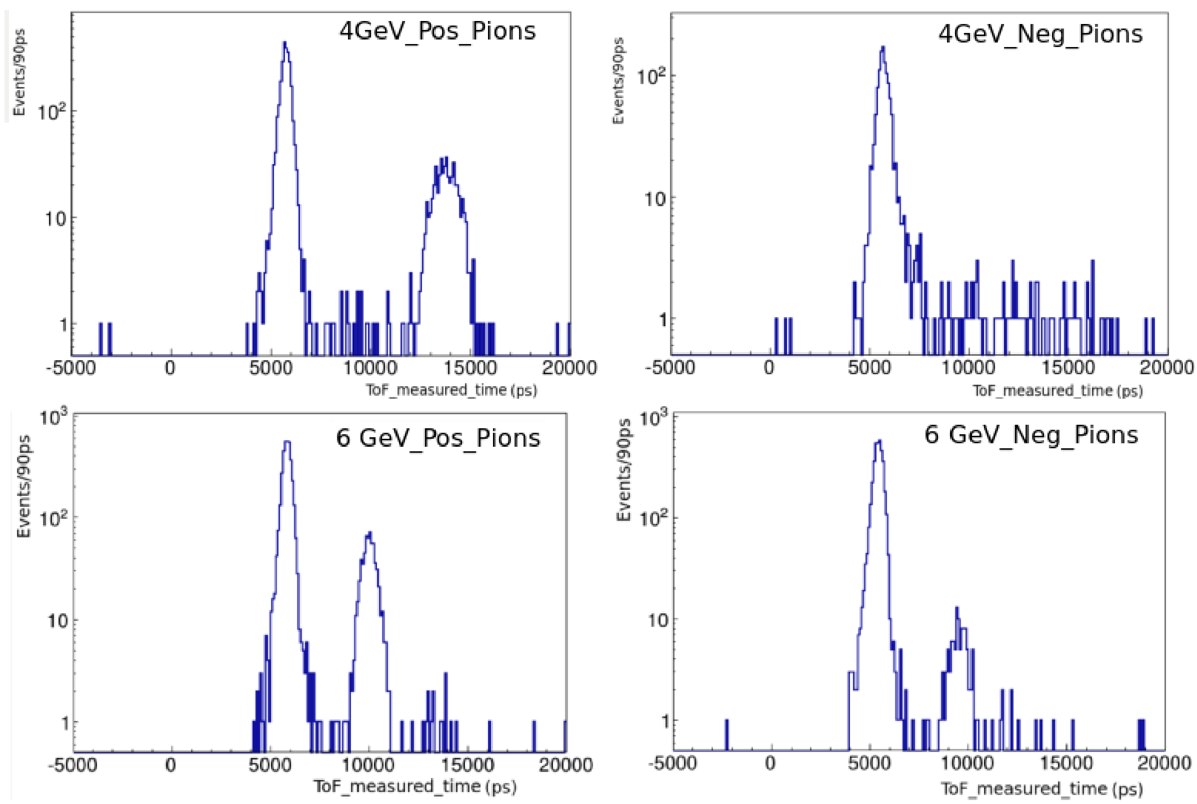


**Figure 4.2:** ToF histograms for events in the $4GeV\_Pos\_Pions$ (contamination interval $\sim$ $[7\ 500, 11\ 500](ps)$), $4GeV\_Neg\_Pions$ (contamination interval $\sim$ $[8\ 200, 11\ 000](ps)$), $6GeV\_Pos\_Pions$ (contamination interval $\sim$ $[7\ 500, 8\ 500](ps)$) and $6GeV\_Neg\_Pions$ (contamination interval $\sim$ $[7\ 000, 8\ 200](ps)$) folders (Data-Run-1).

Figure 4.2 shows ToF histograms for a kind of medium energies, the 2 main peaks are more noticeable for most of the folders, except for the $4GeV\_Neg\_Pions$ where the antiproton peak is not noticeable. We notice immediately that the production rate for antimatter is lower (or just antiprotons are less stable) so we have less antiprotons than protons produced (look at the 6GeV histograms).

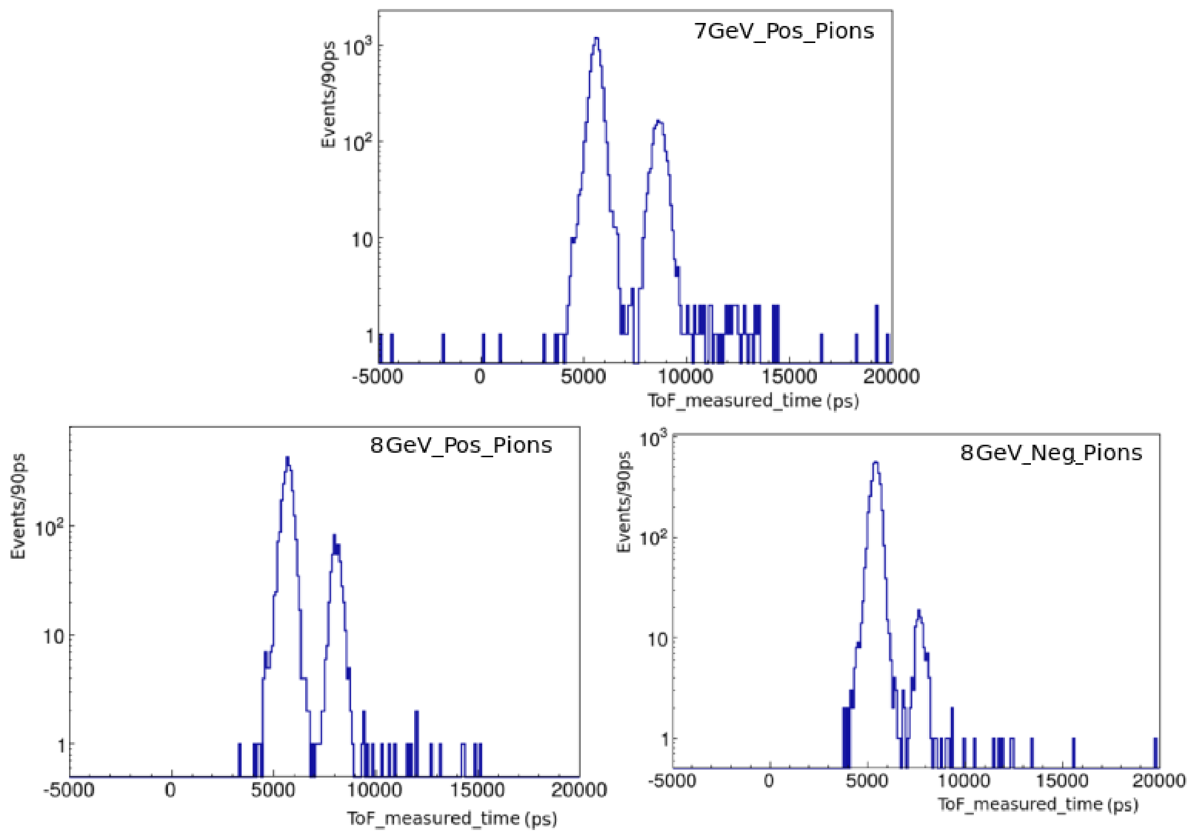


**Figure 4.3:** ToF histograms for events in the $7GeV\_Pos\_Pions$ (small contamination interval $\sim$ $[7\ 000, 7\ 500](ps)$), $8GeV\_Pos\_Pions$ and $8GeV\_Neg\_Pions$ folders (Data-Run-1).

Figure 4.3 shows the ToF histograms for higher energies, we notice that there is almost no contamination interval and that the pion and proton peaks approach each other as the energy increases, in the ultrarelativistic limit the difference between the 2 peaks is of the order of the resolution of the system ($\sim\ 100ps$). We notice that as the energy increases we tend to have more protons (and antiprotons) being produced, there may be that some protons come from upstream and some from the Al target. Until now we can make a fit on both peaks and estimate the number of events (particles) in each of them and perform an eye-scanning of the events in the indicated contamination intervals, the only issue to determine until now is if we are actually considering one particles events or not (**because the effect of the Veto was not considered yet**) and how to determine the number of muons in the pion peak for each case (energy and polarity of the beam). For energies greater than 8GeV it is not possible to separate protons and pions using ToF (nor using dE/dx) but fortunately at those energies other process (DIS) dominates the neutrino interaction inside the MINER$\nu$A main detector.

**Data-Run-2 ToF histograms**

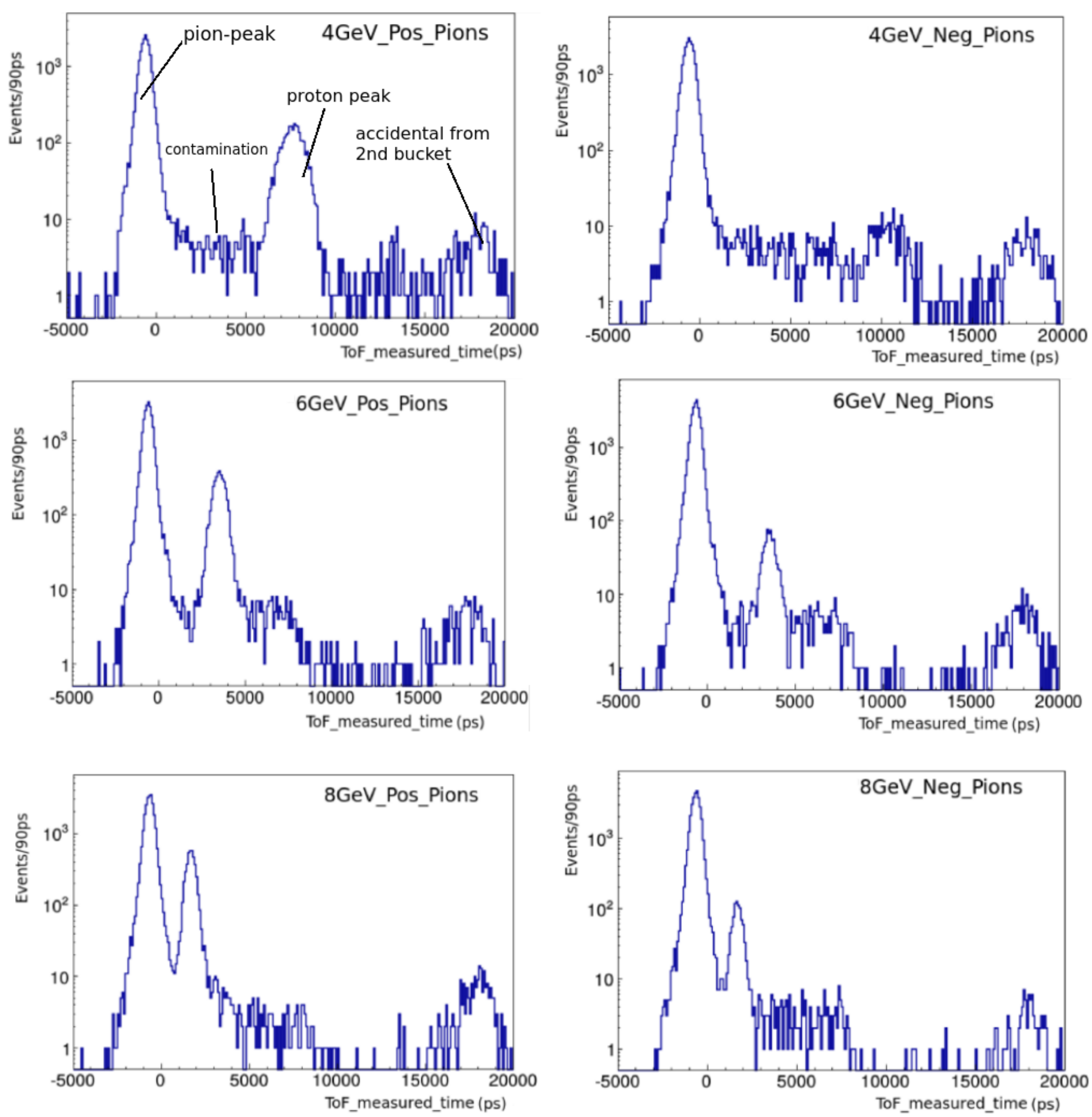


**Figure 4.4:** ToF histograms for events in the indicated folders for 4, 6, and 8 GeV (Data-Run-2) for both positive and negative polarities.

Figure 4.4 shows the ToF histograms for Data-Run-2 folders, there we can see clearly the proton (antiproton) peaks for each energy, the contamination interval (which decreases as the energy increases), and some accidental peaks which may be due to particles from the beginning of the second bucket, this is conceiveable because each bucket time interval is of $\sim 19\ 000ps$ and the time interval presented in the histograms is of $\sim 25\ 000ps$.

The contamination intervals for Data-Run-2 histograms are the following: For $4GeV\_Pos\_Pions$ $\sim\ [2\ 000, 5\ 000](ps)$, for $4GeV\_Neg\_Pions \sim\ [2\ 500, 4\ 000](ps)$, for $6GeV\_Pos\_Pions$ $\sim [1\ 500, 2\ 500](ps)$ and for $6GeV\_Neg\_Pions \sim [1\ 300, 2\ 000](ps)$. For the 8GeV samples it is not possible to choose a contamination interval because the 2 peaks almost merge each other.

## 4.3 Analysis of the contamination between the $\pi$ & $p$ peaks in the ToF histograms

Using the fact that the script permits to create Arachne links for the selected events and that we already know what is the pattern of the energy deposited in the detector by charged particles passing through it (Section 3.3), we can eye-scan events in the contamination interval and fill a spreadsheet with the kinds of particles we expect to find there to calculate their frequencies. Below are some results of the contamination scanning just for the $4GeV$ samples for Data-Run-2. Figure 4.5 shows the selected contamination-histograms and the spreadsheets indicating the number of events (and frequency) of each kind. We can see that almost half of those events corresponds to muons, for the $Pos$ sample 114 Events were scanned and for the $Neg$ one a total of 83 Events.

Something that was not expected was the outcome of some cosmic muons in the sample (these look like a muon but appear at a high angle with respect to the axis of the beam). This was not expected because for an event to appear in the histograms it had to made the trigger fire (so pass along the 3 scintillators as explained in Section 1.3) and the 2 ToF stations to fire, this means that the particles should have passed along a straight line and certainly not look like a cosmic muon; however, here are some hypotheses for them to appear:

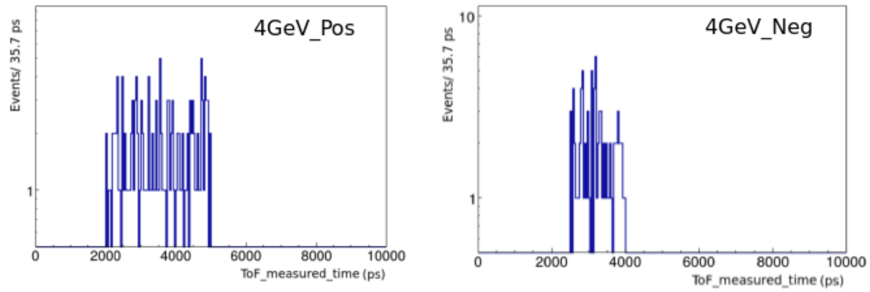


| | Pion-Shape | Muon Beam | Muon Cosmic | Muon (s) beside other particle | electrons | Junk | Low-Activity |
|---|---|---|---|---|---|---|---|
| Number of Events-----> | 28 | 7 | 9 | 24 | 2 | 1 | 12 |
| Percentage------> | 33.7349 | 8.4337 | 10.8434 | 28.9157 | 2.4096 | 1.2048 | 14.4578 |
| | Total % of muons ~48.19% (Considering Junk and Low-Activity Events in total Number of Events) | | | | | | |
| | Total % of muons ~56% (Rejecting Junk and Low-Activity Events in total Number of Events) | | | | | | |

| | Pion-Shape | Muon Beam | Muon Cosmic | 1 or 2-Muons beside other particle | electrons | Junk | Few-Activity |
|---|---|---|---|---|---|---|---|
| Number of Events | 23 | 13 | 10 | 35 | 4 | 5 | 24 |
| Frequency | 20.1754 | 11.4035 | 8.7719 | 30.7018 | 3.5088 | 4.386 | 21.0526 |
| | Total % of muons ~ 50.877 (Considering Junk and Low-Activity Events in total Number of Events) | | | | | | |
| | Total % of muons ~ 68.235 (Rejecting Junk and Low-Activity Events in total Number of Events) | | | | | | |

**Figure 4.5:** contamination histograms and results from the eye-scanning for the $4GeV$ samples of Data-Run-2. In both cases almost half of the events corresponded to muons.

*A beam-particle fired the trigger and ToF-US, it was scattered between the 2 ToF stations and a cosmic muon hit the ToF-2.

*A beam particle fired the trigger, close both ToF stations but then a cosmic passed through the detector .

*Maybe a pion (which fired the Trigger and both ToF Stations) decayed between the start & stop stations and the product was a muon at a certain angle respect to the direction of the parent pion.

The last hypothesis seems more reasonable because many pions decay in their way to the detector, it is also relevant to notice in the spreadsheets the option **Muon(s) beside other particles** (or **1 or 2 muons beside other particles** ), these are events which present more than 1 particle in the Triggered Slice, a situation I baptized as a **party of particles**, below (see Figure 4.6) are shown 2 examples of these kinds of events.

This means that in our sample there are events containing many particles, and the **Goal of the Test-Beam** is to put a **single particle of known energy & polarity into a smaller version of**

**our Main Detector**. For it was relevant to study correlations between the ToF and the Veto systems and to add an extra condition, which is that the Veto should not fire, to get a more pure sample of single-particle events, which are the actual Events of interest, whose efficiency (what fraction they represent of all available physically meaningful Events) is calculated in Section 4.7.

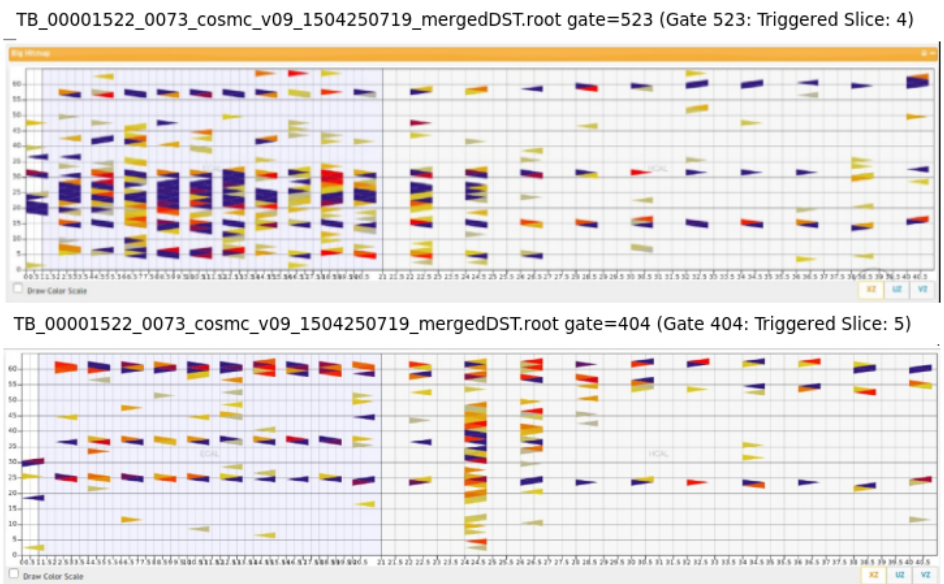


**Figure 4.6:** Party of particles in the scanned sample, maybe because the Veto was not considered (to reject them and select only single-particle Events, as the TB Main Goal demands).

## 4.4 Ideas to isolate $\mu$ from $\pi$

As was indicated above, for both Data-Run 1 & 2, the pion peak for each sample not only contains pions but also muons, because these 2 kinds of particles have almost the same mass (see Figure 1.16 of Section 1.5). Then it is not possible to use ToF to separate the muons there from the pions and we must rely on other tools, like looking at those events in the detector. These tools should exploit the difference in which pions and muons deposit energy in the detector, we expect for example a pion to deposit an almost fixed amount of energy (a narrower distribution) and to pass along the whole detector (activity in the last planes or modules) without showering. A pion will certainly shower in the HCAL region of an ECAL/HCAL configuration if it did not shower in the ECAL (see Figure 3.11 ) and even with more probability in the superHCAL of the second configuration (Figure 4.6 (at the bottom) shows a pion showering in the module corresponding to the HCAL part of the superHCAL).

If we consider (this was a initial hypothesis, which is actually not true) that the probability of a pion to shower inside the detector increases with the decrease in its energy (because it will be more time inside the detector and will have more time to interact and shower) then we can look at events that present activity in the last 4 planes and label them as muons, this would work for low Energy samples (less than 4 GeV). What occurs is that low energy pions deposit less energy which is therefore closer to the energy deposited by muons (muons always deposit less energy because it is deposited only via ionization).

For higher energies however, some energetic pions may not have enough time to interact (again, this was an initial hypothesis!) and will pass along the whole detector looking like a muon, but they will deposit more energy (on average) than a muon, so for high Energy samples a cut in the total-PE (or total energy deposited) will be reliable, as will be presented below (where we verify that this cut works better as the energy increases).

Other interesting variables to look at are the $dE/dx$, which can be calculated for a given module or as an average over all modules and the total number of Hits in a given module (for muons this number is almost always fixed, equal to 2 or 3). Until now, we can separate muon-like from pion-like events using the previous mentioned variables and then calculate their $dE/dx$ to see what would be the pattern to expect for pure samples of muons and pions. Early estimations presented below correspond to $Pos$ samples of Data-Run-2 for 4, 6 and 8 GeV.

### 4.4.1 Cuts in $PE$ & $LP$. Analysis of $dE/dx$ over modules

Above we have discussed the importance of being able to separate the muons present in the pion sample. We can use a PE cut for energies higher than 4GeV to get a sample of almost pure muons and other containing mainly pions and plot a dE/dx histogram over modules to see if we can find a characteristic pattern for each sample. This procedure is outlined below for Data-Run-2 folders of 4, 6 and 8 GeV ($Pos$ samples because they have better statistics).

To calculate the $dE/dx$ for each module (total energy deposited in that module) we can rely on the following formula, considering that each hit took place in a given module and deposited a given value of PE, we can use dictionaries in python (see Appendix-B) as an elegant way to deal with this issue (the keys of the dictionaries are the modules and they stored the energy deposited for that module):

$$\left.\frac{dE}{dx}\right|_{(\text{module\_\{j\}})} = \sum_{\{\ \text{i / event.hit\_module[i] = j}\}} \text{ModuleMultiplier(event.hit\_pe[i],event.hit\_module[i])}$$

The sum is over all hits $i$ that took place in module $j$, note that the Branches $hit\_pe$ and $hit\_module$ are lists containing the values of the PE deposited by hit $i$ and the module (plane in the TB detector) in which that hit occurred, respectively. The lenght of these lists is obviously the total number of hits for the selected event, which equals the value of the Branch $n\_rawhits$. The ModuleMultipler function permits to calculate the actual energy deposited in that module considering a given configuration of the detector, for the analysis presented below it was set in the Tracker/superHCAL configuration (Data-Run-2) and to find the $dE/dx$ values for different modules, dictionaries were used in a clever way.

It is relevant to say that there were 2 different ways in which this analysis was performed, each with a specific procedure but with the same goal in mind.

*In a first stage the events in the pion sample are separated, then a PE cut (which is actually a histogram of the total number of photoelectrons) is performed to isolate muon-like events as indicated in the figures below (inside the green arrows) and the remaining of events were considered as pion-like. Then for each subset of events (muon and pion like) a $dE/dx$ was calculated for each of the modules considering ALL events in the Folder which specifies energy and polarity.

*Since the functions dE/dx vs modules calculated by summing the contributions of ALL events in the folder are not physically meaningful, or, in other words, a 2D histogram of dE/dx which can tell us more information about each individual event is more reliable, it was a second stage in which, to increase the purity of the sample only events near the center of the muon peak were taken a muon-like and events at the right of the pion peak as pion-like. Then with this more pure sample, 2D histograms of dE/dx, total-PE and total-Strips hit were constructed. The code in Appendix-B was actually made for this second stage.

Below are presented the results for the 4, 6 and 8 GeV ($Pos$ polarities) of Data-Run-2 in the following order: First a ToF histogram indicating the interval cut to retain pion and muons, then the PE histogram for these events to be able to separate muon like from pion like events, then the functions dE/dx for the contribution of ALL the events in the folder that passed the previously mentioned cuts (for both muon and pion like events), then are shown 2D histograms for dE/dx, total-PE and total-Hits for almost pure samples (obtained following the procedure mentioned for the second stage).

$*4GeV\_Pos\_Pions$ (Data-Run-2):

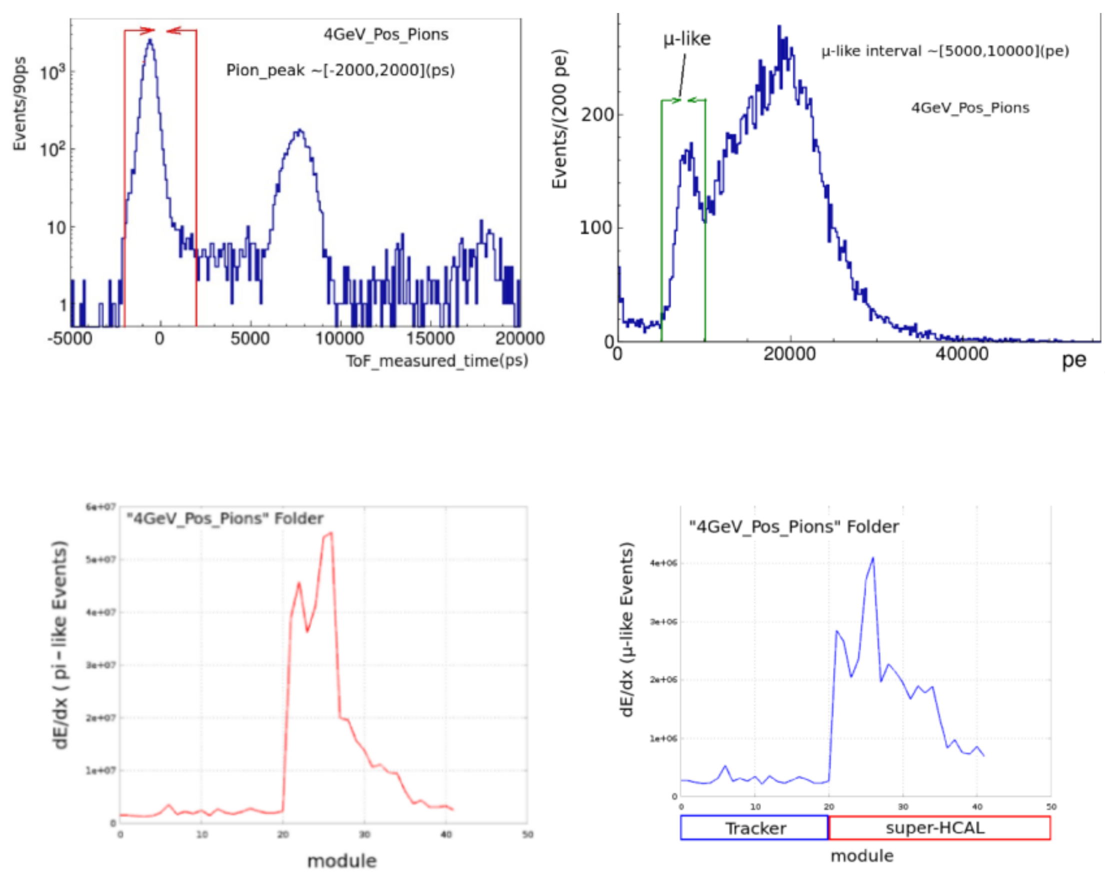


**Figure 4.7:** Cuts to get the muon and pion samples and dE/dx of all those events in the Folder $4GeV\_Pos\_Pions$

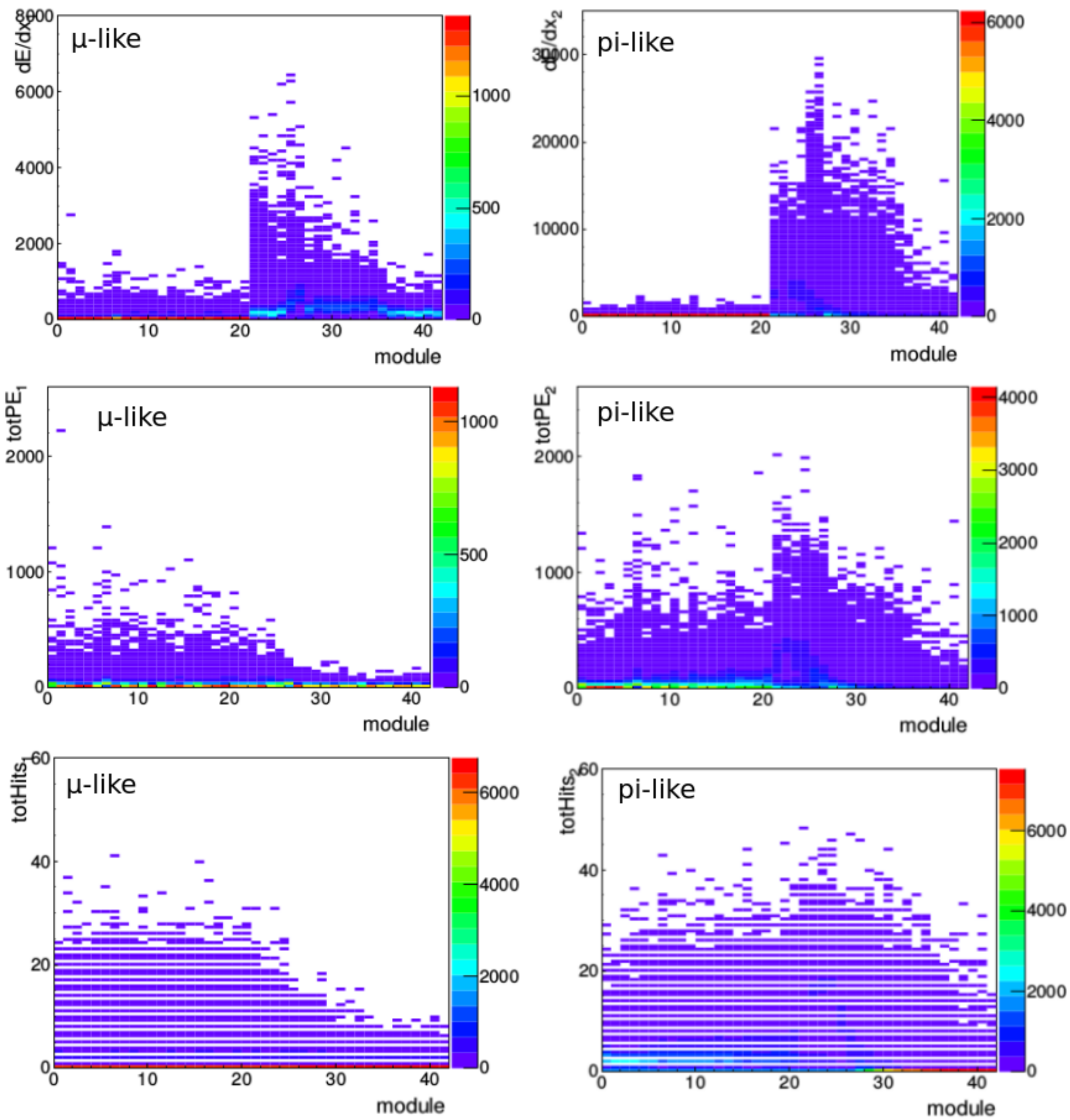


**Figure 4.8:** 2D Histograms of the dE/dx, total PE and total Number of Hits for muon like and pion like Events in the folder $4GeV\_Pos\_Pions$ of Data-Run-2.

$*6GeV\_Pos\_Pions$ (Data-Run-2):

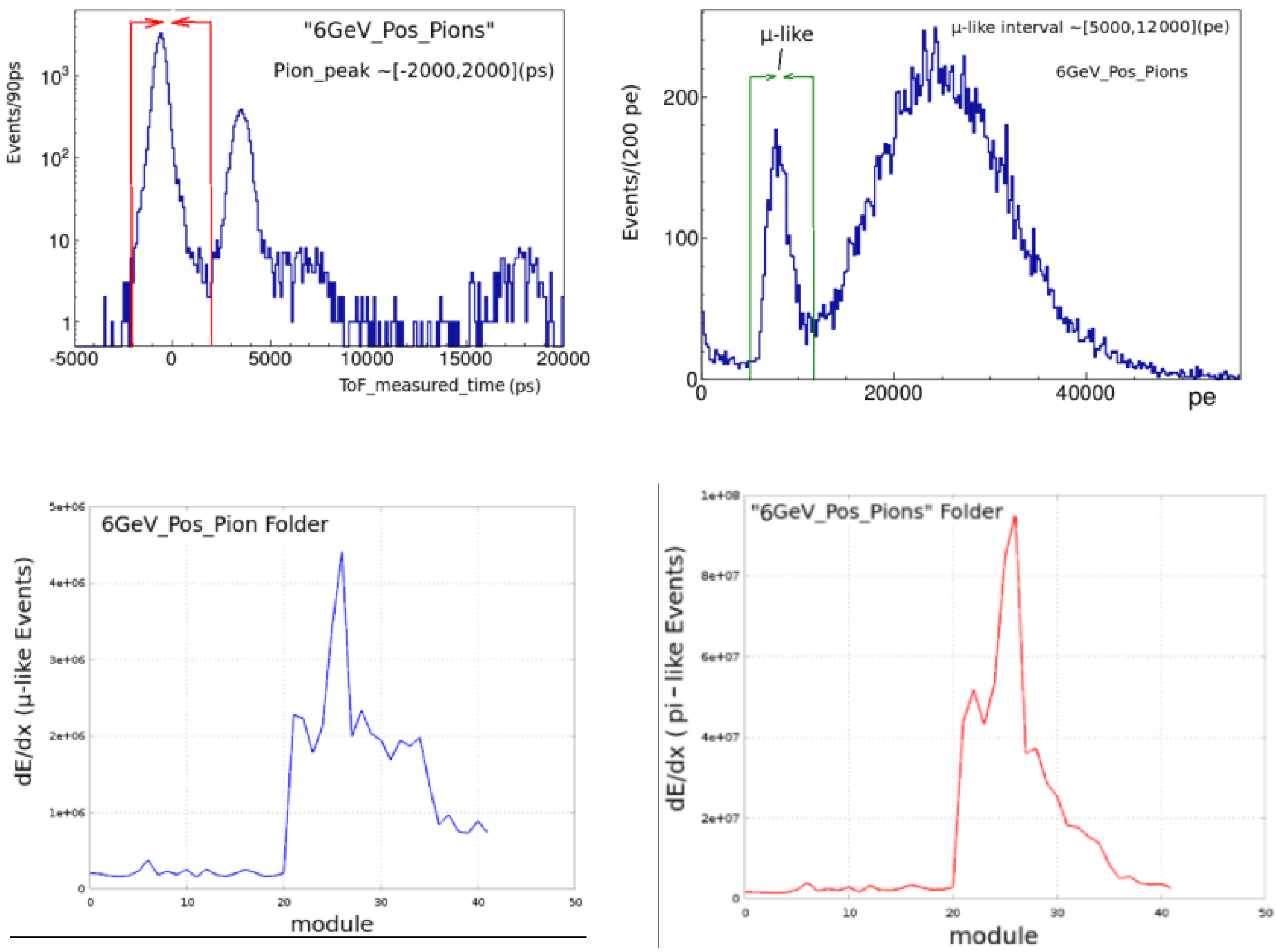


**Figure 4.9:** Cuts to get the muon and pion samples and dE/dx of all those events in the Folder $6GeV\_Pos\_Pions$

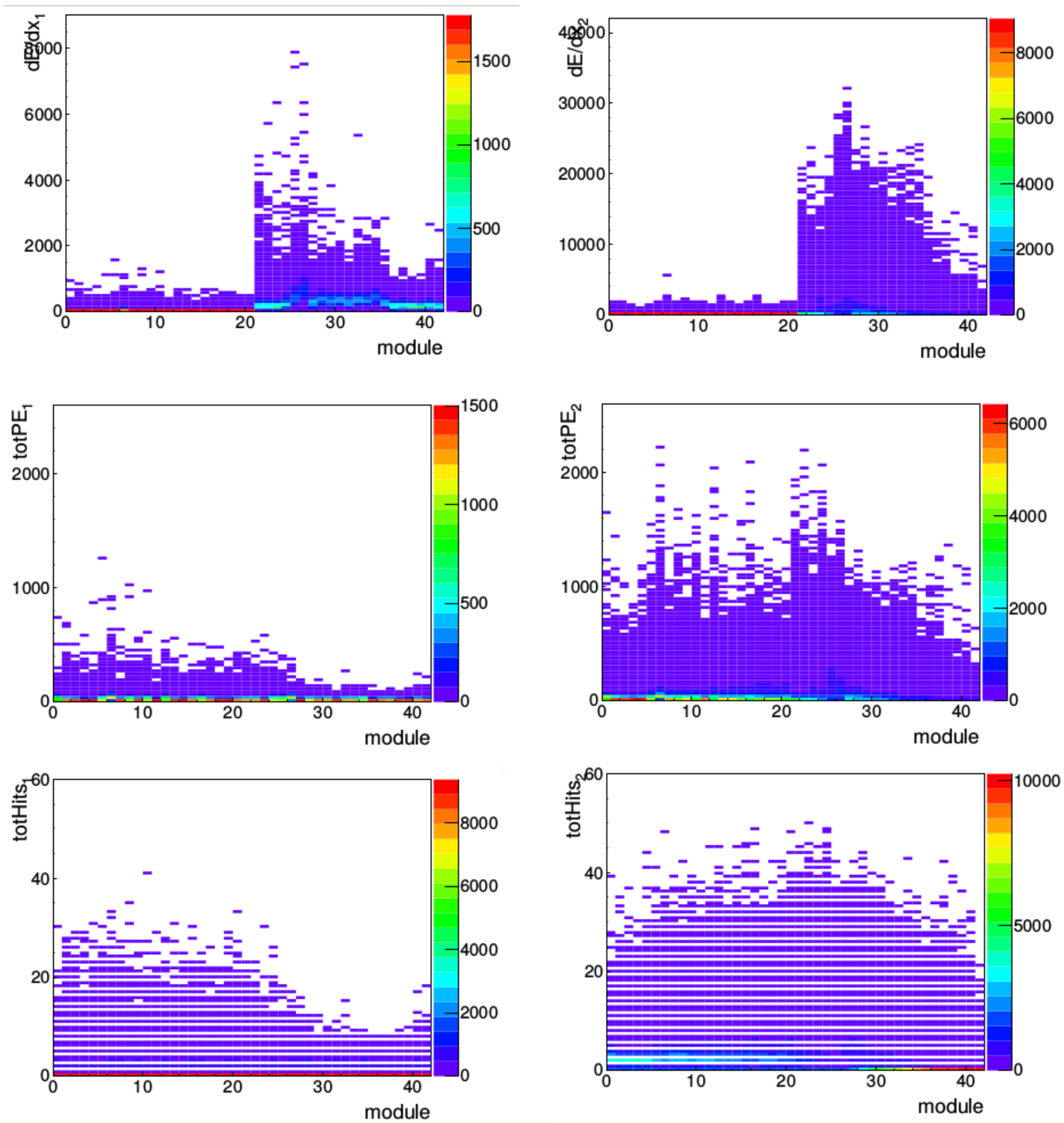


**Figure 4.10:** 2D Histograms of the dE/dx, total PE and total Number of Hits for muon like and pion like Events in the folder $6GeV\_Pos\_Pions$ of Data-Run-2. Pion-like Events at the right & muon-like at the left.

$*8GeV\_Pos\_Pions$ (Data-Run-2):

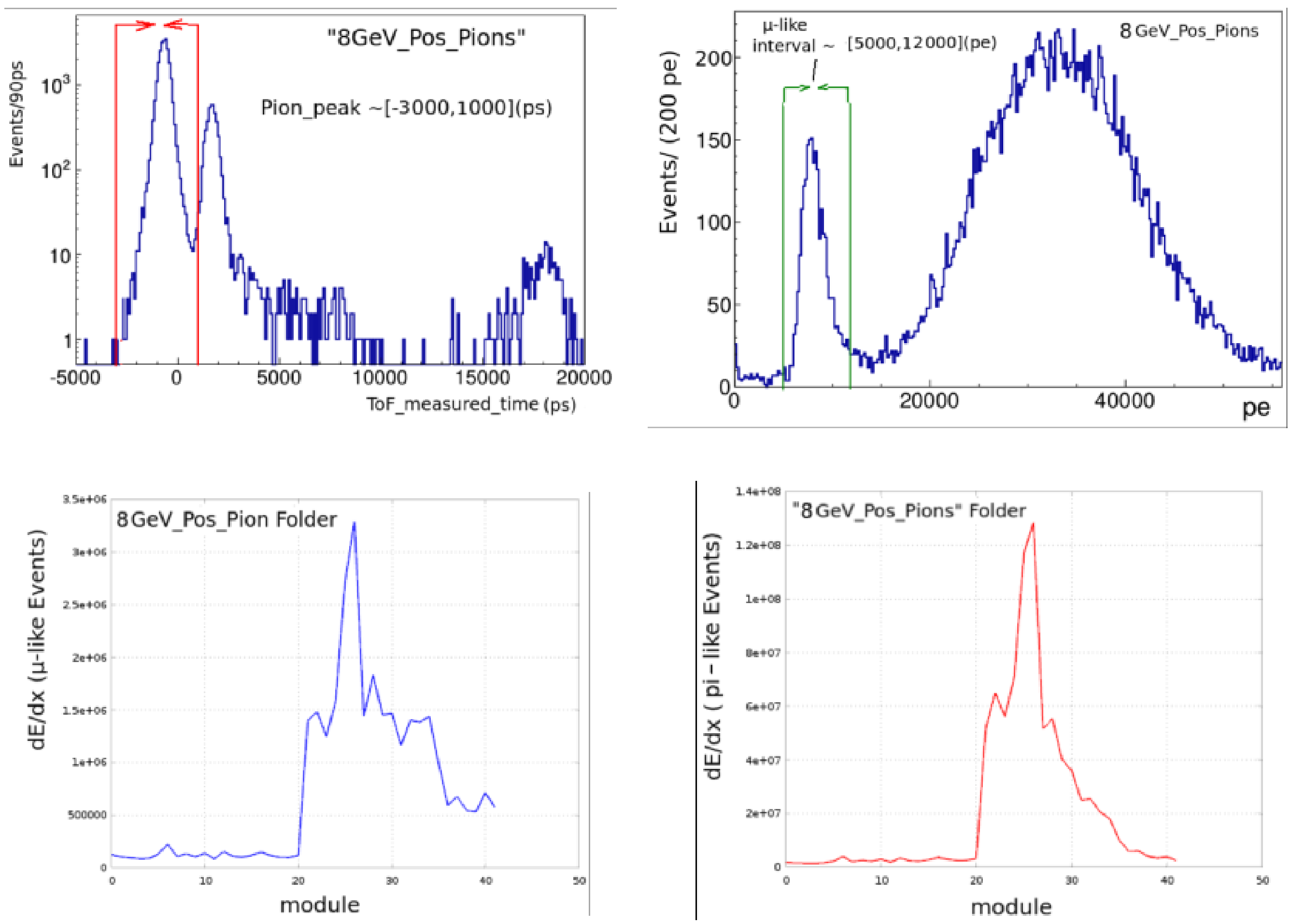


**Figure 4.11:** Cuts to get the muon and pion samples and dE/dx of all those events in the Folder $8GeV\_Pos\_Pions$

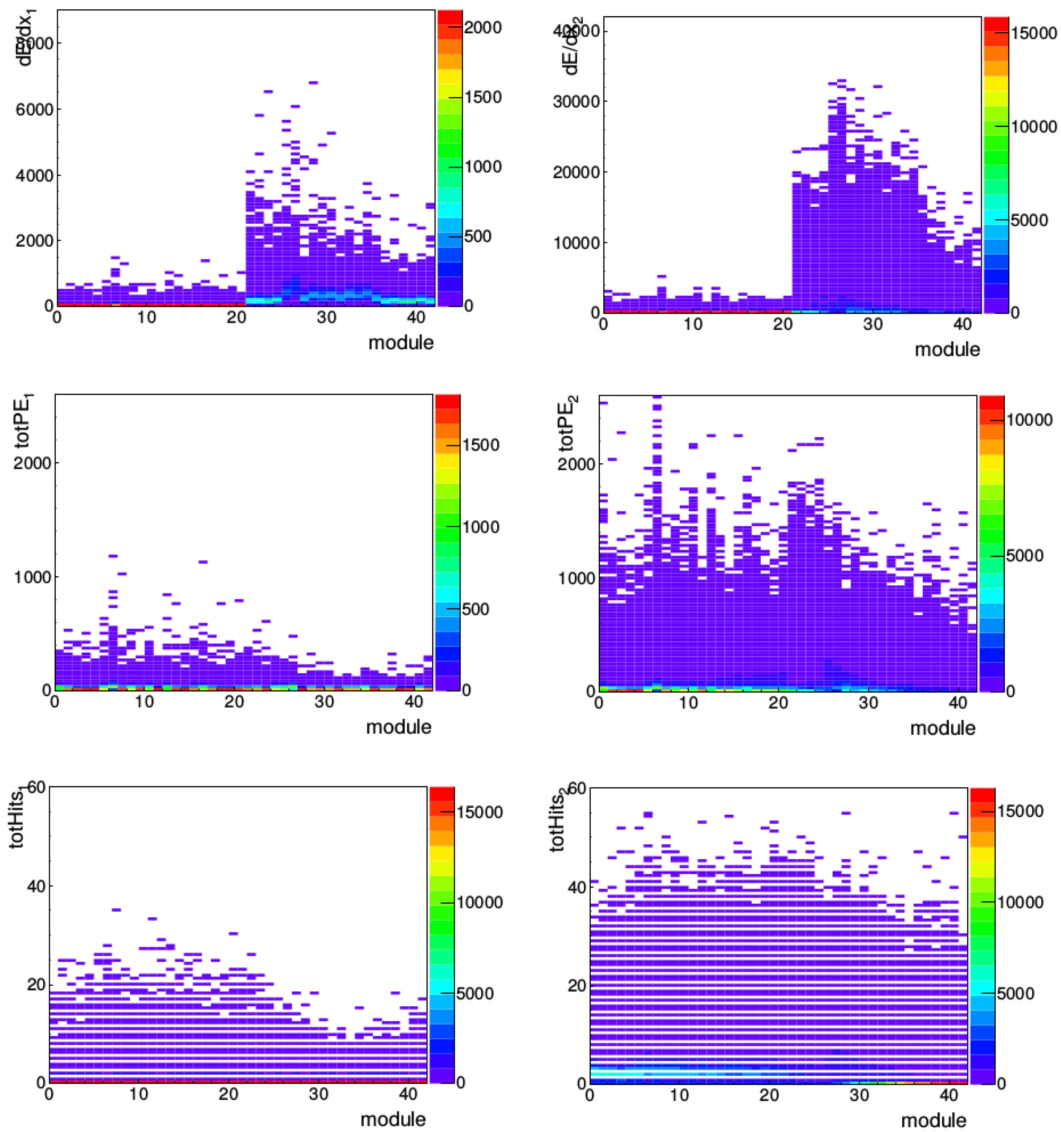


**Figure 4.12:** 2D Histograms of the dE/dx, total PE and total Number of Hits for muon like and pion like Events in the folder $8GeV\_Pos\_Pions$ of Data-Run-2. Pion-like Events at the right & muon-like at the left.

Looking at the previous Figures we can find some interesting features about those results: **The cut in PE improves as the energy of the events increases**, so the accuracy of getting almost pure muons and pions increases. We can see in the function of dE/dx for that sums the contributions for all events in the folder that the rate at which this function decreases (over the modules) is greater for pion than for muon like events. In the 2D histograms we notice that the values of dE/dx values of pion like events attain values a lot higher than those for muon like events (approximately 5 times the value of dE/dx for 4GeV sample), the idea is to continue working with these variables to find the best tool to use to separate the muon from the pions present in the pion peak. Once this best tool is obtained it can be applied to all folders of Data-Run-1 or 2 to find out what is the particle composition of the beam.

## 4.5 Analysis of the Spatial Distribution of the Beam using the Veto Counters

Since the Veto paddles are arranged in a definite and known way in physical space and they send a signal each time a charged particle hits any of them (they have scintillators attached to PMTs), it was interesting to see if looking at correlations among them and counting how many times each of them (or more than one, since some of them overlap spatially, as explained below) send a signal we can have some information about the spatial distribution of the secondary beam and how much it is centered. Figure 4.13 shows a diagram of the spatial distribution of the Veto paddles (12 in total, each one related to a Veto Counter Branch), where we can see that there are correlations among some of them, this means that each time one of them fires there is other that should also fire, this issue can be exploited to construct a correlation matrix and them perform a mapping (line 151 of Appendix-C) to study the spatial distribution of the beam.

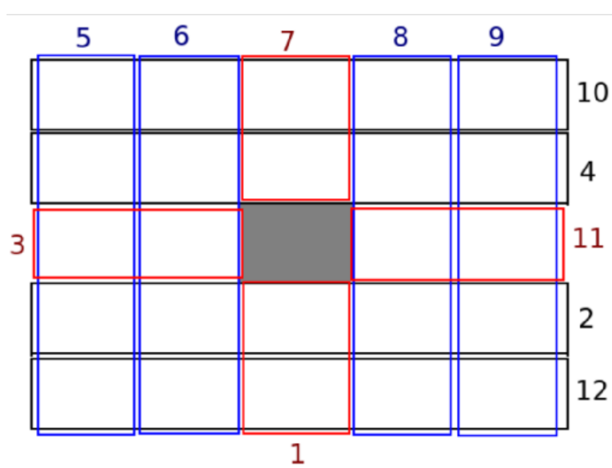


**Figure 4.13:** Spatial configuration of the Veto paddles where correlations among them are noticeable. The idea is to use this “map” to find the spatial distribution of the beam by looking at a correlation matrix of Veto Counters.

Some things that were not difficult to find are: The number of times each counter fired for each Energy & the correlation-matrix for each Energy (Spatial correlation only). The previously shown (Figure 4.13) spatial correlation permits multiple possibilities because there are many cases of overlapping of more than 2 veto paddles in actual physical space, then we require time information (at what specific time each counter fired for each event) in order to actually locate one unique point in space. The next Figure (4.14) shows the correlation matrix and a histogram of the total number of times each counter fired (looking at ALL events in the folder). We can notice a degree of correlation between counters and that counters 3 and 5 did not fire at all (they are actually not working now according to Test Beam experts).

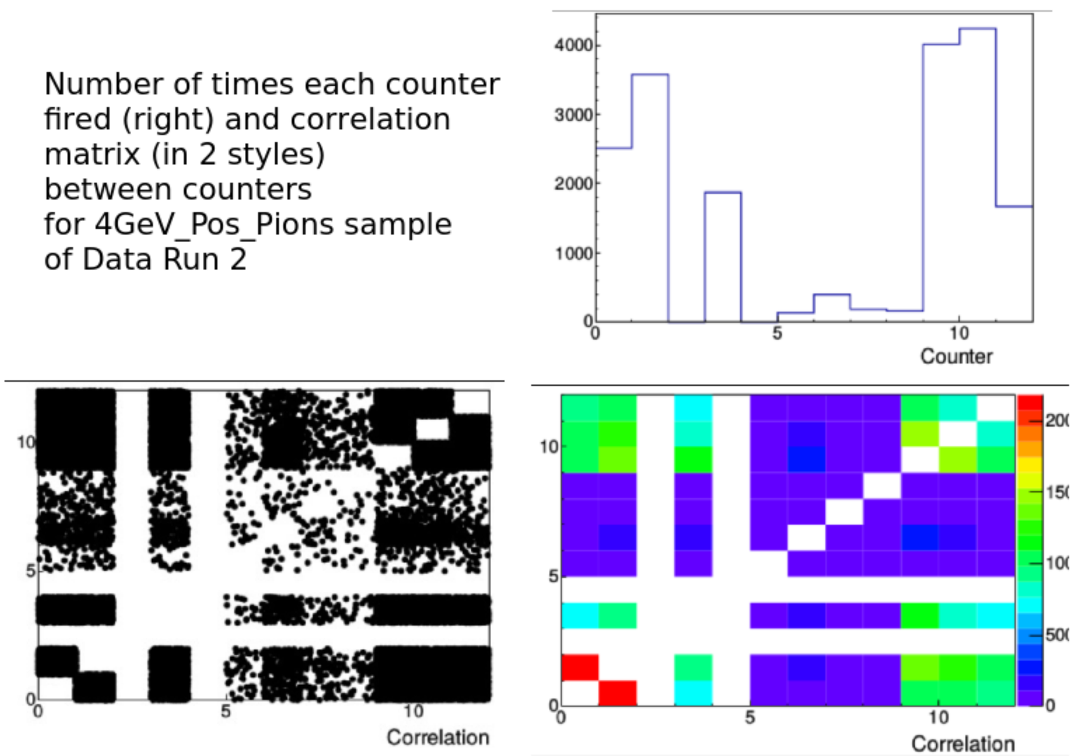


**Figure 4.14:** Each time counter $i$ fired we can look at what other counter $j$ different than $i$ also fired and add this to the correlation matrix, in that way we can find a degree of correlation between counters.

From the correlation matrix we can go to analyze the spatial distribution performing an elegant mapping shown in Appendix-C; however there is a problem: In the correlation-matrix attached previously a point in the histogram is attached each time 2 (space-correlated) counters fired, but this provides more events than the number of real physical events due to the lack of time-information (not available yet in the DSTs). Once time info is available we will be able to locate the real-points in space. To see why time information is important to locate a unique point in space consider the following situation:

Suppose that counters 2,4,6 and 8 fired then we have the 3 possibilities for points to allocate to the correlation-matrix (considering only spatial correlations), as shown in Figure 4.15:

$\{(6,4),(2,8)\}$ (2 points) or $\{(6,2),(8,4)\}$ (2 points) or even $\{(6,2),(8,4),(6,4),(2,8)\}$ (4 points).

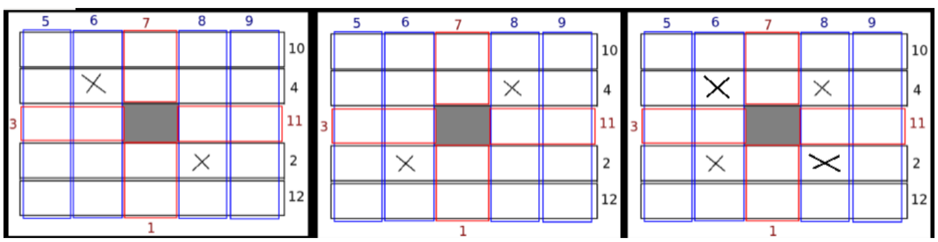


**Figure 4.15:** 3 possibilities for the counters that sent a signal considering only spatial correlation among counters, without time correlation we are considering the 3 cases while filling the correlation matrix.

To choose among these 3 possibilities we require time information because only spatial information leads to more possibilities, once time information is avaible (not yet in the DSTs) we can choose one of the 3 possibilities and attach that point to the correlation matrix and with the aid of the mapping to a given point in real space. The best that can be done now is the following: each time a veto counter fires, choose other at random among those counters correlated to it (this is done with the usage of dictionaries where each key is a counter which opens a list of counters correlated to it) and fill the correlation matrix, then with the mapping locate a random point in physical space. This is like doing a simulation of the beam, knowing the spatial correlation we guess what would have happened to locate a unique point in space and not be lead to choose all 3 possibilities avaible. Figure 4.16 show such a kind of simulation for the 1.77 GeV Pos Pion folder of Data-Run-1, although the sample has a very poor statistics it shows something we actually expect.

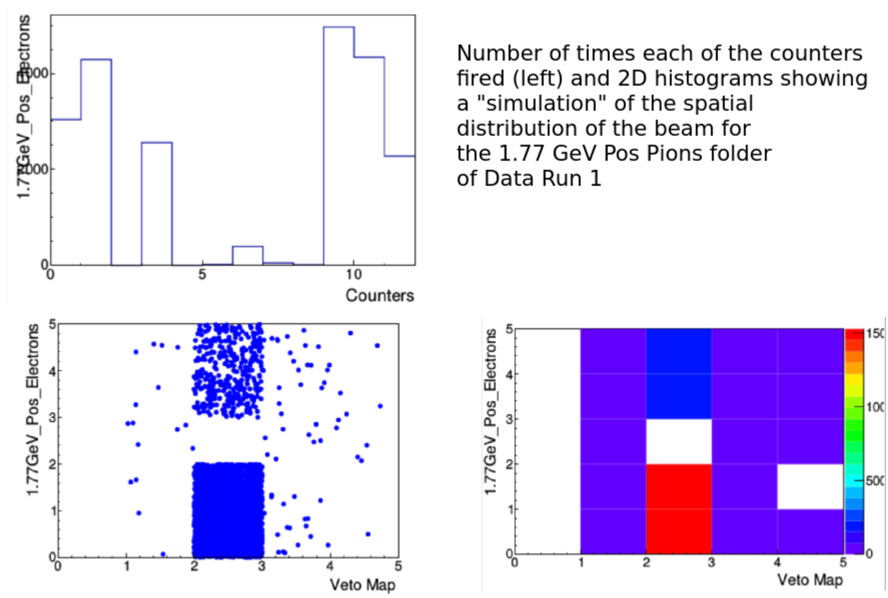


**Figure 4.16:** Number of times each of the counter fires and spatial distribution of simulated points, these histograms were obtained from the correlation matrix by doing an elegant mapping to spatial locations (Appendix-C).

## 4.6 Correlation ToF-Veto & Veto Sanity Check

As it was stated previously (Section 4.3) the **Goal of the Test Beam** is to have only a single particle passing through its Detector, for this reason it was useful to see any correlation between the ToF and the Veto, we expected that among those events that passed through both ToF stations no one of them to fire the Veto or that fraction to be very small because the Veto paddles and the ToF stations almost don't overlap spatially.

The next Figures show the number of Events that passed the ToF cuts and the fraction of them that also made the Veto fire for both Data Run 1 and 2, the fraction was higher than expected so it was necessary to see if we were looking for Veto Events inside the Minerva Readout window or inside the 300 ns window cetered at the time in which the Veto fired. Something that is relevant is that the fraction of events decreases as the energy increases, this was expected because as the energy increases the beam is more focused so less particles scatter and hit the Veto paddles.

| Data-Run-1 | (Pion-Folders) | | | |
|---|---|---|---|---|
| | | | | |
| Beam Energy(GeV) | Polarity | Total Events (ToF-cut) | Total Events (ToF-cut & Veto Fired) | Fraction |
| 1.77 | Pos | 5067 | 1097 | 0.2164989145 |
| 2 | Pos | 4550 | 845 | 0.1857142857 |
| 3 | Pos | 2919 | 572 | 0.1959575197 |
| 4 | Pos | 3225 | 442 | 0.1370542636 |
| 6 | Pos | 4222 | 473 | 0.1120322122 |
| 8 | Pos | 3054 | 257 | 0.0841519319 |
| | | | | |
| 2 | Neg | 105 | 33 | 0.3142857143 |
| 3 | Neg | - | - | |
| 4 | Neg | 1361 | 378 | 0.2777369581 |
| 6 | Neg | 3947 | 384 | 0.0972890803 |
| 8 | Neg | 3946 | 334 | 0.0846426761 |

**Figure 4.17:** Number of good ToF Events and fraction of them that also made the Veto fire for Data Run 1.

| Data-Run-2 | (Pion-Folders) | | | |
|---|---|---|---|---|
| | | | | |
| Beam Energy(GeV) | Polarity | Total Events (ToF-cut) | Total Events (ToF-cut & Veto Fired) | Fraction |
| 4 | Pos | 22695 | 5198 | 0.2290372329 |
| 6 | Pos | 26574 | 3881 | 0.1460450064 |
| 8 | Pos | 28989 | 3460 | 0.1193556176 |
| 9 | Pos | 34214 | 3248 | 0.0949318992 |
| 10 | Pos | 33348 | 3163 | 0.0948482668 |
| 16 | Pos | 16477 | 852 | 0.0517084421 |
| | | | | |
| 4 | Neg | 25081 | 6049 | 0.2411785814 |
| 6 | Neg | 30673 | 4953 | 0.1614775209 |
| 8 | Neg | 32548 | 3479 | 0.1068882881 |
| 9 | Neg | 31658 | 2603 | 0.082222503 |
| 10 | Neg | 31904 | 2640 | 0.0827482447 |

**Figure 4.18:** Number of good ToF Events and fraction of them that also made the Veto fire for Data Run 2.

Since the fraction was still quite high it was relevant to find out if the condition used for the Veto to fire considered events inside the Minerva Readout time window or inside the 300 ns time window centered at the point in time in which the Veto fired. The hypothesis was that maybe there was a large fraction of halo muons hitting the Veto paddles.

For this issue it was relevant to count events in which the Veto fired that occurred inside that time window and inside the minerva readout window, the branches to look at and their meaning as well as the number of events for both kinds of Veto conditions are presented below:

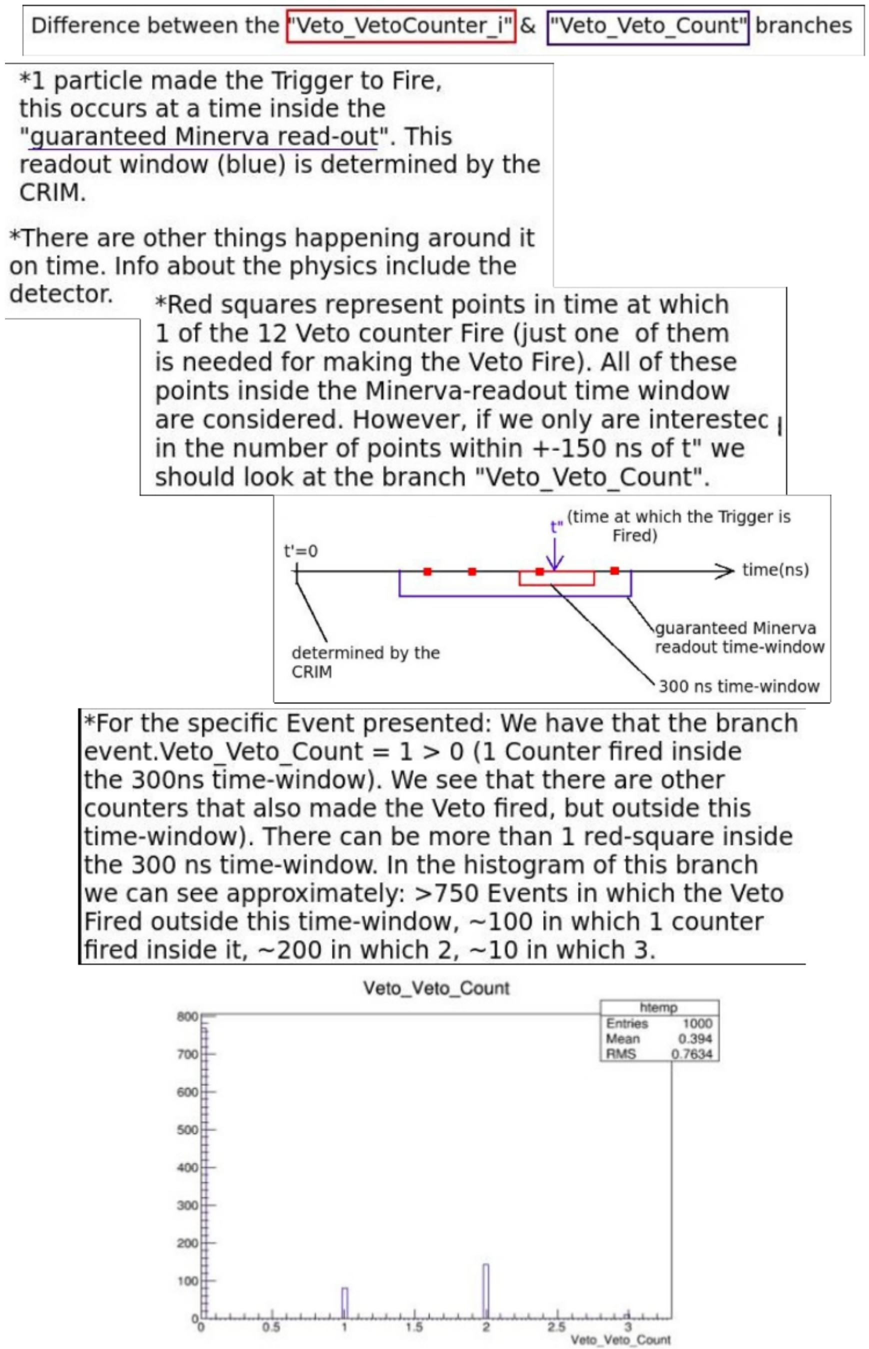


So, in a 1st stage we found the fraction of Good ToF-events (with $ToF\_quality == 1$) that also made the Veto to fire (not necessarily inside the 300 ns window) and in a 2nd stage the fraction of those inside this 300 ns time window. It was really odd to find more veto-events inside the 300 ns window than inside the Minerva readout window, for this reason it was needed a Veto Sanity check to analyze in more detail specific kinds of events but wiping out the ToF condition. The issue was that it was actually a problem with the Veto Count branch related to the electronics and the the other way to consier the Veto to fire (via one of the 12 counters) already considered the events inside the 300 ns time window.

We can present the Veto Sanity check which counts events in which the branch Veto Count is greater than zero but any couter fired and also the number of Events of our interest (of good ToF quality and in which the Veto did not Fire) in the figures of the next Section.

## 4.7 Efficiency of the cut to get physically meaningful Events

Since TB require only 1 particle (of known type & energy) to pass through the detector....we should consider $ToF\_quality == 1$ and the condition that the Veto don't Fire (any of the counters). The idea was to calculate the Efficiency of this last cut with respect to events already $In\_Spill, n\_slices > 0, Triggered$ & $Sliced$. The following table presents all kinds of events considered, where the highlighted type of events are those acceptable for the particle-ID analysis.

| |
|---|
| Events-0: Total Number of Events In_Spill |
| Events-1: Total Number of Events In_Spill & event.n_slices>0 (Activity in the Detector) |
| Events-2: Total Number of Events In_Spill & event.n_slices>0 + Triggered + Sliced |
| Events-3: Total Number of Events of kind-2 & Veto Fired |
| Events-4: Total Number of Events of kind-2 & Veto_Count>0 |
| Events-5: Total Number of Events of kind-2 & Veto_Count>0 & Veto Fired |
| Events-6: Total Number of Events of kind-2 & Veto_Count>0 & Veto did not Fired (odd Events) |
| Events-7: Total Number of Events of kind-2 & ToF_quality==1 & Veto did not Fired (my Events) |

The efficiency of the cuts to get Events of kind 7 is calculated with respect to Events of kind 2, we can construct Arachne links of Events of kind 6 (odd events) and sent them to the TB Experts so they can look at the problem in the Veto Count branch (for the Sanity check), this was already done and it seemed that it was a problem with the electronics.

| Data-Run-1 (Pos) | (Pion-Folders) | | | | | | | |
|---|---|---|---|---|---|---|---|---|
| Energy (GeV) | 1.77 | 2 | 3 | 4 | 6 | 7 | 8 | 16 |
| Polarity | Pos | Pos | Pos | Pos | Pos | Pos | Pos | Pos |
| Events-0 | 13252 | 9414 | 4602 | 4416 | 5407 | 11290 | 9529 | 4163 |
| Events-1 | 12631 | 8836 | 4494 | 4218 | 5189 | 10913 | 9391 | 4089 |
| Events-2 | 11259 | 7942 | 4138 | 4014 | 4988 | 10593 | 9337 | - |
| Events-3 | 5707 | 3473 | 1507 | 1035 | 1002 | 1864 | 1386 | 386 |
| Events-4 | 6226 | 3818 | 1660 | 4014 | 1180 | 2246 | 5031 | 525 |
| Events-5 | 5707 | 3473 | 1507 | 1035 | 1002 | 1864 | 1386 | 386 |
| Events-6 | 519 | 345 | 153 | 2979 | 178 | 382 | 3645 | 139 |
| Events-7 | 3970 | 3705 | 2347 | 2783 | 3749 | 8294 | 2797 | 0 |
| Efficiency(Events-7) | 0.352606803 | 0.466507177 | 0.567182214 | 0.693323368 | 0.751603849 | 0.782969886 | 0.299560887 | |

| Data-Run-1 (Neg) | (Pion-Folders) | | | | | | |
|---|---|---|---|---|---|---|---|
| Energy (GeV) | 2 | 3 | 4 | 6 | 7 | 8 | 12 |
| Polarity | Neg | Neg | Neg | Neg | Neg | Neg | Neg |
| Events-0 | 8032 | 5043 | 2225 | 5046 | 0 | 4642 | 18082 |
| Events-1 | 7902 | 4975 | 2149 | 4806 | 0 | 4481 | 18082 |
| Events-2 | 7215 | 4414 | 2006 | 4652 | 0 | 4400 | 18061 |
| Events-3 | 4926 | 1975 | 854 | 865 | 0 | 614 | 2055 |
| Events-4 | 5315 | 2145 | 931 | 4653 | 0 | 4400 | 2190 |
| Events-5 | 4926 | 1975 | 854 | 865 | 0 | 614 | 2055 |
| Events-6 | 389 | 170 | 77 | 3788 | 0 | 3786 | 135 |
| Events-7 | 72 | 0 | 983 | 3563 | 0 | 3612 | 0 |
| Efficiency(Events-7) | 0.00997921 | 0 | 0.49002991 | 0.765907137 | | 0.820909091 | 0 |

| Data-Run-2 (Pos) | (Pion-Folders) | | | | | | |
|---|---|---|---|---|---|---|---|
| Energy (GeV) | | 4 | 6 | 8 | 9 | 10 | 16 |
| Polarity | | Pos | Pos | Pos | Pos | Pos | Pos |
| Events-0 | | 30392 | 33952 | 34625 | 40009 | 38137 | 18422 |
| Events-1 | | 29923 | 33087 | 33580 | 38966 | 37421 | 18137 |
| Events-2 | | 28575 | 31486 | 32968 | 38221 | 36733 | 17888 |
| Events-3 | | 9621 | 7237 | 5942 | 5741 | 5166 | 1713 |
| Events-4 | | 10406 | 8323 | 6983 | 7019 | 6369 | 2272 |
| Events-5 | | 9621 | 7237 | 5942 | 5741 | 5166 | 1713 |
| Events-6 | | 785 | 1086 | 1041 | 1278 | 1203 | 559 |
| Events-7 | | 17497 | 22693 | 25529 | 30966 | 30185 | 15625 |
| Efficiency(Events-7) | | 0.61231846 | 0.720733024 | 0.774356952 | 0.810182884 | 0.821740669 | 0.873490608 |

| Data-Run-2 (Neg) | (Pion-Folders) | | | | | |
|---|---|---|---|---|---|---|
| Energy (GeV) | | 4 | 6 | 8 | 9 | 10 |
| Polarity | | Neg | Neg | Neg | Neg | Neg |
| Events-0 | | 36067 | 38203 | 38512 | 37827 | 36864 |
| Events-1 | | 35337 | 37356 | 37544 | 36803 | 36004 |
| Events-2 | | 33190 | 35886 | 36691 | 35879 | 35347 |
| Events-3 | | 12356 | 8484 | 6143 | 5160 | 4688 |
| Events-4 | | 13403 | 9688 | 7375 | 6588 | 5894 |
| Events-5 | | 12356 | 8484 | 6143 | 5160 | 4688 |
| Events-6 | | 1047 | 1204 | 1232 | 1428 | 1206 |
| Events-7 | | 19032 | 25720 | 29069 | 29055 | 29264 |
| Efficiency(Events-7) | | 0.573425731 | 0.716714039 | 0.792265133 | 0.809805179 | 0.827906187 |

Some observations about the previous results: It can be noticed that the efficiency of the required cut (Events of interest) tends to increase with Energy. However, it is quite strange that for $8GeV\_Pos\_Pions$ Folder (in purple) this situation is not exhibited. It's interesting also to notice that for the High-energetic folder $12GeV\_Neg\_Pions$ there are no events that passed the $ToF\_quality == 1$ cut. These events are fortunately not relevant for ToF because at these range of energies one cannot separate protons from pions (perhaps that is why no data was taken at that energy). The idea is to construct ToF histograms again but with the previous condition.

## 4.8 Summary of Early Results & work to focus on

The idea was to repeat the procedure starting with Data Run 1 Folders considering the effect of the Veto, because we do not want the Veto to fire (we want single particle events). At this point there was still plenty of work to do in the development of better tools to separate muons from pions in the pion peak, it was better to start looking at Data Run 1 folders because there was already a Monte Carlo simulation of the passage of particles in this configuration of the TB detector (not to be confused with a MC simulation of the secondary beam !), so it was relevant to use the developed tools to the Monte Carlo sample and make comparisons.

The specific tool to use in the separation of muons from pions depends on the energy so it was relevant to find the best tool for each range of energy and then present those results, they will be really useful once the Monte Carlo simulation of the secondary beam is ready (it was not ready at the end of my stay at Fermilab) to make comparisons and to test if the simulation is good enough or there is something to be improved over there.

In the following chapters Results are presented on the composition of the secondary beam (Chapter 5), the methodology to obtain them and a specific way (via an efficiency-purity analysis) to make up the best cut for the isolation of specific species of particles from others (Chapter 6).

# Chapter 5

# Results on the composition of the secondary beam (% $p^{\pm}, \pi^{\pm}, \mu^{\pm}, e^{\pm}$ ) for different energies (8, 6, 4 & 2 GeV) and polarities (+,-)

The previous chapter dealed with the way to find the mandatory conditions needed to select physically meaningful single particle events, which are the following: The beam has to be ON ($In\_spill > 0$), there has to be activity in the detector ($n\_slices > 0$), the event has to take place in the triggered slice (**Triggered** & **Sliced** conditions), all 6 PMTs of the 2 ToF stations have to fire ($ToF\_quality == 1$) & the Veto should not fire ("**not** DidVetoFire(**event**)"condition). With these conditions we can assume that each **Event** corresponds to a **single particle**, so when talking about an Event we mean a particle (the one which fired the Trigger, passed through both ToF stations and did not make the Veto fire) passing through the Test Beam (TB) detector.

We can start by isolating (and counting) **protons** from the ToF histograms (the peak located at the right), then store the Events that are part of the **contamination intervals** (there are usually 2 contamination intervals: 1 in between the pion and proton peaks and 1 at the right of the proton peak) to construct Arachne Links of them in order to find out their particle composition by eye-scanning. For Events in the **pion peak** it was necessary to look at other variables in order to **separate muons and pions** present there, for the case of electrons an initial approach (in next chapter a better tool for looking at them is explained) for counting them was to fit a gaussian in this pion peak and to store events (for eye scanning) in any tail that may appear at the left (because electrons might be present there).

Since there is already a MC (Monte Carlo) simulation of the passage of single particles through the TB detector in the ECAL/HCAL configuration (useful to analyze Data Run 1), we can exploit it in order to separate muons and pions by locating the interval (which varies from histogram to histogram of detector variables) in which muons (or pions) may be present (according to the MC) in order to apply the same cuts to data and in that way separate the muons (or pions) present in the ToF pion peak (for electrons the methodology used was different, as stated before). With the previous conditions imposed to have single-particle events and the procedure to isolate and count each kind of species we could find an estimate of the compostion of the beam for different energies and polarities.

This methodology has been applied to data (Data Run 1) of 8, 6, 4 and 2 GeV for both Positive and Negative polarities of the beam. For the energies of 8, 6 and 4 GeV a cut in the histogram of "Total Energy"(deposited in the TB detector) worked quite well (validated by a MC simulation of pure muons, which tell "where they are located") for separating muons and pions present in the ToF pion peak. Notwithstanding that, for the 2GeV samples it was not possible to rely on a single cut for separating muons and pions present in the ToF pion peak, for that reason it was necessary to look at different detector variables in different regions of the detector in order to find out which one was the "best cut" (a combination of different variables) for performing the separation (in the next chapter a detailed analysis of the cuts to the be applied to the 2GeV samples for separating different particle species is outlined).

In order to perform the above mentioned analysis for all these energies and polarities of the beam several histograms were constructed ($\sim 750$), many events were eye-scanned and different scripts with cuts in different intervals for different variables were written [89]. This chapter presents the procedure followed just for the 8 & 2 GeV (+) samples because the same procedure that was applied to the 8 GeV sample was applied also to the 6 & 4 GeV samples. Results are presented as well as the most important histograms used for both locating muons and comparing patterns of isolated particles (after applying the cut) and pure particles (MC) in order to test the cuts.

The way in which the MC simulation of pure particles is useful for locating the muon (or pion) intervals is the following: We construct histograms of pure muons (MC) for different variables and compare it with data, then we can notice **in what intervals of a specific variable there are certainly no muons**. The usage of muons is more reliable because they have narrower and more localized distributions (so they tell us where they are located) whereas pions usually have more spread and non-localized distributions (a pion may actually look like a muon if it passes through the whole detector without showering & may look like an electron if it showers in the ECAL). The next Figure shows this criteria for locating pions knowing where muons are located with the aid of a MC simulation of muons.

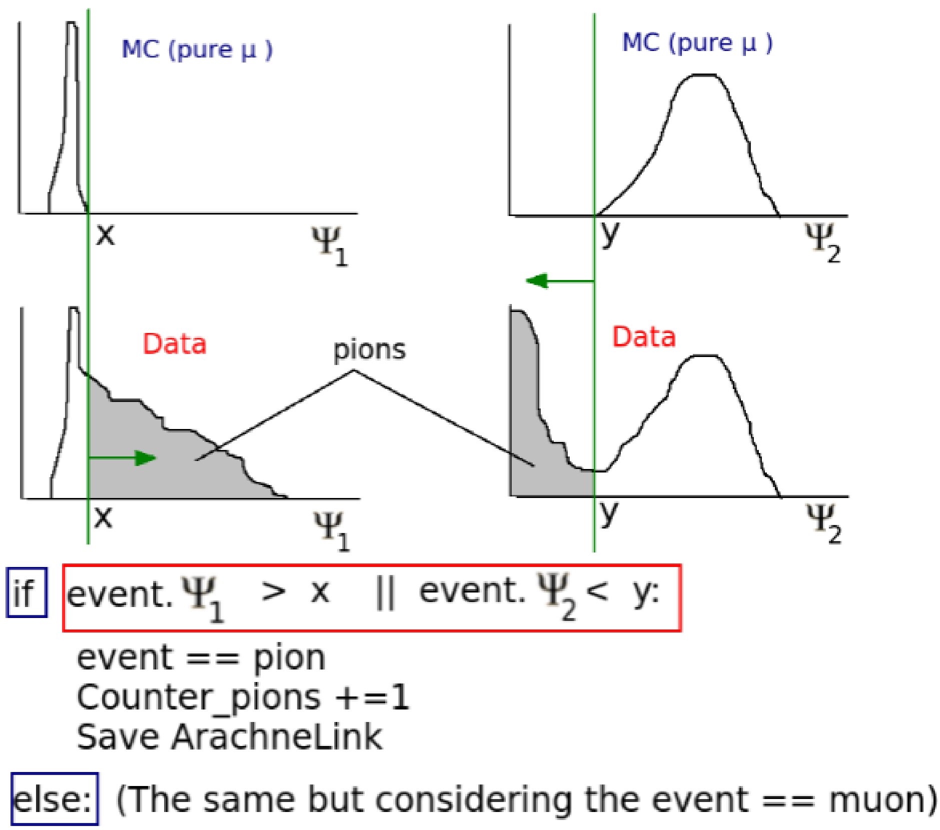


**Figure 5.1:** Muons have usually narrower distributions so they tell us where they are and in this way we can locate pions. This figure shows the usage of 2 different arbitrary variables ($\psi_1$ & $\psi_2$) to make up the cut that looks at pions (the cut that looks for muons will be the negation of this statement).

Before moving on it is also important to show the main Detector-Variables (also called $\mu$-ID variables) constructed to separate muons and pions present in the ToF pion peak. Four kinds of variables and five regions of the detector were analyzed, which gives us a total of 20 different variables that can be used to separate muons and pions, these have been very useful for the 2GeV samples because one variable was not enough to make up the cut for this separation. All these variables can be contructed from the definition of **python-dictionaries** that contain the dE/dx, total-PE and total-Hits for all 42 modules (modules as keys that open the respective values) of the TB detector. The next figure presents these variables and how they were constructed.

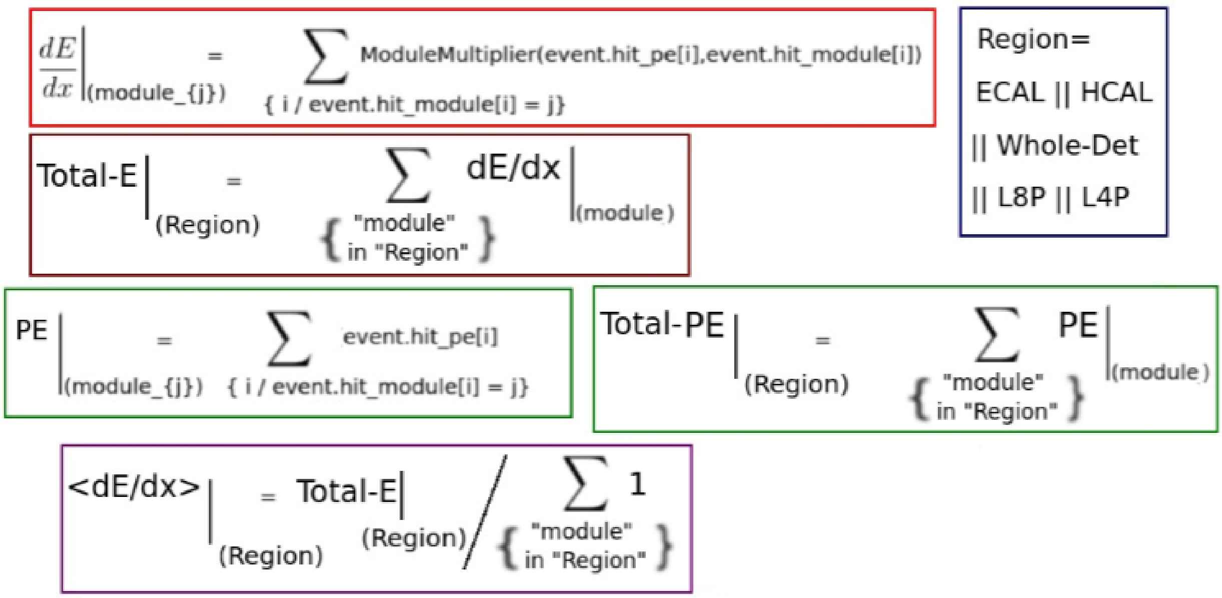


**Figure 5.2:** From the python dictionaries of dE/dx, total-PE & total-Hits for each module we can construct a total of 20 variables considering 4 kinds of variables (Total-E, Total-PE, $< dE/dx >$, Total-Hits) over 5 regions of the detector for each of them (Total-Detector, ECAL, HCAL, L8P & L4P).

## 5.1 Procedure established for the 8 GeV $\pi^+$ sample

Here is explained the methodology followed for the 8 GeV $\pi^+$ sample. We start from the ToF histogram (Figure 5.3) where the main intervals are indicated. We can see the gaussian fits in both the pion (left) and proton (right) peaks and it is indicated that at the left of the pion peak some electrons may be present, so those events were stored to be eye-scanned. In this case all events considered have to be in the first bucket ($\sim$ 19 ns). As mentioned earlier, the particle composition of the contamination intervals was determined via eye-scanning.

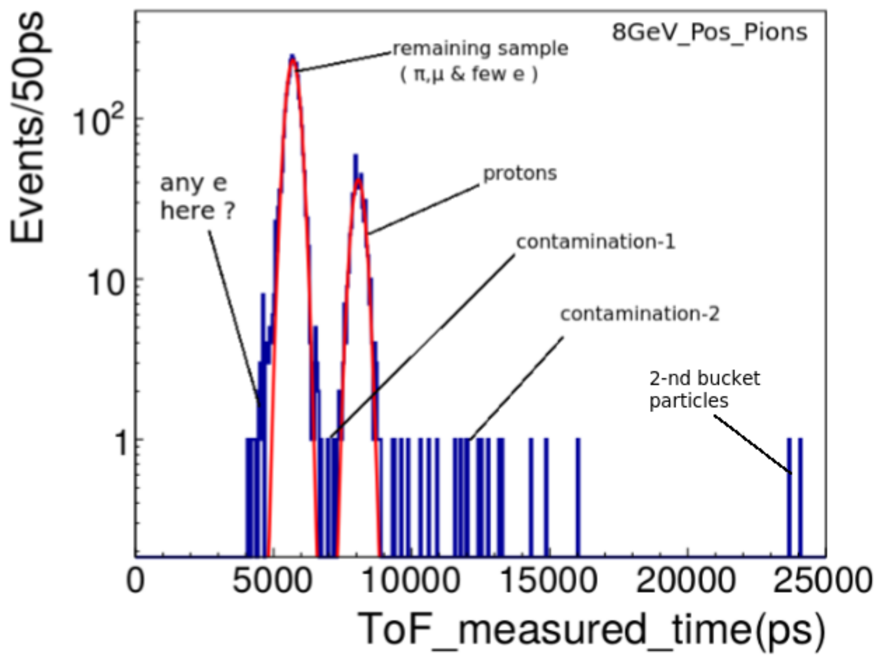


**Figure 5.3:** ToF histogram for the 8 GeV $\pi^+$ sample showing the main intervals to be analyzed according to the methodology established. The left peak is the $\pi$-peak which contains $\pi^+$, $\mu^+$ & some $e^+$. The right peak is the proton-peak.

The specific intervals considered, together with their composition, are presented below. But let us first show the histogram of the "Total-Energy" (deposited in the Detector) for a sample of pure (MC) muons, a sample of pure (MC) pions and the Data at hand **for events present in the ToF $\pi$ peak**. We can clearly see from the histogram of pure (MC) muons that they tell us where they are located, whereas pions have a wider spectrum and some of them ($\sim 4\%$ at 8 GeV) look like muons (these pions may have passed through the whole detector without showering). Then the MC sample of pure muons tell us the interval in which to cut in order to separate muons from pions. We can test this isolation by comparing 2D histograms (which may be of the variable **dE/dx vs. module**, for example) of pure (MC) muons and isolated muons (Figure 5.4). It is very important to indicate the the unit "u" for the Energy deposited in different regions of the detector is estimated in the final section of this chapter.

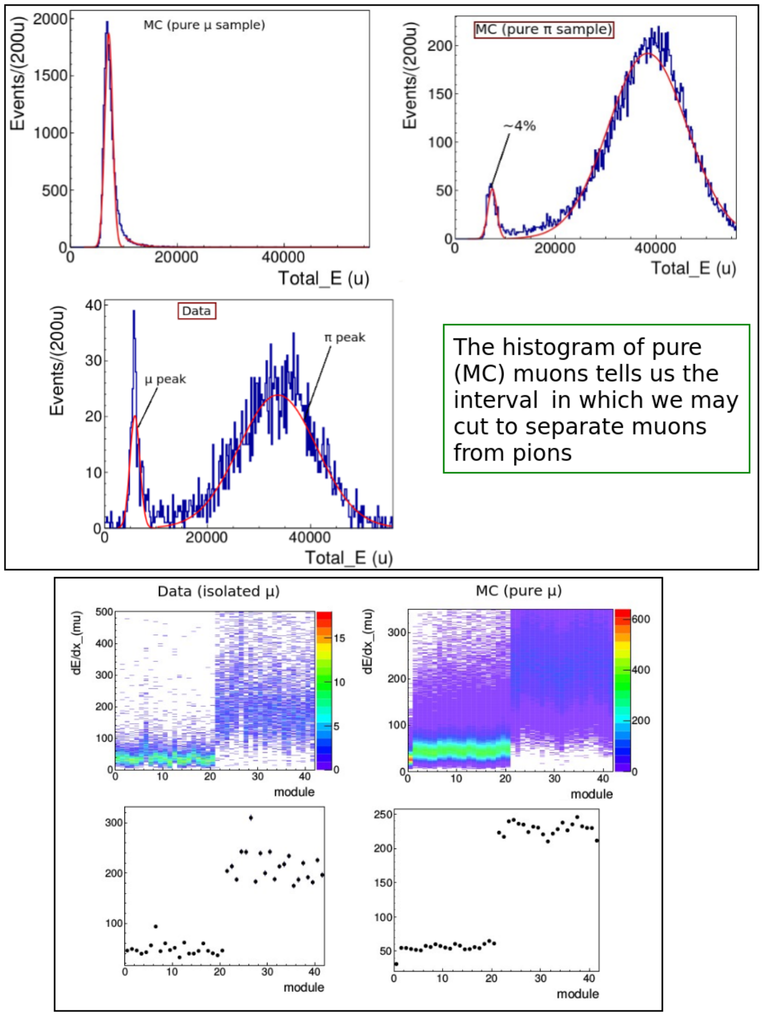


**Figure 5.4:** UP: Histograms of the "Total Energy" deposited in the TB detector for pure (MC) muons, pure (MC) pions & Events (Data) in the ToF $\pi$-peak (interval presented in the previous Figure). DOWN: 2D histograms of dE/dx vs. module for isolated (from Data) $\mu$ & for pure (MC) $\mu$. We notice that the patterns agree as expected due to the separation of the $\mu$ & $\pi$ peaks in the Total-E histogram. The red spot in module-0 (1st-plane) present in the MC sample is discussed at the end of this chapter. The respective profileX histograms are presented below.

### Results for the 8 GeV $\pi^+$ sample

The relevant intervals (in the **ToF histogram**) and their composition are the following (for the Pion-Interval there are other 2 intervals indicated that are located in the **Total-E histogram**, there is indicated also the number of $e^+$ counted at a specific region at the left of the ToF Pion-peak):

*Contamination-2 Interval (at the right of the Proton-peak) = $< 9\,100, 16\,500 >$ $(ps)$: $17p, 1\mu$

*There is no Contamination-1 Interval ($p$ & $\pi$ peaks very close together)

*Proton-peak Interval = $< 7\,000, 9\,000 >$ $(ps)$: $510p$

*Pion-peak Interval = $< 3\,800, 7\,000 >$ $(ps)$:
$\{\mu$-Interval = $< 0, 10\,000 >$ $(u)$ : $329\mu$,
$\pi$-Interval = $< 10\,000, 56\,000 >$ $(u)$ : $(2464 - (5))\pi$,
$5e$ found in the ToF interval $< 3\,900, 4\,650 >$ $(ps)\}$ $\Longrightarrow$ From the total number of $\pi$ counted we have substracted the number of $e$ (assuming that some $\pi$ may be confused as $e$, because $\mu$ will almost never look like $e$).

$\Longrightarrow$ The rough composition of the beam of 8 $GeV\pi^+$ ($\sim$ 3 321 particles (Events) identified) is presented in the next Figure (the relative error is calculated as $1/\sqrt{N_k}$, where $N_k$ is the respective number of each of the species $k = \pi, p, \mu, e$):

| Particle: | Number | Percentage | Relative error |
|---|---|---|---|
| proton | 527 | 15.87% | 0.043561 |
| pion | 2459 | 74.04% | 0.020166 |
| muon | 330 | 9.94% | 0.055048 |
| electron | 5 | 0.15% | 0.447214 |

Total 3 321 "located" events == particles

**Figure 5.5:** Estimation of the beam composition for the $8GeV\pi^+$ sample. It is relevant to indicate that for this particular case all these particles have + charge, so "electron" actually means "positron".

## 5.2 Procedure established for the 2 GeV $\pi^+$ sample

For the $2GeV$ samples it was not possible to rely on a single cut to separate $\mu$ & $\pi$ present in the ToF Pion-peak (see Figure 5.12) because the $\mu$ & $\pi$ peaks in the Total-E histogram almost merge each other. For that reason 5 different kinds of cuts were constucted, each of them looking at a different kind of variable and being a combination of cuts in that specific variable over different regions of the detector. The first 4 cuts are related to a specific kind of variable and the 5th cut is a combination of the first 4 cuts (as summarized in next Figure). Let us label these cuts as CUT-$i$ (where $i = 1, ..., 5$), each of them is looking at $\pi$ taking advantage of the MC sample of pure $\mu$ to locate them (as explained above, by knowing where the $\mu$ are we can locate the $\pi$):

CUT-1: looks at Energy deposited in different regions of the TB detector

CUT-2: looks at PE deposited in different regions of the TB detector

CUT-3: looks at the $< dE/dx >$ in different regions of the TB detector

CUT-4: looks at the Number of Hits in in different regions of the TB detector

CUT-5: A combination of All previous cuts

$$\boxed{CUT\_\boxed{i} \equiv \bigcup_{k=1}^{5} \{sub\_cut\_\boxed{i}\_\boxed{k} \equiv Var\_\boxed{i}\_\boxed{k} \in \boxed{I_k}\}}$$

$$\boxed{i = E, PE, Ave\_dE/dx, Hits} \;\; ; \;\; \boxed{k = Total, ECAL, HCAL, L8P, L4P}$$

$\boxed{I_k}$: A $\pi$-interval in histogram of variable $Var\_i\_k$

$$\boxed{CUT\_5 \equiv \bigcup_{j=1}^{4} CUT\_j}$$

**Figure 5.6:** 5 Cuts that look at $\pi$ in the ToF Pion peak for the 2GeV samples.

Let us show the way in which CUT-1 was built up by looking at the histograms of Energy deposited over different regions of the detector for Events in the ToF Pion-peak (the ToF histogram is shown in Figure 5.12), **adding these cuts** into a single one and to show its logic statement (for the other variables the procedure is similar). The next figures show this procedure and the final logic statement constructed for CUT-1:

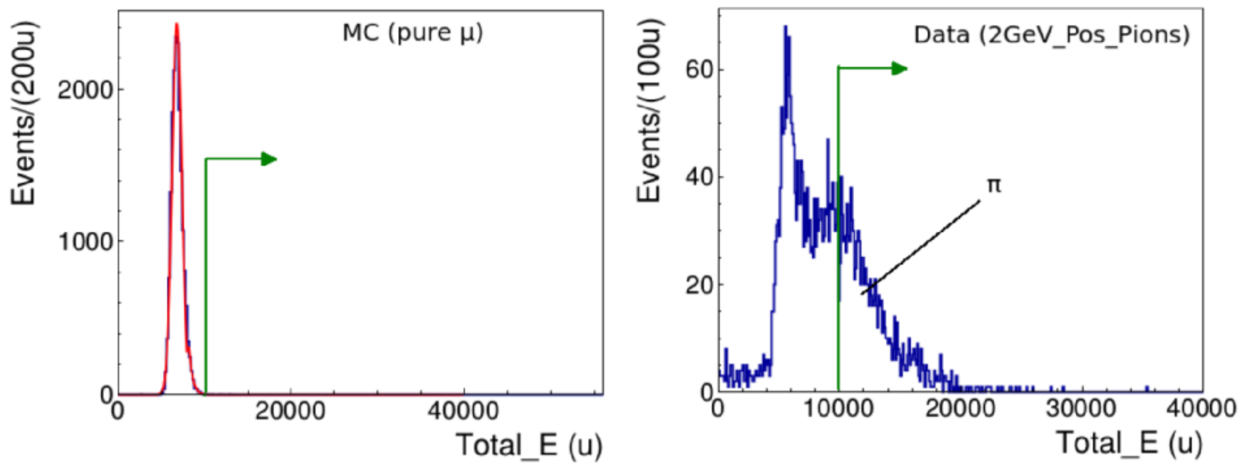


**Figure 5.7:** We can say from the MC sample of pure $\mu$ that events with values of $Total\_E > 10\,000$ are certainly not $\mu$, so we considered those events as $\pi$. But due to the overlapping of the $\mu$ & $\pi$ peaks we need other variables to make up the cut (Figures below).

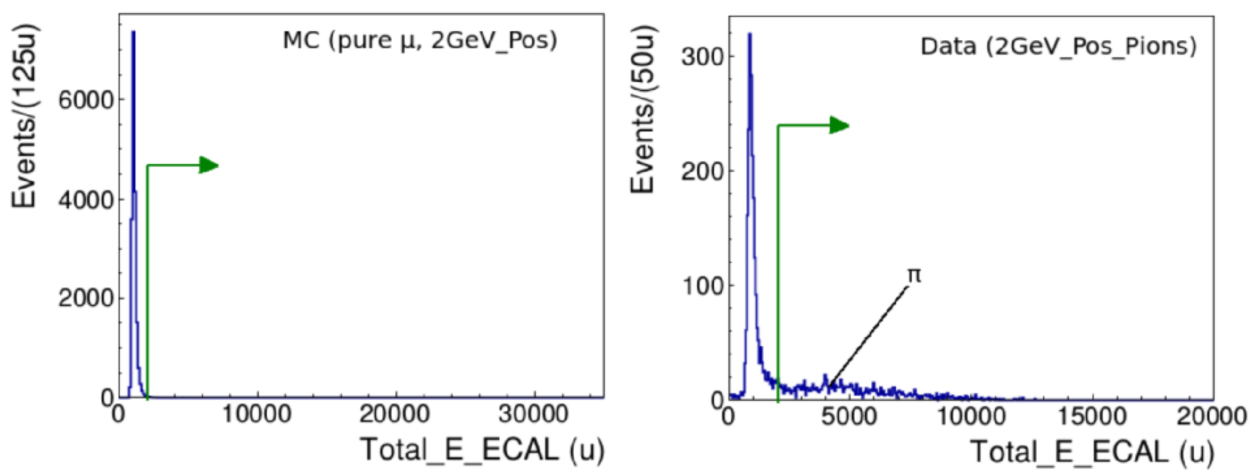


**Figure 5.8:** From the MC sample of pure $\mu$ we can say that events with $Total\_E\_ECAL > 2\,000$ are certainly not $\mu$

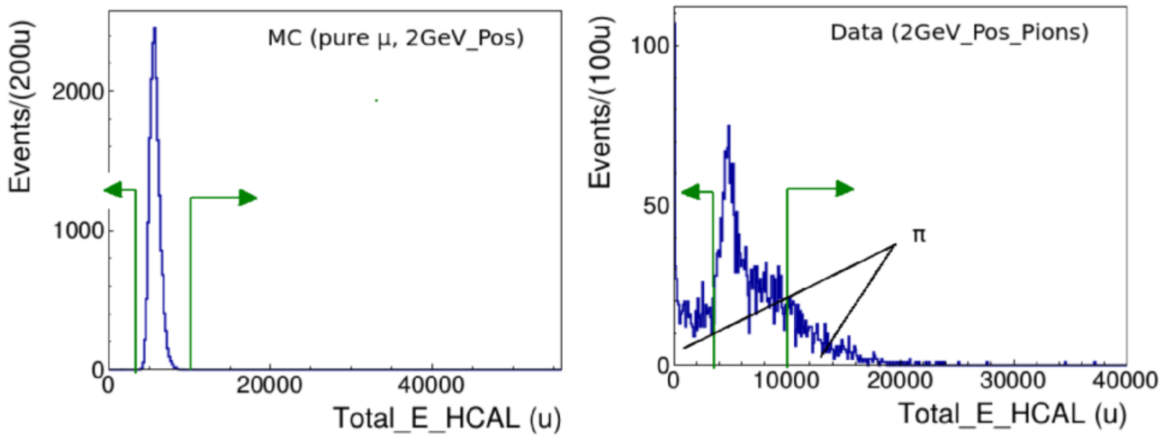


**Figure 5.9:** From the MC sample of pure $\mu$ we can say that events with values of $Total\_E\_HCAL > 10\,000$ **or** $< 4\,000$ are certainly not $\mu$

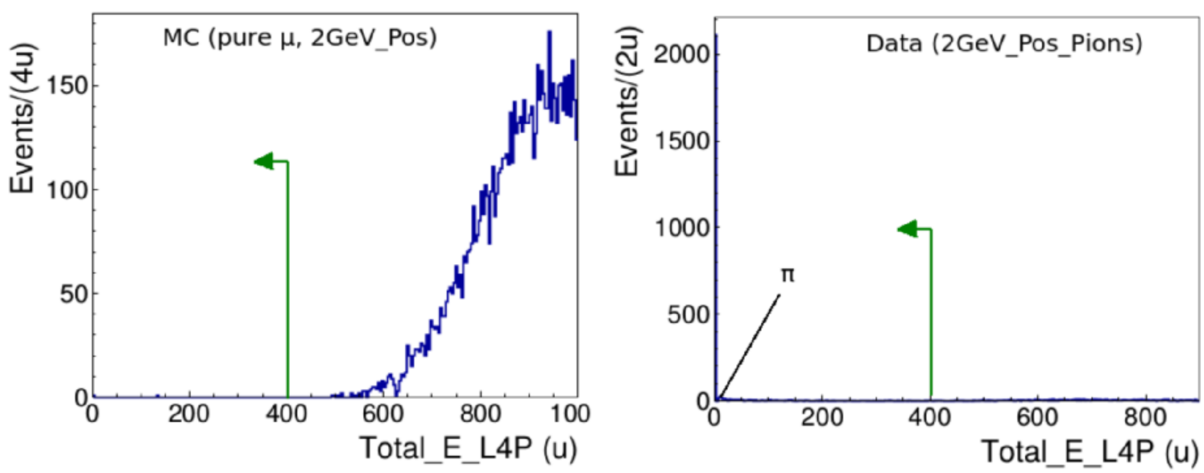


**Figure 5.10:** From the MC sample of pure $\mu$ we can say that events with values of $Total\_E\_L4P < 400$ are certainly not $\mu$. A similar situation is observed for the $Total\_E\_L8P$ variable (histogram not shown here).

```
        if 10000<=S_E_tot or 2000<=S_E_ecal or 10000<=S_E_hcal or
S_E_hcal<=4000  or S_E_L8P<=400 or S_E_L4P<=400:   #pi-like events
        {Counter, ArachneLinks, construction of 2D-pion-histograms
         (dE/dx, Total-PE, Total-Hits vs. module)}

        else: #mu-like events

        {Counter, ArachneLinks, construction of 2D-muon-histograms
         (dE/dx, Total-PE, Total-Hits vs. module)}
```

**Figure 5.11:** With the aid of the previous histograms it was possible to locate the interval for each variable and make up the logic statement for the CUT-1 that looks at $\pi$. In this statement $S\_E\_xyz$ is the counter of the total Energy over region $xyz$ (total, ecal, hcal, L8P, L4P) of the TB detector.

Before presenting Results for each of the CUT-$i$ it is relevant to indicate the **Intervals considered** (starting from the ToF ones) and their composition (then the logic for each of the CUT-$i$ is indicated). The next Figure shows the ToF histogram for the 2GeV $\pi^+$ sample, where we can locate immediately all the relevant intervals.

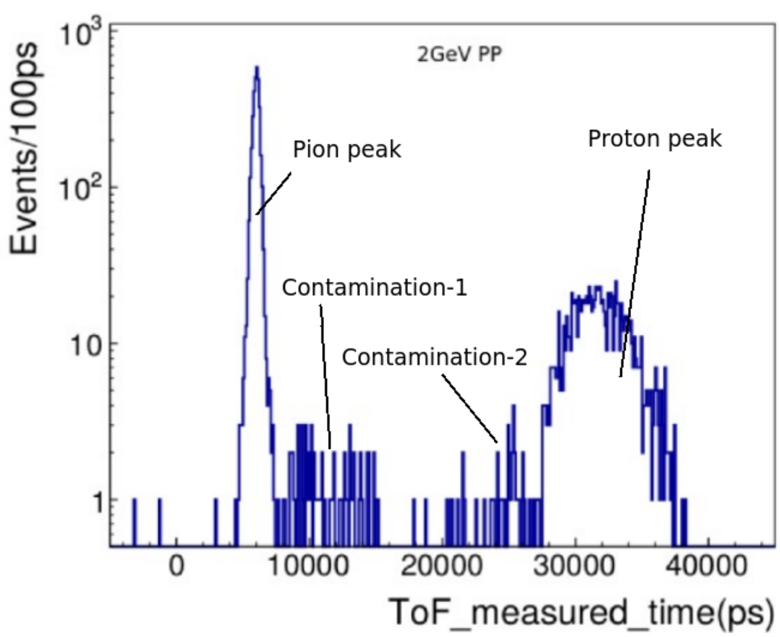


**Figure 5.12:** ToF histogram for the 2GeV $\pi^+$ sample showing the relevant intervals.

**Results for the 2 GeV $\pi^+$ sample**

*Contamination-2 Interval = $< 16\,000, 26\,000 >$ $(ps)$: $29p, 6\mu, 1e$

*Contamination-1 Interval = $< 8\,000, 16\,000 >$ $(ps)$: $34\pi, 29\mu, 5e$

*Proton-peak Interval = $< 26\,000, 39\,000 >$ $(ps)$: $1\,105p$

*Pion-peak Interval = $< 4\,000, 8\,000 >$ $(ps)$:
{ -CUT-1: $749\mu, 2\,623\pi$; -CUT-2: $444\mu, 2\,928\pi$; -CUT-3: $663\mu, 2\,709\pi$; -CUT-4: $518\mu, 2\,854\pi$; -CUT-5: $272\mu, 3\,100\pi$ }
No electrons found in the tail at the left of the Pion-peak $\sim < 4\,000, 4\,500 >$ $(ps)$

$\Longrightarrow$ The rough composition of the beam of $2\ GeV\pi^+$ ($\sim 4\,581$ particles (Events) identified) is presented in the next figure (the relative error is calculated as $1/\sqrt{N_k}$, where $N_k$ is the respective number of each of the species $k = \pi, p, \mu, e$). It is relevant to point out that showers at the right of the proton peak were considered to be protons, but they may be pions from the second bucket (it is also important to stress the fact that these numbers are estimations, there will never be a perfect particle ID technique for reasons explained in the last Section of this Chapter).

| Particle: | Number | Percentage | Relative error | |
|---|---|---|---|---|
| proton | 1134 | 24.75 % | 0.029695694 | |
| electron | 6 | 0.13 % | 0.40824829 | |
| pion | 2657 | 58.00 % | 0.019400111 | CUT-1 |
| muon | 784 | 17.11 % | 0.035714286 | CUT-1 |
| pion | 2962 | 64.66 % | 0.018374159 | CUT-2 |
| muon | 479 | 10.46 % | 0.045691166 | CUT-2 |
| pion | 2743 | 59.88 % | 0.019093568 | CUT-3 |
| muon | 698 | 15.24 % | 0.037850558 | CUT-3 |
| pion | 2888 | 63.04 % | 0.018608 | CUT-4 |
| muon | 553 | 12.07 % | 0.042524 | CUT-4 |
| pion | 3134 | 68.41 % | 0.01786284 | CUT-5 |
| muon | 307 | 6.70 % | 0.057073015 | CUT-5 |

Total 4581 "located" events == particles

**Figure 5.13:** Estimation of the beam composition for the $2GeV\pi^+$ sample for different ways to look at $\pi$ in the ToF Pion-peak.

*The logic statements for each of the CUT-$i$ are presented in the following figures (the intervals and logic statement for CUT-1 were already presented):

```
(CUT-2)"Cut considering the "Total_PE" in different Regions":

                  µ (MC-sample)           pi (Data-sample)

-Total_PE:        µ ~ <1000, 2000> ---->  pi ~ <2000, >
-Total_PE_ECAL:   µ ~ <0,1000>     ---->  pi ~ <1000, >
-Total_PE_HCAL:   µ ~ <0,800>      ---->  pi ~ <800, >
-Total_PE_L8P:    µ ~ <150,400>    ---->  pi ~ <0,150>
-Total_PE_L4P:    µ ~ <50,250>     ---->  pi ~ <0,50>
```

```
               if 2000<=S_PE_tot or 1000<=S_PE_ecal or 800<=S_PE_hcal or
S_PE_hcal<=350 or S_PE_L8P<=150 or S_PE_L4P<=50:   #pi-like events
```

```
(CUT-3)"Cut considering the "Ave_dE/dx":
                  µ (MC-sample)           pi (Data-sample)

-Ave_dEdx_Total:  µ ~ <100,225> ---->   pi ~ <225,1000>
-Ave_dEdx_ECAL:   µ ~ <0,100>   ---->   pi ~ <100,1000>
-Ave_dEdx_HCAL:   µ ~ <200,400> ---->   pi ~ <400,2000>
-Ave_dE/dx_L8P:   µ ~ <150,400> ---->   pi ~ <0,150>
-Ave_dE/dx_L4P:   µ ~ <100, 600>---->   pi ~ <0,100>
```

```
               if 225<=S_E_tot/42 or 100<=S_E_ecal/21 or 400<=S_E_hcal/21 or
S_E_hcal/21<=200 or S_E_L8P/8<=150 or S_E_L4P/4<=100:   #pi-like events
```

```
(CUT-4)"Cut considering the "Total_Hits:

                  µ (MC-sample)           pi (Data-sample)

-Total_Hits:        µ ~ <100,200>----> pi ~ <200,600>
-Total_Hits_ECAL:   µ ~ <50,125> ----> pi ~ <125,400>
-Total_Hits_HCAL:   µ ~ <50,100> ----> pi ~ <0,50> or <120,>
-Total_Hits_L8P:    µ ~ <20,50>  ----> pi ~ <0,15>
-Total_Hits_L4P:    µ ~ <8,30>   ----> pi ~ <0,7>
```

```
               if 200<=S_hits_tot or 125<=S_hits_ecal or S_hits_hcal<=50
or 120<=S_hits_hcal or S_hits_L8P<=15 or S_hits_L4P<=7:   #pi-like events
```

```
(CUT-5)"Using ALL previous cuts"
```

```
               if 10000<=S_E_tot or 2000<=S_E_ecal or 10000<=S_E_hcal or
S_E_hcal<=4000 or S_E_L8P<=400 or S_E_L4P<=400 or 2000<=S_PE_tot or 1000<=S_PE_ecal
or 800<=S_PE_hcal or S_PE_hcal<=350 or S_PE_L8P<=150 or S_PE_L4P<=50 or
225<=S_E_tot/42 or 100<=S_E_ecal/21 or 400<=S_E_hcal/21 or S_E_hcal/21<=200 or
S_E_L8P/8<=150 or S_E_L4P/4<=100 or 200<=S_hits_tot or 125<=S_hits_ecal or
S_hits_hcal<=50 or 120<=S_hits_hcal or S_hits_L8P<=15 or S_hits_L4P<=7:#pi-like events
```

**Figure 5.14:** CUTS-$i$ for $i = 2, ..., 5$ (Relevant Intervals & logic statements presented). The construction of CUT-1 was already explained in detail.

## 5.3 Intervals & Results for All the other samples

Here are presented Results on the composition of the beam for the other samples, only the most important histograms are attached together with the relevant intervals considered.

**Results for the 8 GeV $\pi^-$ sample**

A similar procedure to the one used for the 8 GeV $\pi^+$ sample was followed, the ToF histogram & the Total-E histogram (used for the separation of $\pi$ & $p$ present in the ToF Pion-peak) are presented below together with the relevant Intervals and their composition.

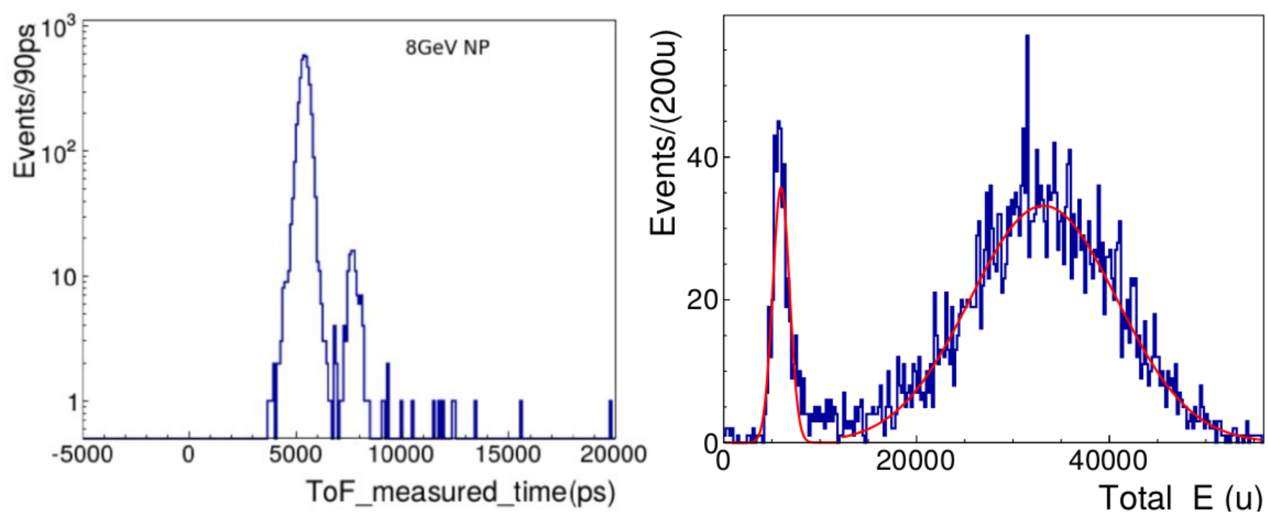


**Figure 5.15:** Left: ToF histogram for the 8 GeV $\pi^-$ sample. Right: Total-E histogram for Events in the ToF Pion-peak (of the histogram at the left).

*Contamination-2 Interval (at the right of the Proton-peak) = $< 8\,800, 16\,000 >$ $(ps)$: $13p$

*Contamination-1 Interval (between the $p$ & $\pi$ peaks) = $< 6\,650, 7\,000 >$ $(ps)$: $2e, 4\pi, 1\mu$

*Proton-peak Interval = $< 7\,000, 8\,800 >$ $(ps)$: $105p$

*Pion-peak Interval = $< 3\,400, 6\,650 >$ $(ps)$:
$\{\mu$-Interval = $< 0, 12\,000 >$ $(u)$ : $510\mu$,
$\pi$-Interval = $< 12\,000, 56\,000 >$ $(u)$ : $(3\,352 - (6))\pi$,

$6e$ found in the ToF interval $< 3\ 400, 4\ 500 >$ $(ps)\}$ $\Longrightarrow$ From the total number of $\pi$ counted we have substracted the number of $e$ (assuming that some $\pi$ may be confused as $e$, because $\mu$ will almost never look like $e$).

$\Longrightarrow$ The rough composition of the beam of $8\ GeV\pi^-$ ($\sim$ 3 987 particles (Events) identified) is presented in the next Figure (the relative error is calculated as $1/\sqrt{N_k}$, where $N_k$ is the respective number of each of the species $k = \pi, p, \mu, e$):

| Particle: | Number | Percentage | Relative error |
|---|---|---|---|
| (-)Polarity | | | |
| proton | 118 | 2.96 % | 0.092057 |
| pion | 3350 | 84.02 % | 0.017277 |
| muon | 511 | 12.82 % | 0.044237 |
| electron | 8 | 0.20 % | 0.353553 |
| Total | 3 987 "located" events == particles | | |

**Figure 5.16:** Estimation of the beam composition for the $8GeV\pi^-$ sample.

**Results for the 6 GeV $\pi^+$ sample**

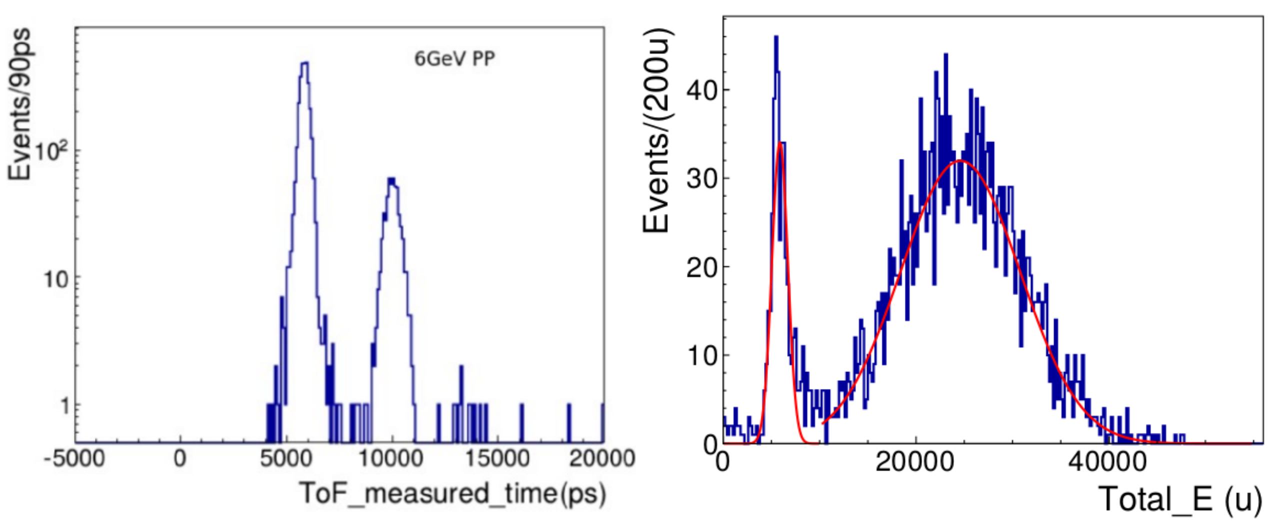


**Figure 5.17:** Left: ToF histogram for the 6 GeV $\pi^+$ sample. Right: Total-E histogram for Events in the ToF Pion-peak (of the histogram at the left).

*Contamination-2 Interval (at the right of the Proton-peak) = $< 12\,000, 16\,000 >$ $(ps)$: $4p, 2e$

*Contamination-1 Interval (between the $p$ & $\pi$ peaks) = $< 7\,800, 8\,980 >$ $(ps)$: $1e, 6\pi, 4\mu$

*Proton-peak Interval = $< 8\,980, 11\,250 >$ $(ps)$: $539p$

*Pion-peak Interval = $< 4\,000, 7\,800 >$ $(ps)$:
$\{\mu$-Interval = $< 0, 10\,000 >$ $(u)$ : $472\mu$,
$\pi$-Interval = $< 10\,000, 55\,000 >$ $(u)$ : $(2\,628 - (1))\pi$,
$1e$ found in the ToF interval $< 4\,000, 4\,500 >$ $(ps)\}$ $\Longrightarrow$ From the total number of $\pi$ counted we have substracted the number of $e$ (assuming that some $\pi$ may be confused as $e$, because $\mu$ will almost never look like $e$).

$\Longrightarrow$ The rough composition of the beam of 6 $GeV \pi^{+}$ ($\sim$ 3 656 particles (Events) identified) is presented in the next Figure (the relative error is calculated as $1/\sqrt{N_k}$, where $N_k$ is the respective number of each of the species $k = \pi, p, \mu, e$):

| Particle: (+)polarity | Number | Percentage | Relative error |
|---|---|---|---|
| proton | 543 | 14.85 % | 0.042914 |
| pion | 2633 | 72.02 % | 0.019488 |
| muon | 476 | 13.02 % | 0.045835 |
| electron | 4 | 0.11 % | 0.500000 |
| Total | 3 656 "located" events == particles | | |

**Figure 5.18:** Estimation of the beam composition for the $6 GeV \pi^{+}$ sample.

### Results for the 6 GeV $\pi^{-}$ sample

*Contamination-2 Interval (at the right of the Proton-peak) = $< 10\,700, 16\,000 >$ $(ps)$: $10p, 1\mu$

*Contamination-1 Interval (between the $p$ & $\pi$ peaks) = $< 7\,000, 8\,100 >$ $(ps)$: $2\pi, 1\mu$

*Proton-peak Interval = $< 8\,200, 10\,700 >$ $(ps)$: $95p$

*Pion-peak Interval = $< 3\,800, 7\,000 >$ $(ps)$:
$\{\mu$-Interval = $< 0, 10\,000 >$ $(u)$ : $481\mu$,
$\pi$-Interval = $< 10\,000, 55\,000 >$ $(u)$ : $(2\,955 - (4))\pi$,

$4e$ found in the ToF interval $< 3\,800, 4\,500 > (ps)\}$ $\Longrightarrow$ From the total number of $\pi$ counted we have substracted the number of $e$ (assuming that some $\pi$ may be confused as $e$, because $\mu$ will almost never look like $e$).

$\Longrightarrow$ The rough composition of the beam of $6\ GeV \pi^-$ ($\sim 3\,545$ particles (Events) identified) is presented in the next Figure (the relative error is calculated as $1/\sqrt{N_k}$, where $N_k$ is the respective number of each of the species $k = \pi, p, \mu, e$):

| Particle: | Number | Percentage | Relative error |
|---|---|---|---|
| (-)polarity | | | |
| proton | 105 | 2.96 % | 0.097590 |
| pion | 2953 | 83.3 % | 0.018402 |
| muon | 483 | 13.62 % | 0.045502 |
| electron | 4 | 0.11 % | 0.500000 |
| Total | 3 545 "located" events == particles | | |

**Figure 5.19:** Estimation of the beam composition for the $6GeV\pi^-$ sample.

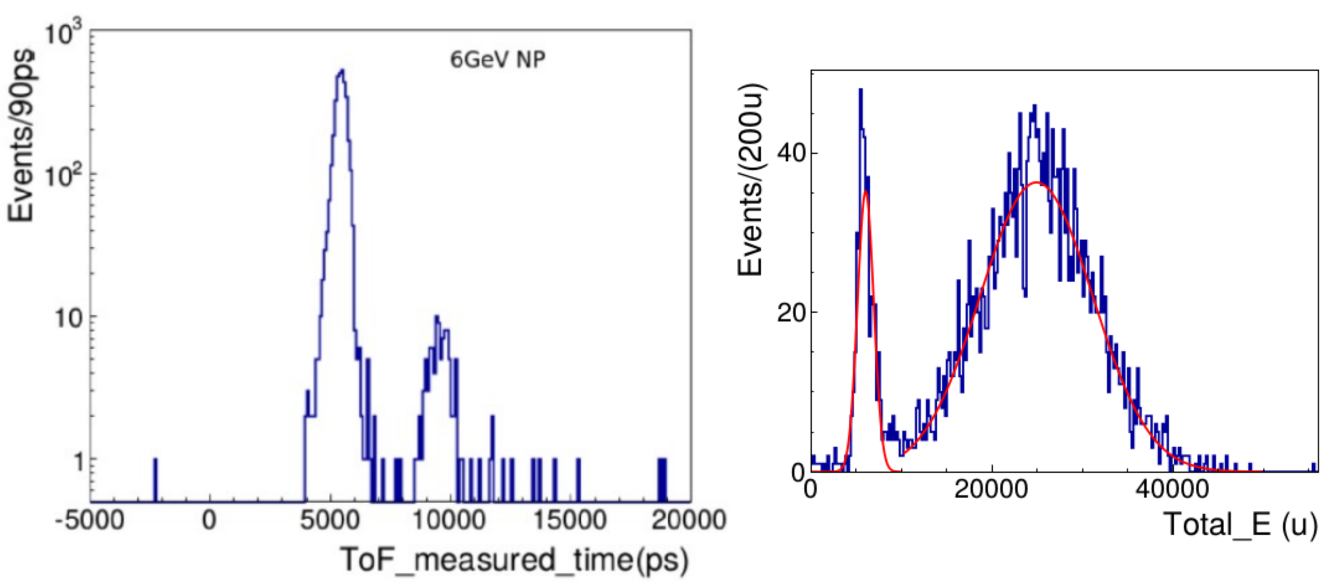


**Figure 5.20:** Left: ToF histogram for the 6 GeV $\pi^-$ sample. Right: Total-E histogram for Events in the ToF Pion-peak (of the histogram at the left).

### Results for the 4 GeV $\pi^+$ sample

*Contamination-2 Interval (at the right of the Proton-peak) = $< 17\,000, 20\,000 > (ps)$: $4p$

*Contamination-1 Interval (between the $p$ & $\pi$ peaks) = $< 7\,500, 11\,500 > (ps)$: $2e, 20\pi, 7\mu$

*Proton-peak Interval = $< 11\,500, 16\,500 > (ps)$: $580p$

*Pion-peak Interval = $< 3\,500, 7\,500 > (ps)$:
$\{\mu$-Interval = $< 0, 8\,000 > (u) : 498\mu$,
$\pi$-Interval = $< 8\,000, 45\,000 > (u) : (2\,446 - (1))\pi$,
$1e$ found in the ToF interval $< 3\,500, 4\,000 > (ps)\} \Longrightarrow$ From the total number of $\pi$ counted we have substracted the number of $e$ (assuming that some $\pi$ may be confused as $e$, because $\mu$ will almost never look like $e$).

$\Longrightarrow$ The rough composition of the beam of $4\ GeV \pi^+$ ($\sim$ 3 557 particles (Events) identified) is presented in the next Figure (the relative error is calculated as $1/\sqrt{N_k}$, where $N_k$ is the respective number of each of the species $k = \pi, p, \mu, e$):

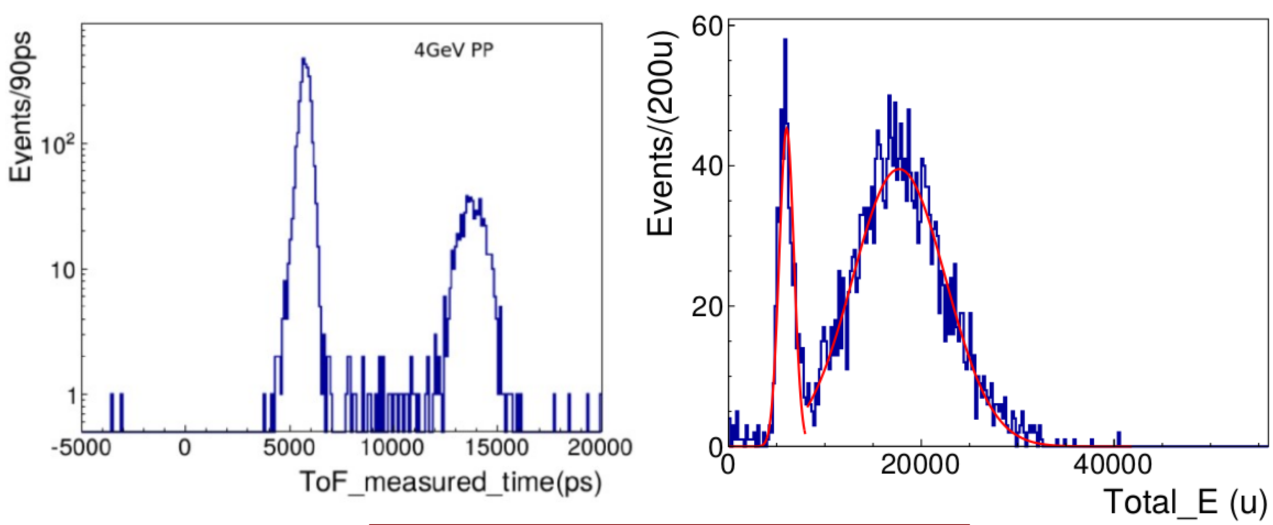


| Particle: (+)polarity | Number | Percentage | Relative error |
|---|---|---|---|
| proton | 584 | 16.41 % | 0.041380 |
| pion | 2465 | 69.30 % | 0.020141 |
| muon | 505 | 14.2 % | 0.044499 |
| electron | 3 | 0.08 % | 0.577350 |

Total 3 557 "located" events == particles

**Figure 5.21:** Relevant histograms & Estimation of the beam composition for the $4GeV\pi^+$ sample.

### Results for the 4 GeV $\pi^-$ sample

*Contamination-2 Interval (at the right of the Proton-peak) = $< 17\,800, 21\,000 >$ $(ps)$: $4p$

*Contamination-1 Interval (between the $p$ & $\pi$ peaks) = $< 7\,800, 14\,500 >$ $(ps)$: $5e, 40\pi, 17\mu$

*Proton-peak Interval = $< 14\,500, 17\,700 >$ $(ps)$: $34p$

*Pion-peak Interval = $< 4\,000, 7\,800 >$ $(ps)$:
$\{\mu$-Interval = $< 0, 8\,000 >$ $(u)$ : $286\mu$,
$\pi$-Interval = $< 8\,000, 45\,000 >$ $(u)$ : $(1\,143 - (1))\pi$,
$1e$ found in the ToF interval $< 3\,500, 5\,000 >$ $(ps)\}$ $\Longrightarrow$ From the total number of $\pi$ counted we have substracted the number of $e$ (assuming that some $\pi$ may be confused as $e$, because $\mu$ will almost never look like $e$).

$\Longrightarrow$ The rough composition of the beam of $4\ GeV \pi^-$ ($\sim$ 1 529 particles (Events) identified) is presented in the next Figure (the relative error is calculated as $1/\sqrt{N_k}$, where $N_k$ is the respective number of each of the species $k = \pi, p, \mu, e$):

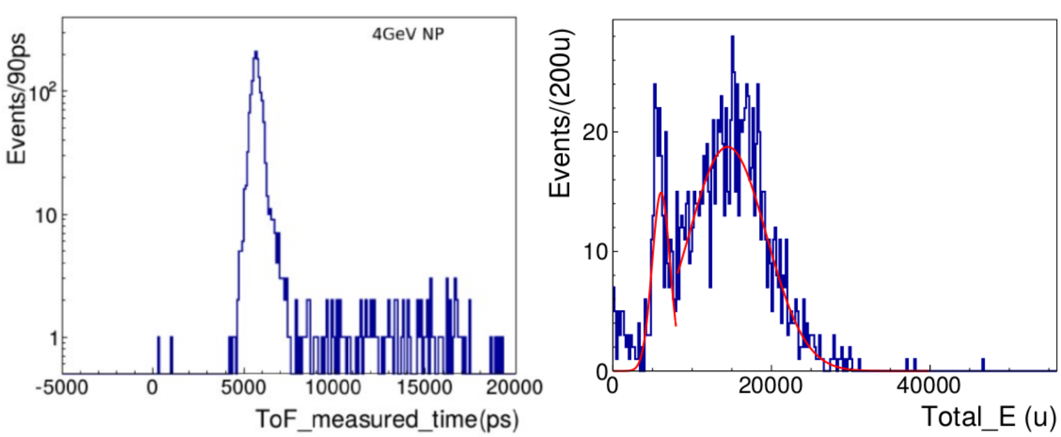


| Particle: (-)polarity | Number | Percentage | Relative error |
|---|---|---|---|
| proton | 38 | 2.5 % | 0.162221 |
| pion | 1182 | 77.3 % | 0.029086 |
| muon | 303 | 19.82 % | 0.057448 |
| electron | 6 | 0.39 % | 0.408248 |
| Total | 1 529 | "located" events == particles | |

**Figure 5.22:** Relevant histograms & Estimation of the beam composition for the $4GeV\pi^-$ sample.

**Results for the 2 GeV $\pi^-$ sample**

*Contamination-2 Interval = $< 30\,000, 31\,000 >$ $(ps)$: 0 particles

*Contamination-1 Interval = $< 12\,000, 16\,000 >$ $(ps)$: $2\pi, 1\mu$

*Proton-peak Interval = $< 20\,000, 25\,000 >$ $(ps)$: $3p$

*Pion-peak Interval = $< 4\,000, 8\,000 >$ $(ps)$:
{ -CUT-1: $48\mu, 90\pi$; -CUT-2: $47\mu, 91\pi$; -CUT-3: $48\mu, 90\pi$; -CUT-4: $13\mu, 125\pi$; -CUT-5: $12\mu, 126\pi$ }
No electrons found in the tail at the left of the Pion-peak $\sim < 4\,000, 4\,500 >$ $(ps)$

$\Longrightarrow$ The rough composition of the beam of 2 $GeV\pi^-$ ($\sim$ 144 particles (Events) identified) is presented in the next figure (the relative error is calculated as $1/\sqrt{N_k}$, where $N_k$ is the respective number of each of the species $k = \pi, p, \mu, e$). We notice that the statistics is very poor when compared to the positive-polarity sample (antiprotons are less stable).

| Particle: (-)polarity | Number | Percentage | Relative error | |
|---|---|---|---|---|
| proton | 3 | 2.08 % | 0.57735 | |
| electron | 0 | 0 % | 0 | |
| pion | 92 | 63.89 % | 0.10426 | CUT-1 |
| muon | 49 | 34.03 % | 0.14286 | |
| pion | 93 | 64.6 % | 0.10370 | CUT-2 |
| muon | 48 | 33.3 % | 0.14434 | |
| pion | 92 | 63.89 % | 0.10426 | CUT-3 |
| muon | 49 | 34.03 % | 0.14286 | |
| pion | 127 | 88.19 % | 0.088736 | CUT-4 |
| muon | 14 | 9.72 % | 0.267261 | |
| pion | 128 | 88.89 % | 0.088388 | CUT-5 |
| muon | 13 | 9.03 % | 0.277350 | |

Total 144 "located" events == particles

**Figure 5.23:** Estimation of the beam composition for the $2GeV\pi^-$ sample for different ways to look at $\pi$ in the ToF Pion-peak.

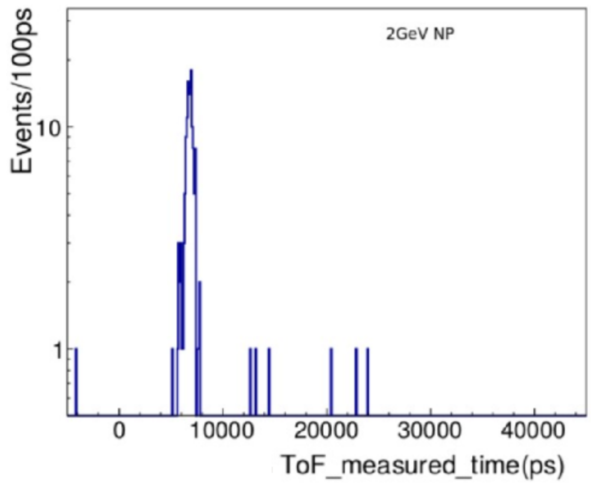


**Figure 5.24:** ToF histogram for the $2GeV\pi^{-}$, the poor statistic of this sample is immediately noticeable (there are almost no antiprotons).

*The logic statements for each of the CUT-$i$ (that look at $\pi$, in the same way as the ones used for the positive-polarity sample) are presented in the following Figures:

```
(CUT-1)"Cut considering the "Total_E" in different regions":

                μ (MC-sample)          pi (Data-sample)

-Total_E:      μ ~ <5000,10000>; pi ~ <10000,>
-Total_E_ECAL: μ ~ <0,2000>;     pi ~ <2000, >
-Total_E_HCAL: μ ~ <4000,10000>; pi ~ <8000, >
-Total_E_L8P:  μ ~ <500, >;      pi ~ <0,400>
-Total_E_L4P:  μ ~ <500, >;      pi ~ <0,400>
```

```
                 if 10000<=S_E_tot or 2000<=S_E_ecal or 8000<=S_E_hcal or
S_E_L8P<=400 or S_E_L4P<=400:   #pi-like events
```

```
(CUT-2)"Cut considering the "Total_PE":

                μ (MC-sample)           pi (Data-sample)

-Total_PE:      μ ~ <1000, 2000>;  pi ~ <2000, >
-Total_PE_ECAL: μ ~ <0,1000>;      pi ~ <1000, >
-Total_PE_HCAL: μ ~ <400,800>;     pi ~ <800, >
-Total_PE_L8P:  μ ~ <100,400>;     pi ~ <0,100>
-Total_PE_L4P:  μ ~ <50,200>;      pi ~ <0,30>
```

```
                 if 2000<=S_PE_tot or 1000<=S_PE_ecal or 800<=S_PE_hcal or
S_PE_L8P<=100 or S_PE_L4P<=30:   #pi-like events
```

```
(CUT-3)"Cut considering the "Ave_dE/dx":

                 μ (MC-sample)           pi (Data-sample)

-Ave_dEdx_Total:  μ ~ <100,225>;   pi ~ <225,1000>
-Ave_dEdx_ECAL:   μ ~ <0,100>;     pi ~ <100,1000>
-Ave_dEdx_HCAL:   μ ~ <200,400>;   pi ~ <400,2000>
-Ave_dE/dx_L8P:   μ ~ <150,450>;   pi ~ <0,100>
-Ave_dE/dx_L4P:   μ ~ <100, 600>;  pi ~ <0,100>
```

```
                if 225<=S_E_tot/42 or 100<=S_E_ecal/21 or 400<=S_E_hcal/21 or
S_E_L8P/8<=100 or S_E_L4P/4<=100:   #pi-like events
```

```
(CUT-4)"Cut considering the "Total_Hits:

                 μ (MC-sample)           pi (Data-sample)

-Total_Hits:        μ ~ <100,200>;      pi ~ <200,600>
-Total_Hits_ECAL:   μ ~ <50,125>;       pi ~ <125,400>
-Total_Hits_HCAL:   μ ~ <50,100>;       pi ~ <0,50> or <120,>
-Total_Hits_L8P:    μ ~ <20,50>;        pi ~ <0,15>
-Total_Hits_L4P:    μ ~ <8,30>;         pi ~ <0,7>
```

```
                if 200<=S_hits_tot or 125<=S_hits_ecal or S_hits_hcal<=50 or
120<=S_hits_hcal or S_hits_L8P<=15 or S_hits_L4P<=7:
```

```
(CUT-5)"Using ALL previous cuts"
```

```
                if 10000<=S_E_tot or 2000<=S_E_ecal or 8000<=S_E_hcal or
S_E_L8P<=400 or S_E_L4P<=400 or 2000<=S_PE_tot or 1000<=S_PE_ecal or 800<=S_PE_hcal
or S_PE_L8P<=100 or S_PE_L4P<=30 or 225<=S_E_tot/42 or 100<=S_E_ecal/21 or
400<=S_E_hcal/21 or S_E_L8P/8<=100 or S_E_L4P/4<=100 or 200<=S_hits_tot or
125<=S_hits_ecal or S_hits_hcal<=50 or 120<=S_hits_hcal or S_hits_L8P<=15 or
S_hits_L4P<=7:
```

## 5.4 Relevant Observations & Summary of Results

The previous Results presented on the composition of the secondary beam (% $p^{\pm}, \pi^{\pm}, \mu^{\pm}, e^{\pm}$ ) at different energies and polarities are important for the Test Beam to test the efficiency of its beamline & main detector devices (for example, the efficiency of the Cerenkov and the Lied shield in rejecting electrons and of the ToF in separating $\pi$ and $p$) and also for the MINER$\nu$A experiment to have more tools available for the identification of specific species passing through its main detector (along its ECAL/HCAL region). Only results for Data Run 1 (ECAL/HCAL configuration of the detector) have been presented because the beam is actually the same for both Data Run 1 & 2, but the detector configuration for Data Run 1 makes it easier to perform a systematic analysis via the definition of specific variables over different regions of the detector.

In this chapter only the most relevant histograms have been presented and the 2D histograms of pure and isolated species ($\mu$ & $\pi$) have been omitted although they can be found in [89].

There are some specific details that are relevant to discuss: What unit of energy corresponds to the unit "u"used for all histograms of Energy related variables (Energy deposited over different regions of the detector)?, Why there is a red-spot in the 2D histogram of **dE/dx vs. module** for the Monte Carlo sample of pure $\mu$ in module-0 ? (there is also other interesting feature in this module for the **total-PE vs module** in Data) & What are the limitations of the logic used so far for the 2GeV samples that has been set to look at $\pi$ (Figure 5.6). The last point related to the need to change the logic is important to analyze in detail the cuts used for the 2GeV samples in order to reduce their number and in that way reduce the **systematic uncertainties** (that cannot be reduced with increasing the statistics) introduced by each of them.

To estimate the exact units for the unit of energy "$u$" we can rely on the histogram for Total-Energy for the $8GeV\pi^+$ sample. From there we can assure that $56\ 000\ u < 8GeV$, because even if the particle of 8GeV managed to deposit all of its energy inside the detector it will deposit a less amount of energy which depend on the detector response at different energies. This implies that $u \leq 1.43 \times 10^5 eV \sim 2.3 \times 10^{-14} J$

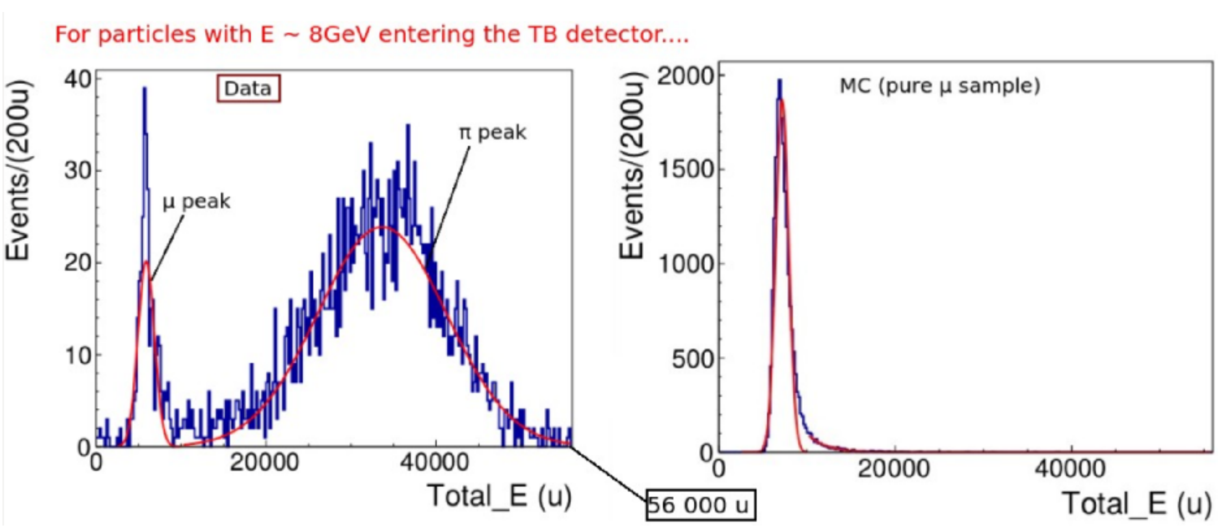


**Figure 5.25:** For any particle entering the TB detector at a given energy, we can find a limit for the unit "$u$" based on the upper limit for the energy deposited. From this: $u \leq 1.43 \times 10^5 eV \sim 2.3 \times 10^{-14} J$.

With respect to the red spot appearing in module-0 for the MC sample of pure $\mu$ it seems that some attenuation lenght was assumed that made the dE/dx to appear too low, this module-0 was not present in Test Beam 1 and that experiment was the starting point for the development of the MC simulation for Test Beam 2. Regarding the higher value of PE for module-0, it seems that due to the fact that this plane is actually a half-plane (it only contains 32 strips instead of 64), the attenuation distance is on average shorter, which implies higher light-yield for this module [90]. This issue of course is not a problem because for other planes the pattern is as expected.

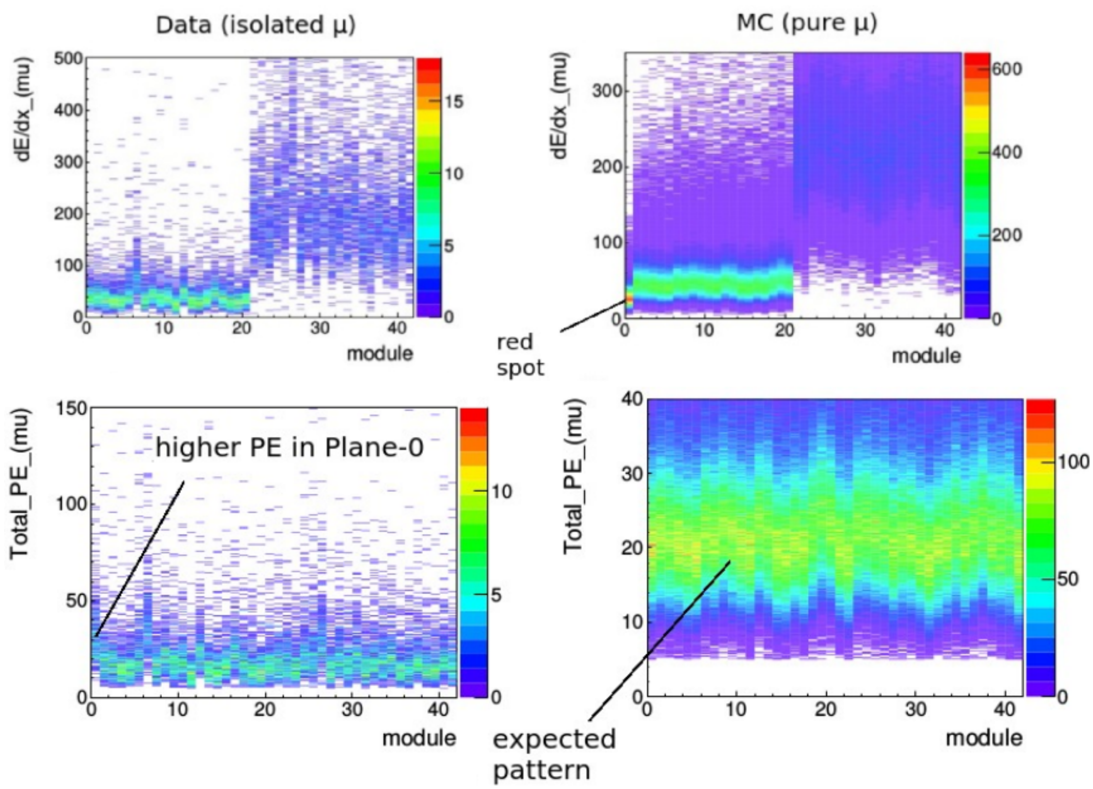


**Figure 5.26:** Some features taking place in module-0 of the TB detector: A lower value of dE/dx for the MC & a higher value of PE for Data. For the remaining planes it is obtained the expected pattern.

With respect to the logic used for locating $\pi$ for events in the ToF Pion-peak (Figure 5.6), it is relevant to point out that the union of cuts is not reliable because it makes it difficult to perform any Efficiency-Purity analysis and to analyze the effect of one specific cut on another one. It is also important to state that for the specific cuts of type CUT-$i$ used, there may be some useless cuts making up a specific CUT-$i$, this is bad because the higher the number of cuts we introduce, the greater the systematic uncertainty in the results obtained on the **composition of the beam**. For this reason in next Chapter a change in the logic is performed together with an Efficiency-Purity analysis to make up the best cut for separating specific species at $2GeV$ (where more than 1 cut is mandatory for this separation).

Finally, let us end this Chapter presenting a summary of the Results (estimations) obtained on the composition of the beam based on different cuts for different energies and polarities of the secondary beam:

| Energy(GeV) | Polarity | %p | %π | %μ | %e | |
|---|---|---|---|---|---|---|
| 8 | Pos | 15.87 | 74.04 | 9.94 | 0.15 | |
| 6 | Pos | 14.85 | 72.02 | 13.02 | 0.11 | |
| 4 | Pos | 16.43 | 69.34 | 14.2 | 0.03 | |
| 2 | Pos | 24.75 | 58 | 17.11 | 0.13 | CUT-1 |
| 2 | Pos | 24.75 | 64.66 | 10.46 | 0.13 | CUT-2 |
| 2 | Pos | 24.75 | 59.88 | 15.24 | 0.13 | CUT-3 |
| 2 | Pos | 24.75 | 63.04 | 12.07 | 0.13 | CUT-4 |
| 2 | Pos | 24.75 | 68.41 | 6.7 | 0.13 | CUT-5 |

| Energy(GeV) | Polarity | %p | %π | %μ | %e | |
|---|---|---|---|---|---|---|
| 8 | Neg | 2.96 | 84.02 | 12.82 | 0.2 | |
| 6 | Neg | 2.96 | 83.3 | 13.62 | 0.11 | |
| 4 | Neg | 2.5 | 77.3 | 19.82 | 8.39 | |
| 2 | Neg | 2.08 | 63.89 | 34.03 | 0 | CUT-1 |
| 2 | Neg | 2.08 | 64.6 | 33.3 | 0 | CUT-2 |
| 2 | Neg | 2.08 | 63.89 | 34.03 | 0 | CUT-3 |
| 2 | Neg | 2.08 | 88.19 | 9.72 | 0 | CUT-4 |
| 2 | Neg | 2.08 | 88.89 | 9.03 | 0 | CUT-5 |

**Figure 5.27:** Particle Composition of the Secondary Beam for different Energies & Polarities. For the 2GeV samples it is shown the specific CUT-$i$ used for getting those results.

# Chapter 6

# Efficiency-Purity analysis to find the optimum cuts to separate different species for the 2GeV sample

It was stated at the end of the previous Chapter why it is important to reduce the number of cuts employed for the isolation of a specific kind of particle species (to reduce systematic uncertainties) for the 2 GeV samples. The cuts of type CUT-$i$ presented there were made up as unions of cuts over different specific variables (each CUT-$i$ being the union of 5 variables among a total of 20 of them) and looked at $\pi$. Since these 20 variables can be used in the separation of $\mu$ from $\pi$, we can analyze each of them and the effect of 1 after another. For that purpose it is better to **change the logic** and seek for the best cut for the isolation of species as an intersection instead of as a union. Figure 6.1 present the logic that would look at $\mu$ insted of $\pi$ (which is just the negation of the one used in the previous Chapter) & the definition of the Variables $Var\_i\_\beta$. It is relevant to point out that this analysis is performed on Positive Polarity particles.

It is relevant to point out that for the analysis that is presented in this Chapter, Monte Carlo simulations of single-particle species were mandatory. However, there was a problem found in the MC while constructing shower-shape scripts (this was an idea to separate $\mu$ by considering that they deposit a number of hits less than a certain fixed number for all modules==planes of the TB-Detector). The issue is that there are several Events in the MC sample that have Hits with values of PE less than 3 (as explained in Figure 6.2), this means that those hits are not physically meaningful (this occurs because the MC is just a simulation !). In this way the variable of kind “Hits ” (a subset of the set of variables $Var\_i\_\beta$) is affected and for this reason it was necessary to introduce an extra condition in the scripts for this analysis: For each Event only consider Hits with a PE higher than 3.

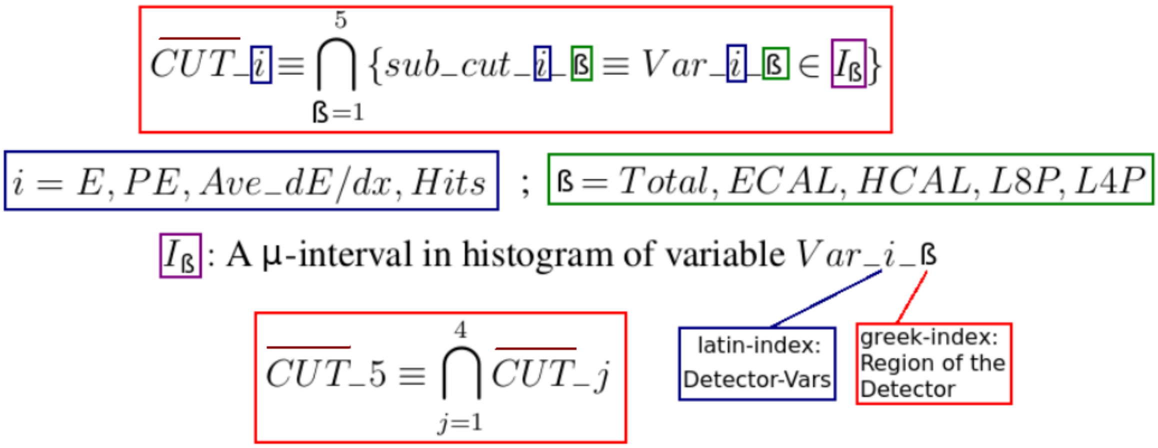


**Figure 6.1:** Logic of the cuts that look at $\mu$. The variables of kind $Var\_i\_\beta$ are presented there. It is relevant to keep in mind that the (sub)cut of type $i\_\beta$ looks for Events in the $\mu$-Interval $I_\mu$ so it is mandatory to find the optimum $I_\mu$ for each of the 20 Variables $Var\_i\_\beta$.

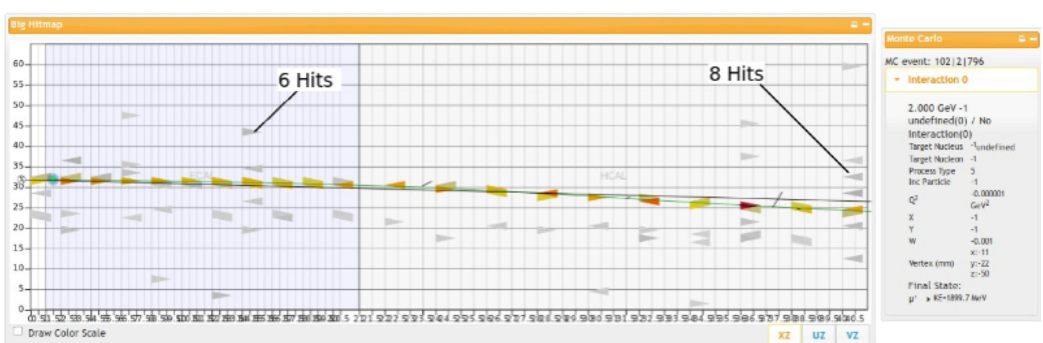


**Figure 6.2:** Many Events in the MC sample contain hits with PE less than 3, this feature was found out while developing shower-shape scripts. It was necessary to repeat the analysis with the condition that for each Event only those Hits with $PE >= 3$ to be considered.

What is presented next is an **Efficiency-Purity Analysis** of the 20 cuts that look at isolating $\mu$ from $\pi$. The idea is to end with a cut that results to be the intersection of the 2 Best Cuts (among the 20 ones) with regard to their value of Efficiency ($\xi$) & Purity ($\mathcal{P}$). For each of the variables $Var\_i\_\beta$ we can find the optimum $\mu$-Interval $I_{\mu}^{i\beta}$. Figure 6.3 presents this methodology to find the optimum $\mu$-Interval for each variable and the definitions of Efficiency & Purity are summarized in Figure 6.4 together with the necessary conditions for those definitions to hold and the way to calculate their respective uncertainties [91].

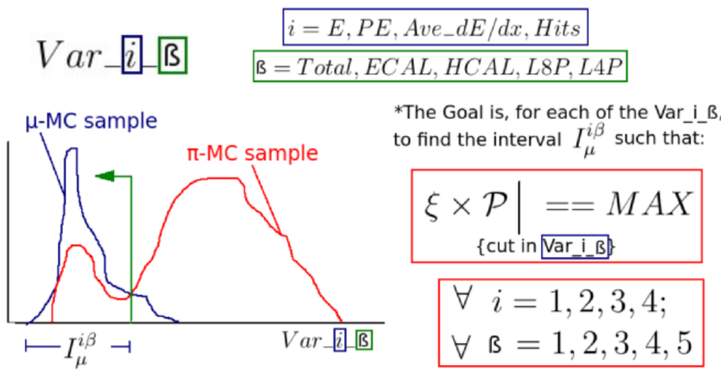


**Figure 6.3:** For each of the Variables $Var\_i\_\beta$ the optimum cut to look at $\mu$ is the one that maximizes the product $\xi \times \mathcal{P}$.

$$\xi = \frac{\text{μ-Events( Var\_i\_ß } \in I_{\mu}^{i\beta}\text{)}}{\text{μ-Events (All μ-histogram)}} \equiv \frac{N_p}{N_p + N_f}$$

$$\mathcal{P} = \frac{\text{μ-Events( Var\_i\_ß } \in I_{\mu}^{i\beta}\text{)}}{\text{μ-Events( Var\_i\_ß } \in I_{\mu}^{i\beta}\text{) + π-Events (Var\_i\_ß } \in I_{\mu}^{i\beta}\text{)}} \equiv \frac{N_s}{N_s + N_b}$$

Conditions:

- The total number $N_0 = N_P + N_f \sim Po(\lambda)$
- Total Number of Events in the μ & π histograms should be equal (== normalized histograms) for a proper calculation of the Purity
- With that assumption & considering errors in the previous numbers as, $\delta N_p = \sqrt{N_p},\ \delta N_f = \sqrt{N_f}$ we can find the respective errors in the Effic & Pur (to plot 2D graphs with error bars & analyze correlations among cuts) using a propagation of errors formula:

$$\Delta\xi = [\xi(1-\xi)/N_0]^{1/2}\ ;\ \Delta\mathcal{P} = [\mathcal{P}(1-\mathcal{P})/N_s + N_b\ ]^{1/2}$$

**Figure 6.4:** Definitions of Efficiency & Purity. For these to hold the total number of Events should follow a Poisson distribution & the Total Number of Events for both histograms should match. The uncertainties in $\xi$ & $\mathcal{P}$ are defined at the bottom [91].

Next an $\xi - \mathcal{P}$ Analysis is applied to make up the best cut that separates: $\mu$ from $\pi$, $e$ from $\mu$ and $e$ from $\pi$. For each case the specific methodology is explained in detail. At the end it is presented the **Tool developed** and the way it should be applied to Data in order to find the Identity of any Event (Particle) that comes from Test Beam Data.

## 6.1 $\xi - \mathcal{P}$ Analysis to make up the Optimum-Cut to separate $\mu^+$ from $\pi^+$

In **Appendix E** are presented histograms of pure (MC) $\mu^+$ & $\pi^+$ samples together in a single Canvas for each of the 20 variables $Var\_i\_\beta$ and the interval $I_\mu$ that maximizes the product $\xi \times \mathcal{P}$ (highlighted). Here are presented plots of $\xi$, $\mathcal{P}$, $\xi \times \mathcal{P}$ vs. Cut & a 2D plot of $\mathcal{P}$ vs. $\xi$. After having selected the **best among the 20 cuts** we outline the methodology followed to pick up the second cut in order to make up the "optimum-cut" for separating $\mu^+$ from $\pi^+$ (as an intersection of the 2 cuts chosen among the 20 ones avaible).
*For the 20 cuts whose intervals in their respective histograms are presented in Appendix E:

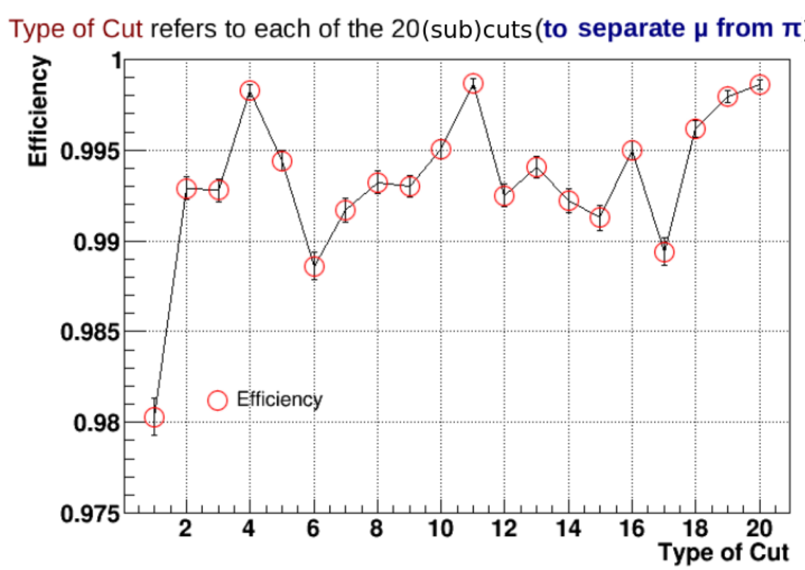


**Figure 6.5:** Efficiency for each of the 20 cuts (each maximizing the product $\xi \times \mathcal{P}$ in the respective variable $Var\_i\_\beta$) that can be used to separate $\mu^+$ from $\pi^+$.

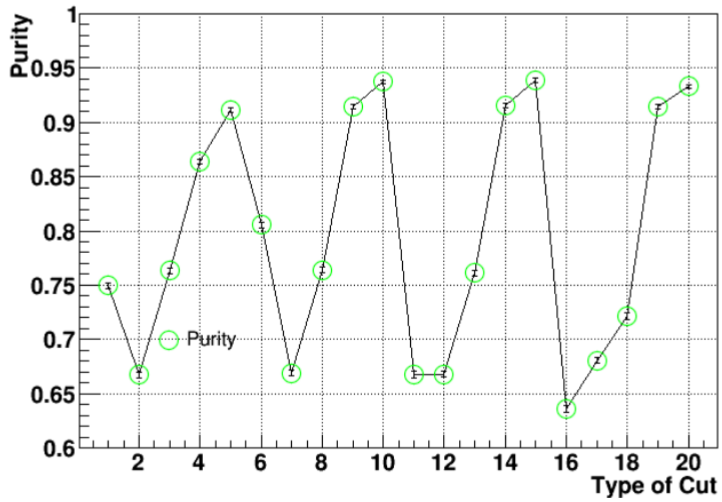


**Figure 6.6:** Purity for each of the 20 cuts (each maximizing the product $\xi \times \mathcal{P}$ in the respective variable $Var\_i\_\beta$) that can be used to separate $\mu^+$ from $\pi^+$.

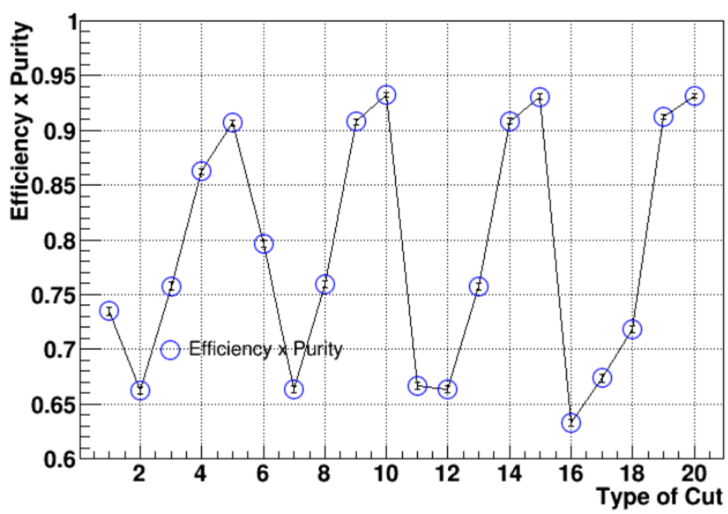


**Figure 6.7:** Efficiency $\times$ Purity for each of the 20 cuts (each maximizing the product $\xi \times \mathcal{P}$ in the respective variable $Var\_i\_\beta$) that can be used to separate $\mu^+$ from $\pi^+$.

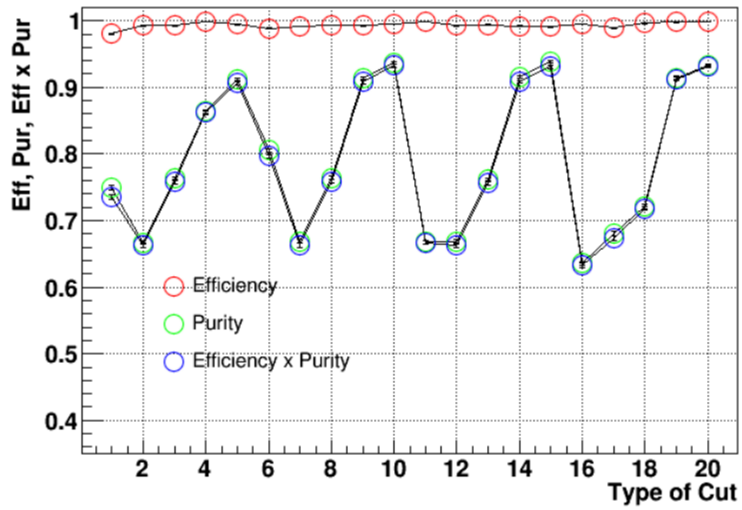


**Figure 6.8:** All the 3 previous quantities in a single plot.

*A 2D Plot of $\mathcal{P}$ vs. $\xi$ is also interesting because it permits to locate what are the best cuts and which of them have similar features.

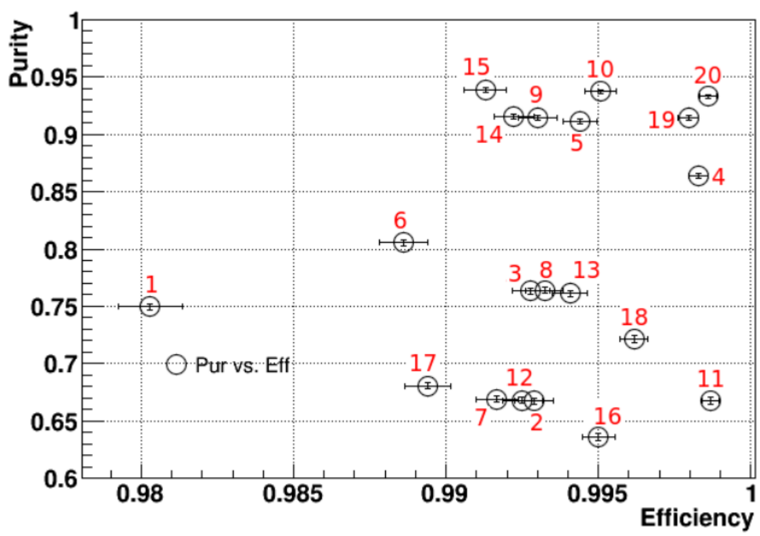


**Figure 6.9:** $\mathcal{P}$ vs. $\xi$ for each of the 20 cuts (each correponding to a different variable). This plot permits to analyze correlations among different cuts (points close together correspond to cuts that have a similar effect in Data) and also to locate the best ones.

From the previous plots we notice that **cuts 5,10,15,20** (L4P vars) are the best ones. After them we have the cuts in L8P vars as shown in the next Figure. The idea is to plot histograms of other Vars for events in the $\mu$-interval (for the best cut) in order to see which could be the **best second cut**. However, there are some relevant remarks to point out: The Purity of the cuts calculated previously cannot be used for Data because for the Data sample we do not know the ratio of $\pi$ to $\mu$, **since there is no MC simulation of the secondary beam**...then we tried to estimate the background for both $\pi$ & $\mu$ in another way, in other to find an estimation of the number of these species. Below the Methodology followed is outlined.

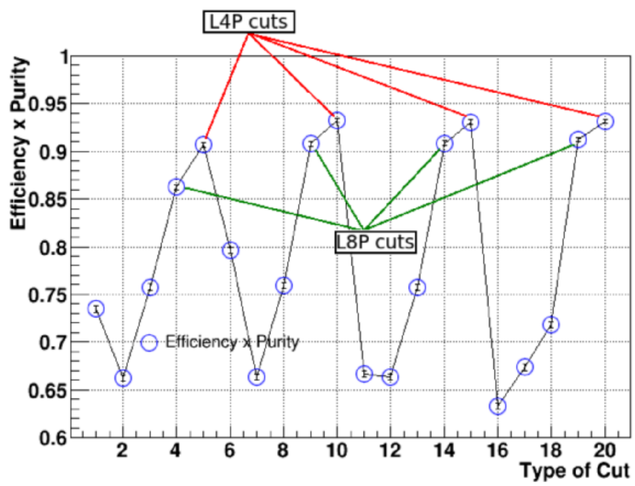


**Figure 6.10:** This plot shows that the cuts in the L4P are the best ones (because those have the largest value of $\xi \times \mathcal{P}$), followed by the ones in the L8P.

***Methodology followed** (a suggestion made by my supervisor at Fermilab, Dr. Leo Bellantoni)

-From the best cuts we select 1 of them (let's call it in Variable $x_1$) to retain events in the $\mu$-Interval ($I_\mu$).

-Plot the histograms of other variables for events in the selected $\mu$-Interval ($I_\mu$) to see which variable (let's call it $x_2$) separates better the $\mu$ & $\pi$ present there. Select the remaining $\mu$ in the new $\mu$-interval ($I'_\mu$ ) in this new histogram.

-Plot also the histogram of the same variable ($x_1$) in that interval in log-scale...to see if we ought to change the $\mu$-Interval in order to improve the cut.

-8 candidates (because their histograms showed a better separation of $\mu$ from $\pi$) were selected as the second cut (to add to the one cited above) and the most efficient (in selecting $\mu$) among them was chosen.

-Then we can make up the cut to retain $\mu$ as well as the cut to retain $\pi$ (which is the negation of the other). The next Figure presents the logic of the optimum-cut constructed and the relevant numbers to calculate: efficiencies ($\xi_{\mu\mu}$, $\xi_{\pi\pi}$), fractions of $\mu$ looking as $\pi$ ($\xi_{\mu\pi}$) and viceversa ($\xi_{\pi\mu}$).

- Cut_μ =={ $x_1 \in I_\mu$ && $x_2 \in I'_\mu$ }
- Cut_π == { $x_1 \in I_\pi$ || { $x_1 \in I_\mu$ && $x_2 \in I'_\pi$ } }

  (*)=={ $x_1 \in I_\pi$ || $x_2 \in I'_\pi$ } == ~ Cut_μ

$$\boxed{\begin{aligned} I_\pi &= I_\mu^c \\ I'_\pi &= I_\mu^{\prime c} \end{aligned}}$$

- Applying these cuts to the MC samples of pure μ & π we can find the efficiencies:
  - Fraction of μ looking as μ(pass the Cut_μ): $\xi_{\mu\mu}$
  - Fraction of μ looking as π: $\xi_{\mu\pi} = 1 - \xi_{\mu\mu}$
  - The same for the case of π: $\xi_{\pi\pi}$, $\xi_{\pi\mu} = 1 - \xi_{\pi\pi}$

**Figure 6.11:** Logic of the cut (intersection of 2 of the 20 cuts) to look at $\mu$ (& $\pi$). The relevant fractions ($\xi_{\mu\mu}, \xi_{\mu\pi}, \xi_{\pi\mu}$) are presented and the intervals for the first ($I_\mu$) & second cut ($I'_\mu$).

Choosing the **best cut** $x_1$ as $Hits\_L4P$ (**Figure E.20** of Appendix E) we make a plot of events in an interval a bit larger ($< 4, 12 >$) than the initial $\mu$-Interval ($< 4, 10 >$) for the same variable $x_1$ to correct this $\mu$-interval (log-scale used) as is shown in Figure 6.12. Choosing 8 candidates for the variable $x_2$ ($Total\_E, Total\_E\_HCAL, Total\_PE, Total\_PE\_HCAL,$ $< dE/dx >\_\ Total, < dE/dx >\_\ HCAL, Total\_Hits\_HCAL, \&\ Total\_Hits\_L8P$), after plotting their histograms for Events in which $x_1 \in I_\mu$ & after calculating the numbers $\xi_{\mu\mu}$, $\xi_{\mu\pi}$, $\xi_{\pi\pi}$, $\xi_{\pi\mu}$ it was found that $x_2 = Total\_PE\_HCAL$ maximized the efficiency for selecting $\mu$ (Figure 6.13 shows this result together with its histogram for Events that have $x_1$ in $I_\mu$ & the new $\mu$-Interval $I'_\mu$ in which to cut on variable $x_2 = Total\_PE\_HCAL$)

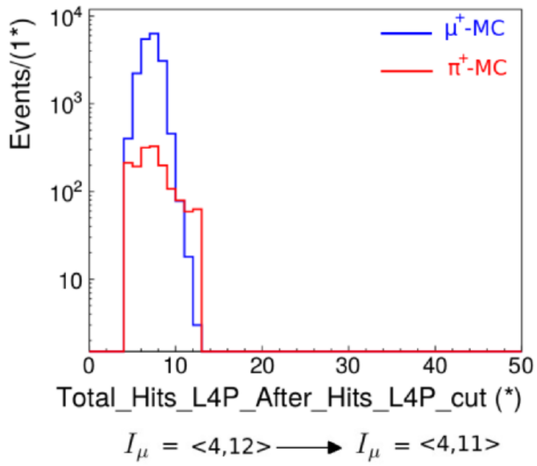


**Figure 6.12:** Histogram of variable $x_1$ for events such that $x_1 \in I_\mu$ in log scale (in an interval a bit larger than $I_\mu$). This shows that a slight change in the interval was relevant to improve the cut (to improve a little the efficiency of selecting $\mu$).

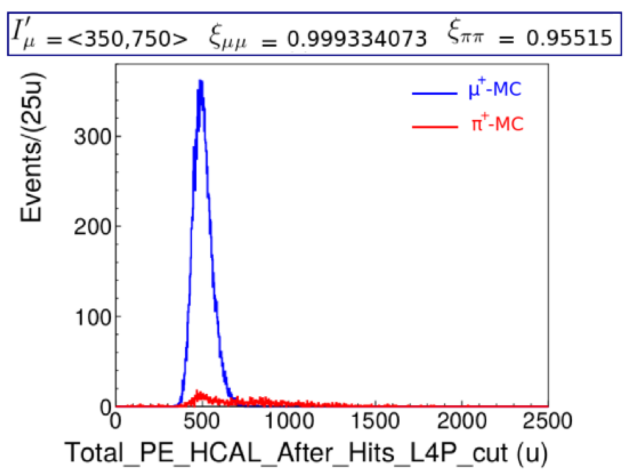


**Figure 6.13:** Histogram of variable $x_2$ for events such that $x_1 \in I_\mu$. The new $\mu$-Interval ($I'_\mu$) for variable $x_2$ that maximizes the efficiency of selecting $\mu$ ($\xi_{\mu\mu}$) is $I'_\mu =< 350, 750 >$.

After having constructed this cut to separate $\mu$ from $\pi$ we can estimate the numbers for each of the species (applying the cut to Events that come from the ToF Pion-peak) and the background for each case using the following formulas (This is to be applied after the initial numbers of $\mu$ & $\pi$ have been calculated):

- Relations that may be used:

$$
\begin{aligned}
N^0_\mu &\equiv N^{Data}_\mu \\
N'_\mu &= N^0_\mu/\xi_{\mu\mu} \\
N_{\pi\mu} &= N'_\pi\,\xi_{\pi\mu} \\
N''_\mu &= N'_\mu - N_{\pi\mu} = N'_\mu - N'_\pi\,\xi_{\pi\mu}
\end{aligned}
\qquad
\begin{aligned}
N^0_\pi &\equiv N^{Data}_\pi \\
N'_\pi &= N^0_\pi/\xi_{\pi\pi} \\
N_{\mu\pi} &= N'_\mu\,\xi_{\mu\pi} \\
N''_\pi &= N'_\pi - N_{\mu\pi} = N'_\pi - N'_\mu\,\xi_{\mu\pi}
\end{aligned}
$$

**Figure 6.14:** Iterative relations to estimate the particle composition of a given Data sample (composed of $\mu$ & $\pi$), this is called correction by efficiency. A way to estimate the background in terms of the fraction of a given species looking like the other is also presented.

## 6.2 $\xi - \mathcal{P}$ Analysis to make up the Optimum-Cut to separate $e^+$ from $\mu^+$

A similar analysis was performed to make up the optimum-cut to separate $e^+$ from $\mu^+$. For this case, as is outlined below, the cuts were excellent and only one of them was enough. This actually verifies what was expected when the TB detector was constructed: The separation between $e^+$ & $\mu^+$ should be almost perfect, since all positrons (that behave like electrons) will be stoped at the ECAL and all muons will pass through the whole detector, depositing energy in the Last-Planes. Despite this fact, the analysis was performed in order to verify that the logic used in the scripts was good and to find out which of the variables was the best one in separating $e^+$ from $\mu^+$. **Appendix F** presents histograms of pure (MC) $e^+$ & $\mu^+$ in the same way as were presented before for the case of $\mu^+$ & $\pi^+$.

*For the 20 cuts whose intervals in their respective histograms are presented in **Appendix F**:

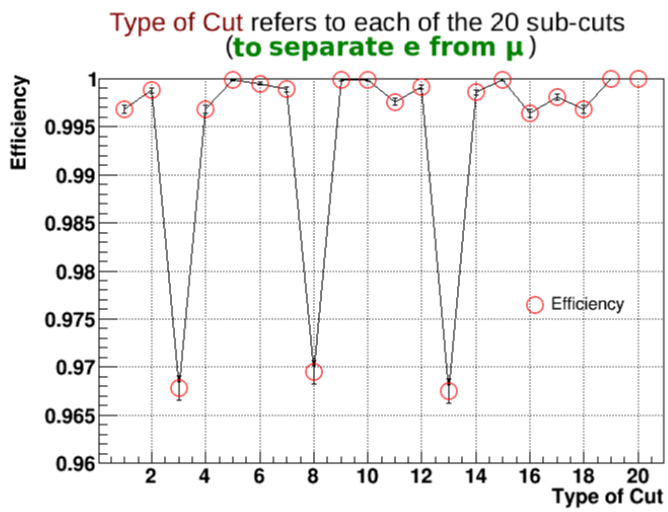


**Figure 6.15:** Efficiency for each of the 20 cuts (each maximizing the product $\xi \times \mathcal{P}$ in the respective variable $Var\_i\_\beta$) that can be used to separate $e^+$ from $\mu^+$.

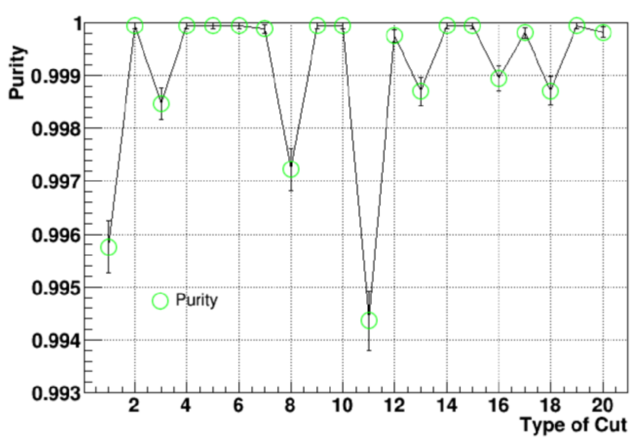


**Figure 6.16:** Purity for each of the 20 cuts (each maximizing the product $\xi \times \mathcal{P}$ in the respective variable $Var\_i\_\beta$) that can be used to separate $e^+$ from $\mu^+$.

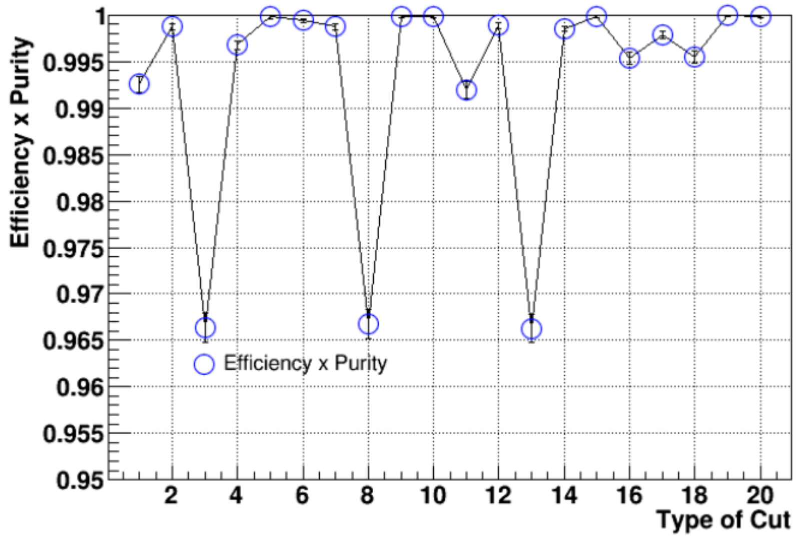


**Figure 6.17:** Efficiency $\times$ Purity for each of the 20 cuts (each maximizing the product $\xi \times \mathcal{P}$ in the respective variable $Var\_i\_\beta$) that can be used to separate $e^+$ from $\mu^+$.

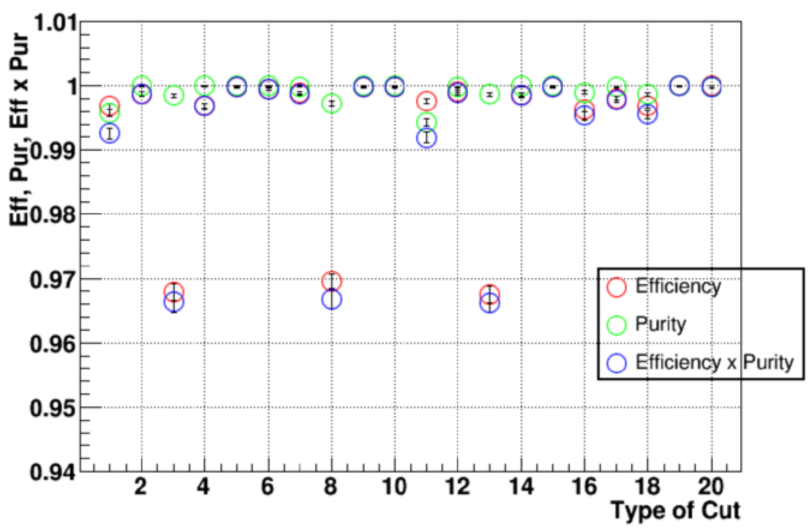


**Figure 6.18:** All the 3 previous quantities in a single plot.

*A 2D Plot of $\mathcal{P}$ vs. $\xi$ in this case shows that there are many excellent cuts that can be applied, this can be seen in the previous histograms since many of them showed the peaks for $\mu$ & $e$ well separated.

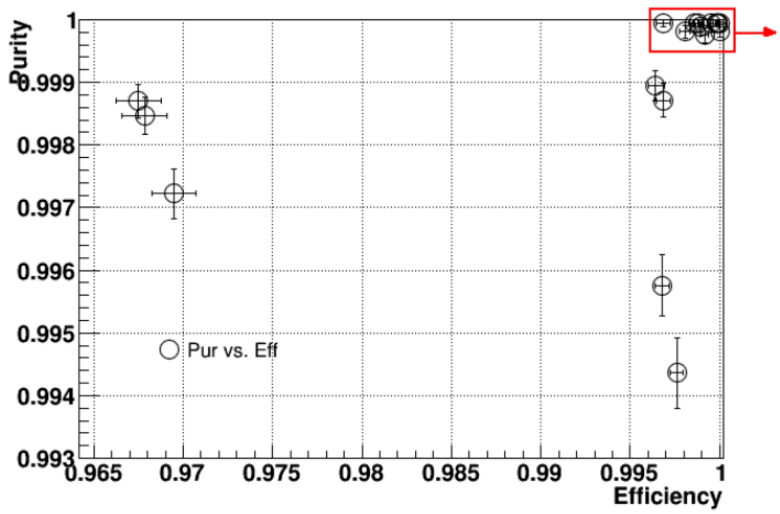


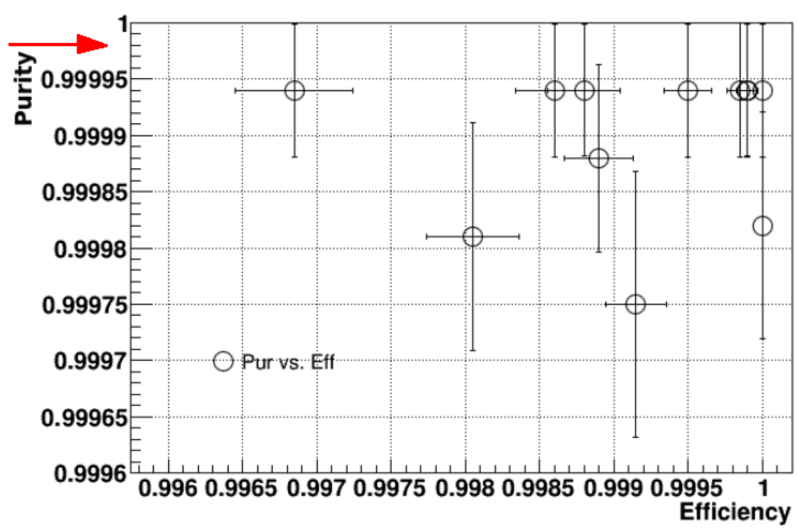


**Figure 6.19:** $\mathcal{P}$ vs. $\xi$ for each of the 20 cuts (each correponding to a different variable) that separate $e^+$ from $\mu^+$. This plot permits to analyze correlations among different cuts (points close together correspond to cuts that have a similar effect in Data) and also to locate the best ones. In this case we see an accumulation of very good cuts at the right top corner.

***Some observations about the $e - \mu$ separation:**

We notice there are many good cuts that separate $e$ from $\mu$, many cuts in $LP - Vars$ are almost perfect. We expect that electrons will almost never arrive at the $LP$ so this is physically expected. I believe that the **best-cut** ($Hits\_L8P$) is enough for a very good separation. The best cuts to separate any $e$ that may be in a $\mu$ sample would be the ones with highest values of the product $\xi \times \mathcal{P}$ as shown in the next Figure:

| Var_i_ß | $\xi \times \mathcal{P}$ |
|---|---|
| Hits_L8P | 0.99994 |
| PE_L8P,PE_L4P, <dE/dx>_L4P | 0.99984 |
| Hits_L4P | 0.99982 |
| E_L4P | 0.99979 |

**Figure 6.20:** This table shows the best cuts together with their value of $\xi \times \mathcal{P}$. Their histograms and the relevant intervals $I_e$ can be found in Appendix F.

## 6.3 $\xi - \mathcal{P}$ Analysis to make up the Optimum-Cut to separate $e^+$ from $\pi^+$

In the same fashion, an Efficiency-Purity analysis has been developed to find the best cut to separate $e^+$ from $\pi^+$, these are actually the most difficult samples to separate each other because there is still a non-negligible probability that a $\pi^+$ will shower in the ECAL region of the detector and in that way look like an $e^+$ (both kinds of particle species tend to shower inside the detector). On the other hand, as is presented in the histograms below, since both kinds of particles make showers inside the detector there is really difficult to separate them by looking at the Last-Plane ($LP$) variables. A similar analysis to the one performed for the $\mu - \pi$ separation was done for this case, the only change is that we deal with $e$-Intervals $I_e$ & $I'_e$ and seek for the optimum-cut that maximizes the efficiency in finding $e^+$ ($\xi_{ee}$). The relevant histograms for variables $Var\_i\_\beta$ & the intervals $I_e$ for each one are shown in **Appendix G**.

*For the 20 cuts whose intervals in their respective histograms are presented in **Appendix G**, only 12 of them are useful, since for the $LP$-Vars it was not possible to perform any cut (no interval presented & no points attached in those plots):

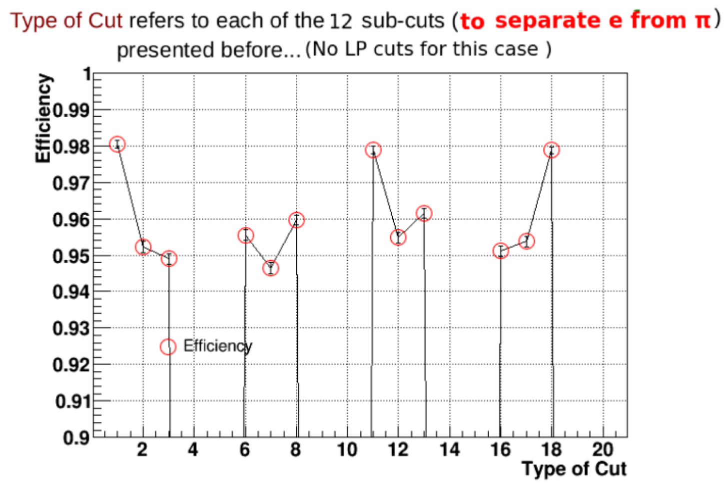


**Figure 6.21:** Efficiency for each of the 12 cuts (each maximizing the product $\xi \times \mathcal{P}$ in the respective variable $Var\_i\_\beta$) that can be used to separate $e^+$ from $\pi^+$.

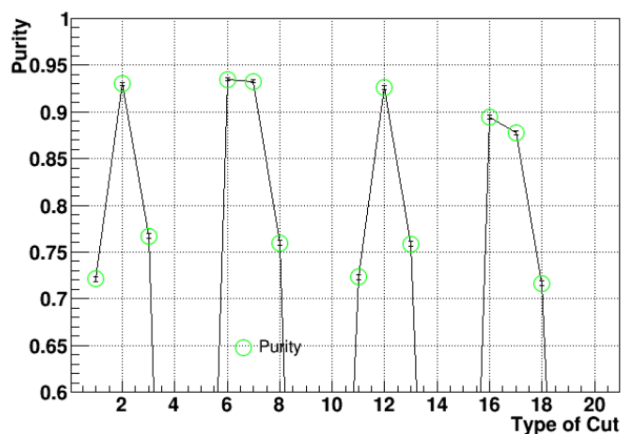


**Figure 6.22:** Purity for each of the 12 cuts (each maximizing the product $\xi \times \mathcal{P}$ in the respective variable $Var\_i\_\beta$) that can be used to separate $e^+$ from $\pi^+$.

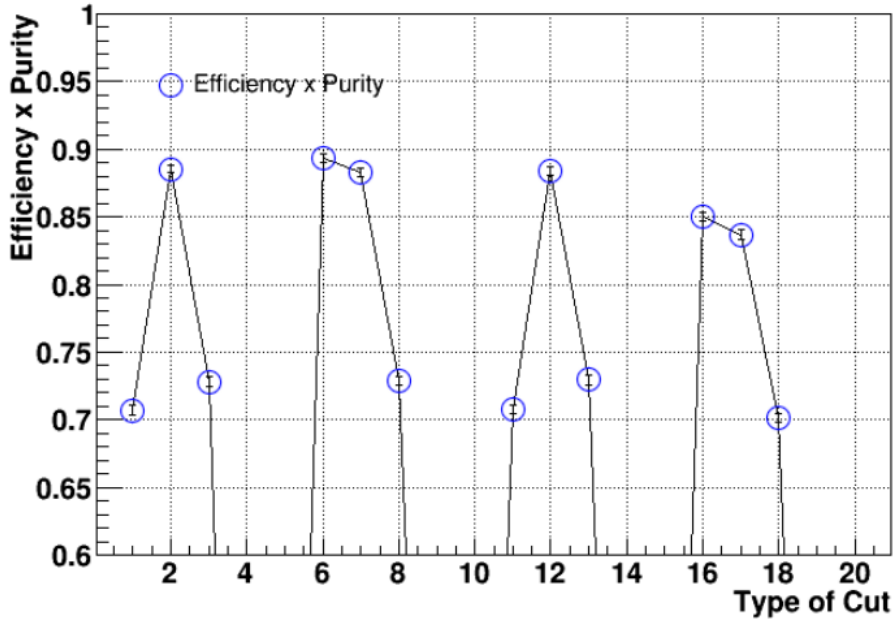


**Figure 6.23:** Efficiency $\times$ Purity for each of the 12 cuts (each maximizing the product $\xi \times \mathcal{P}$ in the respective variable $Var\_i\_\beta$) that can be used to separate $e^+$ from $\pi^+$.

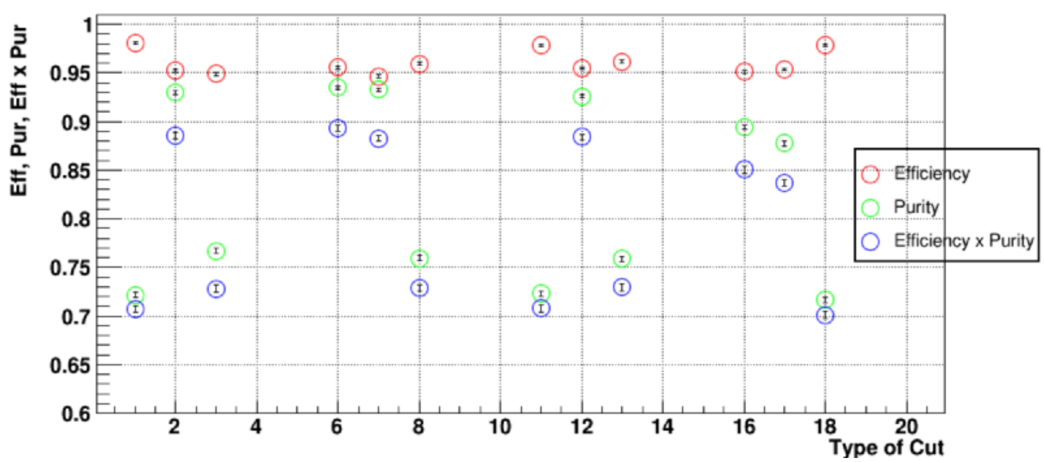


**Figure 6.24:** All the 3 previous quantities in a single plot.

*A 2D Plot of $\mathcal{P}$ vs. $\xi$ is also interesting because it permits to locate what are the best cuts and which of them have similar features.

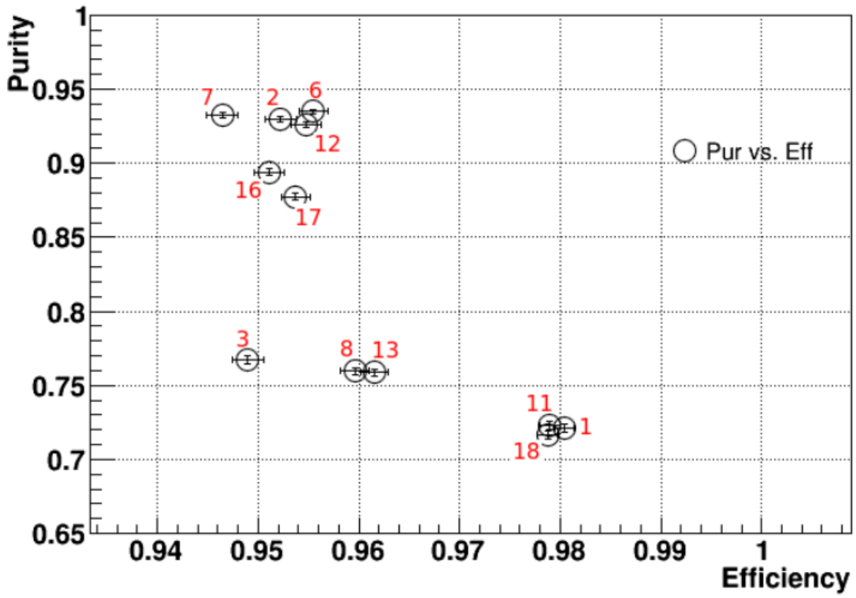


**Figure 6.25:** $\mathcal{P}$ vs. $\xi$ for each of the 12 cuts to separate $e^+$ from $\pi^+$. This plot permits to analyze correlations among different cuts (points close together correspond to cuts that have a similar effect in Data) and also to locate the best ones.

***Methodology followed** (in the same way as for the $\mu - \pi$ separation)

-Select the best cut as the one in Variable $x_1$ to retain events in the $e$-Interval ($I_e$).

-Plot the histograms of other variables for events in the selected $e$-Interval ($I_e$) to see which variable (let's call it $x_2$) separates better the $e$ & $\pi$ present there. Select the remaining $e$ in the new $e$-interval ($I'_e$ ) in this new histogram.

-Plot also the histogram of the same variable ($x_1$) in that interval in log-scale...to see if we ought to change the $e$-Interval in order to improve the cut (for this case was not necessary to change the $I_e$).

-3 candidates (whose histograms showed a better separation of $e$ from $\pi$) were selected as the second cut (to add to the one cited above) and the most efficient (in selecting $e$) among them was chosen (it was not possible to find more than 3 candidates since for the other variables there was full overlapping between $e$ & $\pi$ histograms).

-Then we can make up the cut to retain $e$ as well as the cut to retain $\pi$ (which is the negation of the other). The logic of this optimum-cut and the relevant numbers to calculate (efficiencies ($\xi_{ee}$, $\xi_{\pi\pi}$), fractions of $e$ looking as $\pi$ ($\xi_{e\pi}$) and viceversa ($\xi_{\pi e}$)) follow the same pattern as in the case of the $\mu - \pi$ separation.
*Choosing $x_1$ as $Total\_PE$ (Figure G.5 of Appendix G) we make a plot of events in the initial $e$-Interval for the same variable $x_1$ to see if it was necessary to correct this $e$-interval (log-scale used):

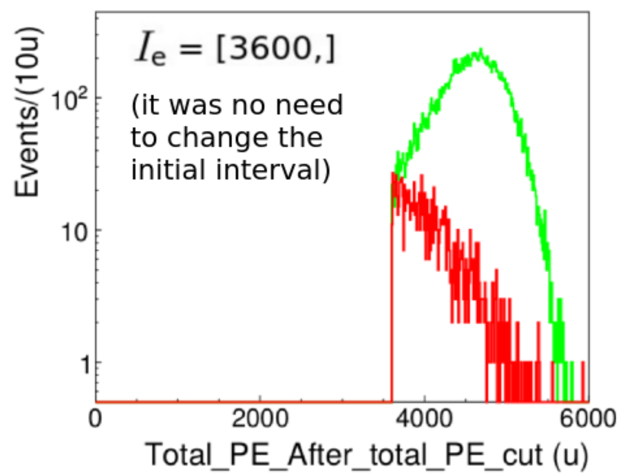


**Figure 6.26:** Histogram of variable $x_1$ for events such that $x_1 \in I_\mu$ in log scale (in an interval a bit larger than $I_\mu$). In this case it was not necessary to change the initial interval $I_e$.

Choosing the only 3 possible candidates for the variable $x_2$ ($Total\_E, Ave\_dE/dx, Total\_Hits$), after plotting their histograms for Events in which $x_1 \in I_e$ & after calculating the numbers $\xi_{ee}$, $\xi_{e\pi}$, $\xi_{\pi\pi}$, $\xi_{\pi e}$ it was found that $x_2 = Total\_Hits$ maximized the efficiency for selecting $e$ (Figure 6.27 shows this result together with its histogram for Events that have $x_1$ in $I_e$ & the new $e$-Interval $I'_e$ selected). After having constructed this cut to separate $e$ from $\pi$ we can estimate the numbers for each of the species (applying the cut to Events who are the $\pi$ separated from the ToF Pion-peak using the cut that separates $\mu$ from $\pi$ in a first stage) and the background for each case using the formulas presented in Figure 6.28 (it is relevant to stay again that these relations are to be applied to the already separated $\pi$ in order to isolate any $e$ present there).

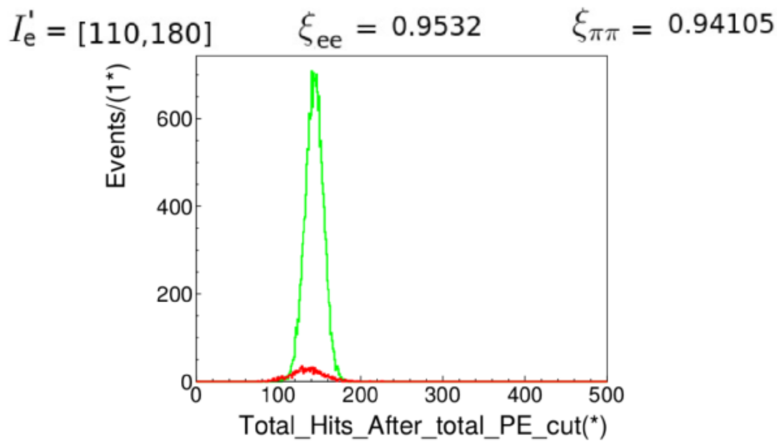


**Figure 6.27:** Histogram of variable $x_2$ for events such that $x_1 \in I_e$. The new $e$-Interval ($I'_e$) for variable $x_2$ that maximizes the efficiency of selecting $e$ ($\xi_{ee}$) is $I'_e = [110, 180]$.

$$\boxed{\begin{aligned} N^0_{e} &\equiv N_{e}^{\text{isolated }\pi\text{ (cut\_}\mu\pi)} \\ N'_{e} &= N^0_{e}/\xi_{ee} \\ N_{\pi e} &= N'_{\pi}\,\xi_{\pi e} \\ N''_{e} &= N'_{e} - N_{\pi e} = N'_{e} - N'_{\pi}\,\xi_{\pi e} \end{aligned}} \quad \boxed{\begin{aligned} N^0_{\pi} &\equiv N_{\pi}^{\text{isolated }\pi\text{ (cut\_}\mu\pi)} \\ N'_{\pi} &= N^0_{\pi}/\xi_{\pi\pi} \\ N_{e\pi} &= N'_{e}\,\xi_{e\pi} \\ N''_{\pi} &= N'_{\pi} - N_{e\pi} = N'_{\pi} - N'_{e}\,\xi_{e\pi} \end{aligned}}$$

Cut_e =={ $x_1 \in I_e$ && $x_2 \in I'_e$ }    Cut_π == ~Cut_e

**Figure 6.28:** Iterative relations to estimate the particle composition of a given Pion Data sample (composed of some $e$ & previously isolated $\pi$ from the ToF Pion peak), this is called correction by efficiency. A way to estimate the background in terms of the fraction of a given species looking like the other is also presented.

## 6.4 Procedure established to apply the Tool developed for the $2GeV$ samples

Here are summarized the optimum-cuts developed for the separation of each of the 3 kinds of particle species ($e, \mu, \pi$). Using the notation $Cut\_i\_j$ for the optimum-cut that separates the species of kind $i$ from the ones of kind $j$ (where $i, j = e, \mu, \pi$), the cut that separates the species of kind $j$ from the one of kind $i$ can be calculated as the negation of the previous one: $Cut\_j\_i =\sim Cut\_i\_j$. The optimum-cuts that have been calculated from the previous Efficiency-Purity analysis are the following:

Cut_μ_π == {Hits_L4P ∈ [4,12] && PE_HCAL ∈ [350,750] }

Cut_e_μ == {Hits_L8P ∈ [0,5]}

Cut_e_π == {Total_PE ∈ [3600,] && Total_Hits ∈ [110,180]}

**Figure 6.29:** Here is the final Tool developed from the Efficiency-Purity analysis: The optimum cut to separate species $i$ from $j$ for the 2GeV sample, where $i, j = e^+, \mu^+, \pi^+$ and $Cut\_j\_i =\sim Cut\_i\_j$.

These cuts permit us to construct the logic to find out the identity of any Event (Particle) from Test Beam Data, for both $\pi$-Folders (Events containing mainly $\pi$ selected with the Cerenkov and the Lead Shield used to reject $e$) & $e$-Folders (Events containing mainly $e$, selected with the Cerenkov device). The procedure is outlined in the Figure below:

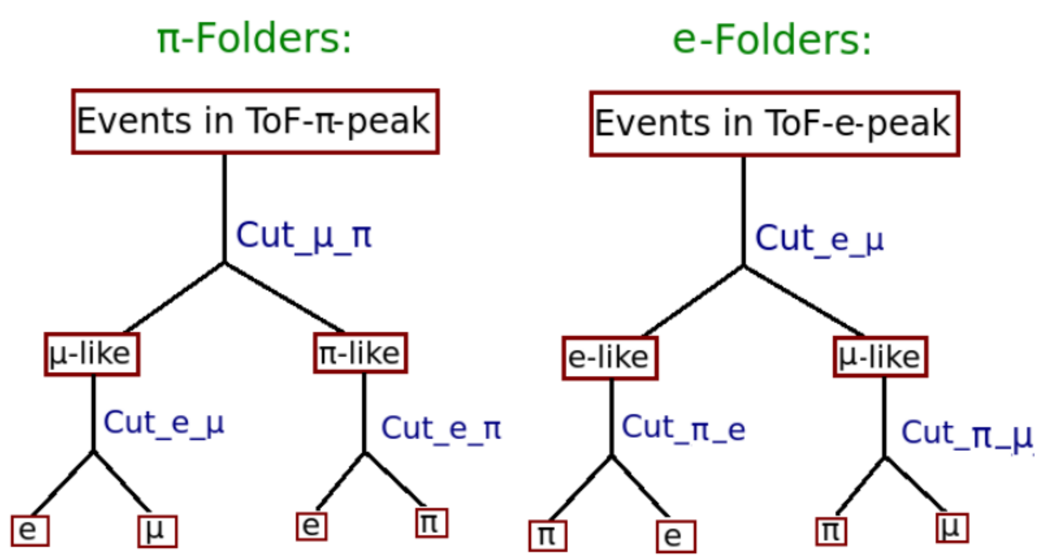


**Figure 6.30:** Here is presented the logic procedure to follow to apply the developed Tool to Events (Particles from the left ToF peak) comming from Pion Folders (Left) & Electron Folders (Right). At the end of the procedure we get the isolated species.

There may be other ways to perform a PID analysis as there are many ways to solve a problem in physics; however, the usage of the variables $Var\_i\_\beta$ has been proven to be useful and agreed with the physical expectations. These confirmed not only that the scripts were properly made but that the experimental devices along the beamline and the TB-detector configurations were set properly to accomplish their purpose: Give to the beam a given value of energy and polarity, select 1 specific particle to enter the detector & have a detector in a configuration that permits to analyze different energy-deposition patterns inside it.

Notwithstanding that, it is important to point out that there will not be possible to develop perfect PID algorithms because the beamline devices and DAQ-elements are not 100% efficient, this was confirmed while eye-scanning some events in the contamination intervals, which showed more than 1 particle entering the detector despite having imposed the $No\_Veto$ condition, used only the triggered slice & the $ToF\_quality = 1$. It is also relevant to point out that the an Efficiency-Purity analysis would permit us to separate any other kind of particle species (like Kaons or Deuterons) that may be present in the beam because it is based on Monte Carlo simulations and the Monte Carlo permits to simulate any kind of particle species (only 3 species were analyzed because the fractions for the others are negligible).

It is also relevant to point out that this Efficiency-Purity analysis was developed only for the 2 GeV Positive Polarity sample because the statistics for the negative sample was very poor (there were almost no antiprotons & the pion peak had a lot less events), but in any case the same procedure can be applied to them or to particle of any energy because the Monte Carlo permits to model almost everything that has been studied theoretically (is a simulation). I should also mention that this analysis presents a **procedure to make up an optimum Tool for particle isolation**, the estimations we can get at the moment are not fully reliable yet (as those Results presented in the previous Chapter) because the Data under analysis is not fully callibrated yet, Test Beam experts are currently working on the improvement of the Data I worked with, which was mainly Raw Data.

# Chapter 7

# Conclusions

This work presented results (they are actually estimations since I worked with Data not fully calibrated yet) on the composition of the Medium-Energy ($\sim$ 1.5-8 GeV) MINER$\nu$A Test Beam experiment as well as efficient tools (algorithms) for the identification of specific kinds of particle species ($p^{\pm}, \pi^{\pm}, \mu^{\pm}, e^{\pm}$). This is very important for the MINER$\nu$A experiment since these tools permit us to identify a specific kind of particle passing through the ECAL/HCAL region of its main detector & in that way be able to reconstruct any Event that took place (a particular neutrino interaction) inside it. The results are also important for the Accelerator-Division because they are interested in analyzing the composition of the delivered beam in order to see what needs to be improved in their operations & will also be relevant for comparison with results from a Monte Carlo simulation of the secondary beam (not ready yet). The results presented permit also to test the efficiency of the Test Beam devices and to improve the way in which they are calibrated and arranged spatially in order to increase the purity of the beam that enters the Test Beam detector (as it was shown there are many $\mu^{\pm}$ and some $e^{\pm}$ beside the desired $\pi^{\pm}$).

As it was stated at the end of the last Chapter, the definition of the Detector-Variables $Var\_i\_\beta$ for the separation of different species is just a particular case in which we can separate between different species exploiting the fact that different species will have a different behaviour inside the Detector. There may be other variables to look at but these have proven to be valuable and permitted to verify that the way the detector was constructed (the configuration) is useful in discriminating between different species. They also permitted the development of an Efficiency-Purity analysis that would be useful to separate any other kind of species that may be present in the secondary beam (like kaons and Deuterons) because this analysis is based on Monte Carlo simulations of the “ideal way” these particles (the ones we wish to analyze since the Monte Carlo permits any species to be simulated) would behave inside our detector.

The specific algorithms developed for particle-ID may be used as a starting point for the development of other particle-ID scripts or to start looking at completely different kind of variables. They have also been useful, beside other sophisticated tools used to perform Data Analysis in MINER$\nu$A, as a tool for the identification of charged pions in the work performed in our last publication [101] because it was mandatory to be able to separate between different species, specially between $\mu^{\pm}$ and $\pi^{\pm}$ in the ECAL/HCAL region of the MINER$\nu$A main detector, in order to recontruct the specific neutrino interaction that took place & to retain events in which charged pions were produced to calculate their respective frequency, which tend to the value of their respective cross sections when the statistics is high, due to the Law of Large Numbers.

The work performed required the understanding of many theoretical, computational and experimental concepts in the field of Experimental High Energy Physics. For this reason, working in an experiment at Fermilab and in that way having the support of the staff of scientists and other students has been very important. Is not just the learning of theoretical issues and programming but seeing how “physics is done” (by taking shifts to control the DAQ, studying the Test Beam detector & beamline elements) and dealing with real data comming from a very complex disposition of experimental devices the way in which one does this specific kind of research. Research on Data Analysis requires both an understanding of how the experimental devices work & of the physical concepts and phenomena taking place.

Finally, I would like to point out the importance of working in a collaboration because these kinds of experiments are so complex that many researches working in different areas are required, for this reason it is very important for our home institution Universidad Nacional de Ingenieria (UNI) to continue being part of this collaboration.

# Bibliography

[1] https://minerva.fnal.gov/

[2] J. HYLEN ET AL., NuMI Technical Design Handbook, Internal NuMI report (2003).

[3] D. HARRIS, *Goals of Test Beam II*. Minerva Internal Note docdb-10090 (2014).

[4] C. J. SOLANO SALINAS & MINER$\nu$A COLLABORATION, *MINERvA neutrino detector response measured with test beam data*, Nucl. Inst. Meth. A789, pp 28-42 (2015).

[5] http://ftbf.fnal.gov

[6] http://www.fnal.gov/

[7] S. E. KOPP, *The NuMI beam at FNAL and its use for cross-section measurements*, arXiv:0709.2737 [hep-ex].

[8] MINOS COLLABORATION:D.G. MICHAEL ET AL., *Observation of Muon Neutrino Disappearance with the MINOS Detector in the NuMI Neutrino Beam*, Phys. Rev. Lett. 97 (2006)191801.

[9] K. HURTADO, PHD. THESIS : *Measurement of the Muon Neutrino Double-Differential Charged Current Quasi-Elastic Like Cross Section on a Hydrocarbon Target at* $E_\nu \sim 3.5\ GeV$

[10] G.N. PERDUE ET AL. (MINERVA COLLABORATION) *The MINERvA data acquisition system and infrastructure*, Nucl. Inst. and Met., Phys. Res. Sect. A, 694(0):179 - 192, (2012).

[11] L. BELLANTONI, *Into / Physics of Test Beam*, Minerva Internal Note docdb-10770 (2015).

[12] *ROOT— A Data Analysis Framework*, https://root.cern.ch/drupal/

[13] J. KLEYKAMP, *Wire chamber tracks*, Minerva Internal Note docdb-11068 (2015).

[14] Photomultiplier Tubes, Hamamatsu Handbook, Third Edition (2007).

[15] BERKELEY LABORATORY, *Nuclear Science-A Guide to the Nuclear Science Wall Chart*, http://www.lbl.gov/abc/wallchart/teachersguide/pdf/Chap11.pdf

[16] A. NORRICK, *Use of Test Beam Data*, Minerva Internal Note docdb-11252 (2015).

[17] A. BERCELLIE, *Test Beam Status Update*, Minerva Internal Note docdb-10968 (2015).

[18] J. KLEYKAMP, *Merging Data for Testbeam II*, Minerva Internal Note docdb-10790 (2015).

[19] L. BELLANTONI, G. SAVAGE, *Time of Flight for MINERvA Testbeam II and MTest Facility*, Minerva Internal Note docdb-10750 (2015).

[20] H. BUDD, *Procedures for Testing PMT Boxes at Lab G*, Minerva Internal Note docdb-9269.

[21] H. BUDD, *FEB replacement procedure new format*, Minerva Internal Note docdb-6108.

[22] H. BUDD, *Turning the MINERvA Detector ON and OFF*, Minerva Internal Note docdb-6438.

[23] VON BAYER, O. HAHN, L. MEITNER, Phys. Zeitschrift, 12, January, 1911, p. 378

[24] CHADWICK, J., Verh. Deutsch. Phys. Ges., 16, 383 (1914)

[25] C.D. ELLIS, B.A. WOOSTER, *The average energy of desintegration of Radium*, E,Proc. Roy. Soc. A117(1927) 109-123

[26] B. PONTECORVO, *Mesonium and anti-mesonium*, Zh. Eksp. Teor. Fiz. 33, 549â551. reproduced and translated in Sov. Phys. JETP 6, 429 (1957).

[27] Z. MAKI, M. NAKAGAWA, AND S. SAKATA, *Remarks on the Unified Model of Elementary Particles*, Progress of Theoretical Physics 28, 870 (1962)

[28] B. PONTECORVO, *Neutrino Experiments and the Problem of Conservation of Leptonic Charge*, Zh. Eksp. Teor. Fiz. 53, 1717. reproduced and translated in Sov. Phys. JETP 26, 984 (1968).

[29] Brookhaven's Alternating Gradient Synchroton, Science 5 December 1958: Vol. 128 no. 3336 pp. 1393-1401.

[30] F. J. HASERT ET AL. (GARGAMELLE), *Observation of neutrino-like interactions without muon or electron in the Gargamelle neutrino experiment*, Phys. Lett. B46 (1973) 138.

[31] M. L. PERL, *The Discovery of the tau lepton*, In *Stanford 1992, The rise of the standard model* 79-100

[32] K. KODAMA ET AL. [DONUT COLLABORATION], *Observation of tau neutrino interactions*, Phys. Lett. B 504, 218 (2001).

[33] ALEPH COLLABORATION:D. DECAMP ET AL., *Determination of the Number of Light Neutrino Species*, Phys. Lett. B 231(1989)519.

[34] DELPHI COLLABORATION:P.A. AARNIO ET AL., *Measurement of the Mass and Width of the Z0 Paricle from Multi-Hadronic Final States Produced in the e+ e- Annihilation*, Phys. Lett. B 231 (1989)539.

[35] L3 COLLABORATION:B. ADEVA ET AL., *A Determination of the Properties of the Neutral Inter- mediate Vector Boson Z0*, phys. Lett. B 231 (1989)509.

[36] OPAL COLLABORATION:M.Z. AKRAWY ET AL., *Measurement of the Z0 Mass and Width with the OPAL Detector at LEP*, Phys. Lett. B bf 231 (1989)530.

[37] C. ATHANASSOPOULOS ET AL., *Candidate Events in a Search for Anti-Muon-Neutrino - Anti- Electron-Neutrino Oscillations*, Phys. Rev. Lett. 75, 2650, 1995.

[38] TINA J. LEITNER, *Neutrino Interactions with Nucleons and Nuclei*, (2005)

[39] C.S. WU ET AL., , Phys. Rev. 105 (1957)1413.

[40] M. GOLDHABER, L. GRODZINS, AND A.W. SUNYAR, *Helicity of neutrinos*, Phys. Rev. 109 (1958)1015.

[41] E. K. Akhmedov, 1997, hep-ph/9705451, Fourth International Solar Neutrino Conference, Heidelberg, Germany, 8-11 Apr 1997.

[42] R. DAVIS, *A review of the Homestake solar neutrino experiment*, Prog. Nucl. Phys. 32, p13 (1994).

[43] K. LANDE, Proceedings of Neutrino 96, p25.

[44] V. N. GAVRIN, *Solar neutrino and Cr-51 results from SAGE*, Proceedings of Neutrino 96, p14.

[45] P. ANSELMANN ET AL., *Solar neutrinos observed by GALLEX at Gran Sasso*, Phys. Lett. B285 (1992) 376-389

[46] K. ABE ET AL. (SUPER-KAMIOKANDE COLLABORATION), *Solar neutrino results in Super- Kamiokande-I*, Phys.Rev.D73:112001,(2006).

[47] SNO COLLABORATION, *Independent Measurement of the Total Active 8B Solar Neutrino Flux Using an Array of He3 Proportional Counters at the Sudbury Neutrino Observatory*, Phys. Rev. Lett. 101, 111301(2008).

[48] W.N. COTTINGHAM AND D.A GREENWOOD, *An Introduction to the Standard Model of Par- ticle Physics*, Second Editions, Cambridge University, xv,42 (2001).

[49] T. KAJITA ET. AL., Proceedings of Neutrino 98 ,Nucl.Phys.Proc.Suppl. 77 (1999) Takayama, Japan, June 4-9, 1998.

[50] R. M. BIONTA ET. AL., Phys. Rev. Lett. 58, p1494 (1987)

[51] W. W. M. ALLISON ET. AL., Phys. Lett. B391, p491 (1997)

[52] CH. BERGER ET. AL., Phys. Lett. B227, p489 (1994).

[53] M. AGLIETTA ET. AL., Europhys. Lett. 8, p611 (1989).

[54] T. KAJITA, *Atmospheric neutrinos*, New J. Phys. 6 (2004) 194.

[55] THE SUPER-KAMIOKANDE COLLABORATION, *Evidence for oscillation of atmospheric neutrinos*, Phys. Rev. Lett. 81 (1998) 1562-1567

[56] D. PERKINS, *Introduction to High Energy Physics*, 4th edition, Cambridge University Press, 246 (2000).

[57] K. ZUBER, *Neutrino Physics*, Institute of Physics Publishing Bristol and Philadelphia, Oxford, 22,32,57(2004).

[58] A. THOMAS AND W. WEISE, *The structure of the nucleon*, Wiley-VCH, 8 (2001).

[59] D. GRIFFITS, *Introduction to Elementary Particles*, John Wiley and Sons, Inc, (1987).

[60] C.J. SOLANO SALINAS, K. HURTADO, C. ROMERO., *Introduction to Particle Physics*, AIP Conf.Proc.1123:13-29,2009.

[61] C. GIUNTI AND C. KIM, *Fundamentals of Neutrino Physics and Astrophysics*, 193 (2007).

[62] J. L. HEWETT ET AL., *Fundamental Physics at the Intensity Frontier*, arXiv:1205.2671[hepex].

[63] R. PLACAKYTE, *Parton Distribution Functions*, arXiv:1111.5452 [hep-ph].

[64] D. REIN AND L. M. SEHGAL, *Neutrino Excitation of Baryon Resonances and Single Pion Production*, Annals Phys. 133 (1981) 79.

[65] P.A RODRIGUEZ, *Comparing pion production models to MiniBooNE data*, arXiv:1402.4709 [hep-ex]

[66] V. T. MCGARY, *NC Coherent pi0 Production in the MiniBooNE Antineutrino Data*, arXiv:0806.2347 [hep-ex].

[67] C. H. LLEWELLYN SMITH, Phys. Rep., 3, 261, 1972.

[68] S. K. SINGH AND E. OSET, *Quasielastic neutrino (anti-neutrino) reactions in nuclei and the axial vector form-factor of the nucleon*, Nucl. Phys. A542 (1992) 587â615.

[69] S. GALSTER ET AL., *Elastic electron - deuteron scattering and the electric neutron form-factor at four momentum transfers*, Nucl. Phys. B32 (1971) 221â237.

[70] NAMBU, YOICHIRO, *Axial Vector Current Conservation in Weak Interactions*, Phys. Rev. Lett. V4 (1960)

[71] H. S. BUDD, A. BODEK, AND J. ARRINGTON, *Modeling quasi-elastic form factors for electron and neutrino scattering*, arXiv:hep-ex/0308005.

[72] V. BERNARD, L. ELOUADRHIRI AND U. G. MEISSNER, *Axial Structure of the Nucleon*, J. Phys. G28, R1 (2002), hep-ph/0107088.

[73] SHNEOR R ET AL., Phys. Rev. Lett. 99:072501 (2007)

[74] SARGSIAN MM ET AL., Phys. Rev. C 71:044615 (2005)

[75] SCHIAVILLA R ET AL., Phys. Rev. Lett. 98:132501 (2007)

[76] H. GALLAGHER, G. GARVER AND G.P.ZELLER, *Neutrino-Nucleus Interactions*, Annual Review of Nuclear and Particle Science 2011. 61:355â78.

[77] M.B. BARBARO, *Nuclear effects in charged-current quasielastic neutrino- nucleus scattering*, J.Phys.Conf.Ser. 336:012024 (2011).

[78] SINGH, S. K., AND E. OSET, Nucl. Phys. A542, 587.

[79] AGUILAR-AREVALO ET AL., 2010a, Phys. Rev. D 81, 092005.

[80] LYUBUSHKIN, V., ET AL., 2009, Eur. Phys. J. C 63, 355.

[81] J. A. FORMAGGIO AND G. P. ZELLER, *From eV to EeV: Neutrino Cross Sections Across Energy Scales*, Rev. Mod. Phys. 84, 1307 (2012), arXiv:1305.7513 [hep-ex].

[82] A. A. AGUILAR-AREVALO ET AL. (MINIBOONE COLLABORATION), *First measurement of the muon neutrino charged current quasielastic double differential cross section*, Phys. Rev. D 81, 092005 - Published 28 May 2010.

[83] A. FIORENTINI ET. ALL (MINERVA COLLABORATION), *Measurement of Muon Neutrino Quasi-Elastic Scattering on a Hydrocarbon Target at $E_\nu \sim 3.5GeV$*, Phys. Rev. Lett. 111, 022502 (2013). Ì

[84] J. SOULIÉ, *C++ Language Tutorial*, http://www.cplusplus.com/doc/tutorial/.

[85] C. J. SOLANO SALINAS & MINER$\nu$A COLLABORATION, *Arachne - A web-based event viewer for MINERvA*, Nucl.Inst.Meth. 676 (2012) 44-49.

[86] http://www.nevis.columbia.edu/ seligman/root-class/

[87] A. ZEGARRA, Minerva Internal Note docdb-10977, p.23.

[88] D. HARRIS, *INSS 2011 Detector Technology Lecture*, Minerva Internal Note docdb-10819.

[89] A. ZEGARRA, *RESULTS PID Pion Folders Data-Run-1*, Minerva Internal Note docdb-11341.

[90] A. ZEGARRA, *pid-update-sep-17*, Minerva Internal Note docdb-11424.

[91] CRAIG BLOCKER, *Uncertainties on Efficiencies*, Brandeis University. August 4, 2004.

[92] C. J. SOLANO SALINAS & MINER$\nu$A COLLABORATION, *Demonstration of Communication using Neutrinos*, Modern Physics Letters A Vol.27, (2012)1250077

[93] C. J. SOLANO SALINAS & MINER$\nu$A COLLABORATION, *The MINERvA Data Acquisition System and Infrastructure*, Nucl.Inst.Meth.A694(2012)179-192

[94] C. J. SOLANO SALINAS & MINER$\nu$A COLLABORATION, *Measurement of Muon Antineutrino Quasielastic Scattering on a Hydrocarbon Target at $E_\nu \sim 3.5\ GeV$*, PhysRevLett.111.022501.

[95] C. J. SOLANO SALINAS & MINER$\nu$A COLLABORATION, *Measurement of Muon Neutrino Quasielastic Scattering on a Hydrocarbon Target at $E_\nu \sim 3.5\ GeV$*, PhysRevLett.111.022502.

[96] C. J. SOLANO SALINAS & MINER$\nu$A COLLABORATION, *Design, calibration, and performance of the MINERvA detector*, NuclInstMethA743(2014)130-159.

[97] C. J. SOLANO SALINAS & MINER$\nu$A COLLABORATION, *Measurement of Ratios of $\nu_\mu$ Charged-Current Cross Sections on C, Fe, and Pb to CH at Neutrino Energies 2-20 GeV.*, PhysRevLett.112.231801.

[98] C. J. SOLANO SALINAS & MINER$\nu$A COLLABORATION, *Measurement of Coherent Production of $\pi^\pm$ in Neutrino and Anti-Neutrino Beams on Carbon from $E_\nu$ of 1.5-20 GeV*, PhysRevLett.113.261802.

[99] C. J. SOLANO SALINAS & MINER$\nu$A COLLABORATION, *Measurement of muon plus proton final states in $\nu_\mu$ Interactions on Hydrocarbon at $< E_\nu >= 4.2\ GeV$*, Phys.Rev.D91:071301.2015.

[100] C. J. SOLANO SALINAS & MINER$\nu$A COLLABORATION, *Single neutral pion production by charged-current $\overline{\nu}_\mu$ interactions on hydrocarbon at $< E_\nu >= 3.6\ GeV$*, PhysLettB749-2015-130-136.

[101] A. ZEGARRA, G. SALAZAR, C. J. SOLANO SALINAS & MINERVA COLLABORATION, *Charged pion production in $\nu_\mu$ interactions on hydrocarbon at $E_\nu = 4.0\ GeV$*, Phys. Rev. D92, 092008 (2015)

# Appendix A

# Pyroot scripts to construct ToF histograms & select contamination intervals

```python
from ROOT import *
import os
import sys
import myPlotStyle
import re

class HTML:
  def __init__(self,Types):
    self.Data=dict()
    for type in Types:
      if type=="":
        continue
      self.Data[type]=[]
  def AddType(self,Type):
    for datum in self.Data:
      if Type==datum:
        print "Type already exists!"
        return
    self.Data[Type]=[]
  def OpenHtml(self,Type,filename):
    self.Data[Type].append(open(filename,"w"))
    self.Data[Type][-1].write("<html><div>\n")
  def CloseHtml(self,Type,index):
    self.Data[Type][index].write("</div></html>\n")
    self.Data[Type][index].close()
  def CloseAll(self,index):
    for datum in self.Data:
      self.CloseHtml(datum,index)
  def GetLastHtml(self,Type):
    return self.Data[Type][-1]

def DrGranCoolTool(gate,inputdst,outfile,slice):
#NOTE!  Gate in Arachne=ev_gate-1
  outstring = ""
  outstring+= "<p><a href=";
  outstring+= "http://minerva05.fnal.gov/Arachne/arachne.html?entry=%d"%gate
  outstring+="&filename=%s&filetype=dst> \t%s\tgate=%d</a></p>"%
(inputdst,os.path.basename(inputdst),gate)
```

```
  outstring+="<p> Gate "+str(gate)+": Triggered Slice: "+str(slice)+"</p>"
  outfile.write(outstring)

#def DidVetoFire(event):
#  if event.Veto_VetoCounter_1>0 or event.Veto_VetoCounter_2>0 or event.Veto_VetoCounter_3>0 or event.Veto_VetoCounter_4>0 or event.Veto_VetoCounter_5>0 or #event.Veto_VetoCounter_6>0 or event.Veto_VetoCounter_7>0 or event.Veto_VetoCounter_8>0 or event.Veto_VetoCounter_9>0 or event.Veto_VetoCounter_10>0 or #event.Veto_VetoCounter_11>0 or event.Veto_VetoCounter_12>0:
#    return True
#  else:
#    return False

def ModuleMultiplier(pe,module):
  #ECAL/HCAL Multiplier
  if module<0:
    return 0
  elif module==0:
    return pe*1.3
  elif module>0 and module<21:
    return pe*2.1
  elif module>=21 and module<42:
    return pe*10.7
  #TRAK/SuperHCAL
#  if module<0:
#    return 0
#  elif module>=0 and module<21:
#    return pe*1.2551
#  elif module>=21 and module<=24:
#    return pe*10.7271
#  elif module>=25 and module<=35:
#    return pe*20.1991
#  elif module>=36 and module<=41:
#    return pe*10.7271
```

```
def GetTrigTime(event,hit):#This gets the time of the trigger
  qtick=0
  if event.hit_quarter_ticks[hit]==0:
    qtick=4
  return (0.5/53.1032e6)*1e9*(event.hit_sys_ticks[hit]+event.hit_delay_ticks[hit]+0.25*event.hit_quarter_ticks[hit])

def IsSliceTriggered(minmax,triggertime):#This finds the slice that was triggered
  trigdelta=80
  truetime=triggertime-740#offset is ~540 ns
  triglo=truetime-trigdelta
  trighi=truetime+trigdelta
  if triglo>minmax[1] and trighi>minmax[1]:#trig range above slice range
    return False
  elif triglo<minmax[0] and trighi<minmax[0]:#trig range below slice range
    return False
  elif triglo>minmax[0] and triglo<minmax[1]:
    return True
  elif trighi>minmax[0] and trighi<minmax[1]:
    return True

#########################################################################
myPlotStyle.myPlotStyle()#Sets a fixed plot format

#The merged DSTs live in /minerva/data/testbeam2/run1datamerged/(directory)/TB_*_mergedDST.root
#I found it advantageous to separate the analysis according the directories
dirs=["1.77GeV_Pos_Pions",
      "2GeV_Pos_Pions",
      "2GeV_Neg_Pions",
      "3GeV_Pos_Pions",
      "3GeV_Neg_Pions",
      "4GeV_Pos_Pions",
      "4GeV_Neg_Pions",
      "6GeV_Pos_Pions",
      "6GeV_Neg_Pions",
      "7GeV_Pos_Pions",
      "7GeV_Neg_Pions"]
```

```
#HTML is a class I wrote (you can find it above).  Here, we are creating the class witl
the types of events we want to look at so we can call them later.  In this case, the
only events look at are those that passed all the cuts shown below (not yet a time-cut
html_files=HTML(["AllEvents"])

#List of histograms
AllEventshists=[]
#Contaminationhists=[]

for dir in dirs:
  #This returns a list of files in the directory
  input_files = os.popen("ls /minerva/data/testbeam2/run1datamerged/%s/*mergedDST.root
(dir)).readlines()

  AllEventshists.append(TH1D("AllEvents"+dir,";ToF_measured_time;",280,-5000,20000))
  #Contaminationhists.append(TH1D
("Contamination"+dir,";ToF_measured_time;",-5000,20000))

  #This opens an html file called "ArachneLinks_Run1_(directory).html"
  #Whenever we put an event in type "AllEvents", it writes a link to the event
  #in ArachneLinks_Run1_(directory).html
  html_files.OpenHtml("AllEvents","ArachneLinks_Run1_"+dir+"_AllEvents.html")
  #html_files.OpenHtml("Contamination","ArachneLinks_Run1_"+dir+"_NoVeto.html")

  #This creates a TChain in which you can add TTree to with the name "minerva"
  roottree = TChain("minerva")

  for infile in input_files:
    filename = infile.split()[0]
    print filename
    roottree.Add(filename)#This adds the TTree in the file to the chain

  nEntries=roottree.GetEntries()

  counter=0
```

```
  for iEvent, event in enumerate(roottree): #Loop through the events in the chain
    #If In_spill is larger than 0.5, then the event occured in a spill
    #n_slices tell you how many slices there are in an event
    #If n_slices=0, nothing happened in the detector
    if event.In_spill>0.5 and event.n_slices>0:
      #This is just a counter of the number of events
      if int(iEvent)/100>counter:
        print "Gate: %i/%i" % ((int(iEvent)/100)*100,nEntries)
        counter=int(iEvent)/100

      trigtime=0
      triggered=false

      totpe=dict()
      timedist=dict()
      sliceminmax=dict()

      for i in range(event.n_slices):#ignore slice 0
        timedist[i+1]=[]
        totpe[i+1]=0

      #Some variables come in arrays.  You will need to loop over these arrays to get the values
      for i in range(event.n_rawhits):
        #This returns the trigger time for each event. If there was no trigger, then the "triggered" flag remains false
        if event.hit_disc_fired[i]==1 and event.hit_croc[i]==1 and event.hit_chain[i]==0 and event.hit_board[i]==5 and event.hit_pixel[i]==7:
          trigtime=GetTrigTime(event,i)
          triggered=true

        #Here is where I'd write code to get the values of the variables you want for each event.
        #For instance, here I'm grabbing the pe for each hit and summing them together (this part relevant for the dE/dx and PE calculation)
```

```
        if event.hit_pe[i]>=0 and event.hit_time_slice[i]>0:
          #ModuleMultiplier takes in account passive material in the detector
          if event.hit_time_slice[i]>event.n_slices:#This shouldn't happen
            continue
          totpe[event.hit_time_slice[i]]+=ModuleMultiplier(event.hit_pe[i],event.hit_module[i])
          timedist[event.hit_time_slice[i]].append(event.hit_time_raw[i])

      #This goes through and finds the slice in which the trigger occurred
      triggerslice=0
      sliced=false
      for sl in timedist:
        if len(timedist[sl])!=0:
          sliceminmax[sl]=[min(timedist[sl]),max(timedist[sl])]
      if triggered:
        for slmm in sliceminmax:
          if sliceminmax[slmm][0]==sliceminmax[slmm][1]:
            break
          if IsSliceTriggered(sliceminmax[slmm],trigtime):
            triggerslice=slmm
            sliced=true
            break

        #Here is where we output the results.  Write events into html files, write events into histograms, etc.
        if sliced:
          if event.ToF_quality==1:#and event.ToF_measured_time > t1 and event.ToF_measured_time < t2:
                                  #To be used after locating contamination interval <t1,t2>  for each folder
            DrGranCoolTool(event.ev_gate-1,roottree.GetCurrentFile().GetName(),html_files.GetLastHtml("AllEvents"),triggerslice)
            AllEventshists[-1].Fill(event.ToF_measured_time)
html_files.CloseAll(-1)#Closes all html files

gROOT.SetBatch()
outfile="Run1_ToF_histograms.pdf"
c=TCanvas()
c.Print(outfile+"[")
for AEhist in AllEventshists:
  gPad.SetLogy()
  AEhist.Draw()
  c.Print(outfile)
#for nvhist in Contaminationhists:
#  nvhist.Draw()
#  c.Print(outfile)
```

# Appendix B

# Script for constructing dE/dx histograms

```
from ROOT import *
import os
import sys
import myPlotStyle
import re

class HTML:
  def __init__(self,Types):
    self.Data=dict()
    for type in Types:
      if type=="":
        continue
      self.Data[type]=[]
  def AddType(self,Type):
    for datum in self.Data:
      if Type==datum:
        print "Type already exists!"
        return
    self.Data[Type]=[]
  def OpenHtml(self,Type,filename):
    self.Data[Type].append(open(filename,"w"))
    self.Data[Type][-1].write("<html><div>\n")
  def CloseHtml(self,Type,index):
    self.Data[Type][index].write("</div></html>\n")
    self.Data[Type][index].close()
  def CloseAll(self,index):
    for datum in self.Data:
      self.CloseHtml(datum,index)
  def GetLastHtml(self,Type):
    return self.Data[Type][-1]

def DrGranCoolTool(gate,inputdst,outfile,slice):
#NOTE!  Gate in Arachne=ev_gate-1
  outstring = ""
  outstring+= "<p><a href=";
  outstring+= "http://minerva05.fnal.gov/Arachne/arachne.html?entry=%d"%gate
  outstring+="&filename=%s&filetype=dst> \t%s\tgate=%d</a></p>"%
(inputdst,os.path.basename(inputdst),gate)
```

```
  outstring+="<p> Gate "+str(gate)+": Triggered Slice: "+str(slice)+"</p>"
  outfile.write(outstring)

#def DidVetoFire(event):
#  if event.Veto_VetoCounter_1>0 or event.Veto_VetoCounter_2>0 or
event.Veto_VetoCounter_3>0 or event.Veto_VetoCounter_4>0 or event.Veto_VetoCounter_5>0
or #event.Veto_VetoCounter_6>0 or event.Veto_VetoCounter_7>0 or
event.Veto_VetoCounter_8>0 or event.Veto_VetoCounter_9>0 or event.Veto_VetoCounter_10>0
or #event.Veto_VetoCounter_11>0 or event.Veto_VetoCounter_12>0:
#    return True
#  else:
#    return False

def ModuleMultiplier(pe,module):
  #ECAL/HCAL Multiplier
  #if module<0:
  #  return 0
  #elif module==0:
  #  return pe*1.3
  #elif module>0 and module<21:
  #  return pe*2.1
  #elif module>=21 and module<42:
  #  return pe*10.7
  #TRAK/SuperHCAL
  if module<0:
    return 0
  elif module>=0 and module<21:
    return pe*1.2551
  elif module>=21 and module<=24:
    return pe*10.7271
  elif module>=25 and module<=35:
    return pe*20.1991
  elif module>=36 and module<=41:
    return pe*10.7271

```

```
def GetTrigTime(event,hit):#This gets the time of the trigger
  qtick=0
  if event.hit_quarter_ticks[hit]==0:
    qtick=4
  return (0.5/53.1032e6)*1e9*(event.hit_sys_ticks[hit]+event.hit_delay_ticks[hit]+0.25*event.hit_quarter_ticks[hit])

def IsSliceTriggered(minmax,triggertime):#This finds the slice that was triggered
  trigdelta=80
  truetime=triggertime-740#offset is ~540 ns
  triglo=truetime-trigdelta
  trighi=truetime+trigdelta
  if triglo>minmax[1] and trighi>minmax[1]:#trig range above slice range
    return False
  elif triglo<minmax[0] and trighi<minmax[0]:#trig range below slice range
    return False
  elif triglo>minmax[0] and triglo<minmax[1]:
    return True
  elif trighi>minmax[0] and trighi<minmax[1]:
    return True

#######################################################################
myPlotStyle.myPlotStyle()#Sets a fixed plot format

#The merged DSTs live in /minerva/data/testbeam2/run2datamerged/(directory)/TB_*_mergedDST.root
#I found it advantageous to separate the analysis according the directories
dirs=["4GeV_Pos_Pions"]
#     "4GeV_Neg_Pions",
#      "6GeV_Pos_Pions",
#      "6GeV_Neg_Pions",
#      "8GeV_Pos_Pions",
#      "8GeV_Neg_Pions",
#      "9GeV_Pos_Pions",
#      "9GeV_Neg_Pions"]
      #"10GeV_Pos_Pions",
      #"10GeV_Neg_Pions",
      #"16GeV_Pos_Pions"]
```

```
#HTML is a class I wrote (you can find it above).  Here, we are creating the class with the types of events we want to look at so we can call them later.
#In this case, the events are those that passed the ToF cuts and then the dE/dx is constructed for pi and mu like events.
html_files=HTML(["All_hists"])

#List of histograms

PE_hists=[]

dEdx1_hists = []
dEdx2_hists = []
totPE1_hists = []
totPE2_hists = []
totHits1_hists = []
totHits2_hists = []

for dir in dirs:
  #This returns a list of files in the directory
  input_files = os.popen("ls /minerva/data/testbeam2/run2datamerged/%s/*mergedDST.root"%(dir)).readlines()

  PE_hists.append(TH1D("PE_hists"+dir,";pe; Events",280,0,56000))
  dEdx1_hists.append(TH2D("dEdx1_hists"+dir,";module; dE/dx_{1}",42,0,42,100,0,8000)) #1 stands for mu-like and 2 for pi-like
  dEdx2_hists.append(TH2D("dEdx2_hists"+dir,";module; dE/dx_{2}",42,0,42,100,0,35000))
  totPE1_hists.append(TH2D("totPE1_hists"+dir,";module; totPE_{1}",42,0,42,100,0,2600))
  totPE2_hists.append(TH2D("totPE2_hists"+dir,";module; totPE_{2}",42,0,42,100,0,2600))
  totHits1_hists.append(TH2D("totHits1_hists"+dir,";module; totHits_{1}",42,0,42,100,0,60))
  totHits2_hists.append(TH2D("totHits2_hists"+dir,";module; totHits_{2}",42,0,42,100,0,60))

  #This opens an html file called "ArachneLinks_Run2_(directory).html"
  #in ArachneLinks_Run2_(directory).html
  #html_files.OpenHtml("All_hists","ArachneLinks_Run2_"+dir+"_PE.html")
  #html_files.OpenHtml("Contamination","ArachneLinks_Run2_"+dir+"_NoVeto.html")
```

```
#This creates a TChain in which you can add TTree to with the name "minerva"
roottree = TChain("minerva")

for infile in input_files:
  filename = infile.split()[0]
  print filename
  roottree.Add(filename)#This adds the TTree in the file to the chain

nEntries=roottree.GetEntries()

counter=0

for iEvent, event in enumerate(roottree): #Loop through the events in the chain
      #If In_spill is larger than 0.5, then the event occured in a spill
      #n_slices tell you how many slices there are in an event
      #If n_slices=0, nothing happened in the detector
  dEdx1=dict() #This contains the modules as keys and for each value the dE/dx for events with pe < E_critic(mu-like)
  dEdx2=dict()#This contains the modules as keys and for each value the dE/dx for events with pe > E_critic (pi-like)
  totPE1=dict()
  totPE2=dict()
  totHits1=dict()
  totHits2=dict()

  dEdx1[-1]=0  #THIS ODD MODULE-NUMBERS MAY DEPEND ON THE FOLDER
  dEdx1[-99]=0
  dEdx2[-1]=0
  dEdx2[-99]=0

  totPE1[-1]=0
  totPE1[-99]=0
  totPE2[-1]=0
  totPE2[-99]=0

```

```
    totHits1[-1]=0
    totHits1[-99]=0
    totHits2[-1]=0
    totHits2[-99]=0

    for i in range(42):
      dEdx1[i]=0
      dEdx2[i]=0
      totPE1[i]=0
      totPE2[i]=0
      totHits1[i]=0
      totHits2[i]=0

    if event.In_spill>0.5 and event.n_slices>0:
        #This is just a counter of the number of events
      if int(iEvent)/100>counter:
        print "Gate: %i/%i" % ((int(iEvent)/100)*100,nEntries)
        counter=int(iEvent)/100

      trigtime=0
      triggered=false

      totpe=dict()
      timedist=dict()
      sliceminmax=dict()

      for i in range(event.n_slices):#ignore slice 0
        timedist[i+1]=[]
        totpe[i+1]=0

      #Some variables come in arrays.  We need to loop over these arrays to get the values
      for i in range(event.n_rawhits):
        #This returns the trigger time for each event. If there was no trigger, then the "triggered" flag remains false
        if event.hit_disc_fired[i]==1 and event.hit_croc[i]==1 and event.hit_chain[i]==0 and event.hit_board[i]==5 and event.hit_pixel[i]==7:
```

```
        if event.hit_disc_fired[i]==1 and event.hit_croc[i]==1 and event.hit_chain[i]==0 and event.hit_board[i]==5 and event.hit_pixel[i]==7:
          trigtime=GetTrigTime(event,i)
          triggered=true

        if event.hit_pe[i]>=0 and event.hit_time_slice[i]>0:
          #ModuleMultiplier takes in account passive material in the detector
            if event.hit_time_slice[i]>event.n_slices:#This shouldn't happen
              continue
            totpe[event.hit_time_slice[i]]+=ModuleMultiplier(event.hit_pe[i],event.hit_module[i])
            timedist[event.hit_time_slice[i]].append(event.hit_time_raw[i])

      #This goes through and finds the slice in which the trigger occurred
      triggerslice=0
      sliced=false
      for sl in timedist:
          if len(timedist[sl])!=0:
            sliceminmax[sl]=[min(timedist[sl]),max(timedist[sl])]
      if triggered:
          for slmm in sliceminmax:
            if sliceminmax[slmm][0]==sliceminmax[slmm][1]:
              break
            if IsSliceTriggered(sliceminmax[slmm],trigtime):
              triggerslice=slmm
              sliced=true
              break

        #Here is where you output the results.  Write events into html files, write events into histograms, etc.
          if sliced:
            if event.ToF_quality==1 and event.ToF_measured_time > -3000 and event.ToF_measured_time < 1000:
              PE_hists[-1].Fill(totpe[triggerslice])
              if totpe[triggerslice] > 7000 and totpe[triggerslice] < 9000: #These are mu-like events
```

```
                for i in range(event.n_rawhits):
                  if event.hit_time_slice[i]==triggerslice:
                    dEdx1[event.hit_module[i]]+=ModuleMultiplier(event.hit_pe[i],event.hit_module[i])
                    totPE1[event.hit_module[i]]+=event.hit_pe[i]
                    totHits1[event.hit_module[i]]+=1

              elif totpe[triggerslice] > 20000 and totpe[triggerslice] < 35000: #These are pi-like events
                for i in range(event.n_rawhits):
                  if event.hit_time_slice[i]==triggerslice:
                    dEdx2[event.hit_module[i]]+=ModuleMultiplier(event.hit_pe[i],event.hit_module[i])
                    totPE2[event.hit_module[i]]+=event.hit_pe[i]
                    totHits2[event.hit_module[i]]+=1
              else:
                  continue

                    #NOW FOR THE SELECTED EVENTS AND THE DICTIONARIES CONSTRUCTED WE PROCEED TO FILL THE 2D-HISTOGRAMS:
              for i in dEdx1:
                if dEdx1[i]>5:
                  dEdx1_hists[-1].Fill(i,dEdx1[i])
                if dEdx2[i]>5:
                  dEdx2_hists[-1].Fill(i,dEdx2[i])
                if totPE1[i]>5:
                  totPE1_hists[-1].Fill(i,totPE1[i])
                if totPE2[i]>5:
                  totPE2_hists[-1].Fill(i,totPE2[i])
                totHits1_hists[-1].Fill(i,totHits1[i])
                totHits2_hists[-1].Fill(i,totHits2[i])

html_files.CloseAll(-1)#Closes all (if any) html files

gROOT.SetBatch()
outfile="Run2_dEdx_totPE_totHits_mu_pi_4GeV_Pos_Pions.pdf"
c=TCanvas()
c.Print(outfile+"[")
for i in range(len(dEdx1_hists)):
    PE_hists[i].Draw()
    c.Print(outfile)
    dEdx1_hists[i].Draw("colz")
    c.Print(outfile)
    dEdx2_hists[i].Draw("colz")
    c.Print(outfile)
    totPE1_hists[i].Draw("colz")
    c.Print(outfile)
    totPE2_hists[i].Draw("colz")
    c.Print(outfile)
    totHits1_hists[i].Draw("colz")
    c.Print(outfile)
    totHits2_hists[i].Draw("colz")
    c.Print(outfile)
c.Print(outfile+"]")
```

# Appendix C

# Script for analyzing the spatial distribution of the beam

```
#HTML is a class I wrote (you can find it above).  Here, we are creating the class with the types of events we want to look at so we can call them later.  In this case, the only type of events here are those which fired the Veto
html_files=HTML(["Veto"])

#List of histograms
Contador_total_hists=[]
Correlation1_hists=[]
MAP1_hists=[] #This contains blue-point hists containing points when "only one counter fired" (and a random-one is addded)

for dir in dirs:
  #This returns a list of files in the directory
  input_files = os.popen("ls /minerva/data/testbeam2/run1datamerged/%s/*mergedDST.root"%(dir)).readlines()

  Contador_total_hists.append(TH1D("h_Contador_total_"+dir,";Counters;"+dir,12,0,12))
  Correlation1_hists.append(TH2D("h_Correlation_"+dir,";Correlation;"+dir,12,0,12,12,0,12))
  MAP1_hists.append(TH2D("hVetoMap1"+dir,";Veto Map;"+dir,5,0,5,5,0,5))
 #MAP2_hists.append(TH2D("hVetoMap2"+dir,";Veto Map;"+dir,5,0,5,5,0,5))

  #This opens an html file called "ArachneLinks_Run1_(directory).html"
  #Whenever we put an event in type "Veto", it writes a link to the event
  #in ArachneLinks_Run1_(directory).html
  html_files.OpenHtml("Veto","ArachneLinks_Run1_"+dir+"_Veto.html")

  #This creates a TChain in which you can add TTree to with the name "minerva"
  roottree = TChain("minerva")

  for infile in input_files:
    filename = infile.split()[0]
    print filename
    roottree.Add(filename)#This adds the TTree in the file to the chain

  nEntries=roottree.GetEntries()
    #This does the mapping from the correlation matrix to physical space
```

```
  #This does the mapping from the correlation matrix to physical space
VetoPaddles={ 5 : {12:[0,0],
                   2: [0,1],
                   3: [0,2],
                   4: [0,3],
                   10:[0,4]
                  },
              6 : {12:[1,0],
                   2: [1,1],
                   3: [1,2],
                   4: [1,3],
                   10:[1,4]
                  },
              1 : {12:[2,0],
                   2: [2,1]
                  },
              7 : {4: [2,3],
                   10:[2,4]
                  },
              8 : {12:[3,0],
                   2 :[3,1],
                   11:[3,2],
                   4 :[3,3],
                   10:[3,4]
                  },
              9 : {12:[4,0],
                   2 :[4,1],
                   11:[4,2],
                   4 :[4,3],
                   10:[4,4]
                  }
          }

Key_counters=dict()
Key_counters[0]=[1,11]
Key_counters[1]=[4,5,0,7,8]
Key_counters[2]=[4,5]
```

```
Key_counters[3]=[4,5,6,7,8]
Key_counters[4]=[9,3,2,1,11]
Key_counters[5]=[9,3,2,1,11]
Key_counters[6]=[9,3]
Key_counters[7]=[9,3,10,1,11]
Key_counters[8]=[9,3,10,1,11]
Key_counters[9]=[4,5,6,7,8]
Key_counters[10]=[7,8]
Key_counters[11]=[4,5,0,7,8]

counter=0
for iEvent, event in enumerate(roottree): #Loop through the events in the chain
  #If In_spill is larger than 0.5, then the event occured in a spill
  #n_slices tell you how many slices there are in an event
  #If n_slices=0, nothing happened in the detector

  if event.In_spill>0.5 and event.n_slices>0:
    #This is just a counter of the number of events
    if int(iEvent)/100>counter:
      print "Gate: %i/%i" % ((int(iEvent)/100)*100,nEntries)
      counter=int(iEvent)/100

    trigtime=0
    triggered=false

    totpe=dict()
    timedist=dict()
    sliceminmax=dict()

    for i in range(event.n_slices):#ignore slice 0
      timedist[i+1]=[]
      totpe[i+1]=0

    #Some variables come in arrays.  You will need to loop over these arrays to get the values
    for i in range(event.n_rawhits):
```

```
        #This returns the trigger time for each event. If there was no trigger, then the "triggered" flag remains false
        if event.hit_disc_fired[i]==1 and event.hit_croc[i]==1 and event.hit_chain[i]==0 and event.hit_board[i]==5 and event.hit_pixel[i]==7:
          trigtime=GetTrigTime(event,i)
          triggered=true

        if event.hit_pe[i]>=0 and event.hit_time_slice[i]>0:
          #ModuleMultiplier takes in account passive material in the detector
          if event.hit_time_slice[i]>event.n_slices:#This shouldn't happen
            continue
          totpe[event.hit_time_slice[i]]+=ModuleMultiplier(event.hit_pe[i],event.hit_module[i])
          timedist[event.hit_time_slice[i]].append(event.hit_time_raw[i])

      #This goes through and finds the slice in which the trigger occurred
      triggerslice=0
      sliced=false
      for sl in timedist:
        if len(timedist[sl])!=0:
          sliceminmax[sl]=[min(timedist[sl]),max(timedist[sl])]
      if triggered:
        for slmm in sliceminmax:
          if sliceminmax[slmm][0]==sliceminmax[slmm][1]:
            break
          if IsSliceTriggered(sliceminmax[slmm],trigtime):
            triggerslice=slmm
            sliced=true
            break

        #Here is where you output the results.  Write events into html files, write events into histograms, etc.
        if sliced:
          if DidVetoFire(event):#If true, veto fired
            #Flag=0
            Lista_counters=[event.Veto_VetoCounter_1, event.Veto_VetoCounter_2, event.Veto_VetoCounter_3, event.Veto_VetoCounter_4, event.Veto_VetoCounter_5, event.Veto_VetoCounter_6, event.Veto_VetoCounter_7, event.Veto_VetoCounter_8,
```

```
event.Veto_VetoCounter_3, event.Veto_VetoCounter_4, event.Veto_VetoCounter_5,
event.Veto_VetoCounter_6, event.Veto_VetoCounter_7, event.Veto_VetoCounter_8,
event.Veto_VetoCounter_9, event.Veto_VetoCounter_10, event.Veto_VetoCounter_11,
event.Veto_VetoCounter_12]
            for i in range(12):
                if Lista_counters[i]>0:
                    Contador_total_hists[-1].Fill(i)
                    listita=Key_counters[i]
                    j=random.choice(listita)
                    Correlation1_hists[-1].Fill(i,j) #Histogram filled when 1 counter fired (the other chosen randomly among those correlated to it)

  for x in VetoPaddles:
    for y in VetoPaddles[x]:
      MAP1_hists[-1].Fill(VetoPaddles[x][y][0],VetoPaddles[x][y][1],Correlation1_hists[-1].GetBinContent(x,y))

html_files.CloseAll(-1)#Closes all html files

gROOT.SetBatch()
outfile="Run1_Veto-Counters-SpatialRandomMAp-1.77GeV_Pos_Electrons.pdf"
c=TCanvas()
c.Print(outfile+"[")
for vhist in Contador_total_hists:
  vhist.Draw()
  c.Print(outfile)
for Vmaph1 in MAP1_hists:
  Vmaph1.SetMarkerColor(kBlue)
  Vmaph1.Draw()
  c.Print(outfile)
  Vmaph1.Draw("colz")
  c.Print(outfile)
c.Print(outfile+"]")
```

# Appendix D

# Script for counting events of interest (to calculate efficiency of cuts)

```
for dir in dirs:
  #This returns a list of files in the directory
  input_files = os.popen("ls /minerva/data/testbeam2/run2datamerged/%s/*mergedDST.root"%(dir)).readlines()

  Anne_Eventshists.append(TH1D("Anne_Events"+dir,";;",280,-5000,20000))
###  Contaminationhists.append(TH1D("Contamination"+dir,";pe;",-5000,20000))

  #This opens an html file called "ArachneLinks_Run2_(directory).html"
  #Whenever we put an event in type "Veto" or "NoVeto", it writes a link to the event
  #in ArachneLinks_Run2_(directory).html
  html_files.OpenHtml("Anne_Events","ArachneLinks_Run2_"+dir+"_Anne_Events.html")
###  html_files.OpenHtml("Contamination","ArachneLinks_Run2_"+dir+"_NoVeto.html")

  #This creates a TChain in which you can add TTree to with the name "minerva"
  roottree = TChain("minerva")

  for infile in input_files:
    filename = infile.split()[0]
    print filename
    roottree.Add(filename)#This adds the TTree in the file to the chain

  nEntries=roottree.GetEntries()

  contador0=0  #Counts All Events just In_spill
  contador1=0  #Count All Events In_spill && event.n_slices>0 (Activity in the Detector)
  contador2=0  #counts ALL events that satisfied the previous cut + triggered + sliced (events in the triggered slice)
  contador3=0  #counts all events that passed the previous cuts AND in which the Veto fired
  contador4=0  #Counts all events that passed made Veto_Count>0
  contador5=0  #Counts all events that satisfied both previous conditions.
  contador6=0  #Counts all events that passed made Veto_Count>0 AND Veto did not fire (Odd Events)
  contador7=0  #Events of kind 2 AND ToF quality 1 AND Veto did not fire (My Events)

  counter=0
```

```
for iEvent, event in enumerate(roottree): #Loop through the events in the chain
  #If In_spill is larger than 0.5, then the event occured in a spill
  #n_slices tell you how many slices there are in an event
  #If n_slices=0, nothing happened in the detector
  if event.In_spill>0.5:
    contador0+=1

  if event.In_spill>0.5 and event.n_slices>0:
    contador1+=1
    #This is just a counter of the number of events
    if int(iEvent)/100>counter:
      print "Gate: %i/%i" % ((int(iEvent)/100)*100,nEntries)
      counter=int(iEvent)/100

    trigtime=0
    triggered=false

    totpe=dict()
    timedist=dict()
    sliceminmax=dict()

    for i in range(event.n_slices):#ignore slice 0
      timedist[i+1]=[]
      totpe[i+1]=0

    #Some variables come in arrays.  You will need to loop over these arrays to get the values
    for i in range(event.n_rawhits):
      #This returns the trigger time for each event. If there was no trigger, then the "triggered" flag remains false
      if event.hit_disc_fired[i]==1 and event.hit_croc[i]==1 and event.hit_chain[i]==0 and event.hit_board[i]==5 and event.hit_pixel[i]==7:
        trigtime=GetTrigTime(event,i)
        triggered=true

      if event.hit_pe[i]>=0 and event.hit_time_slice[i]>0:
```

```
        if event.hit_pe[i]>=0 and event.hit_time_slice[i]>0:
          #ModuleMultiplier takes in account passive material in the detector
          if event.hit_time_slice[i]>event.n_slices:#This shouldn't happen
            continue
          totpe[event.hit_time_slice[i]]+=ModuleMultiplier(event.hit_pe[i],event.hit_module[i])
          timedist[event.hit_time_slice[i]].append(event.hit_time_raw[i])

      #This goes through and finds the slice in which the trigger occurred
      triggerslice=0
      sliced=false
      for sl in timedist:
        if len(timedist[sl])!=0:
          sliceminmax[sl]=[min(timedist[sl]),max(timedist[sl])]
      if triggered:
        for slmm in sliceminmax:
          if sliceminmax[slmm][0]==sliceminmax[slmm][1]:
            break
          if IsSliceTriggered(sliceminmax[slmm],trigtime):
            triggerslice=slmm
            sliced=true
            break

        #Here is where you output the results.  Write events into html files, write events into histograms, etc.
        if sliced:
         contador2+=1
         if DidVetoFire(event):
            contador3+=1
         if event.Veto_Veto_Count>0:
            contador4+=1
         if DidVetoFire(event) and event.Veto_Veto_Count>0:
            contador5+=1
         if event.Veto_Veto_Count>0 and not DidVetoFire(event):
            contador6+=1  #This is an ODD Event
         if event.ToF_quality==1 and not DidVetoFire(event):
            contador7+=1 #This is an event of interest for Me. generate also Arachne-
```

```
            contador7+=1 #This is an event of interest for Me, generate also Arachne-links for them (using DrGran)
            DrGranCoolTool(event.ev_gate-1,filename,html_files.GetLastHtml("Anne_Events"),triggerslice)

  dirdict[dir]=[contador0, contador1, contador2, contador3, contador4, contador5, contador6, contador7]

html_files.CloseAll(-1)#Closes all html files

gROOT.SetBatch()
outfile="Run2_ToF_VetoCounters2.pdf"
c=TCanvas()
c.Print(outfile+"[")
#for AEhist in AllEventshists:
#  gPad.SetLogy()
#  AEhist.Draw()
#  c.Print(outfile)
#for nvhist in novetohists:
#  nvhist.Draw()
#  c.Print(outfile)
c.Print(outfile+"]")

print "Events-0: Total Number of Events In_Spill";
print "Events-1: Total Number of Events In_Spill & event.n_slices>0 (Activity in the Detector)";
print "Events-2: Total Number of Events In_Spill & event.n_slices>0 + Triggered + Sliced";
print "Events-3: Total Number of Events of kind-2 & Veto Fired";
print "Events-4: Total Number of Events of kind-2 & Veto_Count>0";
print "Events-5: Total Number of Events of kind-2 & Veto_Count>0 & Veto Fired";
print "Events-6: Total Number of Events of kind-2 & Veto_Count>0 & Veto did not Fired (Odd-Events)";
print "Events-7: Total Number of Events of kind-2 & ToF_quality==1 & Veto did not Fired (My-Events)";
print "";
print "Folder  ", "Events-0  ", "Events-1  ", "Events-2  ", "Events-3  ", "Events-4  ", "Events-5  ", "Events-6 ", "Events-7 ";

print "";

for i in dirdict:
    print i, dirdict[i][0], dirdict[i][1], dirdict[i][2], dirdict[i][3], dirdict[i][4], dirdict[i][5], dirdict[i][6], dirdict[i][7] ;
```

# Appendix E

# Histograms of pure (MC) 2 GeV $\mu^+$ & $\pi^+$ samples

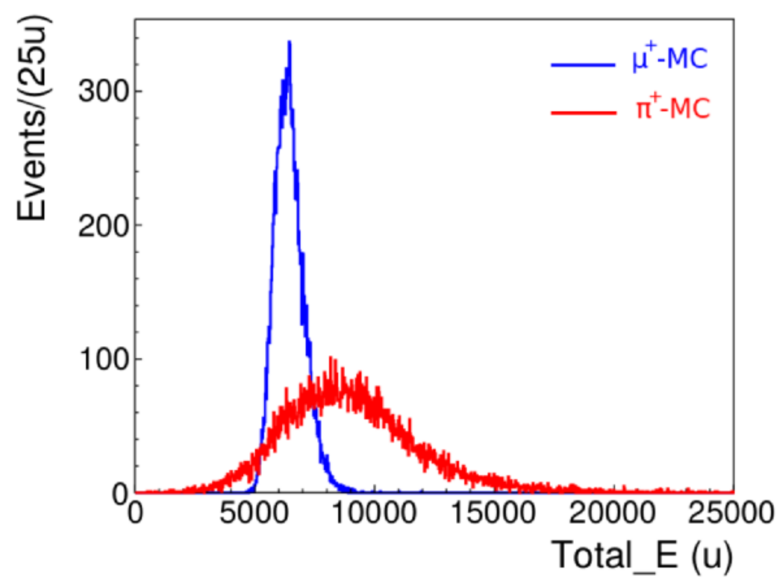


| Var_i_ß_cut(i) | Cut(μ)_Interval | Eff | Deff | Pur | Dpur | Eff*Pur | D(Eff*Pur) |
|---|---|---|---|---|---|---|---|
| | [5000,9000] | 0.99761 | 0.00036346 | 0.67297 | 0.0028703 | 0.67136 | 0.0031081 |
| | [5000,8500] | 0.99462 | 0.00054508 | 0.70826 | 0.0028575 | 0.70444 | 0.0032282 |
| Total_E | [5100,8000] | 0.9803 | 0.0010352 | 0.74958 | 0.0028223 | 0.73481 | 0.0035426 |

**Figure E.1:** Histogram of $Var\_1\_1$ for pure (MC) 2 GeV $\mu^+$ & $\pi^+$ samples.

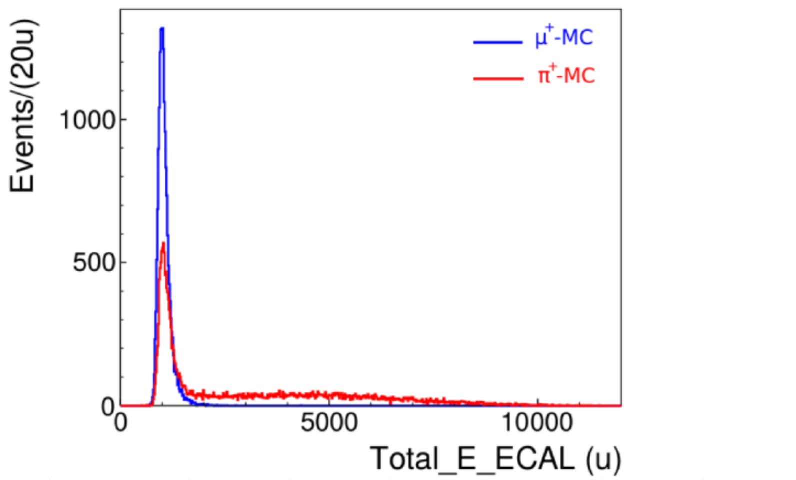


| Var_i_ß_cut(i) | Cut(μ)_Interval | Eff | Deff | Pur | Dpur | Eff*Pur | D(Eff*Pur) |
|---|---|---|---|---|---|---|---|
| | [500,1800] | 0.99612 | 0.00046339 | 0.66338 | 0.0028728 | 0.66081 | 0.003169 |
| Total_E_ECAL | [500,1700] | 0.9929 | 0.00062561 | 0.66723 | 0.0028775 | 0.66249 | 0.0032745 |
| | [500,1900] | 0.99695 | 0.00041093 | 0.65979 | 0.0028712 | 0.65778 | 0.0031336 |

**Figure E.2:** Histogram of $Var\_1\_2$ for pure (MC) 2 GeV $\mu^+$ & $\pi^+$ samples.

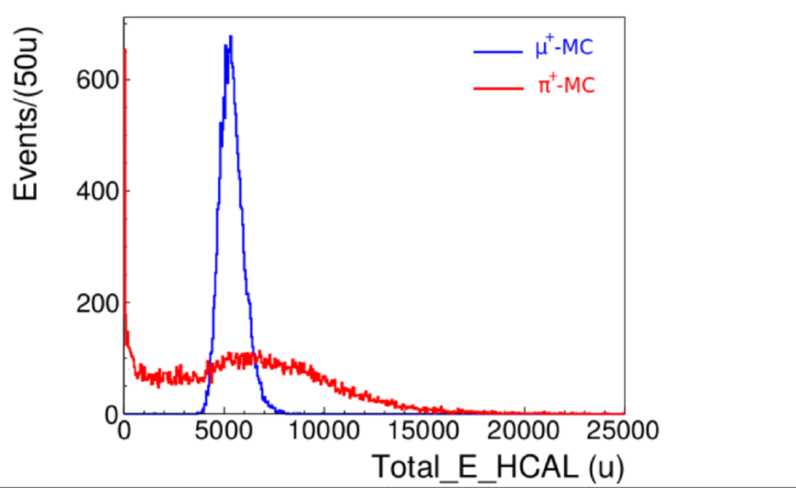


| Var_i_ß_cut(i) | Cut(μ)_Interval | Eff | Deff | Pur | Dpur | Eff*Pur | D(Eff*Pur) |
|---|---|---|---|---|---|---|---|
| | [4000,7500] | 0.99584 | 0.00047959 | 0.75477 | 0.0027902 | 0.75163 | 0.0031405 |
| Total_E_HCAL | [4100,7400] | 0.99279 | 0.00063044 | 0.76325 | 0.0027766 | 0.75774 | 0.0032377 |
| | [4100,7600] | 0.99473 | 0.00053946 | 0.75342 | 0.0027944 | 0.74945 | 0.0031861 |

**Figure E.3:** Histogram of $Var\_1\_3$ for pure (MC) 2 GeV $\mu^+$ & $\pi^+$ samples.

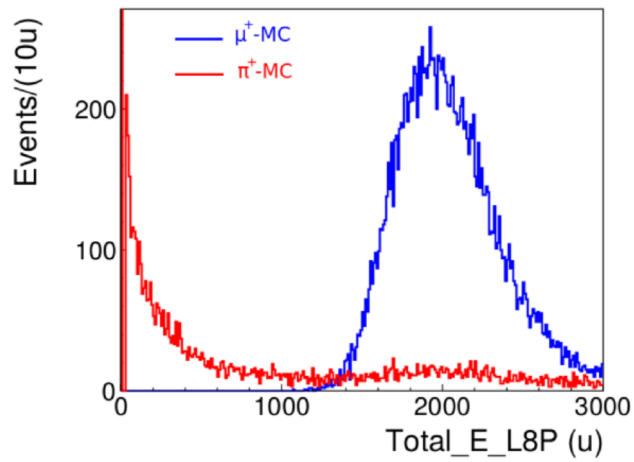


| Var_i_ß_cut(i) | Cut(μ)_Interval | Eff | Deff | Pur | Dpur | Eff*Pur | D(Eff*Pur) |
|---|---|---|---|---|---|---|---|
| | [1200,] | 0.99956 | 0.00015693 | 0.8612 | 0.0023907 | 0.86082 | 0.0025247 |
| Total_E_L8P | [1300,] | 0.99828 | 0.00030871 | 0.8638 | 0.0023768 | 0.86232 | 0.0026394 |
| | [1400,] | 0.99345 | 0.00060084 | 0.86673 | 0.0023648 | 0.86106 | 0.0028701 |

**Figure E.4:** Histogram of $Var\_1\_4$ for pure (MC) 2 GeV $\mu^+$ & $\pi^+$ samples.

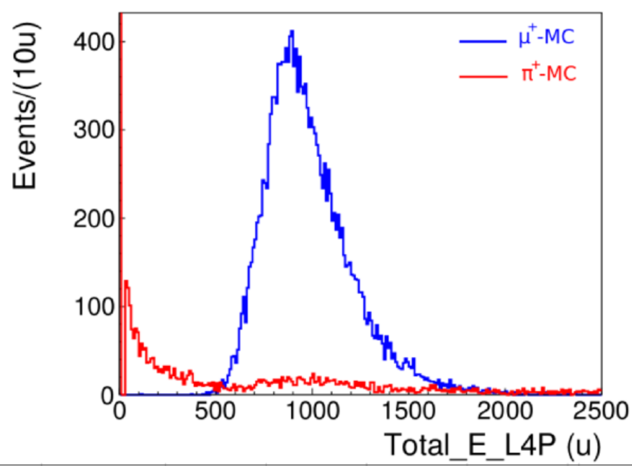


| Var_i_ß_cut(i) | Cut(μ)_Interval | Eff | Deff | Pur | Dpur | Eff*Pur | D(Eff*Pur) |
|---|---|---|---|---|---|---|---|
| Total_E_L4P | [500,1850] | 0.9944 | 0.00055614 | 0.91167 | 0.0020242 | 0.90656 | 0.0025198 |
| | [550,1850] | 0.99212 | 0.00065868 | 0.9135 | 0.0020094 | 0.9063 | 0.0025953 |
| | [600,1850] | 0.98368 | 0.00094373 | 0.91443 | 0.0020091 | 0.89951 | 0.0028393 |

**Figure E.5:** Histogram of $Var\_1\_5$ for pure (MC) 2 GeV $\mu^+$ & $\pi^+$ samples.

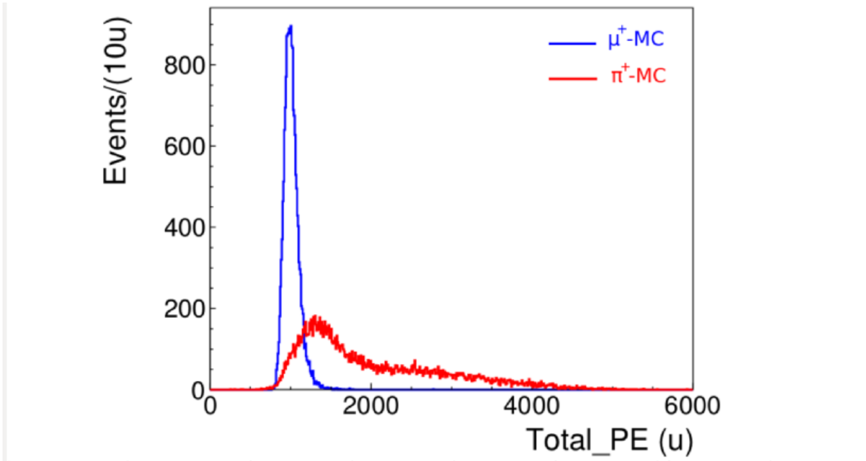


| Var_i_ß_cut(i) | Cut(μ)_Interval | Eff | Deff | Pur | Dpur | Eff*Pur | D(Eff*Pur) |
|---|---|---|---|---|---|---|---|
| | [700,1400] | 0.99612 | 0.00046339 | 0.75735 | 0.0027845 | 0.75441 | 0.0031247 |
| Total_PE | [750,1300] | 0.98862 | 0.00079002 | 0.80561 | 0.0026611 | 0.79645 | 0.0032673 |
| | [700,1500] | 0.99834 | 0.0003037 | 0.71842 | 0.0028423 | 0.71722 | 0.0030557 |

**Figure E.6:** Histogram of $Var\_2\_1$ for pure (MC) 2 GeV $\mu^+$ & $\pi^+$ samples.

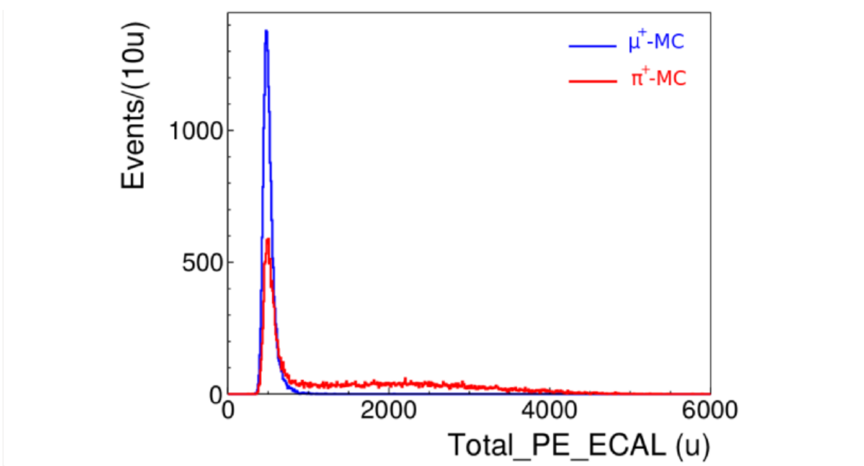


| Var_i_ß_cut(i) | Cut(μ)_Interval | Eff | Deff | Pur | Dpur | Eff*Pur | D(Eff*Pur) |
|---|---|---|---|---|---|---|---|
| | [250,750] | 0.98513 | 0.00090169 | 0.67335 | 0.0028884 | 0.66333 | 0.0034526 |
| | [250,900] | 0.99667 | 0.00042914 | 0.66109 | 0.0028718 | 0.65889 | 0.0031459 |
| Total_PE_ECAL | [250,800] | 0.99168 | 0.00067682 | 0.66909 | 0.0028792 | 0.66352 | 0.0033081 |

**Figure E.7:** Histogram of $Var\_2\_2$ for pure (MC) 2 GeV $\mu^+$ & $\pi^+$ samples.

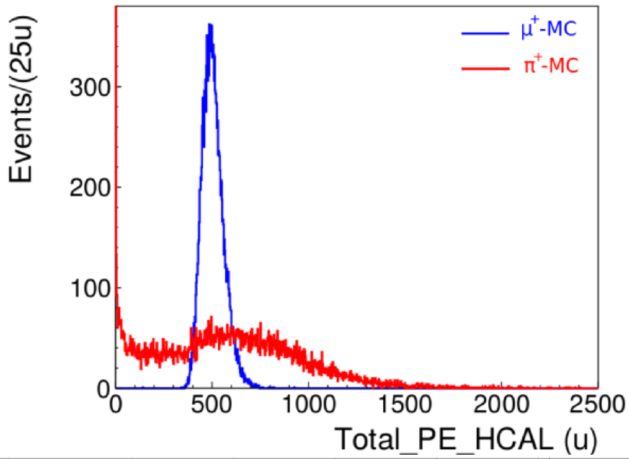


| Var_i_ß_cut(i) | Cut(μ)_Interval | Eff | Deff | Pur | Dpur | Eff*Pur | D(Eff*Pur) |
|---|---|---|---|---|---|---|---|
| | [350,700] | 0.99689 | 0.00041463 | 0.7466 | 0.0028041 | 0.74428 | 0.0031049 |
| | [370,690] | 0.99473 | 0.00053946 | 0.75891 | 0.0027832 | 0.75491 | 0.003178 |
| Total_PE_HCAL | [370,680] | 0.99323 | 0.00061087 | 0.76412 | 0.002774 | 0.75895 | 0.003222 |

**Figure E.8:** Histogram of $Var\_2\_3$ for pure (MC) 2 GeV $\mu^+$ & $\pi^+$ samples.

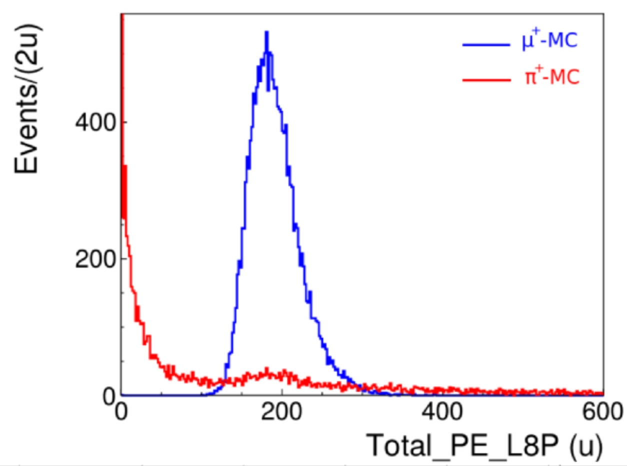


| Var_i_ß_cut(i) | Cut(μ)_Interval | Eff | Deff | Pur | Dpur | Eff*Pur | D(Eff*Pur) |
|---|---|---|---|---|---|---|---|
| | [120,310] | 0.99506 | 0.00052223 | 0.9121 | 0.0020195 | 0.90759 | 0.0024858 |
| Total_PE_L8P | [120,300] | 0.99301 | 0.00062074 | 0.91441 | 0.0019999 | 0.90801 | 0.0025535 |
| | [110,310] | 0.99617 | 0.00046008 | 0.9084 | 0.002052 | 0.90492 | 0.0024621 |

**Figure E.9:** Histogram of $Var\_2\_4$ for pure (MC) 2 GeV $\mu^+$ & $\pi^+$ samples.

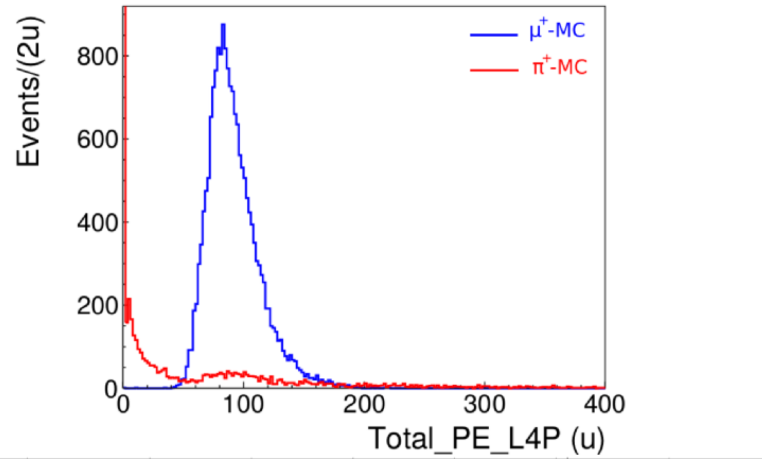


| Var_i_ß_cut(i) | Cut(μ)_Interval | Eff | Deff | Pur | Dpur | Eff*Pur | D(Eff*Pur) |
|---|---|---|---|---|---|---|---|
| | [45,170] | 0.99351 | 0.00059831 | 0.93673 | 0.0017609 | 0.93065 | 0.0023099 |
| Total_PE_L4P | [50,180] | 0.99506 | 0.00052223 | 0.93714 | 0.0017547 | 0.93251 | 0.0022354 |
| | [55,175] | 0.98724 | 0.00083622 | 0.93921 | 0.0017362 | 0.92722 | 0.0024994 |

**Figure E.10:** Histogram of $Var\_2\_5$ for pure (MC) 2 GeV $\mu^+$ & $\pi^+$ samples.

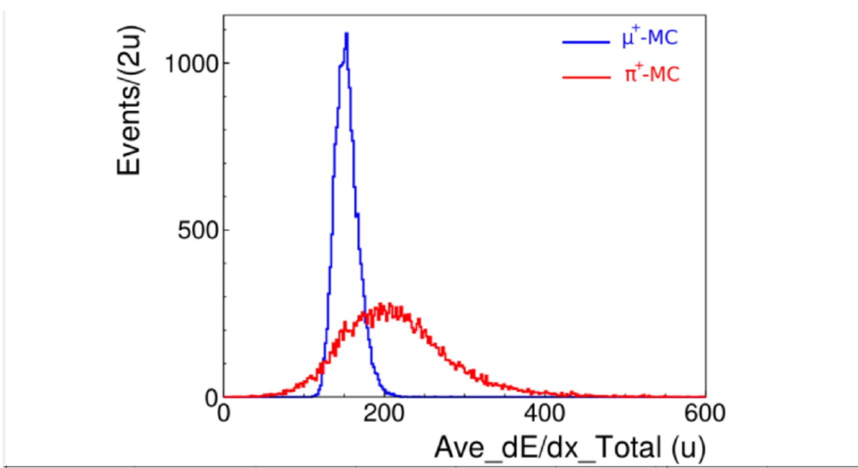


| Var_i_ß_cut(i) | Cut(μ)_Interval | Eff | Deff | Pur | Dpur | Eff*Pur | D(Eff*Pur) |
|---|---|---|---|---|---|---|---|
| | [115,220] | 0.99917 | 0.00021484 | 0.65458 | 0.0028671 | 0.65404 | 0.0030053 |
| | [120,225] | 0.99734 | 0.00038396 | 0.6449 | 0.0028666 | 0.64319 | 0.0031066 |
| Ave_dEdx_Total | [115,215] | 0.99867 | 0.00027168 | 0.6678 | 0.0028692 | 0.66691 | 0.0030468 |

**Figure E.11:** Histogram of $Var\_3\_1$ for pure (MC) 2 GeV $\mu^+$ & $\pi^+$ samples.

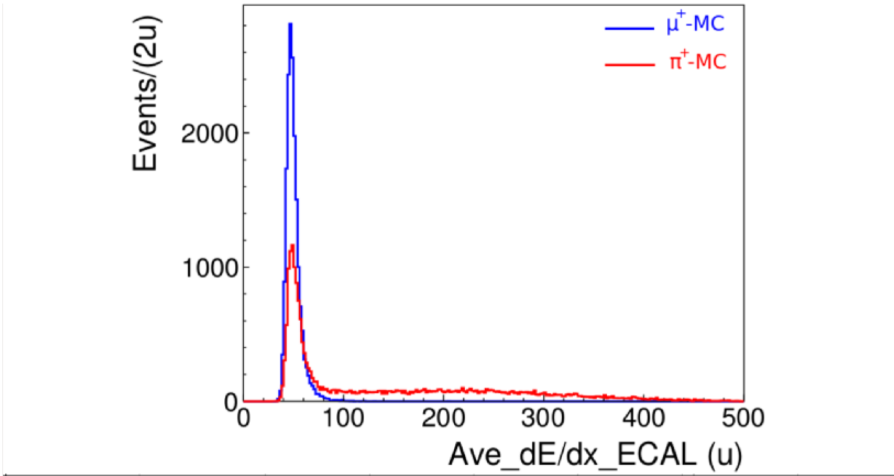


| Var_i_ß_cut(i) | Cut(μ)_Interval | Eff | Deff | Pur | Dpur | Eff*Pur | D(Eff*Pur) |
|---|---|---|---|---|---|---|---|
| Ave_dEdx_ECAL | [30,80] | 0.99251 | 0.00064236 | 0.66804 | 0.0028781 | 0.66303 | 0.0032856 |
| | [30,90] | 0.99684 | 0.00041831 | 0.66021 | 0.0028714 | 0.65812 | 0.0031385 |
| | [30,85] | 0.99567 | 0.00048905 | 0.66401 | 0.0028734 | 0.66114 | 0.0031857 |

**Figure E.12:** Histogram of $Var\_3\_2$ for pure (MC) 2 GeV $\mu^+$ & $\pi^+$ samples.

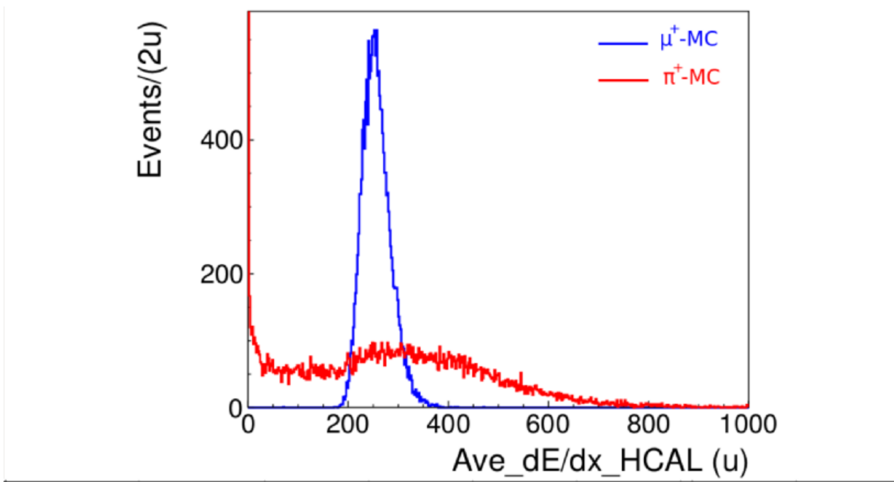


| Var_i_ß_cut(i) | Cut(μ)_Interval | Eff | Deff | Pur | Dpur | Eff*Pur | D(Eff*Pur) |
|---|---|---|---|---|---|---|---|
| Ave_dEdx_HCAL | [190,350] | 0.99406 | 0.00057233 | 0.76135 | 0.002779 | 0.75683 | 0.0031982 |
| | [200,370] | 0.9914 | 0.00068792 | 0.74862 | 0.0028082 | 0.74218 | 0.003299 |
| | [195,360] | 0.99478 | 0.00053663 | 0.75512 | 0.0027909 | 0.75118 | 0.0031816 |

**Figure E.13:** Histogram of $Var\_3\_3$ for pure (MC) 2 GeV $\mu^+$ & $\pi^+$ samples.

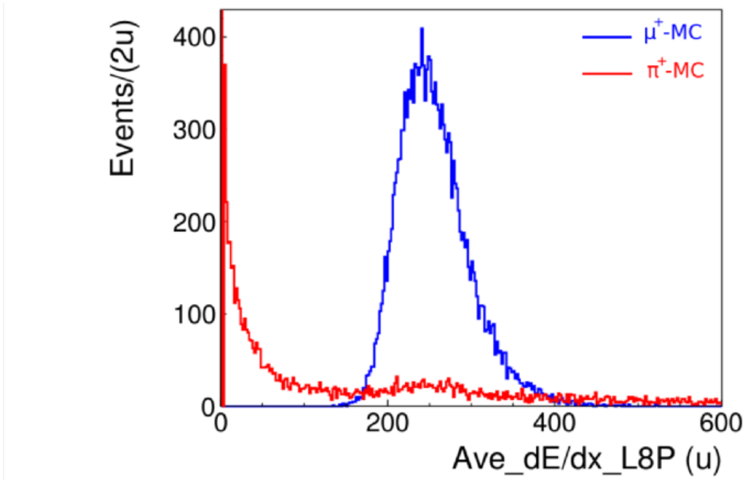


| Var_i_ß_cut(i) | Cut(μ)_Interval | Eff | Deff | Pur | Dpur | Eff*Pur | D(Eff*Pur) |
|---|---|---|---|---|---|---|---|
| | [160,420] | 0.9955 | 0.00049832 | 0.91092 | 0.0020299 | 0.90683 | 0.0024747 |
| | [155,410] | 0.99517 | 0.00051636 | 0.91127 | 0.002027 | 0.90687 | 0.0024878 |
| Ave_dEdx_L8P | [170,410] | 0.99223 | 0.00065406 | 0.91561 | 0.0019892 | 0.9085 | 0.0025726 |

**Figure E.14:** Histogram of $Var\_3\_4$ for pure (MC) 2 GeV $\mu^+$ & $\pi^+$ samples.

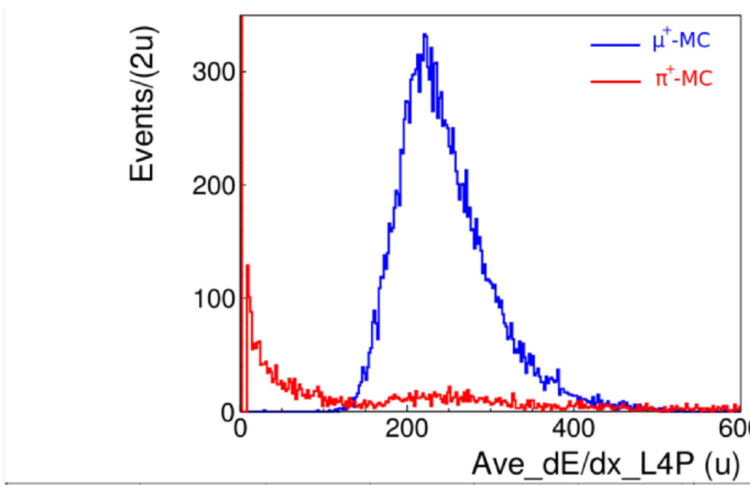


| Var_i_ß_cut(i) | Cut(μ)_Interval | Eff | Deff | Pur | Dpur | Eff*Pur | D(Eff*Pur) |
|---|---|---|---|---|---|---|---|
| | [125,450] | 0.99234 | 0.0006494 | 0.93777 | 0.0017494 | 0.93059 | 0.002345 |
| Ave_dEdx_L4P | [130,445] | 0.99129 | 0.0006923 | 0.93877 | 0.001738 | 0.9306 | 0.0023728 |
| | [120,450] | 0.9929 | 0.00062561 | 0.93696 | 0.0017587 | 0.93031 | 0.0023324 |

**Figure E.15:** Histogram of $Var\_3\_5$ for pure (MC) 2 GeV $\mu^+$ & $\pi^+$ samples.

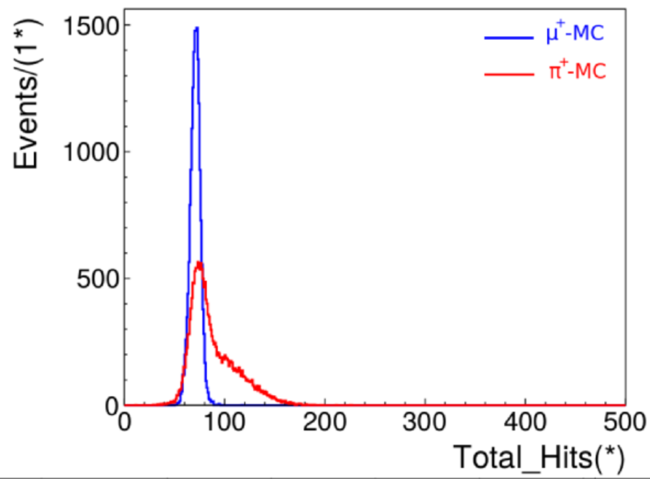


| Var_i_ß_cut(i) | Cut(μ)_Interval | Eff | Deff | Pur | Dpur | Eff*Pur | D(Eff*Pur) |
|---|---|---|---|---|---|---|---|
| | [50,90] | 0.99911 | 0.00022188 | 0.60839 | 0.0028374 | 0.60785 | 0.0029699 |
| | [55,88] | 0.9975 | 0.0003718 | 0.62045 | 0.0028511 | 0.6189 | 0.0030746 |
| Total_Hits | [55,85] | 0.99501 | 0.00052514 | 0.63619 | 0.0028657 | 0.63301 | 0.0031855 |

**Figure E.16:** Histogram of $Var\_4\_1$ for pure (MC) 2 GeV $\mu^+$ & $\pi^+$ samples.

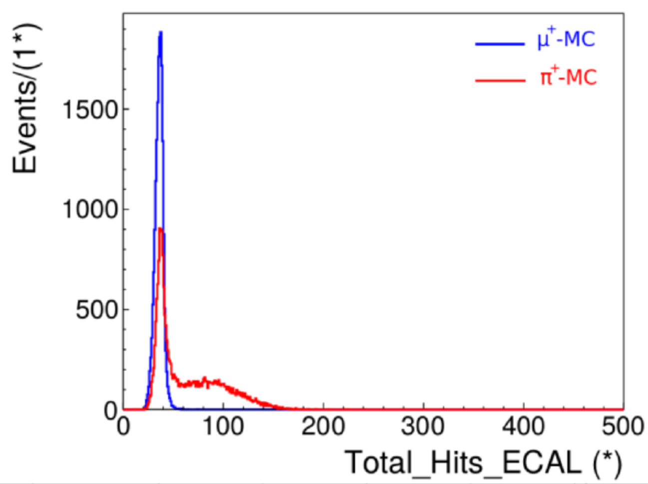


| Var_i_ß_cut(i) | Cut(μ)_Interval | Eff | Deff | Pur | Dpur | Eff*Pur | D(Eff*Pur) |
|---|---|---|---|---|---|---|---|
| | [20,50] | 0.99778 | 0.00035058 | 0.66046 | 0.0028701 | 0.659 | 0.0030953 |
| Total_Hits_ECAL | [20,45] | 0.9894 | 0.00076287 | 0.6807 | 0.0028807 | 0.67349 | 0.0033694 |
| | [20,55] | 0.99933 | 0.00019217 | 0.6452 | 0.0028639 | 0.64477 | 0.002986 |

**Figure E.17:** Histogram of $Var\_4\_2$ for pure (MC) 2 GeV $\mu^+$ & $\pi^+$ samples.

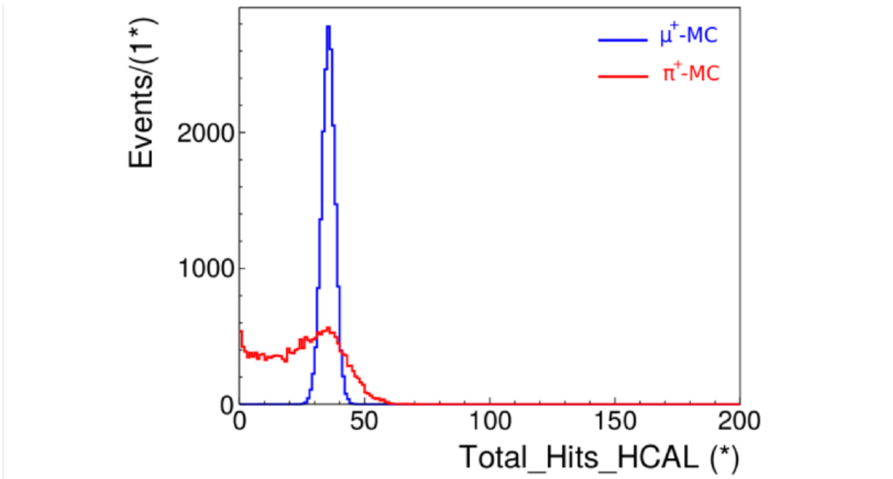


| Var_i_ß_cut(i) | Cut(μ)_Interval | Eff | Deff | Pur | Dpur | Eff*Pur | D(Eff*Pur) |
|---|---|---|---|---|---|---|---|
| | [27,43] | 0.99822 | 0.00031364 | 0.71443 | 0.0028466 | 0.71317 | 0.0030656 |
| | [28,44] | 0.99617 | 0.00046008 | 0.71888 | 0.0028448 | 0.71613 | 0.0031647 |
| Total_Hits_HCAL | [27,42] | 0.99617 | 0.00046008 | 0.7213 | 0.0028421 | 0.71854 | 0.0031631 |

**Figure E.18:** Histogram of $Var\_4\_3$ for pure (MC) 2 GeV $\mu^+$ & $\pi^+$ samples.

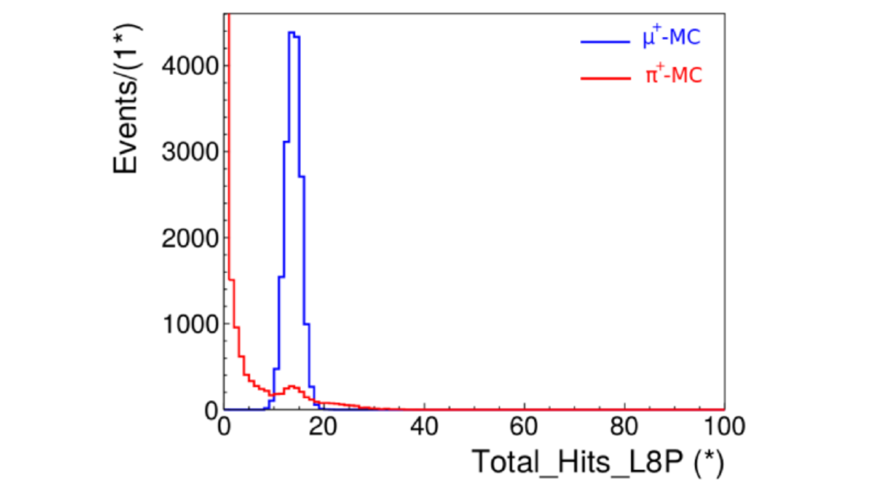


| Var_i_ß_cut(i) | Cut(μ)_Interval | Eff | Deff | Pur | Dpur | Eff*Pur | D(Eff*Pur) |
|---|---|---|---|---|---|---|---|
| Total_Hits_L8P | [9,18] | 0.99795 | 0.00033721 | 0.9145 | 0.001994 | 0.91262 | 0.0022983 |
| | [10,19] | 0.99279 | 0.00063044 | 0.91798 | 0.0019655 | 0.91136 | 0.0025301 |
| | [9,19] | 0.99861 | 0.00027728 | 0.91134 | 0.0020229 | 0.91008 | 0.0022728 |

**Figure E.19:** Histogram of $Var\_4\_4$ for pure (MC) 2 GeV $\mu^+$ & $\pi^+$ samples.

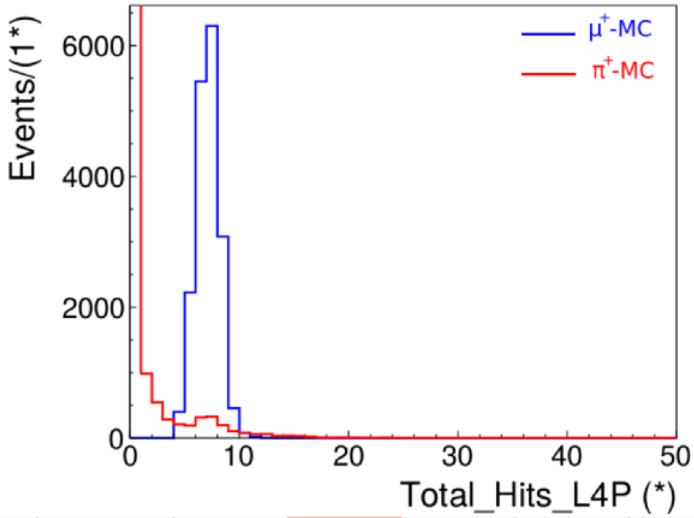


| Var_i_ß_cut(i) | Cut(µ)_Interval | Eff | Deff | Pur | Dpur | Eff*Pur | D(Eff*Pur) |
|---|---|---|---|---|---|---|---|
| | [4,11] | 0.99961 | 0.00014679 | 0.93042 | 0.0018286 | 0.93006 | 0.0019645 |
| Total_Hits_L4P | [4,10] | 0.99861 | 0.00027728 | 0.93292 | 0.0018012 | 0.93163 | 0.0020574 |
| | [4,12] | 0.99978 | 0.00011098 | 0.92771 | 0.0018583 | 0.92751 | 0.0019608 |

**Figure E.20:** Histogram of $Var\_4\_5$ for pure (MC) 2 GeV $\mu^+$ & $\pi^+$ samples.

# Appendix F

# Histograms of pure (MC) 2 GeV $e^+$ & $\mu^+$ samples

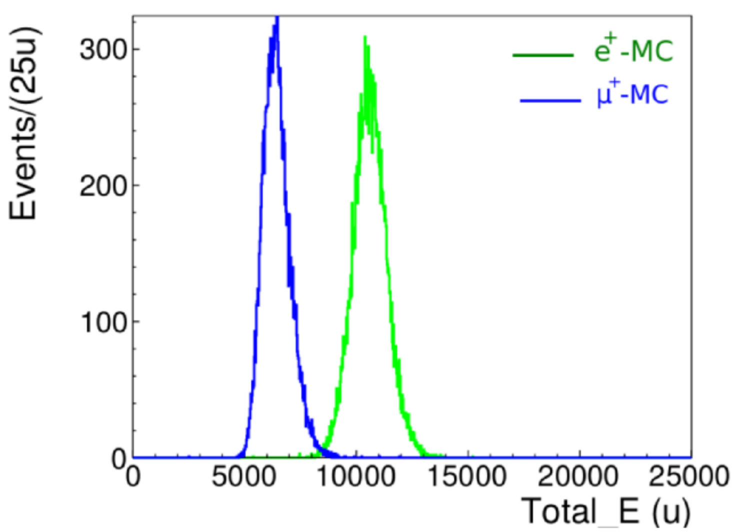


| Var_i_ß_cut(i) | Cut(e)_Interval | Eff | Deff | Pur | Dpur | Eff*Pur | D(Eff*Pur) |
|---|---|---|---|---|---|---|---|
| Total_E | [8500,16000] | 0.9968 | 0.0003994 | 0.99576 | 4.84E-004 | 0.99257 | 8.80E-004 |
| | [8600,16000] | 0.9953 | 0.0004836 | 0.99667 | 4.30E-004 | 0.99198 | 9.10E-004 |
| | [8700,16000] | 0.9932 | 0.0005811 | 0.99731 | 3.89E-004 | 0.99052 | 9.66E-004 |

**Figure F.1:** Histogram of $Var\_1\_1$ for pure (MC) 2 GeV $e^+$ & $\mu^+$ samples.

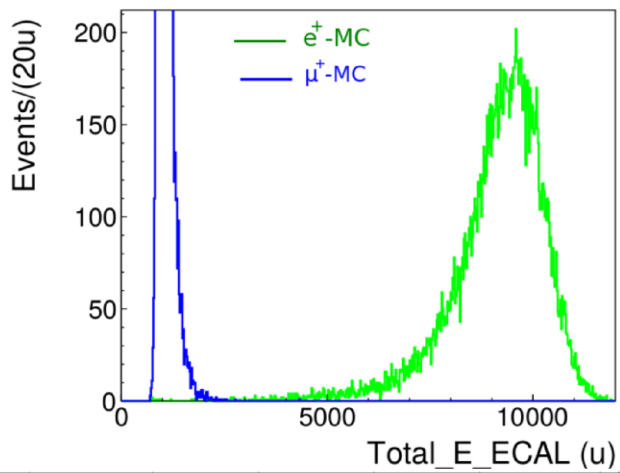


| Var_i_ß_cut(i) | Cut(e)_Interval | Eff | Deff | Pur | Dpur | Eff*Pur | D(Eff*Pur) |
|---|---|---|---|---|---|---|---|
| | [3000,] | 0.9986 | 0.0002644 | 0.99994 | 5.87E-005 | 0.99854 | 3.23E-004 |
| | [3500,] | 0.9979 | 0.0003237 | 0.99994 | 5.89E-005 | 0.99784 | 3.82E-004 |
| Total_E_ECAL | [2800,] | 0.9988 | 0.0002448 | 0.99994 | 5.86E-005 | 0.99874 | 3.03E-004 |

**Figure F.2:** Histogram of $Var\_1\_2$ for pure (MC) 2 GeV $e^+$ & $\mu^+$ samples.

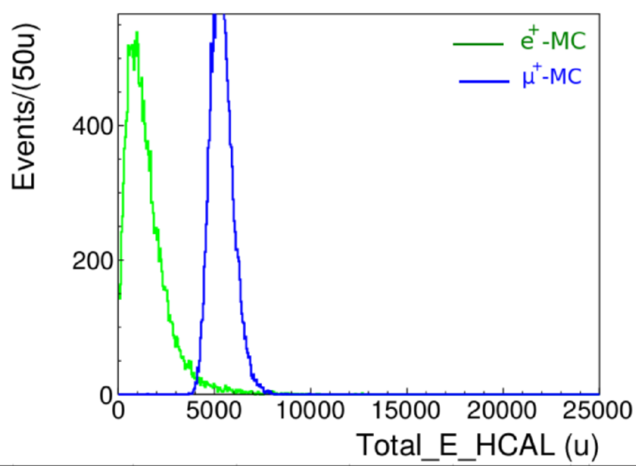


| Var_i_ß_cut(i) | Cut(e)_Interval | Eff | Deff | Pur | Dpur | Eff*Pur | D(Eff*Pur) |
|---|---|---|---|---|---|---|---|
| Total_E_HCAL | [0,4000] | 0.96785 | 0.0012473 | 0.99846 | 2.93E-004 | 0.96636 | 1.53E-003 |
| | [0,4250] | 0.97355 | 0.0011347 | 0.98877 | 7.83E-004 | 0.96262 | 1.88E-003 |
| | [0,4500] | 0.97795 | 0.0010384 | 0.95219 | 1.56E-003 | 0.93119 | 2.51E-003 |

**Figure F.3:** Histogram of $Var\_1\_3$ for pure (MC) 2 GeV $e^+$ & $\mu^+$ samples.

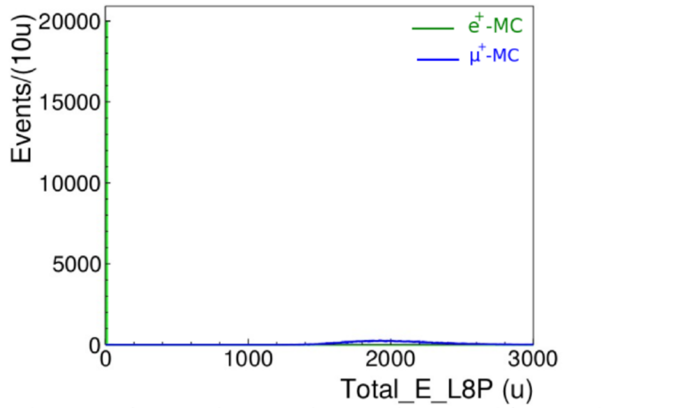


| Var_i_ß_cut(i) | Cut(e)_Interval | Eff | Deff | Pur | Dpur | Eff*Pur | D(Eff*Pur) |
|---|---|---|---|---|---|---|---|
| | [0,20] | 0.99585 | 0.0004546 | 0.99994 | 5.85E-005 | 0.99579 | 5.13E-004 |
| | [0,25] | 0.99585 | 0.0004546 | 0.99994 | 5.86E-005 | 0.99579 | 5.13E-004 |
| Total_E_L8P | [0,50] | 0.99685 | 0.0003962 | 0.99994 | 5.88E-005 | 0.99679 | 4.55E-004 |

**Figure F.4:** Histogram of $Var\_1\_4$ for pure (MC) 2 GeV $e^+$ & $\mu^+$ samples.

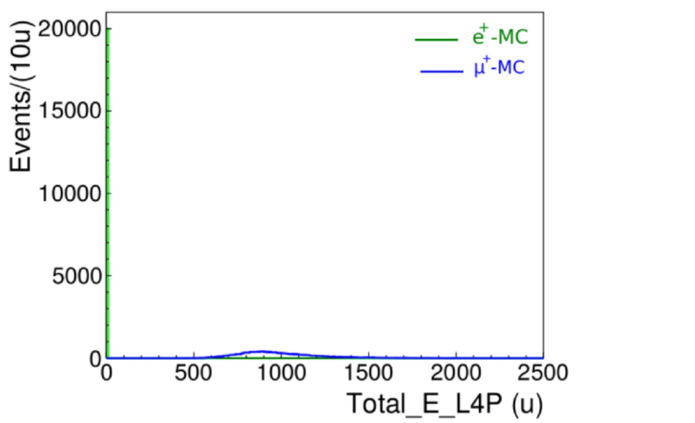


| Var_i_ß_cut(i) | Cut(e)_Interval | Eff | Deff | Pur | Dpur | Eff*Pur | D(Eff*Pur) |
|---|---|---|---|---|---|---|---|
| | [0,15] | 0.99975 | 0.0001118 | 0.99994 | 5.88E-005 | 0.99969 | 1.71E-004 |
| | [0,25] | 0.99975 | 0.0001118 | 0.99994 | 5.89E-005 | 0.99969 | 1.71E-004 |
| Total_E_L4P | [0,50] | 0.99985 | 0.0000866 | 0.99994 | 5.94E-005 | 0.99979 | 1.46E-004 |

**Figure F.5:** Histogram of $Var\_1\_5$ for pure (MC) 2 GeV $e^+$ & $\mu^+$ samples.

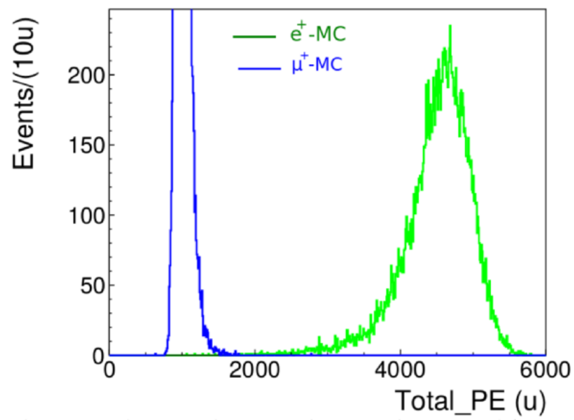


| Var_i_ß_cut(i) | Cut(e)_Interval | Eff | Deff | Pur | Dpur | Eff*Pur | D(Eff*Pur) |
|---|---|---|---|---|---|---|---|
| | [2000,] | 0.9991 | 0.000212 | 0.99994 | 5.87E-005 | 0.99904 | 2.71E-004 |
| Total_PE | [1800,] | 0.9995 | 0.0001581 | 0.99994 | 5.91E-005 | 0.99944 | 2.17E-004 |
| | [1900,] | 0.99935 | 0.0001802 | 0.99994 | 5.86E-005 | 0.99929 | 2.39E-004 |

**Figure F.6:** Histogram of $Var\_2\_1$ for pure (MC) 2 GeV $e^+$ & $\mu^+$ samples.

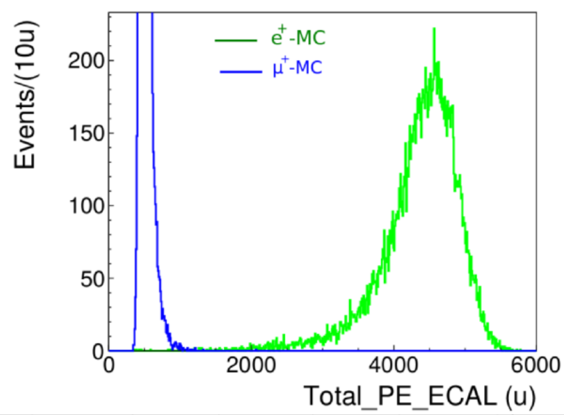


| Var_i_ß_cut(i) | Cut(e)_Interval | Eff | Deff | Pur | Dpur | Eff*Pur | D(Eff*Pur) |
|---|---|---|---|---|---|---|---|
| | [1500,] | 0.9985 | 0.0002737 | 0.99994 | 5.93E-005 | 0.99844 | 3.33E-004 |
| | [1400,] | 0.99875 | 0.0002498 | 0.99994 | 5.87E-005 | 0.99869 | 3.08E-004 |
| Total_PE_ECAL | [1300,] | 0.9989 | 0.0002344 | 0.99988 | 8.34E-005 | 0.99878 | 3.18E-004 |

**Figure F.7:** Histogram of $Var\_2\_2$ for pure (MC) 2 GeV $e^+$ & $\mu^+$ samples.

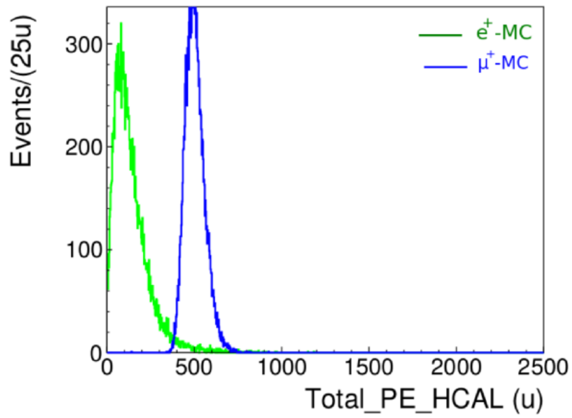


| Var_i_ß_cut(i) | Cut(e)_Interval | Eff | Deff | Pur | Dpur | Eff*Pur | D(Eff*Pur) |
|---|---|---|---|---|---|---|---|
| | [0,400] | 0.974 | 0.0011253 | 0.98599 | 8.71E-004 | 0.96035 | 1.96E-003 |
| Total_PE_HCAL | [0,380] | 0.9695 | 0.0012159 | 0.99722 | 3.93E-004 | 0.96681 | 1.59E-003 |
| | [0,420] | 0.9779 | 0.0010395 | 0.95352 | 1.54E-003 | 0.93245 | 2.49E-003 |

**Figure F.8:** Histogram of $Var\_2\_3$ for pure (MC) 2 GeV $e^+$ & $\mu^+$ samples.

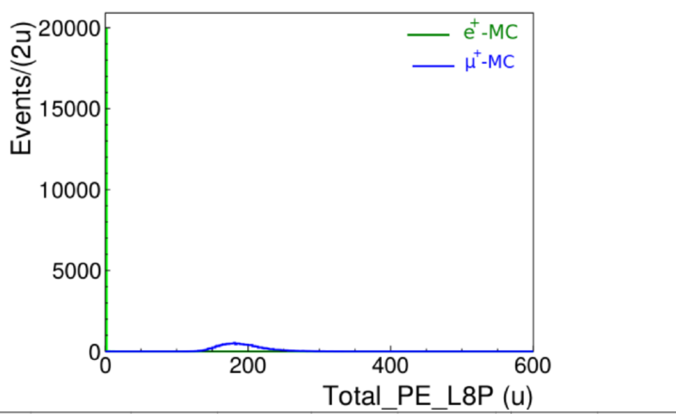


| Var_i_ß_cut(i) | Cut(e)_Interval | Eff | Deff | Pur | Dpur | Eff*Pur | D(Eff*Pur) |
|---|---|---|---|---|---|---|---|
| | [0,15] | 0.9986 | 0.0002644 | 0.99994 | 5.87E-005 | 0.99854 | 3.23E-004 |
| | [0,20] | 0.9989 | 0.0002344 | 0.99994 | 5.89E-005 | 0.99884 | 2.93E-004 |
| Total_PE_L8P | [0,50] | 0.9999 | 0.0000707 | 0.99994 | 5.87E-005 | 0.99984 | 1.29E-004 |

**Figure F.9:** Histogram of $Var\_2\_4$ for pure (MC) 2 GeV $e^+$ & $\mu^+$ samples.

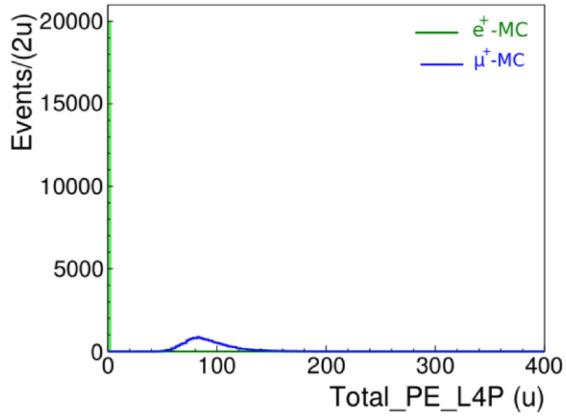


| Var_i_ß_cut(i) | Cut(e)_Interval | Eff | Deff | Pur | Dpur | Eff*Pur | D(Eff*Pur) |
|---|---|---|---|---|---|---|---|
| | [0,8] | 0.9999 | 0.0000707 | 0.99994 | 5.88E-005 | 0.99984 | 1.30E-004 |
| Total_PE_L4P | [0,10] | 0.9999 | 0.0000707 | 0.99994 | 5.87E-005 | 0.99984 | 1.29E-004 |
| | [0,15] | 0.99995 | 0.00005 | 0.99988 | 8.37E-005 | 0.99983 | 1.34E-004 |

**Figure F.10:** Histogram of $Var\_2\_5$ for pure (MC) 2 GeV $e^+$ & $\mu^+$ samples.

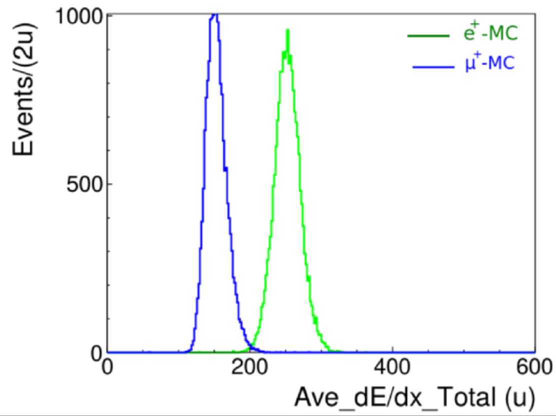


| Var_i_ß_cut(i) | Cut(e)_Interval | Eff | Deff | Pur | Dpur | Eff*Pur | D(Eff*Pur) |
|---|---|---|---|---|---|---|---|
| Ave_dEdx_Total | [200,] | 0.9976 | 0.000346 | 0.99436 | 5.56E-004 | 0.99197 | 8.99E-004 |
| | [190,] | 0.9995 | 0.0001581 | 0.98163 | 9.92E-004 | 0.98114 | 1.15E-003 |
| | [210,] | 0.98995 | 0.0007053 | 0.99815 | 3.20E-004 | 0.98812 | 1.02E-003 |

**Figure F.11:** Histogram of $Var\_3\_1$ for pure (MC) 2 GeV $e^+$ & $\mu^+$ samples.

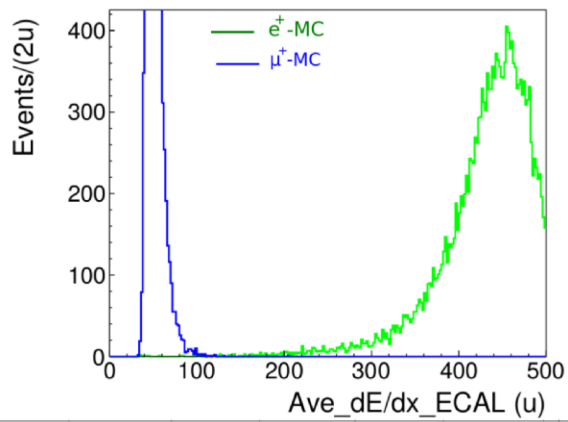


| Var_i_ß_cut(i) | Cut(e)_Interval | Eff | Deff | Pur | Dpur | Eff*Pur | D(Eff*Pur) |
|---|---|---|---|---|---|---|---|
| Ave_dEdx_ECAL | [120,] | 0.99915 | 0.0002061 | 0.99975 | 1.18E-004 | 0.9989 | 3.24E-004 |
| | [140,] | 0.9987 | 0.0002548 | 0.99994 | 5.86E-005 | 0.99864 | 3.13E-004 |
| | [130,] | 0.99885 | 0.0002397 | 0.99988 | 8.30E-005 | 0.99873 | 3.23E-004 |

**Figure F.12:** Histogram of $Var\_3\_2$ for pure (MC) 2 GeV $e^+$ & $\mu^+$ samples.

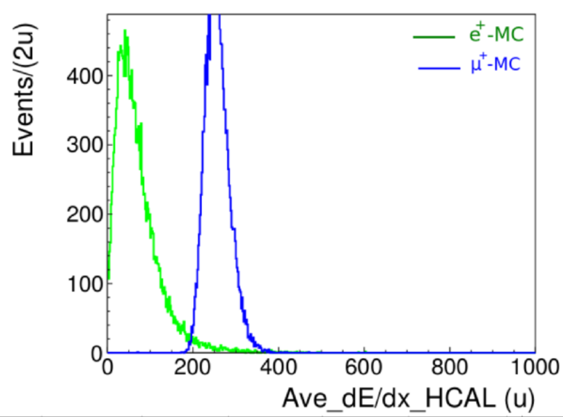


| Var_i_ß_cut(i) | Cut(e)_Interval | Eff | Deff | Pur | Dpur | Eff*Pur | D(Eff*Pur) |
|---|---|---|---|---|---|---|---|
| | [0,180] | 0.9615 | 0.0013605 | 0.99975 | 1.18E-004 | 0.96126 | 1.47E-003 |
| Ave_dEdx_HCAL | [0,190] | 0.9675 | 0.0012539 | 0.9987 | 2.70E-004 | 0.96624 | 1.51E-003 |
| | [0,200] | 0.97235 | 0.0011594 | 0.99183 | 6.69E-004 | 0.96441 | 1.80E-003 |

**Figure F.13:** Histogram of $Var\_3\_3$ for pure (MC) 2 GeV $e^+$ & $\mu^+$ samples.

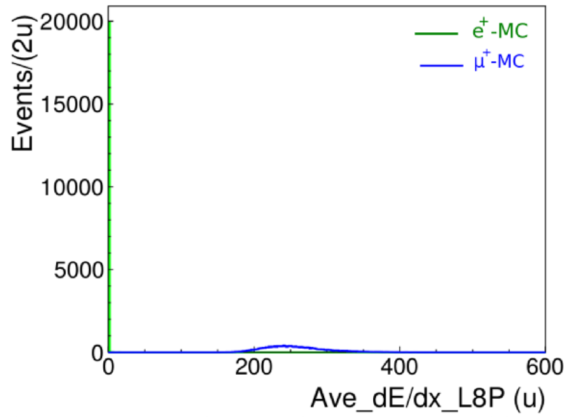


| Var_i_ß_cut(i) | Cut(e)_Interval | Eff | Deff | Pur | Dpur | Eff*Pur | D(Eff*Pur) |
|---|---|---|---|---|---|---|---|
| | [0,10] | 0.9975 | 0.0003531 | 0.99994 | 5.87E-005 | 0.99744 | 4.12E-004 |
| | [0,15] | 0.99815 | 0.0003039 | 0.99994 | 5.87E-005 | 0.99809 | 3.62E-004 |
| Ave_dEdx_L8P | [0,20] | 0.9986 | 0.0002644 | 0.99994 | 5.89E-005 | 0.99854 | 3.23E-004 |

**Figure F.14:** Histogram of $Var\_3\_4$ for pure (MC) 2 GeV $e^+$ & $\mu^+$ samples.

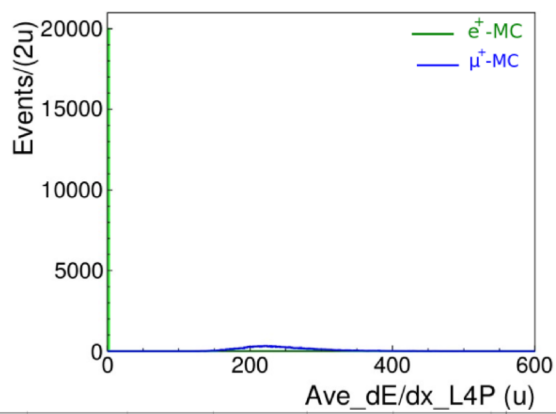


| Var_i_ß_cut(i) | Cut(e)_Interval | Eff | Deff | Pur | Dpur | Eff*Pur | D(Eff*Pur) |
|---|---|---|---|---|---|---|---|
| | [0,10] | 0.99975 | 0.0001118 | 0.99994 | 5.89E-005 | 0.99969 | 1.71E-004 |
| Ave_dEdx_L4P | [0,15] | 0.9999 | 0.0000707 | 0.99994 | 5.90E-005 | 0.99984 | 1.30E-004 |
| | [0,20] | 0.9999 | 0.0000707 | 0.99994 | 5.89E-005 | 0.99984 | 1.30E-004 |

**Figure F.15:** Histogram of $Var\_3\_5$ for pure (MC) 2 GeV $e^+$ & $\mu^+$ samples.

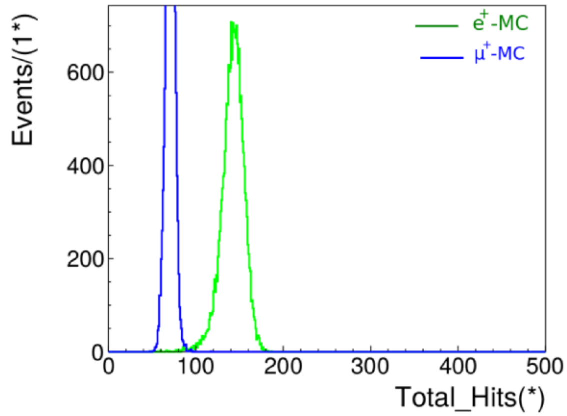


| Var_i_ß_cut(i) | Cut(e)_Interval | Eff | Deff | Pur | Dpur | Eff*Pur | D(Eff*Pur) |
|---|---|---|---|---|---|---|---|
| Total_Hits | [90,] | 0.9964 | 0.0004235 | 0.99895 | 2.41E-004 | 0.99536 | 6.63E-004 |
| | [95,] | 0.995 | 0.0004987 | 0.99969 | 1.31E-004 | 0.99469 | 6.29E-004 |
| | [100,] | 0.99255 | 0.0006081 | 0.99994 | 5.88E-005 | 0.99249 | 6.66E-004 |

**Figure F.16:** Histogram of $Var\_4\_1$ for pure (MC) 2 GeV $e^+$ & $\mu^+$ samples.

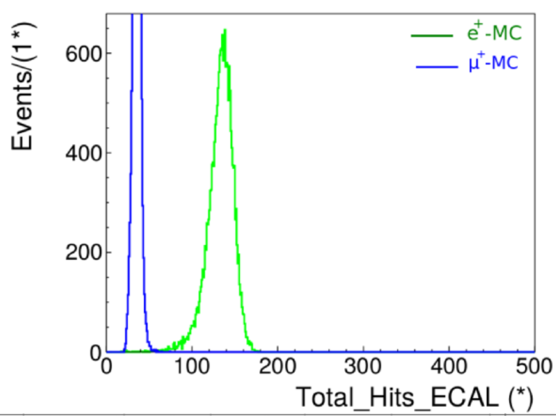


| Var_i_ß_cut(i) | Cut(e)_Interval | Eff | Deff | Pur | Dpur | Eff*Pur | D(Eff*Pur) |
|---|---|---|---|---|---|---|---|
| Total_Hits_ECAL | [60,] | 0.99805 | 0.0003119 | 0.99981 | 1.01E-004 | 0.99787 | 4.13E-004 |
| | [55,] | 0.99875 | 0.0002498 | 0.99894 | 2.43E-004 | 0.99769 | 4.93E-004 |
| | [65,] | 0.9972 | 0.0003736 | 0.99994 | 5.85E-005 | 0.99714 | 4.32E-004 |

**Figure F.17:** Histogram of $Var\_4\_2$ for pure (MC) 2 GeV $e^+$ & $\mu^+$ samples.

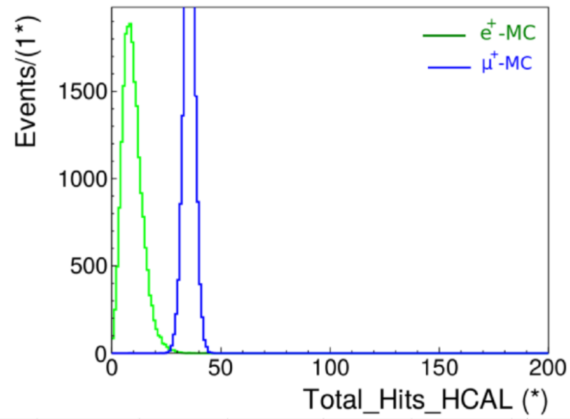


| Var_i_ß_cut(i) | Cut(e)_Interval | Eff | Deff | Pur | Dpur | Eff*Pur | D(Eff*Pur) |
|---|---|---|---|---|---|---|---|
| Total_Hits_HCAL | [0,26] | 0.99685 | 0.0003962 | 0.99871 | 2.68E-004 | 0.99556 | 6.63E-004 |
| | [0,25] | 0.9956 | 0.000468 | 0.99957 | 1.55E-004 | 0.99517 | 6.22E-004 |
| | [0,27] | 0.99775 | 0.000335 | 0.996 | 4.70E-004 | 0.99376 | 8.03E-004 |

**Figure F.18:** Histogram of $Var\_4\_3$ for pure (MC) 2 GeV $e^+$ & $\mu^+$ samples.

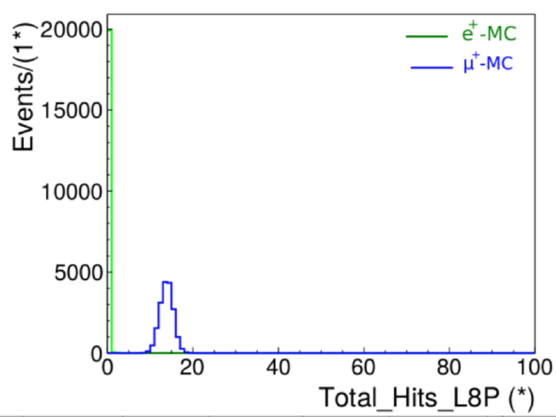


| Var_i_ß_cut(i) | Cut(e)_Interval | Eff | Deff | Pur | Dpur | Eff*Pur | D(Eff*Pur) |
|---|---|---|---|---|---|---|---|
| | [0,3] | 0.99995 | 0.00005 | 0.99994 | 5.86E-005 | 0.99989 | 1.09E-004 |
| Total_Hits_L8P | [0,5] | 1 | 0 | 0.99994 | 5.89E-005 | 0.99994 | 5.89E-005 |
| | [0,8] | 1 | 0 | 0.99883 | 2.55E-004 | 0.99883 | 2.55E-004 |

**Figure F.19:** Histogram of $Var\_4\_4$ for pure (MC) 2 GeV $e^+$ & $\mu^+$ samples.

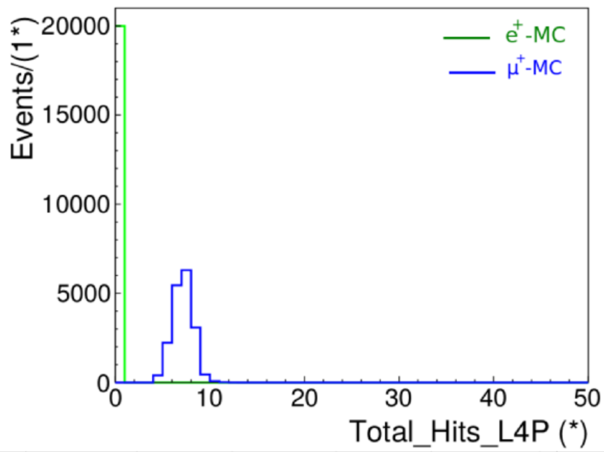


| Var_i_ß_cut(i) | Cut(e)_Interval | Eff | Deff | Pur | Dpur | Eff*Pur | D(Eff*Pur) |
|---|---|---|---|---|---|---|---|
| Total_Hits_L4P | [0,2] | 1 | 0 | 0.99982 | 1.01E-004 | 0.99982 | 1.01E-004 |
| | [0,3] | 1 | 0 | 0.99975 | 1.17E-004 | 0.99975 | 1.17E-004 |
| | [0,4] | 1 | 0 | 0.97566 | 1.13E-003 | 0.97566 | 1.13E-003 |

**Figure F.20:** Histogram of $Var\_4\_5$ for pure (MC) 2 GeV $e^+$ & $\mu^+$ samples.

# Appendix G

# Histograms of pure (MC) 2 GeV $e^+$ & $\pi^+$ samples

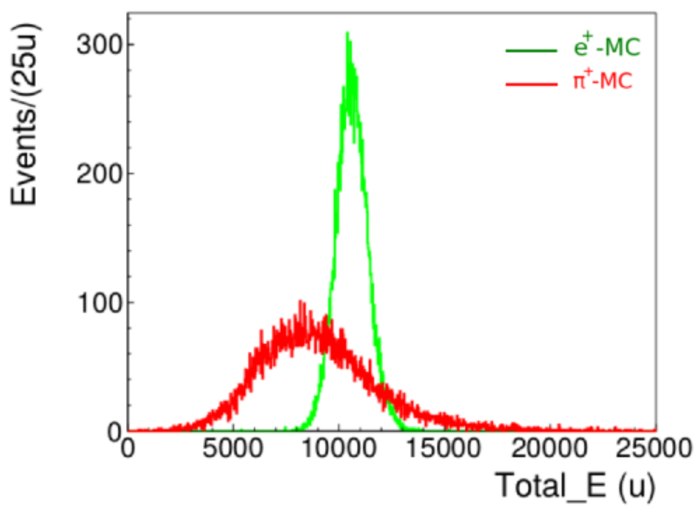


| Var_i_ß_cut(i) | Cut(e)_Interval | Eff | Deff | Pur | Dpur | Eff*Pur | D(Eff*Pur) |
|---|---|---|---|---|---|---|---|
| | [8000,13000] | 0.99725 | 0.0003703 | 0.65259 | 0.0027236 | 0.65079 | 0.0029578 |
| | [8500,13000] | 0.99465 | 0.0005158 | 0.6866 | 0.0027252 | 0.68293 | 0.0030648 |
| Total_E | [9000,13000] | 0.98045 | 0.000979 | 0.72126 | 0.0027193 | 0.70716 | 0.0033723 |

**Figure G.1:** Histogram of $Var\_1\_1$ for pure (MC) 2 GeV $e^+$ & $\pi^+$ samples.

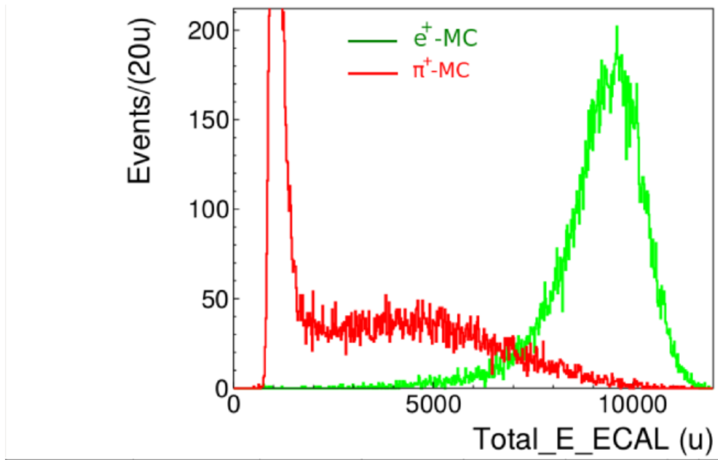


| Var_i_ß_cut(i) | Cut(e)_Interval | Eff | Deff | Pur | Dpur | Eff*Pur | D(Eff*Pur) |
|---|---|---|---|---|---|---|---|
| | [5500,] | 0.98615 | 0.0008264 | 0.85178 | 0.002335 | 0.83998 | 0.0030066 |
| | [6500,] | 0.9689 | 0.0012275 | 0.90602 | 0.0019952 | 0.87784 | 0.0030453 |
| Total_E_ECAL | [7000,] | 0.95225 | 0.0015078 | 0.92984 | 0.0017847 | 0.88544 | 0.0031015 |

**Figure G.2:** Histogram of $Var\_1\_2$ for pure (MC) 2 GeV $e^+$ & $\pi^+$ samples.

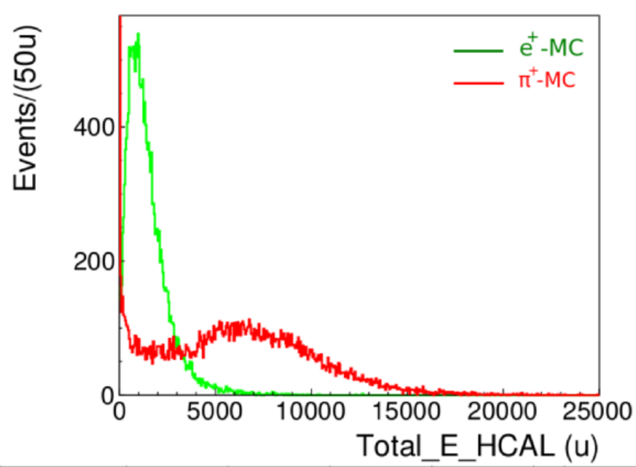


| Var_i_ß_cut(i) | Cut(e)_Interval | Eff | Deff | Pur | Dpur | Eff*Pur | D(Eff*Pur) |
|---|---|---|---|---|---|---|---|
| | [0,3000] | 0.91765 | 0.0019438 | 0.78191 | 0.0026954 | 0.71752 | 0.0039933 |
| Total_E_HCAL | [0,3500] | 0.94895 | 0.0015563 | 0.76708 | 0.0026873 | 0.72792 | 0.0037439 |
| | [0,4000] | 0.96785 | 0.0012473 | 0.75176 | 0.0026921 | 0.72759 | 0.0035433 |

**Figure G.3:** Histogram of $Var\_1\_3$ for pure (MC) 2 GeV $e^+$ & $\pi^+$ samples.

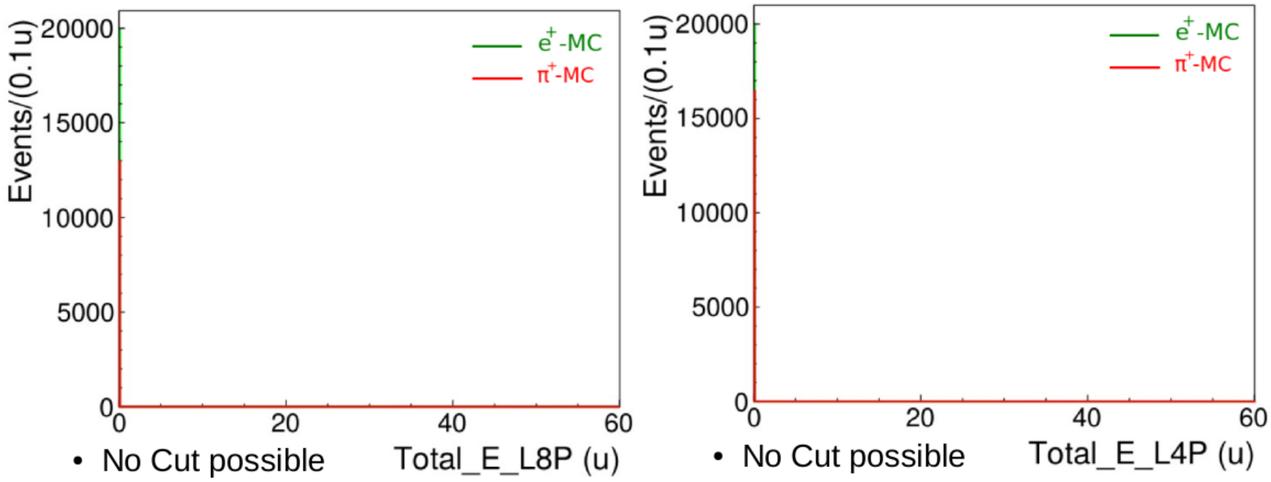


**Figure G.4:** Histograms of $Var\_1\_4$ & $Var\_1\_5$ (no possible cut) for pure (MC) 2 GeV $e^+$ & $\pi^+$ samples.

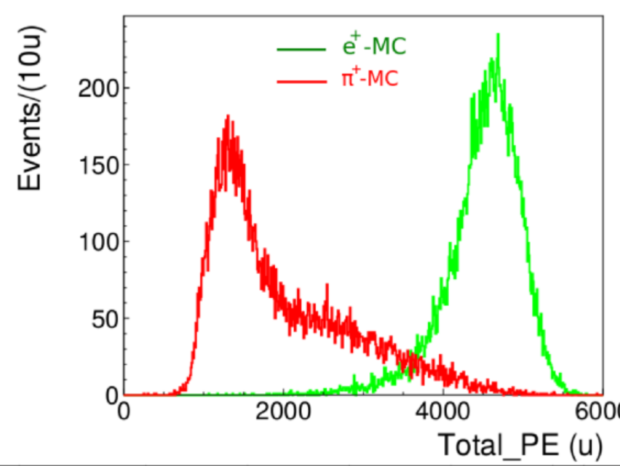


| Var_i_ß_cut(i) | Cut(e)_Interval | Eff | Deff | Pur | Dpur | Eff*Pur | D(Eff*Pur) |
|---|---|---|---|---|---|---|---|
| | [3500,] | 0.9637 | 0.0013225 | 0.92526 | 0.0018221 | 0.89167 | 0.0029796 |
| Total_PE | [3600,] | 0.9555 | 0.0014581 | 0.93484 | 0.0017262 | 0.89324 | 0.0030125 |
| | [3400,] | 0.9709 | 0.0011886 | 0.91564 | 0.0019085 | 0.889 | 0.0029412 |

**Figure G.5:** Histogram of $Var\_2\_1$ for pure (MC) 2 GeV $e^+$ & $\pi^+$ samples.

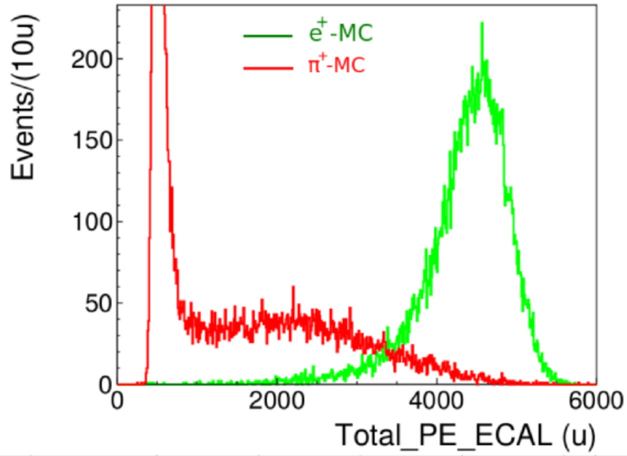


| Var_i_ß_cut(i) | Cut(e)_Interval | Eff | Deff | Pur | Dpur | | Eff*Pur | D(Eff*Pur) |
|---|---|---|---|---|---|---|---|---|
| | [3500,] | 0.93445 | 0.00175 | 0.93943 | 0.0016912 | | 0.87785 | 0.0032244 |
| Total_PE_ECAL | [3400,] | 0.94645 | 0.0015919 | 0.93274 | 0.0017582 | | 0.88279 | 0.0031489 |
| | [3300,] | 0.95605 | 0.0014495 | 0.92274 | 0.0018548 | | 0.88218 | 0.0031108 |

**Figure G.6:** Histogram of $Var\_2\_2$ for pure (MC) 2 GeV $e^+$ & $\pi^+$ samples.

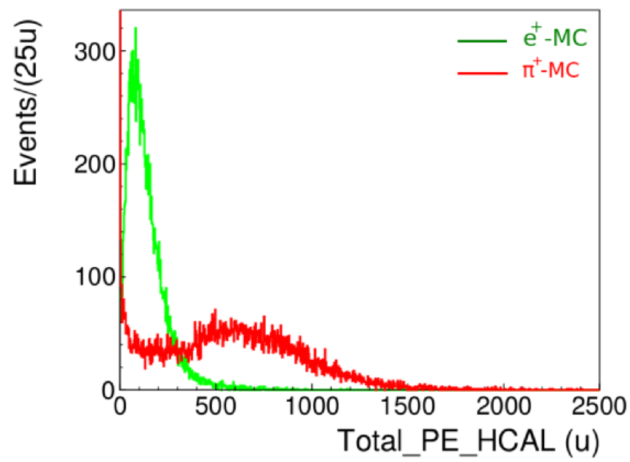


| Var_i_ß_cut(i) | Cut(e)_Interval | Eff | Deff | Pur | Dpur | | Eff*Pur | D(Eff*Pur) |
|---|---|---|---|---|---|---|---|---|
| Total_PE_HCAL | [0,350] | 0.9596 | 0.0013923 | 0.75951 | 0.0026886 | | 0.72882 | 0.0036374 |
| | [0,300] | 0.9337 | 0.0017593 | 0.77563 | 0.0026886 | | 0.7242 | 0.0038749 |
| | [0,340] | 0.95455 | 0.0014728 | 0.76239 | 0.0026896 | | 0.72774 | 0.0036903 |

**Figure G.7:** Histogram of $Var\_2\_3$ for pure (MC) 2 GeV $e^+$ & $\pi^+$ samples.

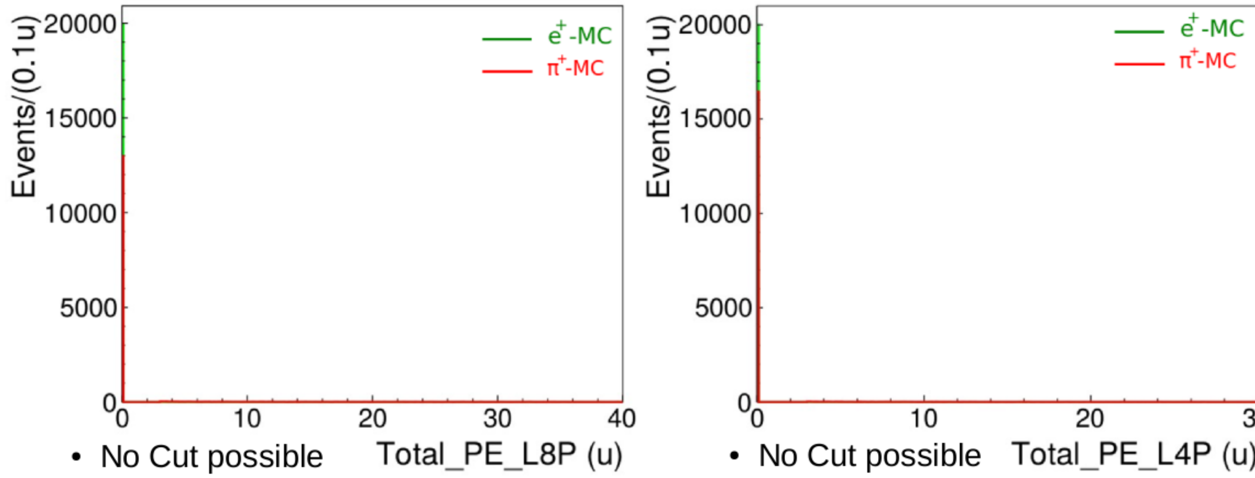


**Figure G.8:** Histograms of $Var\_2\_4$ & $Var\_2\_5$ (no possible cut) for pure (MC) 2 GeV $e^+$ & $\pi^+$ samples.

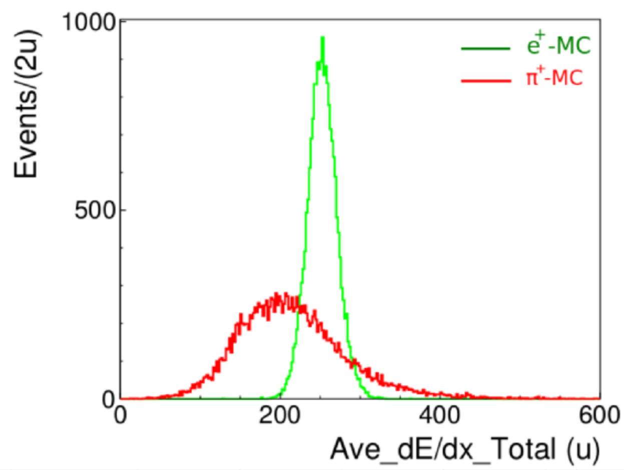


| Var_i_ß_cut(i) | Cut(e)_Interval | Eff | Deff | Pur | Dpur | | Eff*Pur | D(Eff*Pur) |
|---|---|---|---|---|---|---|---|---|
| | [200,320] | 0.99685 | 0.0003962 | 0.67277 | 0.0027256 | | 0.67066 | 0.0029836 |
| | [210,310] | 0.98805 | 0.0007683 | 0.70899 | 0.0027208 | | 0.70052 | 0.003233 |
| Ave_dEdx_Total | [215,310] | 0.97895 | 0.0010151 | 0.72306 | 0.0027194 | | 0.70784 | 0.0033961 |

**Figure G.9:** Histogram of $Var\_3\_1$ for pure (MC) 2 GeV $e^+$ & $\pi^+$ samples.

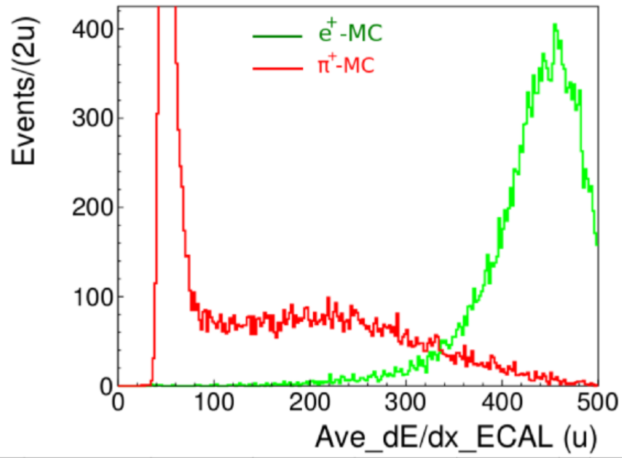


| Var_i_ß_cut(i) | Cut(e)_Interval | Eff | Deff | Pur | Dpur | | Eff*Pur | D(Eff*Pur) |
|---|---|---|---|---|---|---|---|---|
| | [340,] | 0.9448 | 0.0016148 | 0.93558 | 0.0017274 | | 0.88394 | 0.0031429 |
| Ave_dEdx_ECAL | [330,] | 0.9548 | 0.001469 | 0.92587 | 0.0018242 | | 0.88402 | 0.0031019 |
| | [350,] | 0.9328 | 0.0017704 | 0.9426 | 0.0016533 | | 0.87926 | 0.003211 |

**Figure G.10:** Histogram of $Var\_3\_2$ for pure (MC) 2 GeV $e^+$ & $\pi^+$ samples.

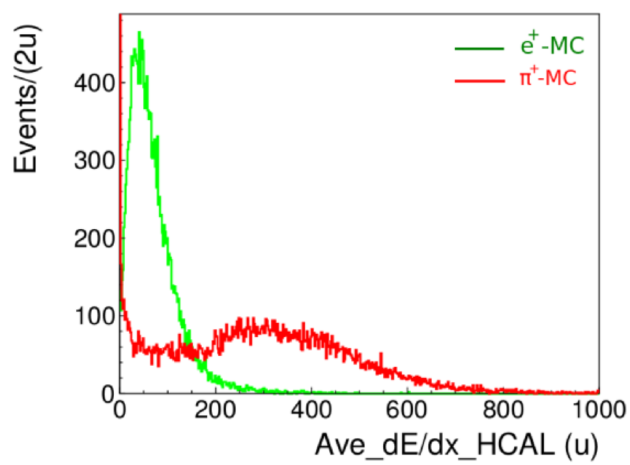


| Var_i_ß_cut(i) | Cut(e)_Interval | Eff | Deff | Pur | Dpur | | Eff*Pur | D(Eff*Pur) |
|---|---|---|---|---|---|---|---|---|
| | [0,170] | 0.95235 | 0.0015063 | 0.76469 | 0.0026878 | | 0.72826 | 0.0037116 |
| Ave_dEdx_HCAL | [0,180] | 0.9615 | 0.0013605 | 0.75858 | 0.0026878 | | 0.72937 | 0.0036164 |
| | [0,190] | 0.9675 | 0.0012539 | 0.75204 | 0.0026921 | | 0.7276 | 0.0035476 |

**Figure G.11:** Histogram of $Var\_3\_3$ for pure (MC) 2 GeV $e^+$ & $\pi^+$ samples.

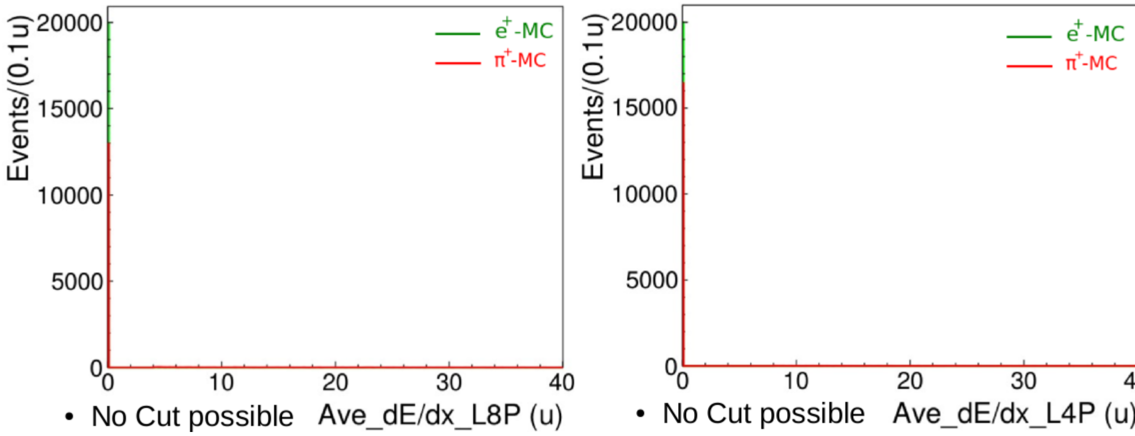


**Figure G.12:** Histograms of $Var\_3\_4$ & $Var\_3\_5$ (no possible cut) for pure (MC) 2 GeV $e^+$ & $\pi^+$ samples.

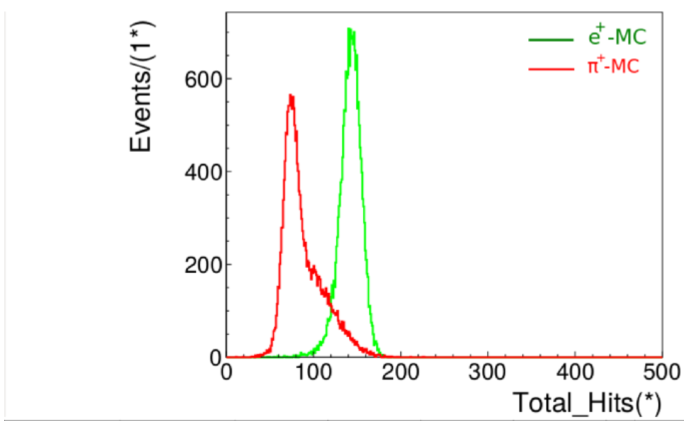


| Var i ß cut(i) | Cut(e) Interval | Eff | Deff | Pur | Dpur | Eff*Pur | D(Eff*Pur) |
|---|---|---|---|---|---|---|---|
| Total_Hits | [120,] | 0.9511 | 0.0015249 | 0.89414 | 0.0021093 | 0.85042 | 0.0033697 |
| | [125,] | 0.9146 | 0.0019762 | 0.91264 | 0.0019945 | 0.8347 | 0.0036277 |
| | [115,] | 0.971 | 0.0011866 | 0.87152 | 0.0022417 | 0.84624 | 0.0032108 |

**Figure G.13:** Histogram of $Var\_4\_1$ for pure (MC) 2 GeV $e^+$ & $\pi^+$ samples.

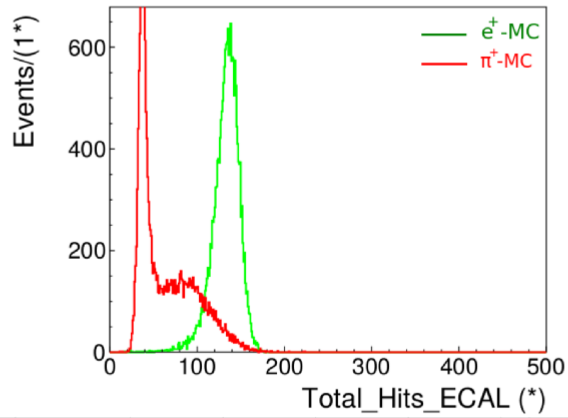


| Var i ß cut(i) | Cut(e) Interval | Eff | Deff | Pur | Dpur | | Eff*Pur | D(Eff*Pur) |
|---|---|---|---|---|---|---|---|---|
| | [100,] | 0.96835 | 0.0012379 | 0.85668 | 0.0023304 | | 0.82957 | 0.0033172 |
| | [110,] | 0.92985 | 0.0018059 | 0.89568 | 0.0021214 | | 0.83285 | 0.0035901 |
| Total_Hits_ECAL | [105,] | 0.95375 | 0.0014851 | 0.87746 | 0.002224 | | 0.83687 | 0.0034243 |

**Figure G.14:** Histogram of $Var\_4\_2$ for pure (MC) 2 GeV $e^+$ & $\pi^+$ samples.

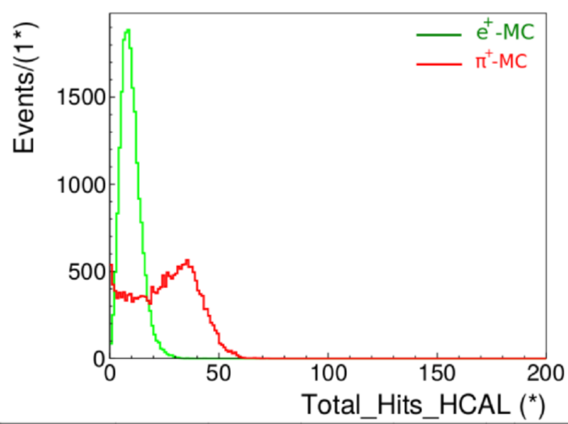


| Var i ß cut(i) | Cut(e) Interval | Eff | Deff | Pur | Dpur | | Eff*Pur | D(Eff*Pur) |
|---|---|---|---|---|---|---|---|---|
| Total_Hits_HCAL | [0,20] | 0.97875 | 0.0010198 | 0.7164 | 0.0027268 | | 0.70118 | 0.0033994 |
| | [0,25] | 0.9956 | 0.000468 | 0.66969 | 0.0027276 | | 0.66675 | 0.003029 |
| | [0,30] | 0.9994 | 0.0001732 | 0.62073 | 0.0027039 | | 0.62035 | 0.0028098 |

**Figure G.15:** Histogram of $Var\_4\_3$ for pure (MC) 2 GeV $e^+$ & $\pi^+$ samples.

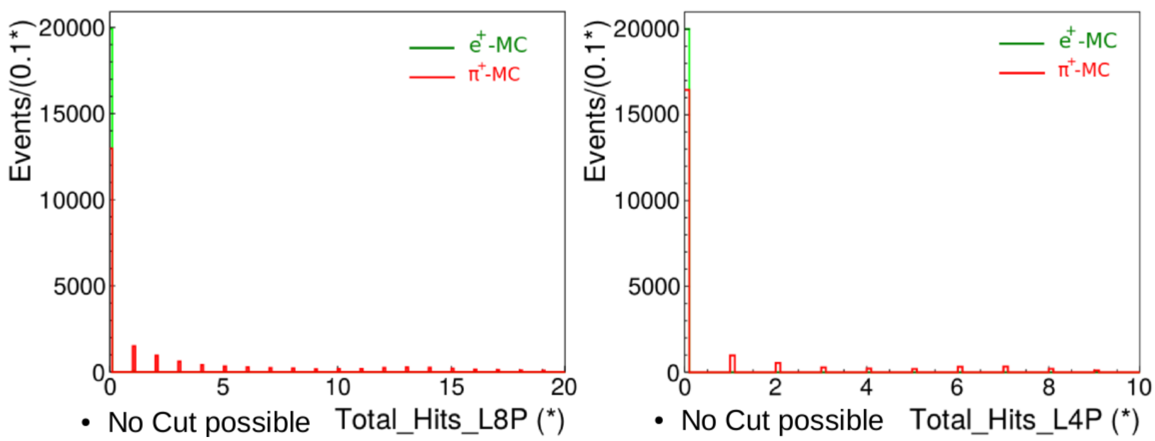


**Figure G.16:** Histograms of $Var\_4\_4$ & $Var\_4\_5$ (no possible cut) for pure (MC) 2 GeV $e^+$ & $\pi^+$ samples.

# Appendix H

# Summary of main contributions to MINER$\nu$A & other physical issues

As has been outlined in this work, the development of particle-ID tools is crucial to be able to distinguish specific particle species moving, and thus depositing energy in a specific way, inside the MINERvA Main & Test Beam detectors. The identification of muons is extremely important to avoid their confusion with some pions that may reach the ECAL/HCAL region of the MINERvA Main detector and in this way permits us to reconstruct properly the Event (which is a specific neutrino interaction, as detailed in Chapter 2). It is also important to be able to locate some rock muons that may be present and wipe them out from the Event we wish to reconstruct, since those particles do not come from neutrino interactions but from the NuMI beam (rock muons are those muons that did not decay and managed to arrive at the MINERvA main detector).

The methodology presented in Chapter 6 for making up the Optimum-Tool (based on an Efficiency-Purity analysis) to locate specific particle species can also be followed for locating specific species inside the MINERvA Main Detector with a slight modification of the *ModuleMultiplier* function (that should consider now the Main Detector Modules in the Tracker-Region) & the definition of other variables similar to the $Var\_i\_\beta$ for the tracker region. The importance of the Methodology established in that Chapter is that one can make up the Optimum-Tool to locate any charged particle species at any energy moving inside the MINERvA Main & Test Beam detectors with the aid of Monte Carlo simulations of single particles moving inside the detectors.

As it was stated in Chapter 1, it was necessary to look at the Detector (& construct Detector Variables) to separate muons from pions present in the Time of Flight (ToF) Pion peak because the time difference between muons and pions is smaller than the resolution of the ToF device ($\sim 10^2 ps$). To see this we can use the relativistic equations of Figure 1.15, considering the lowest possible energy (which permits a better separation of species) in which $p \sim 1GeV/c$, the fact that the masses of the proton, pion and muon are $m_p \sim 1\ 800m_e,\ m_\pi \sim 273m_e,\ m_\mu \sim 207m_e$ ($m_e$ being the mass of the electron) & the following approximations (using the SI system of units for each quantity):

$$p \sim 1GeV/c \sim 10^{-18}, \quad c \sim 10^8, \quad m_e \sim 10^{-31}, \quad distance \sim 10^2$$

then we can estimate the time difference between the muons and pions ($\delta t_{\mu\pi}$) & between the pions and protons ($\delta t_{\pi p}$) using the equation present in Figure 1.15:

$$\delta t_{\mu\pi} \sim 1ps, \quad \delta t_{\pi p} \sim 10^2 ps$$

Then we notice (from this estimation) that the ToF device has problems in separating pions from muons because their time difference is smaller than the resolution of the system (even at a low energy like 1GeV) whereas the time difference between pions and protons is almost of the order (or even larger) of the resolution of the ToF device.

Other interesting feature of this experiment is that we deal with very tiny time intervals (all of the order of $ns$) in which we expect specific interactions or events to take place (1 bucket $\sim 19ns$, Minerva Readout window $\sim 300ns$, Time in which the Gate is open to receive the beam $\sim 16ns$) & also deal with neutrino interactions that take place in a very short region of the space (called the vertex), which ideally would be a point but due to limitations of the MINERvA detector spatial-resolution we are able only to have a precision of $mm$ when the vertex is reconstructed (the size must be always less than 3 cm to have certainty that the vertex was located). The size of the vertex is usually taken as the RMS (standard deviation) of the Track Position Resolution, which physically represents the spatial uncertainty in locating the actual vertex from which final state particles come from. Although this thesis does not deal with this issue, more information about it can be found in the NIM paper (Reference [96]). The next Figure shows that the vertex usually has a size of the order of $mm$. With better detector technologies we would be able to achieve better resolution (smaller sizes for the vertex) in the reconstruction of the vertex (it would be great to attain sizes of the order of $nm$).

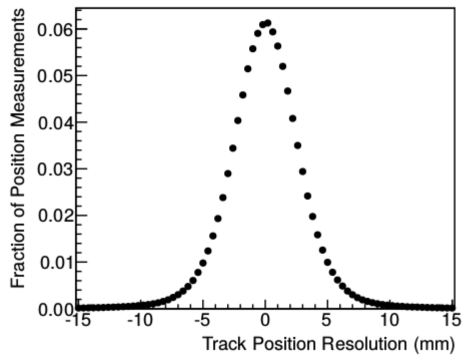


**Figure H.1:** Resolution of the fitted positions along a track relative to the measured cluster positions for a sample of data rock muons. The RMS of the distribution is $3.1mm$ [96].

Other interesting issue would be the usage of muons (because they deposit energy via ionization in an almost constant & predicted way along its trajectory and do not produce showers) to study properties and composition of materials, this is like trying to infer what would be the *ModuleMultiplier* function (which provides information on the composition of the material) for a given piece of matter over which we make muons to pass through and then analyze the response of that material to them (attaching PMTs to specific spots to record the response of the material to the passage of muons).